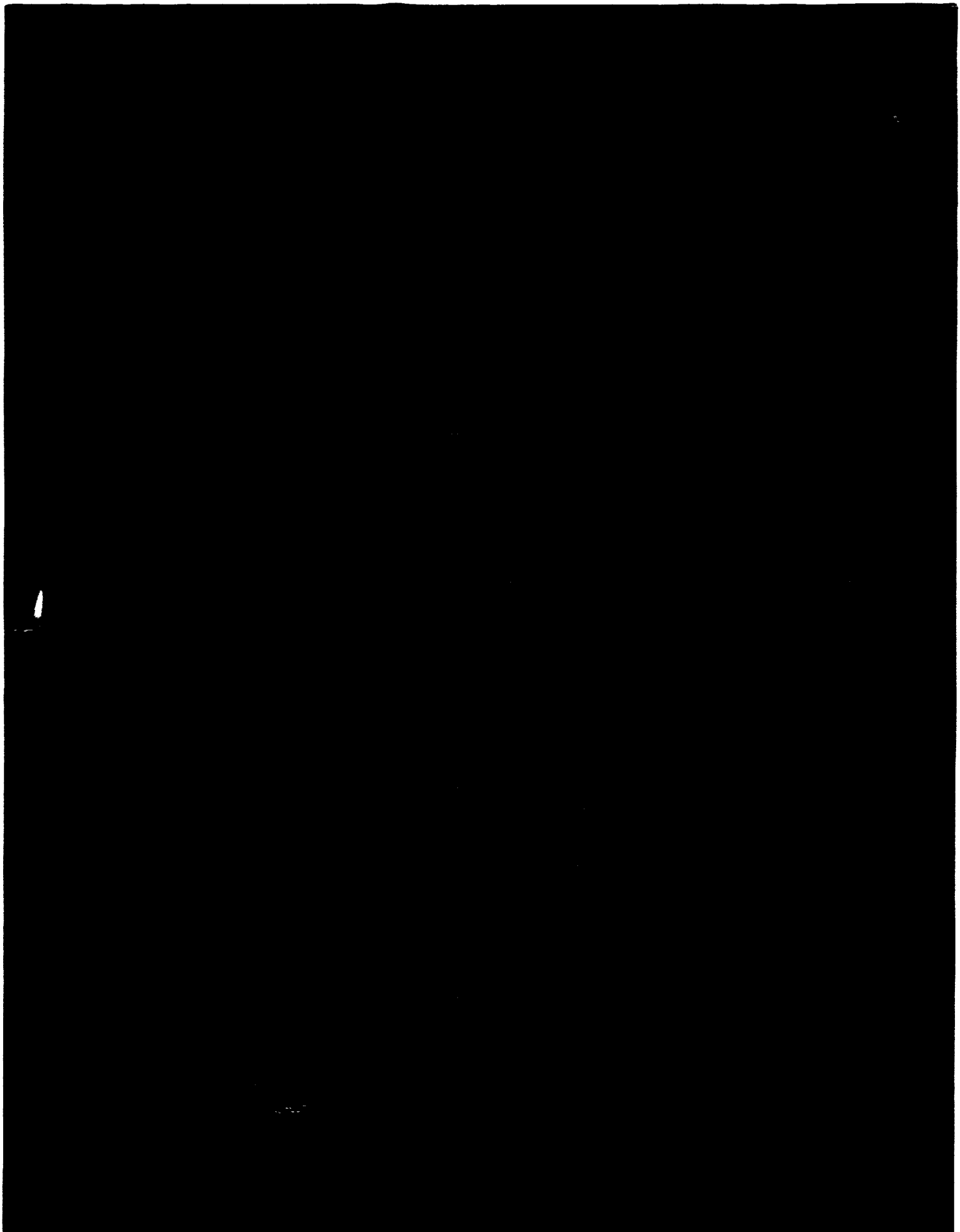

NASA CR-566

# ACOUSTIC PREDICTION METHODS FOR ROCKET ENGINES, INCLUDING THE EFFECTS OF CLUSTERED ENGINES AND DEFLECTED EXHAUST FLOW

By R. C. Potter and M. J. Crocker



Prepared under Contract No. NAS 8-11071 by
WYLE LABORATORIES
Huntsville, Ala.

for George C. Marshall Space Flight Center

NATIONAL AERONAUTICS AND SPACE ADMINISTRATION

For sale by the Clearinghouse for Federal Scientific and Technical Information
Springfield, Virginia 22151 – Price $3.25

TABLE OF CONTENTS

LIST OF FIGURES

# LIST OF SYMBOLS

| | |
|---|---|
| $a$ | distance from center line of free jet to outer boundary of core |
| $a$ | shock parameter |
| $a$ | speed of sound |
| $A$ | cross-sectional area of jet |
| $b$ | momentum width parameter |
| $b$ | shock parameter |
| $C$ | coefficient of specific heat for a gas at constant pressure |
| $C_p$ | coefficient of specific heat for a gas at constant pressure |
| $d$ | width of two-dimensional impinging flow |
| $D$ | diameter of jet flow; exit diameter |
| $f$ | frequency |
| $f_1\left(\frac{y}{y_0}\right)$ | deflected jet shape parameter |
| $f_2\left(\frac{h}{h_0}\right)$ | deflected jet shape parameter |
| $f_3\left(\frac{h}{h_0}\right)$ | deflected jet shape parameter |
| $F(T)$ | function of temperature |
| $g$ | gravitational constant |
| $h$ | shock parameter |
| $h$ | vertical height above deflection plane in deflected jet |
| $h_1$ | thickness of two-dimensional deflected jet, (downplane) |
| $h_2$ | thickness of two-dimensional deflected jet, (up plane) |
| $J$ | mechanical equivalent of heat |
| $k$ | shock parameter |
| $K_1$, $K_2$ | clustered nozzle parameters |
| $^oK$ | degree Kelvin |
| $m$ | molecular weight |
| $\dot{m}$ | mass flow |
| $M$ | Mach number of flow |
| $\bar{M}$ | momentum of flow |
| $n$ | number of rockets |
| $n_p$ | number of rockets on perimeter of cluster |
| $p$ | static pressure |
| $P$ | clustered nozzle parameter |
| $q$ | dynamic pressure |
| $q_{yh}$ | dynamic pressure at position y and height h in deflected jet |
| $q_{y0}$ | dynamic pressure at position y on ground plane of deflected jet |

| | |
|---|---|
| $q_{max\ h}$ | dynamic pressure measured at height h on center line of deflected jet |
| $q_{max\ 0}$ | dynamic pressure measured at ground plane on center line of deflected jet |
| r | radial distance from center line of jet to point considered |
| R | exit radius of nozzle |
| R | distance to point |
| $\underline{R}$ | gas constant |
| $\underline{R}_u$ | universal gas constant |
| $^oR$ | degree Rankine |
| S | Strouhal Number |
| t | thrust |
| T | static temperature |
| $\overline{T}$ | total temperature |
| u | velocity at any radial position in jet stream |
| U | maximum velocity at downstream station considered |
| $\overline{U}$ | mean velocity at downstream station considered |
| V | velocity |
| V | representative velocity, defined in Chapter 5 |
| $V_{max\ 0}$ | velocity measured at ground plane on center line of deflected jet |
| W | acoustic power, watts |
| $W_m$ | mechanical power of jet stream, watts |
| x | distance downstream from nozzle exit |
| $x_t$ | distance to the core tip from the nozzle exit |
| y | horizontal distance measured from center-line of deflected jet |
| $y_h$ | horizontal distance measured from center-line of deflected jet to point where $q_{yh} = \frac{1}{2} q_{max\ h}$ |
| $y_0$ | horizontal distance measured on ground plane from center-line of deflected jet to point where $q_{y0} = \frac{1}{2} q_{max\ 0}$ |

## GREEK ALPHABET

| | |
|---|---|
| $\alpha$ | clusted nozzle area ratio |
| $\alpha$ | shock angle |
| $\beta$ | clustered nozzle density ratio |
| $\gamma$ | ratio of specific heats |
| $\delta$ | flow deflection angle |
| $\eta$ | jet parameter = $(r - a) / b$ |
| $\theta$ | angle measured from rocket exhaust flow direction |
| $\theta$ | angle measured in plane perpendicular to flow for a deflected jet |
| $\theta$ | clustered nozzle velocity ratio |
| $\xi$ | shock wave angle |
| $\rho$ | density |

## SUBSCRIPTS

| | |
|---|---|
| a | refers to atmospheric conditions |
| c | refers to characteristic values |
| e | refers to nozzle exit conditions |
| i | refers to conditions just before impingement of a deflected jet |
| t | refers to throat conditions |
| * | refers to critical conditions in flow |

## SUMMARY

In this report, existing methods to predict the noise generated by rocket motors are examined and calculated values compared with measured results. A method of allocating a spectrum of acoustic sources with distance downstream from the nozzle exit is produced. The final result is shown as a single normalized curve, which fits well all the reported results. It is based on measurements of acoustic sound power level on a boundary just outside and at 10 degrees to the rocket exhaust flow.

Methods to predict the noise fields generated by clustered rocket engines and deflected rocket exhaust flows are given, based on an analysis of the flow pattern produced. The flow patterns are solved in terms of the rocket flow parameters, nozzle, missile and deflector geometry, and the atmospheric conditions. The prediction method developed in the first part of this report is applied to the various segments of the flows to obtain the resultant noise fields. Comparison of predicted results with experimentally measured values indicates the usefulness of this method, which appears to cover well the whole range of rocket measurements reported.

# 1.0 INTRODUCTION

Much theoretical and experimental research has been accomplished towards the prediction of the noise generated by jets during the last fifteen years. More recently, increasing effort has been directed towards the prediction of the noise generated by rockets. However, despite all these efforts by many investigators, it is impossible today to predict completely the total noise field resulting from either a rocket with an arbitrary nozzle geometry or a deflected rocket flow.

This report reviews existing prediction techniques proposed for calculating the near and far field noise produced by jet and rocket flows. It examines in detail the noise field of a rocket flow from a single circular nozzle. In this examination, the methods of Reference 18 are extended and applied to recently published rocket data and thus normalized acoustic power generation and radiation characteristics over the entire length of the rocket flow are obtained.

The report also develops methods for predicting the flow and noise from clustered rocket nozzles. The methods rely heavily on the fact that similar flows produce similar noise. Thus, once the appropriate flow parameters are defined in terms which may be related to the flow from the simple circular nozzle, the noise for the complex flow is obtained by similarity.

This concept is also extended to the last portion of the report in which the prediction of noise generation and radiation of a deflected rocket flow is considered. In this case primary emphasis is placed on developing an appropriate model of the deflected flow. This development is frought with difficulties, since little good experimental data exists on which to base the necessary assumptions for the theoretical model; however, despite these difficulties, useful techniques are developed for the prediction of deflected flow noise.

## 2.0 ROCKET NOISE PREDICTION TECHNIQUES, AND FAR FIELD SOUND MEASUREMENTS.

### 2.1 Requirements of a Prediction Technique.

A complete prediction technique for rocket noise should allow the noise field to be determined fully, for a given flow configuration. Thus when the vehicle and engine geometry, exhaust flow parameters and atmospheric conditions are known, it should be possible to determine the noise at any point, both in the near and far field. Normally, this requires a determination of the total sound power produced by the rocket at each frequency, and then details of how this sound is directed away from the turbulent exhaust flow. These results can be used with the inverse square law of distance and atmospheric attenuation to obtain the sound field at the required points. It may also be necessary to make some allowance for refraction and reflection.

It has been the practice to present specialized prediction techniques, concerned with only one range of positions, such as the sound propagated back on to the missile structure itself. Also special methods have been suggested to account for reflected and other non-normal mixing flows. These have been used in an attempt to obtain accurate results by limiting the range of the variables. However, it should be possible by going to a more basic method to obtain a technique that should cover all cases of rocket exhaust. This technique obviously must be linked to details of the exhaust flow of the rocket, and in the limit, would be a complete description of the noise generating mechanism of the turbulent mixing flow.

The number of parameters to be considered for rocket noise is greater than for the case of the slower turbojet flow. This increase results not only on account of the higher velocities and thrust encountered with rockets, but also because the exhaust gas formed will have much different properties to the air with which it is mixing. The prediction technique should be applicable to thrusts ranging from a 1000 lb. rocket with a total noise power of $2.0 \times 10^4$ watts, to a rocket whose thrust is measured in millions of pounds and total acoustic power can equal $5.0 \times 10^7$ watts. It is important that the prediction method covers this wide range if the full effect of rocket scaling is to be understood. The increasing cost of large rockets means that the use of scale models in development work is increasing and full advantage, acoustically, must be taken of these tests. There is no reason why acoustic model testing should not become a part of the normal design process as is aerodynamic model testing.

Morgan (References 1 and 2) has studied the use of acoustic scale models extensively, and he suggests that the noise generated by a rocket depends primarily on the velocity density and exit Mach number. Therefore, the prediction method will have to cover a wide range of velocities and temperatures; velocities up to values of 10,000 ft/sec at an exit Mach number greater than 3, and temperatures as high as $4000^\circ$ R. In

addition the rocket can be either over or under expanded depending on the nozzle design, and it is possible for the conditions to completely reverse as the missile rises through the atmosphere. For these reasons it has been suggested by Cole et al. in Reference 3 that the critical speed of sound in the gas is another suitable parameter to be considered. Since the pressure ratio of the nozzle at launch conditions will normally be above the critical value, then the critical speed of sound in the exhaust gas will be the gas velocity at the nozzle throat.

Morgan, in Reference 1, suggested that the noise produced by a rocket is not especially dependent on such properties of the gas as thermal capacity and molecular weight. On this argument, he was able to replace the rocket gas by helium in his model. However, it will be shown in this report that the thermal properties of the exhaust gas are important in determining the flow characteristics of the exhaust mixing process and these depend on both the average molecular weight of the gas and the specific heats. In Section 4 on clustered rockets, it is shown that variations in the thermal properties can cause changes in the resultant flow velocities of up to 25 per cent. Since the noise production of a given volume of gas depends upon some high power of the velocity, a variation of this magnitude is critical.

Typical gases found in the rocket exhaust are carbon dioxide, carbon monoxide, steam, hydrogen and various halogen gases, such as potassium chloride which will occur in some solid rockets. The values of the specific heat at constant pressure for these gases are listed in Table 1.

TABLE 1*

SPECIFIC HEAT AT CONSTANT PRESSURE

| Gas | m | $\gamma$ 288°K, 1atm. | $C_p$ (cal/gr. °K) 288°K, 1 atm. | $C_p$ (cal/gr. °K) 1400°K, 10 atm. |
|---|---|---|---|---|
| $O_2$ | 32 | 1.401 | 0.2178 | 0.268 |
| $N_2$ | 28 | 1.404 | 0.2477 | 0.376 |
| $CO_2$ | 44 | 1.304 | 0.1989 | 0.303 |
| CO | 28 | 1.404 | 0.2478 | - |
| $H_2$ | 2 | 1.410 | 3.389 | 3.45 |
| $H_2O$ | 18 | 1.324 | 0.4820 (373°K) | 0.515 (1000°K) |
| Air | 29 | 1.403 (273°K) | 0.2398 (273°K) | 0.29 |
| | | 1.316 (2073°K) | | |

* Reference - American Institute of Physics Handbook, McGraw Hill Book Co. (1963)

For a turbojet engine the thermal properties of the gas are very similar to air since only a small part of the oxygen in the air will be burned. However, the exhaust gas of a rocket contains a large percentage of the lighter gases such as steam and hydrogen with the result that it often has high values of $C_p$, compared to air. Most of the gases are diatomic and so will have similar values for $\gamma$ to air, although the value will be reduced from the theoretical value of 1.40 for a perfect diatomic gas because of the high temperature.

Morgan, in Reference 2, refers to a small solid propellant rocket used as the standard which has a ratio of the specific heats equal to 1.12. The rocket was of the class of composite propellants, also called Hetrogeneous propellants, and Zucrow in Reference 4, suggests that the value of specific heat ratio of the exhaust gas for these rockets is between 1.2 and 1.27. From the value of the gas constant for the model rocket exhaust gas reported by Morgan, the average molecular weight of the exhaust gas calculates as 28.5. This agrees with the suggested values for solid rockets given by Zucrow. The average molecular weight values are similar to air, so the extremely low values for the ratio of specific heats means the gas molecules must contain several atoms. These must therefore be of the light atoms, such as hydrogen, to keep the average molecular weight low. Typical reported values of specific heat ratio equal to 1.25 are most likely to represent the actual conditions, and the lower values measured are probably in error. The fact that the specific heat for rocket exhaust gas can be up to three times greater than that of air, means that the mixing process of the gas with the atmosphere will be changed from that of the simple air jet. Therefore, any attempt to directly scale up jet engine acoustic data to fit rocket flows will not be suitable to obtain accurate results. The thermal properties of the exhaust gas will normally be implied if a complete description of the exhaust flow at the rocket exit is given. This means the pressure, density, velocity, temperature and Mach number of the flow should be specified. Also full details of the geometry of the nozzles, missile and deflectors are required.

The prediction technique should then take these given conditions and allow an estimate of the flow to be made, from which the acoustic field can be obtained.

## 2.2 Prediction Methods for Rocket Noise

Although a theoretical approach to calculate the noise power produced by a rocket, based purely on the given flow parameters of density, velocity, nozzle dimensions and atmospheric conditions, would be most desirable, such a simple straight forward approach does not appear immediately possible. The simple $V^8D^2$ law of Lighthill, (Reference 5), which gave such a good correlation between experimental results and theoretical calculations for a subsonic jet, does not appear to be directly applicable to the case of rockets. In fact, at the high exhaust velocities of present day rockets, the simple application of the law gives the meaningless result that over 100 per cent of the rocket jet propulsive power is converted into noise. The $V^8$ relationship

no longer holds, as the Mach number of the exhaust increases and tends to become a $V^3$ law as the exit Mach number becomes greater than 3. (This value corresponds to hot rocket flows at velocities near 9,000 ft/sec). Also Lighthill's basic theory of sound generation breaks down when the convection velocity of the eddies in the turbulent mixing region approaches a speed of Mach 1. The present inability to extend the theory, in its present form, to include the high speed flows of rockets means that it has become necessary to fall back upon semi-expirical methods based on experimental measurements. This has led to a variety of expressions for the total acoustic power produced, mostly based on variations of Lighthill's parameter, and each backed up by certain experimental evidence. Naturally enough, each method is sufficient for estimating the acoustic power generated from rockets similar to those used for the experimental configuration. However, when they are extrapolated to other flows they generally become inaccurate. Other methods of estimating the total noise have been suggested from empirical expressions based on the rocket propulsive power. While it is inherently obvious that the noise power must be related to the jet flow, the exact relationship will be very complicated, depending on details of the turbulent mixing process. However, it is not likely that a simple expression will predict the noise completely, since the flow of the gases from the rocket exit can be at a wide variety of temperatures, pressures, densities and velocities. An additional factor is that the exhaust gases will be different from the atmosphere into which they are mixing. Therefore, it is to be expected that any prediction method should include full allowance for all these variables.

Once the overall acoustic power has been determined, the next requirement is for a frequency analysis of this power, and the various experimentally measured spectra have been non-dimensionlised on a variety of terms. First attempts have been based on a Strouhal number relationship and a variety of velocities and dimensions have been suggested. Finally some idea of the directivity of the sound pattern produced is required. Again most suggested relationships are based on experimental results for a given group of rockets. These are for fully developed undeflected rocket exhausts. In order to estimate values for deflected or clustered rockets it is normally necessary to compare results with similar flows. The problem is not really one of estimating what the directivity pattern looks like in the far field, but is more an examination of the directivity of individual sources in the rocket exhaust itself.

This leads to the other group of prediction methods. Here the rocket exhaust is replaced by a series of sources, each radiating at a certain frequency and each positioned at a different downstream station. A directivity pattern has to be allocated to each source and the final sound pressure level at the required point is obtained by simple addition. An example of this method applied to near field noise is given by Dyer in Reference 6 and extended by Wilhold in Reference 7, to cover the case of a deflected rocket stream. Dyer is concerned with the acoustic loading on the rocket structure and he presents an empirical spectrum of noise measured on the rocket that is the average value of many experimental results. It will not be suitable for extension to flows where the rocket exhaust is greatly different from that used to obtain the spectrum. The method used in Reference 7 is different in that two measurements must be made in

order to allocate the sources down the mixing flow. Again the author was concerned with the noise field on the rocket and he suggests that the measuring points be set at each end of the rocket. An assumption must be made regarding the directional properties of the sound radiation for each frequency source, and for the deflected flow case it is assumed that all sources regardless of position, radiate equally to the point under consideration.

The technique of replacing the rocket exhaust by one source containing all frequencies is more useful for estimating far field pressure levels. An expression for the directivity is still required, as is some method of estimating the magnitude of the source. Normally one measurement is necessary to estimate the source strength and spectrum, and the directivity is assumed from other results. The location of the apparent sources can also be obtained from near field pressure measurements on the jet boundary. It will be shown in Section 3 that this method is fairly accurate at estimating the total power produced, despite complications expected due to these measurements being made in the hydrodynamic regions of the sound field.

When the rocket is moving, various additional factors must be considered in estimating the noise. First, the exact velocity and directional relationship between the source and the receiver must be calculated. This process is explained most fully by Eldred, Roberts and White (Reference 8) who show how the frequency shift and variation in total power heard depends on the geometry of the source and receiver. Secondly there is the change in the overall power produced due to the different mixing process formed. The velocity difference between the exhaust and the atmosphere will be reduced, and this effect can normally be allowed for by substituting the smaller velocity difference, instead of the rocket exhaust velocity directly into the noise prediction formula. However, it must be remembered that the motion of the rocket is usually accompanied by an increase in the mixing region volume; for example the initial region, defined by the core length, will lengthen. Once again the indications are that the complete prediction method will not be attained until a full understanding of the mixing flow and the noise generation processes are obtained.

## 2.3 Comparison of Prediction Methods with Experimental Far Field Noise Data

In a calculation of the total noise power produced by a high speed flow, the parameters necessary to describe the flow must be given and should be used as part of the calculation. Initially the single rocket will be considered, and since it is assumed that all rocket exhausts mix in a like manner, the description of the flow at the nozzle exit is sufficient. This can be given as Mach number, velocity and density of the flow, and also the nozzle diameter.

Von Gierke in Reference 9 suggests the following empirical expression to calculate the total acoustic power generated by the rocket.

$$OAPWL = 78 + 13.5 \log_{10} W_m \qquad 2.1$$

where

$W_m$ is the mechanical power of the jet stream in watts

$$W_m = 0.676\, V_e\, t \qquad 2.2$$

$t$ is the thrust in lbs.,

and $V_e$ is the gas velocity at the nozzle exit in feet/sec.

The second expression for overall power is based on a modification of Lighthill's parameter and is given by Eldred in Reference 8.

$$W_a = 5 \times 10^{-5} \cdot \left( \frac{\rho_a \, V_c^8 \, A_c}{a_a^5} \right) \cdot F(T) \qquad 2.3$$

The parameters in this expression are measured in the foot, slug and second system and the constant is such that the answers are in watts. The subscript a refers to the surrounding atmosphere and F(T) is a function of temperature.

The values of area and velocity taken are certain characteristic values. In Reference 8, it is found that the acoustic velocity in the rocket exhaust stream, which will be the fluid velocity at the nozzle throat, is the best characteristic velocity of the rocket. The area $A_c$ is based on the throat area but is equivalent to the area that would allow flow at the acoustic velocity and at the exit density. In Reference 8 it is found that this expression fits a series of measured results, both for jets and rockets, except at the highest temperature and velocity flows and so a correction factor must be added.

Equations 2.1 and 2.3, have been derived by fitting partially derived functions to measured experimental results. The basis for equation 2.3 is that Lighthill's basic parameter is typical of the noise producing mechanism, and the velocity of sound in the flow is fully representative of the flow conditions. The experiments used to determine both these expressions were concerned with large high thrust full scale rockets. They will therefore be checked out by comparing their estimated values against independent experimental results for small solid fueled rockets. Morgan, in Reference 1, measured the completed acoustic field of a small solid rocket motor, Mayes, Lanford and Hubbard, in Reference 10, and Cole, England and Powell in Reference 11, also give noise measurements for a range of small

solid fueled engines. These acoustic measurements allow the total acoustic power output to be calculated. In order that the expression of Equation 2.3 can be used, details of the flow of the fluid through the nozzle are needed, so that the conditions at the throat can be estimated. References 1 and 10 included complete information concerning the rocket exhaust and by assuming isentropic flow, the complete flow including details of the nozzle physical measurements can be obtained. Mayes et al., in Reference 10, have given more than sufficient information on the nozzle dimensions and flow parameters, allowing a check on these calculations. The throat area was calculated from the given exit conditions and found to be in agreement with the measured values. In Reference 11, the flow details were not complete enough to enable a full solution of the flow through the nozzle to be found. However, two values of the exit velocity were assumed, one certainly below and the other above the true velocity. Table II lists the calculations, which were completed using the expressions of Appendix C.

TABLE II

CALCULATION OF THE CRITICAL VELOCITIES AND DIAMETERS

| Ref. | $V_e$ ft/sec | $D_e$ ft. | $a_e$ ft/sec | $\rho_e$ lb/ft$^3$ | $p_e$ lb/in$^2$ | $\frac{R}{}$ ft lb/lb$^\circ$R | $\gamma$ | $V_t = a_*$ ft/sec | $D_t$ ft | $p_t$ lb/in$^2$ | $\rho_t$ lb/ft$^3$ |
|---|---|---|---|---|---|---|---|---|---|---|---|
| 1 | 8600 | 0.194 | 2760 | 0.0065 | 9.4 | 57.8 | 1.12 | 3370 | 0.067 | 362 | 0.165 |
| 10 | 8065 | 0.550 | 2350 | 0.0183 | 17.3 | 57* | 1.25* | 3470 | 0.147 | 958 | 0.460 |
| 11a | 11500* | 0.217 | 1690 | 0.00739 | 3.5 | 57* | 1.25* | 2650 | 0.0832 | 511 | 0.214 |
| 11b | 6850* | 0.217 | 1690 | 0.0189 | 3.8 | 57* | 1.25* | 2650 | 0.0832 | 511 | 0.332 |

Values * are estimated in order that the flow may be solved. Nozzle C of Reference 10 checked by calculating the throat diameter and comparing it with measured results. For Reference 10, only the flow throughout nozzle C was fully calculated since all the nozzles were very similar and within the same range, and also certain of the far field results were suspect. This point will be mentioned later. The total value of the acoustic power produced was then calculated from the far field results, and the flow parameters substituted into the various expressions.

The value of acoustic power obtained by assuming that 0.5 per cent of the jet stream mechanical power is converted into acoustic power was calculated for each example and the various results are shown in Figure 1. The different symbols represent the expressions used. Examination of the results shows that the first expression due to

Von Gierke, Reference 9, generally tends to underestimate the measured value of acoustic power. The expression due to Eldred et al. in Reference 3 seems to generally overestimate the answers. In actual fact, examination of the results suggests that taking 0.5 per cent of the jet stream power gives good results for the range of rockets considered. The examples taken are all for small solid rockets ranging in thrust from 400 up to 6,000 pounds.

For the second expression, the throat velocity was taken as the critical velocity, and this will be the critical speed of sound in the rocket since the pressure ratio will normally be well above critical. This value of $a_*$ will be constant for the gas flowing through the nozzle, and will have the same value at the nozzle exit. It has been suggested that this critical speed of sound may be important because it is the same as the sonic velocity downstream in the jet. This assumption is based on the heat loss being negligible. While it is agreed that conservation of heat in the exhaust stream is a fair assumption, the air that mixes into the exhaust stream radically changes its thermal properties. Thus the sonic velocity of the flow at the tip of the core bears only the minimum resemblance to the critical velocity of the exhaust gas in the nozzle. What seems more likely is that since the critical velocity is dependent on the thermal and physical properties of the fluid, it helps to describe the basic flow parameters, which in turn decide the total acoustic power produced.

The throat conditions are more typical of the flow conditions of the rocket exhaust, since the exit conditions can be considerably changed by nozzle design. Equation 2.3 suggests that the more basic properties of the flow are those that are more critical to the acoustic power generated. Figure 2 shows the suggested temperature correction.

Acoustic measurements for several large solid and liquid fueled rockets are given in References 12, 13, 14 and 15, but none gives the complete acoustic field, which would allow the total noise produced to be calculated. A major problem with large rockets is setting up a sufficient number of microphones to cover the whole sound field. However, the various measurements made in these references will allow a check of any prediction method for certain selected points.

Once a value for the total noise has been predicted, the frequency spectrum of the sound is then required. A single normalized curve, based on the flow parameters, is the most suitable way of presenting this. The frequency is non-dimensionalized as a Strouhal number, and the power in each cycle is related to the overall sound produced. The far field results of References 3,6,10 and 11 were taken and normalized in Figures 3 to 8. In Figure 3 the Strouhal number is based on the exit velocity and diameter, and the results include the generalized curve given by Cole et al. (Reference 3) for several large rockets. Although the results collapse at the higher Strouhal number, the results at low Strouhal numbers

(low frequencies) are in complete disagreement.

Figure 4 shows these results replotted on the basis of a Strouhal number formed from the sonic velocity of the exhaust gas at the nozzle exit. This velocity will be related to the actual flow velocity and the thermal properties of the gas. Also shown on this figure is the smooth curve through the experimental points of the large rockets of Reference 3 which also includes model jets. The curve through some typical turbojet results as reported in Reference 9 is also given. Again, while fair agreement is reached for the higher frequency part of the spectrum, it is the low frequency end that shows a large scatter, with the turbojet results again showing much lower values.

Figures 5,6 and 7 show the results plotted on the basis of certain throat dimensions, and a variety of velocities. These curves all show some scatter and none seems an appreciable improvement upon any other.

Figure 8 shows the results plotted against a Strouhal number given by,

$$S = \frac{f D_c a_*}{V_c a_a}$$

where f is the frequency,

$$D_c = D_t \left[ \left( \frac{2}{\gamma + 1} \right)^{\gamma/\gamma-1} \quad \frac{p_t}{p_a} \right]^{1/2} = D_t \frac{p_s \text{ throat}}{p_a}$$

$D_t$ is the throat diameter

$p_t$ is the total pressure at the throat

$p_{s\ \text{throat}}$ is the static pressure at the throat

$p_a$ is the pressure of the atmosphere into which the rocket is mixing

and $V_c$ is the critical velocity, taken as the velocity at the throat.

This normalization was suggested by Eldred in Reference 8, and the smooth curve in Figure 8 is the mean of the experimental results reported there. It is seen to give a very good collapse, especially considering that the results of Reference 8 also included rockets, turbo-jet and model results. For a rocket, where the nozzle pressure ratio will be greater than critical, $V_c = a_*$ the critical velocity at the throat. Hence the Strouhal number reduces to

$$S = \frac{f D_c}{a_a} \qquad 2.4$$

The exact reason why the speed of sound in the surrounding atmosphere should be so important is open to speculation, although the critical diameter used does contain rather more additional information than a straight dimension and so the rocket flow parameters are indirectly involved. The atmosphere also is important as is the stationary air withwhich the rocket exhaust mixes and produces noise. The curve is not concerned with total acoustic power produced, but indicates the distribution of the power in the various frequencies. Figure 8 appears to give the best collapse for all the data considered here. It will be noted that the parameters are the same as used in expression 2.3 for the total acoustic power, which tended to overestimate the total power produced by the smaller rockets. The main drawback in the use of these expressions is the necessity to calculate a special diameter based on the flow conditions.

There is another method of sound prediction where the estimates of the spectrum levels are calculated directly without a prior computation of the overall power level. This method is used by Wilhold, Guest and Jones (Reference 16), and is based on the work of Dyer (Reference 6). Basically it is assumed in the system that the rocket exhaust stream can be replaced by an array of sources each at a different frequency. The high frequency sources are located close to the nozzle exit with the low frequency sources occuring further downstream. Dyer showed that the sound pressure level at a point on the rocket structure can be represented by :

$$SPL_f = \frac{A(f)\,\beta^2(\phi f)\,G^2(kR)}{R^2} \qquad 2.5$$

Where

$A(f)$ is the source strength emmission in the direction of the structure.

$\beta^2(\phi f)$ is a term to allow for unsymmetrical flow

$G^2(kR)$ is a term to allow for near field effects

$k$ is the propagation constant $= 2\pi f/a$

and

$R$ is the distance from the source to the point under consideration.

Dyer presents a curve of the source strength function against frequency as a generalized function through measured experimental points.

The method is extended by Wilhold, Guest and Jones to obtain the far field noise produced by a large moving rocket. Whereas Dyer was only concerned with noise radiated back to exite the missile structure; Wilhold et al. present

a method to give the whole sound field. The source strength function given by Dyer includes a reduction on account of the smaller quantity of sound radiated in the forward direction but that which is given in Reference 16 is for an average sound production. Both expressions relate the acoustic power directly to the jet stream mechanical power. For high speed rocket flows, it has been measured that the acoustic efficiency, (the rate of conversion of mechanical to acoustic power) falls off from being proportional to $V^5$ for low subsonic jets, to a constant value of approximately 0.5 per cent for rocket flows at exit Mach numbers greater than 3. Dyer explains this effect as being due to the sound power increasing with the exhaust velocity, to become an appreciable fraction of the turbulent power, and any further increase in sound power then tends to damp the turbulence. He suggests that a form of equilibrium would exist between the sound power and the turbulent flow. Lighthill (Reference 17), however, disagrees with this idea, and he suggests that the acoustic power formed is so small compared to the viscous power dissapated in the turbulent flow that it is extremely unlikely to have any effect on the basic turbulent flow. He suggests that the apparent reduction in the rate of rise of acoustic efficiency is due in some part to the reduced turbulence at the high Mach numbers and also due to the directional pattern of the sound emmission caused by the convection of the sound sources in the turbulent exhaust. The turbulent reduction is due to aerodynamic viscous forces rather than acoustic loading, and is not sufficient to account for the decrease in acoustic radiation efficiency rise alone. Settlement of these arguments will have to wait until a more detailed experimental analysis of rocket flow is available, which in turn depends on development of the necessary instrumentation.

A description of the directivity of the noise radiation is required, once the overall value and the spectrum of the acoustic power output has been determined. If the far field position under consideration is sufficiently distant from the rocket exhaust, then the sound can be regarded as originating from a point source. The Average Sound Pressure Level in a given frequency band is calculated on the basis of uniform radiation from a point near the nozzle exit, and then the Directivity Index is applied to allow for the unequal radiation with angle. Five sets of results, from References 1,3,10,11 and 12 have been compared, (only two of the nozzles in Reference 10 being taken because of certain disparities appearing when the results were plotted out). Certain of the Directivity Functions given by Wilhold, Guest and Jones (Reference 16) have been converted to Directivity Indices by integrating the functions to zero power over the surface of a sphere and these are also plotted. In order to estimate the Average Sound Pressure Level from some of the References, the results had to be extrapolated to large angles near $180^{\circ}$, back along the rocket. (In the Figures presented here, the rocket exhaust flow is always taken in the zero angle direction.) For each set of results considered, the Average Sound Pressure Level was first calculated, with an allowance for atmospheric attenuation when necessary. Then the Directivity Indices were determined by subtraction of this Average Sound Power Level from the measured results. The

frequency bands differed slightly in the various references, but the results were interpolated and a consistent set of seven octave bands were considered. Figure 9 presents a plot of the Directivity Indices for the overall sound pressure levels. Only nozzles C and F of Reference 10 are included since all the nozzles in this Reference gave much different results from the others. The results from Reference 3, which are for solid fuel rockets of 100,000 and over pounds of thrust agree very well with the results of References 1 and 11, which are for much smaller rockets. Figures 10 through 16 present the calculated Directivity Indices for the octave bands.

An examination of the results of Reference 10 shows certain inconsistencies. These results are for a series of small solid rockets, approximately 6000 pounds thrust, except for nozzle F whose measured thrust was near 1,000 pounds. The results show three peaks of sound pressure level within the half circle, from the 0 to 180°, which is very different from the single peak given by the other results. A two peak curve with a smaller peak in the 90 - 180 degree quadrant would be acceptable, and certain results, notably those of Cole et al. (Reference 11) show a trend towards the two peak curve at low frequencies. It is suggested then that the results of Reference 10 are not really suitable to be included in this analysis and the overall indication is that they are not too reliable.

At the lower frequencies, all the results agree well in the quadrant except for the curve obtained in Reference 3 for the very large rockets. As the frequency increases, better agreement is found in the forward quadrant, and, except for the results of Reference 10, better agreement also occurs in the rear quadrant. The results of Reference 3 are very similar at all frequencies and do not show the great change measured on the smaller rockets. However, the agreement of the overall results is most encouraging. Some difficulty in estimating the exact Sound Pressure Level at small angles leads to the difference in the curves shown in Figure 9. The values for the small angles reported by Morgan (Reference 1) show larger values, but this is probably due to the fact that these measurements were made at a small radius with the microphone near to the mixing stream and so the results cannot be considered as originating from a single source near the nozzle exit. The microphone would be nearer the low frequency sources far downstream and so would indicate a larger sound pressure level. This effect only becomes negligible if the far field measurements are taken at a great distance from the rocket.

The disparity between the results of the larger and the smaller rockets leads to the question of scale effect and also the effect of exhaust velocity must be considered. The differences between the sound fields of the rocket and the slower turbojet engine have been well documented; the angle of peak sound radiation increases with exhaust velocity. Also since the frequency distribution of the sound sources in the exhaust stream will be directly related to the size of the

rocket, it seems logical to attempt to compare the results on a Strouhal Number Basis. Figure 17 shows the directivity curves, where the Strouhal Number is similar for all nozzles, and based on the center frequency of the octave band. The velocity and diameter at the exit are used, and since all the rockets have similar exit velocities, the scaling is thus based directly on exit diameter. Figure 18 shows another set at a smaller Strouhal Number and the values for a jet engine (Reference 9) have been added. Directivity curves are normally given simply on the basis of frequency alone, as in References 3 and 16, and it must be questioned as to whether this is justified.

Consider two rockets, as in Figure 19, which have equal exhaust velocities but different diameters. Similar frequency sources will exist at approximately equal distances downstream in the core region and at similar conditions; for example, consider the sources at frequencies $f_1$ and $f_2$. Since the mixing region width will be the same here and the maximum velocities equal, the shear of velocity gradient will be similar. However, if the sources are compared at frequency $f_3$, the source for the smaller rocket will be downstream of the core and that for the larger rocket will still be in the core region. The maximum velocities at the two downstream stations will be unequal and hence the velocity gradients will also be different for the two sources. Now the directivity of the radiated sound depends upon the rate of convection of the source in the turbulence and the refraction through the mixing region. Therefore, it is to be expected that different results will be obtained for different sized rockets. Since a velocity effect also exists it would seem more logical to present the directivity curves on some sort of non-dimensional basis rather than a direct frequency basis. A complete description of the directivity effect is needed, for each source at each frequency and at each position in the exhaust. Such a system was developed for the jet in Reference 18, but the approach relied on correlation measurements made near the exhaust stream. Such experimental results are yet unavailable for a rocket flow.

Other far field noise measurements have been reported by Cole et al. (Reference 19), who made a complete study of the noise measured at ground stations during the launching of various missiles. References 13 and 14 contain some measurements made in the far field during the static firing of a large solid propellant rocket, but these are necessarily limited to a plane at $90^{\circ}$ to the rocket exhaust direction.

The results obtained were used, with generalized prediction methods, to calculate the overall power produced and the 1/3 octave band spectrum, and the answers varied over some 10 db. through most of the frequency range. Attempts were made to fit the curve of sound power produced by the small model rocket of Reference 11, to the predicted results by direct scaling. Some fair agreement was obtained between the mean results for the large rockets tested, but the scaled values of

Reference 11 did not agree well at the higher frequencies. Once again some method to account fully for the scale effect is called for. For the large rockets, the overall acoustic power produced was calculated to range from 1/2 per cent of the jet stream mechanical power in Reference 13 to 1/4 per cent of the jet stream power in Reference 14. This was for almost identical rockets and using identical methods, and shows the variation that can be expected using one simple method alone.

## 3.0 NEAR FIELD NOISE

Near field acoustic measurements have been reported for rockets ranging from Saturn (Reference 20) to 400 pound thrust solid fuel rocket motors (Reference 1). The near field may be defined as that region where hydrodynamic effects in addition to acoustic disturbances are possible. Measurements have been made at a series of selected points on rocket structures and also along side of the exhaust stream. However, they are not generally complete in describing the noise field of the rocket since most workers have been more concerned with the noise environment of the rocket itself.

### 3.1 The Directivity Function

The total sound power generated by a rocket exhaust, must pass through a closed boundary containing the rocket exhaust. Therefore, in order to obtain details of the total noise generated, it is necessary to measure results over a complete surface. Figure 20 shows typical near field measurements obtained of the noise fields of a rocket and a jet engine, and indicates the main differences that are observed between them. For the rocket, the sound appears to propagate at a greater angle to the exhaust flow, and secondly, the apparent source of sound is located much further downstream. Contours, such as shown in Figure 20, are useful in that, as well as giving the immediate near field, they also show the main direction of sound radiation. However, series of measurements taken on a line at ten degrees to and just outside of the rocket exhaust prove particularly useful. The total sound power generated by the exhaust passes through this boundary and can be calculated from these measurements. This method is interesting in that the individual measurements made on the ten degree boundary must be mostly concerned with the sound generated in the nearby flow. Because the measuring points are very close to the flow, and can be within one wavelength of the sound at the lower frequencies, certain inaccuracies are to be expected. These are due to the near field effect, the result of interference of the individual sources of noise generation. However, it can be shown that this effect is very slight and can normally be neglected. For example, Morgan in Reference 1,gives far field sound pressure measurements and also the $10^{\circ}$ boundary near field measurements of the noise field of a small solid fueled rocket. The total radiated acoustic power can be calculated from both sets of readings and the results are shown in Figure 21 as the octave band spectrum. It is seen that there is good agreement between the results calculated by the two methods. In order to use the near field results, the $10^{\circ}$ boundary measurements are plotted in each octave band and the source is considered as acting only in that region where the near field sound pressure levels are within 3 db of the maximum value. The relevant boundary area is calculated for each octave band and the total sound power radiated is calculated by use of a directionality factor. The values used here are based on the values given in Figure 30 of Reference 18. The main difference between the two calculated acoustic power spectra is that the near field spectrum peaks at a higher frequency than that for the far field measurements. This means that the

higher frequency sources may be allocated too far down stream and should be moved nearer the nozzle. However, it could also indicate that the low frequency sources should be placed further downstream. The overall values agree to within 0.5 db., which is remarkable considering the difference to be expected due to the near field effect. This might be expected to cause a large disparity, especially with the low frequency results, since the wavelength is greater here. It is therefore concluded that the near field effect can generally be disregarded and also that the directivity curve used in this method must also be reasonably accurate.

This directionality function is shown in Figure 22, where the line is the mean of the results from Figure 30 of Reference 18. Certain values of the Directivity curve were estimated from the results of near field measurements of rockets in Reference 10 and for high speed air jets in Reference 21. It will be seen that the rocket results fall in with the trend of the jet results although slightly larger angles of sound propagation are suggested. Unfortunately, the results are limited to the smaller Strouhal Numbers since full sets of near field measurements are not available from large rockets, although experience with larger rockets indicates that the maximum noise radiation angle to be expected is of the order of 65-70 degrees. (Reference 19). The degree of agreement reached in the above example suggests that this function is sufficiently accurate to be used also in rocket noise estimation. The available results for rockets and high speed flows are at present rather limited and so no real justification can be taken for changing the shape of the curve much from that derived for jets.

## 3.2 Source Distribution

Analysis of the jet engine near field results has shown that the sources can be considered as being distributed in the exhaust near the nozzle exit. However, when the near field results of rockets are analyzed in a similar manner, the sources appear to be distributed further downstream in the exhaust flow. Lighthill, in Reference 17, explains that this is a direct consequence of the constant efficiency of noise production of the rocket exhaust. The turbulent flow will generate noise at a similar efficiency right down to the slow speed region, well beyond the end of the core. Of course, it is recognized that an array of simple sources is only an approximate representation, and in fact, sources of all frequencies will occur at each position in the flow. However, it is interesting to compare the suggested source locations given by several experimenters. Figure 23 shows the source location based on the near field measurements given for several rockets and high speed air jets. The results show general agreement for the rockets, but the values for the Mach 3 air jets of Reference 21 show considerable discrepancies. The near field results used to obtain these values are not given in the reference and so a more detailed analysis of this difference is not possible. It is perhaps more logical to plot these source locations on a non-

dimensional basis and in Figure 24 they are plotted against core length, using the theoretical expression based on Mach number given in Reference 18. This does bring the jet results more into the range of the rocket results, however, they still show completely different trends and indicate that a different mixing process takes place.

It is proposed to discuss the near field rocket results as showing sources containing all frequencies at all stations. It is then necessary to use a directivity function with these sources and it is proposed to use the function given in Figure 22.

## 3.3 The Normalized Source Spectrum

For those rockets and high speed air jets whose complete $10^{o}$ boundary near field results were measured, (References 1, 10 and 21), the total acoustic power generated by various segments of the exhaust stream was calculated. It was necessary in certain cases to interpolate the given near field sound pressure levels so that a complete set of seven octave band measurements was available for each case. For Reference 10 the results were given up to 2500 cps and so only this limited part of the spectrum could be used. The exhaust stream was divided into segments and a constant value of pressure level assumed for each part. Then the total sound generated by each segment in each octave band was calculated from the area of the segment, the mean pressure level and the mean radiation angle as given in Figure 22. Figure 25 presents the generalized spectral density values of the power generated, the results being normalized on the distance from the nozzle to the center of each segment and the exit Mach number. For the higher frequency results the values collapse well into a single generalized curve, but some scatter is recorded for the low Strouhal number results. These values at which scatter occurs are the low frequency results for the segments near to the nozzle exit. It was at these points, that the results were less well documented, and so some disagreement may be expected here. Also shown is the curve for the near field acoustic measurements reported for the J57 engine, in Reference 18, although these are limited to points alongside the initial core region. This line and the general expressions given in Reference 18 fall well across the values calculated here, except at the low Strouhal numbers. It will be noticed that the normalizing function involves the Mach number at the nozzle exit of the rocket stream. In section 2.3 it is suggested that the Mach number at the nozzle throat is a better normalizing parameter and it is shown to be useful in predicting the spectrum and the total noise produced. Therefore the results are replotted in Figure 26 on the basis of a Strouhal number that includes the Mach number of the nozzle throat flow. For supersonic rocket flows, this quantity disappears, leaving a Strouhal number containing the speed of sound in the surrounding atmosphere. While all the rocket results seem to show the same degree of collapse, the curve for the jet engine is moved significantly away from the rocket results. The

reason is most likely due to the fact that the Mach number of the exit flow is important in determining the core dimensions of the flow, and that a typical frequency in the flow is proportional to the width of the mixing region. This result suggests that the width of the mixing region is related to the distance downstream through the exit Mach number. Therefore, although the nozzle throat conditions are important in determining the total sound power produced by the flow, the nozzle exit conditions are more critical in describing the spectrum of sound produced at a given downstream distance.

In Figure 27 the results are normalized on the basis of the momentum width parameter b as defined in Reference 18. This parameter is typical of the width of the mixing region, and was calculated on the basis of the constant density jet equation described in Reference 18. Here, the collapse of the results is as good as in Figure 25, but some better collapse might have been expected, since the rate of growth of the b parameter does not depend linearly on distance downstream. The theory allows the b parameter to grow at a different rate for the initial core region from that for the downstream flow and this should give a better collapse since the frequency will be directly related to the width of the mixing flow. The typical frequency, proportional to $V/b$, would therefore be expected to be more accurate than one proportional to $V/x$. However, the collapse is no better than that in Figure 25 and this is no doubt due to the difference between the details of the hot variable density flow and the constant density flow of the theory used to obtain a value of the width parameter.

In order that this normalized spectrum can be used to predict the actual power of the acoustic energy generated by a rocket exhaust flow, it is necessary to know the overall power produced by each segment of the exhaust. The values calculated for the two rockets and the two air jets referred to here, are given in Figure 28, as power per unit radius length compared to the overall value against the calculated core length downstream. This figure shows some disagreement with expected results, since the values calculated for the Boeing rocket (Reference 1), which has the highest exit flow Mach number, indicate that most of the sound is generated from a region nearer the nozzle exit than do the other results. For the rocket of Reference 10 and the high speed air jets of Reference 11 the maximum sound producing region occurs at about two core lengths downstream of the nozzle exit. Figure 29 shows typical sound pressure levels, measured in the indicated octave bands, for the four flows. These results are the values measured along the $10^{\circ}$ boundary and are plotted against the calculated core length. The maximum sound pressure levels occur at similar regions to those calculated for maximum sound power, as would be expected. The results for the Boeing nozzle are the most complete, but they disagree with the other three sets and also to some extent with the expected results. As explained by Lighthill (Reference 17) it would be expected that a long length of the mixing region should radiate sound at almost equal power.

The results for the nozzle F in Reference 10, shown in Figure 28, are typical of what might be expected. The disagreement obviously calls for a more careful set of near field measurements, which should include complete frequency coverage at many points along the $10^{o}$ boundary. Also directional correlation measurement should be performed at selected points so that details of the sound radiation pattern can be obtained.

## 3.4 Far Field Sound predicted from Near Field Measurements

The results used in obtaining the normalized spectrum of sound power generated per unit length of the rocket stream are based completely on the measured near field values of sound pressure level. In this example the sound level in the far field at a selected point is estimated from these near field results. This is then compared to the measured results.

Starting with the near field results given for the Boeing rocket in Reference 1, the rocket exhaust was divided up into 5 segments each 20 nozzle exit radii long. The total power generated per segment was deduced using the near field sound pressure levels with the Directionality curve of Figure 22. These values were then taken with the mean curve of the results in Figure 25, shown in Figure 30, to obtain the acoustic power output in each octave band for each segment. The point under consideration was chosen as the 60 degree point at 100 nozzle diameters from the exit. The distance from the center of each segment to this point was then computed and the average sound pressure level due to each octave band in each segment was calculated. In order to apply the Directionality Ratio to the average sound pressure level the results given in Reference 18 for the jet engine were taken. This figure is redrawn here as Figure 31. The value of the factor $fx/a_a$ was calculated for each term so that the Directivity Ratio could be obtained. The values of sound pressure level were then obtained and the results added in the various octave bands. These values were then converted to spectral density values by dividing them by the respective band widths and the results are shown in Figure 32, where the measured value in the far field is also shown. The agreement is fair and within 2 db. over most of the range. The maximum error is at the lower frequencies, and also the calculated spectrum does not show such a sharp peak. It is also at the small Strouhal numbers that the normalized source spectrum curve shows the greatest scatter. With more careful measurements at these low frequencies it should be possible to obtain a more consistent set of results and to find better agreement between predicted and measured results.

The second example is taken for the other extreme in rocket motor size and involves an estimate of the sound pressure level for a rocket engine typical

of that used on the Saturn 1 vehicle. From the listed parameters of the rocket (Reference 20) the total noise produced by eight such rockets calculates as 205.7 db. relative to $10^{-13}$ watts, taking the acoustic power as 0.5 percent of the jet stream mechanical power. The sound pressure level was estimated at a point 4.5 kms from the launch point for a vehicle vertically above the launching area, and at a time of 60 seconds from the vehicle lift off. The power produced by the rocket was divided up into various segments, in accordance to a mean line drawn through the results of Figure 28. This mean line is shown in Figure 33 and applies only to rockets whose exit Mach number is in the range 2.5 to 3.2. Then using the normalized spectrum of Figure 30, the power in the various octave bands for each segment was calculated. This is based on the assumption of no mixing of the eight individual nozzles, the combination of the exhaust flows will effect the results, and some indication of the way this alters the noise produced will be seen here. The method of calculating the flow from a cluster is given in Chapter 4.

The various Directivity Indices were calculated from Figure 31 and allowance was also made for atmospheric attenuation. The sound pressure level was calculated as before and the spectural density found. This is plotted in Figure 34. It is compared with the sound pressure level recorded at a similar point during the launch of the Saturn SA3 Vehicle, Reference 24. It is seen that the predicted values agree well with those measured, except at the lower frequencies. The measured spectrum also shows the two peaked curve which is expected from a cluster of rockets as shown in Chapter 4. Otherwise the spectrum shows the same general shape.

Another example was performed, the measuring point being taken as 1.5 Kilometers from the launch point. The example was calculated as before and the sound pressure level spectral density graph obtained when the missile was 29 seconds from lift off. The calculated result is shown in Figure 35 and compared to the value measured at a similar station for the launch of the Saturn SA4, Reference 25. The measured curve shows the classical two peaked spectrum for clustered rockets as predicted in Chapter 4. The calculated value shows a single peaked curve, since no interference of the individual rocket flows was allowed for. The results generally fall into the same regions and the comparison of the calculated and the measured values is exactly as would be expected. The center frequency range levels are reduced at the expense of increases at both low and high frequencies.

The example on the Saturn rocket was further extended to calculate the sound pressure level at a point back on the missile. The angle of propagation for use in Figure 31 was taken as $170^{\circ}$, and the sound pressure level spectral density was calculated exactly as before. The results are shown in Figure 36, and the calculated value was found to be some 8 db. less than the measured value, although it must be remembered that the measured value was

made with the rocket exhaust flow deflected. A further calculation was made for the flow deflected at 90° and this agrees better with the measured values. Also shown is the calculated sound pressure level spectral density curve calculated previously and shown in Figure 35. It is reproduced here to show the difference in the spectrum shape given by the prediction method for these two different observation positions. This far field result shows a spectrum shape with much greater fall-off at the high frequencies. In Figure 37, the similar results are plotted as measured for the Boeing nozzle quoted by Morgan, Reference 1. These results show exactly a similar spectrum change for the noise field produced by this small solid fueled rocket motor. The spectrum shape for the position forward, alongside the rocket case, is much shallower compared to the spectrum for the far field position. The greater value for the far field results in this case is due to the measuring point being much closer to the angle of predominant noise propagation.

Further examples of the prediction method applied to deflected and clustered rocket exhaust flows are given in the next two chapters.

# 4.0 FLOW AND NOISE OF ROCKET CLUSTERS

## 4.1 Introduction

Prediction methods to estimate the noise produced by rocket clusters are normally based on the method for the single nozzle, and the effect of clusters of rockets is estimated simply by adding the results for the individual rockets. However, if the nozzles are set close together, the exhaust flows will combine into one large stream and the resultant noise field generated will be different from that estimated by summing the noise fields of single nozzles.

This section is concerned with producing a simple method of estimating the exhaust flow of a cluster of rocket engines, so that this flow pattern can be used to determine the noise generated. The method is based on calculating the combined flow at some distance downstream from the nozzle exits, and then finding the single nozzle conditions that would also create this downstream flow. The prediction methods of sound generation for single nozzles are then applied to this flow pattern. First they are applied to the equivalent nozzle to produce the combined downstream flow, and secondly to the individual rocket exhausts up to the position of the combined flow. Since the noise producing regions of a rocket flow can extend far downstream, the distribution of the sources in the rocket flow is important. The clustered rocket streams are assumed to generate noise fields individually as far as a combined flow position, while farther downstream the noise produced is not considered to be a sum of that from separate streams but is assumed to be produced by a combined rocket flow.

This method is a direct extension of that used by Eldred, et al. in Reference 18 for the flow of turbojet engines. However, in this case, the process of solving the flow pattern is complicated on two accounts. The first is that the flow can no longer be treated as a constant density flow, since the density and temperature variations will become much more critical. Secondly, the gas exhausting from the rocket nozzle will be much different from that of the surrounding atmosphere into which it is mixing, and its basic thermal properties will be different from air. These complications make the solution of the hot rocket flow very complicated. In order to obtain a solution certain assumptions have to be made, and certain points depend on the results obtained for a constant density jet in Reference 18.

Until more detailed experimental evidence is available concerning hot flows and measurements of the variables, velocity, pressure, density and temperature of the rocket exhaust, are available, the assumptions are best made on the solution developed for the constant density axisymmetric jet. This, at least will mean that the results will have some consistency and all that then may be necessary is to add a simple scaling factor to give the exact results. In fact the results obtained have shown that no such factor is necessary and this would tend to confirm that the assumptions made are accurate within the limitations given. The initial analysis is limited to the case of stationary rockets; i.e. the atmosphere into which the rocket flow is mixing, has no velocity and the resultant flow is not deflected or disturbed in any way.

## 4.2 Velocity Profile Data

It has been shown by Eldred, et al. (Reference 18) that the velocity profile in a jet can be represented by an exponential expression of the type

$$u = U e^{\frac{-\eta^2}{2}} \qquad 4.1$$

where $\eta = \frac{r - a}{b}$

U is the maximum velocity at the downstream station considered,
r is the distance from the center line to the point considered
a is the distance from the center line to the outer boundary of the core
and b is a momentum width parameter which is defined so that the momentum at any station is given by $U\pi(a + b)^2$. (Integration of the velocity expression will show that this result holds.) In the downstream region where no core exits, $a = o$ and $\eta = r/b$. This profile has been matched to measured results by Laurence (Reference 26) and shown to be a good fit for subsonic jets. This profile is chosen instead of the cosine profile preferred by Squire and Trouncer (Reference 27) since it enables the solution of the jet flow equation to be solved more readily and the results extended to concentric and more complicated flows.

A necessary assumption, owing to the lack of experimental data, is that this profile can be applied directly to rocket flows. Since a similar flow process is formed, with a highly sheared mixing region exchanging the momentum of the exhaust gas with the ambient air, it is not unreasonable. On simple aerodynamic considerations, an asymmptotic profile must occur and so the expression of equation 4.1 is considered completely applicable.

The derivation of the solution of the flow for a constant density axisymmetric jet in Reference 18 shows that the momentum width distance b is the thickness of the mixing region from the inner edge of the core to the 0.61 value of the maximum velocity at each station. When no core exists, it is measured from the center line which is the point of maximum velocity. The solution of the jet flow shows that downstream of the core the value of b grows linearly with distance downstream, and that up to the core tip it also approximates to a linear growth. The relationships are derived in terms of the distance to the core tip and this distance can be obtained by the empirically derived expression,

$$\frac{x_t}{R} = 6.9 (1 + 0.38M)^2 \qquad 4.2$$

where $x_t$ is the distance to the core tip from the nozzle exit

R is the exit radius of the nozzle

and M is the Mach number of the jet at the exit.

This expression is matched with experimental results for model jets, turbo-jets, and rockets in Reference 18 and has been shown to be consistant at exit Mach numbers up to 3.5.

The expressions for b are:

$$0 < x < x_t \qquad b = R\frac{x}{x_t} \qquad 4.3$$

$$x_t < x \qquad b = 0.5R(1 + x/x_t) \qquad 4.4$$

where x is the distance downstream from the nozzle exit.

Equations 4.2, 4.3, and 4.4 have all been derived for a constant density jet, however, these results are applied directly to the rocket flow and the effect of the density variation is assumed slight. Experimental measurements of the overall dimensions of the flow have indicated that the critical parameter in estimating the core length is the Mach number of the exit flow and that temperature and density variations only cause small effects. The width of the mixing region, defined by b, is seen to be similar for both the cases of a hot and a cold jet, when scaled on the core length.

## 4.3 Mixing Flows

Consider the case of a multi-exhaust nozzle which is composed of n peripheral circular nozzles. (This analysis is similar to that of Reference 18, but here density and temperature variation have been taken into account.) A sketch of the theoretical model is given in Figure 38, which shows the square velocity profiles at the individual nozzle exits, and the combined velocity profile formed at the downstream position.

R is the nozzle exit radius

U is the maximum velocity at each station

and a and b are the velocity profile parameters, as previously defined.

Subscript 1 refers to the flow of the individual rocket nozzles at the exit plane

2 refers to flow of the total set of the individual nozzles at the exit plane

3 refers to flow from the single equivalent nozzle, equal in exit area and conditions to the n individual nozzles

4 refers to flow from the equivalent jet at the position downstream where the individual rocket flows have mixed to form the combined flow

5 refers to the apparent exit conditions of a single rocket necessary to form the combined flow at position 4

6 refers to the flow of the individual jets at some downstream station, and up to the core tip, $U_6 = U_1$ (Position 6 will be moved downstream as required)

Now the total exit momentum at the nozzle exit is $n \rho_1 U_1^2 \pi R_1^2$. The individual flows then combine to produce the flow at position 4, and the change in momentum is equivalent to the pressure field applied to the rocket. This assumes that all the external atmospheric air is drawn into the flow radially. Then the momentum equation in the axial direction of the flow can be written, assuming that the pressure acting on the outer edge of the rocket mixing flow is $p_a$, the atmospheric pressure:

$$(a_4 + b_4)^2 \pi \rho_4 U_4^2 - n\pi R_1^2 \rho_1 U_1^2 = n\pi R_1^2 p_1 - \pi R_4^2 p_4 + (\pi R_4^2 - n\pi R_1^2) p_a \qquad 4.5$$

where $R_4$ is the radius of the total mixing region at station 4.

In order that equation 4.5 may be made more manageable, and also as a necessary assumption so that the flow may be solved, the static pressure at station 4 will be taken as equal to that of the atmosphere. Since station 4 is positioned at a distance at least equal to the core length downstream of the nozzle exit, this is not an unfair assumption. Also throughout that part of the flight of the rocket in the atmosphere where the rocket exhaust acoustic excitation will occur, the exhaust pressure of the rocket will not be greatly different from the atmosphere pressure.

Then,

$$(a_4 + b_4)^2 \rho_4 U_4^2 - n \rho_1 R_1^2 U_1^2 = (p_1 - p_a) n R_1^2 \qquad 4.6$$

It is now assumed that the outer edges of the individual jets will mix as for the case of a single rocket with no interference, and the velocity on the center line of the individual jets will reduce after the core and eventually equal $U_4$ at the combined jet flow. Then the change in momentum for a single jet is given by

$$\rho_6 b_6^2 U_6^2 - \rho_1 U_1^2 R_1^2 = p_1 R_1^2 - p_6 R_6^2 + p_a (R_6^2 - R_1^2) \qquad 4.7$$

where $U_6$ is the maximum velocity on the center line of the individual jet.

Now by matching the individual jets to the combined flow,

$$b_6 = b_4 \ , \ U_6 = U_4 \ ,$$

$$\rho_6 = \rho_4 \ , \ P_6 = P_4 = P_a$$

On substitution, equation 4.7 becomes

$$\rho_4 b_4^2 U_4^2 - \rho_1 U_1^2 R_1^2 = (p_1 - p_a) R_1^2 \qquad 4.8$$

Solving equations 4.6 and 4.8 gives

$$b_4 = \frac{a_4}{n^{1/2} - 1} \qquad 4.9$$

$$U_4^2 = \frac{R_1^2}{\rho_4 b_4^2} \left[ \rho_1 U_1^2 + (p_1 - p_a) \right] \qquad 4.10$$

At the nozzle exits, the distance of the center line of the individual peripheral rockets from the center line of the cluster is $R_2 - R_1$. By matching the flow, of the nozzles to the combined flow at position 4, it is assumed that the width of the core of the downstream combined flow is also this dimension,

$$a_4 = R_2 - R_1$$

and hence

$$b_4 = \frac{R_2 - R_1}{n^{1/2} - 1} \qquad 4.11$$

$$U_4 = \frac{R_1 (n^{1/2} - 1)}{R_2 - R_1} \left[ \frac{\rho_1 U_1^2 + (p_1 - p_a)}{\rho_4} \right]^{1/2} \qquad 4.12$$

$$a_4 + b_4 = R_5 = (R_2 - R_1)\left(\frac{n^{1/2}}{n^{1/2}-1}\right) \qquad 4.13$$

where $R_5$ is the equivalent exit radius necessary to produce the combined flow at station 4, as if it occured from a single nozzle.

It will be noted from Reference 18 that equations 4.11 and 4.13 are identical expressions to those derived for a constant density jet. This is to be expected since the approach used here assumes that a similar velocity profile relationship occurs for both the hot and the cold flows.

The above method is not sufficient to give the solution for the flow conditions, since insufficient data is available. The value of density of the flow must be known before the velocity can be calculated; however the distance downstream to the combined flow station 4 can be obtained by use of the constant density jet relationships for the b parameter and equations 4.2, 4.3, 4.4 and 4.11.

## 4.4 Mean Velocity and Temperature at the Downstream Position

In order to solve the flow it is necessary to introduce another relationship, and the equation chosen is the conservation of heat. It becomes apparent that this further complicates matters on account of the rocket exhaust flow having different thermal properties to the atmosphere into which it is mixing, and this introduces additional equations, so the whole process becomes very complicated. An exact solution cannot be obtained and it is necessary to assume the value of one unknown in order to obtain a solution.

The previous work has indicated that the momentum radius of the combined downstream flow is approximately $a_4 + b_4$. This can represent the flow leaving an equivalent single nozzle of radius $R_5 = a_4 + b_4$. This value of $R_5$ can be determined from the geometry of the nozzles by the use of equation 4.13. Then the exit area of the downstream flow is:

$$A_5 = \pi(a_4 + b_4)^2$$

$$A_5 = \frac{n\pi(R_2 - R_1)^2}{(n^{1/2}-1)^2} \qquad 4.14$$

The flow at position 5 will be related to the nozzle exit flow, by the equations of continuity, momentum and heat conservation. In effect, the flow at station 4

is replaced by a constant velocity flow at 5 and this is equated to the exit flows. The exit conditions of the rocket nozzles will be indicated by the suffix 3, which represents a single nozzle that is equivalent in total exit area to the cluster. The exit area of the rocket is the sum of the individual exit areas of the cluster.

Thus

$$A_3 = n\pi R_1^2 \qquad 4.15$$

From the continuity of mass flow, the mass flow at 5 equals the mass flow at 3 plus the inflow from the atmosphere. Thus

$$\dot{m}_5 = \dot{m}_a + \dot{m}_3 \qquad 4.16$$

where suffix a refers to the surrounding atmosphere into which the rocket stream is mixing.
Conservation of heat gives

$$C_5\dot{m}_5\bar{T}_5 = C_3\dot{m}_3\bar{T}_3 + C_a\dot{m}_a\bar{T}_a \qquad 4.17$$

where C is the coefficient of specific heat at constant pressure, and $\bar{T}$ is the total temperature.

With static temperatures equation 4.17 becomes

$$\dot{m}_5\left(C_5T_5 + \frac{U_5^2}{2gJ}\right) = \dot{m}_3\left(C_3T_3 + \frac{U_3^2}{2gJ}\right) + \dot{m}_aC_aT_a \qquad 4.18$$

where g is the gravitational constant and J is the mechanical equivalent of heat.

Substituting for $\dot{m}_a$ from equation 4.16, and putting $\dot{m} = \rho AU$

$$\rho_5U_5A_5\left(C_5T_5 + \frac{U_5^2}{2gJ} - T_aC_a\right) = \rho_3U_3A_3\left(C_3T_3 + \frac{U_3^2}{2gJ} - T_aC_a\right) \qquad 4.19$$

The momentum equation is the same as before, and again includes the assumption of air drawn in radially.

$$\rho_5 U_5^2 A_5 - \rho_3 U_3^2 A_3 = A_3 (p_3 - p_5) \qquad 4.20$$

The value of the coefficient of specific heat at station 5 is given by comparison of the mass flows.

$$C_5 = C_a + (C_3 - C_a) \rho_3 U_3 A_3 / \rho_5 U_5 A_5 \qquad 4.21$$

The gas constant for the exhaust fluid at station 5 can be determined from the value of the average molecular weight there.

$$m_5 = m_a + (m_3 - m_a) \rho_3 U_3 A_3 / \rho_5 U_5 A_5 \qquad 4.22$$

and

$$\underline{R}_5 = \underline{R}_u / m_5 \qquad 4.23$$

where $\underline{R}_u$ is the Universal Gas Constant.

Then the gas equation at station 5 gives

$$p_5 = \frac{g \rho_5 \underline{R}_u T_5}{m_a + (m_3 - m_a) \rho_3 U_3 A_3 / \rho_5 U_5 A_5} \qquad 4.24$$

The value of $A_5$ is obtained from equation 4.14 and the value of $p_5$ is assumed to be atmospheric as before. This gives four unknowns, $\rho_5$, $U_5$, $C_5$ and $T_5$, and four equations, 4.19, 4.20, 4.21, and 4.24 involving these unknowns. Hence the flow is soluble.

In order to apply these equations directly to the case of clustered nozzles, the two areas $A_5$ and $A_3$ must be estimated. $A_5$ is given by equation 4.14 and $A_3$ is taken equal to the exit areas of all the nozzles in the cluster. Then the conditions of the imaginary nozzle exit at 5 can be calculated. The downstream

flow, is considered to be one large rocket stream, and the flow up to this combined flow position is considered to be composed of the individual rocket flows. The distance downstream to station 4 is obtained by comparison of the b parameter for the combined flow and the individual rocket flows.

In order to estimate the acoustic power produced by such a cluster or rockets, the sound field is calculated for the two separate portions. For the initial portion, allowance is made for the fact that only the sound produced by the outer mixing portions of the individual rockets is heard; the noise generated by the internal mixing regions is assumed lost and also only that length of the rocket flow up to the combined flow station 4 is considered. This is especially important for high Mach number rockets, since considerable sound power can be generated by the flow far downstream from the nozzle exit. The noise produced by the fully mixed downstream flow is computed, on the basis of a single rocket flow at the exit conditions at station 5, and except for the case of rocket nozzles which are clustered very close together, the flow in this region is sufficiently slow so that the simpler expressions for turbojet noise may be used.

The total noise produced by the cluster is then obtained by summing these two noise fields together, and the small extra effect due to the downstream jet between the assumed exit plane and the calculated downstream mixed position i.e. between points 5 and 4, is neglected. This high frequency noise which is neglected may be considered to be swamped by the high frequency sound produced by the individual rockets upstream.

## 4.5 Solution of the Flow Equations

By substitution and elimination, the six equations 4.19, 4.20, 4.21, 4.22, 4.23, and 4.24 can be reduced to give the velocity at station 5. The value of the cross-sectional area at 5 is calculated from equation 4.14, and expressed as $a$ , which equals $A_5 / A_3$. Then the velocity ratio $\theta$ equals $U_5 / U_3$ is given by

$$\theta^4 a \; K_2 (C_3 - C_a)(m_3 - m_a) / P + \theta^3 a \; K_2 \left[ C_a (m_3 - m_a) \right.$$

$$\left. + (C_3 - C_a) m_a \right] + \theta^2 (a \; K_2 P C_a m_a + U_3^2 / 2gJ) - \theta K_1$$

$$- T_a C_a = 0 \qquad 4.25$$

where $$K_1 = \left( C_3 T_3 + \frac{U_3^2}{2gJ} - T_a C_a \right) / P$$

$$K_2 = \frac{p_a}{g \underline{R}_u \rho_3 P^2}$$

$$P = \frac{p_3 - p_a}{U_3^2 \rho_3} + 1$$

All the terms are expressed in thermal units, so that the dimensions of each expression in equation 4.25 is BTU/lb. weight. The assumption $p_5 = p_a$ has been made in deriving this equation, which gives a direct relationship between $\theta$ and $\alpha$. If the area ratio $\alpha$ is calculated, a solution for $\theta$ can be obtained. However, this involves the solution of a quartic equation which can prove tedious. The other unknowns can be quickly calculated once $\theta$ is known.

$$\frac{\rho_5}{\rho_3} = \beta = \frac{P}{\theta^2 \alpha} \qquad 4.26$$

$$C_5 = C_a + (C_3 - C_a) \frac{\theta}{P} \qquad 4.27$$

$$T_5 = \frac{p_a \left[ P m_a + (m_3 - m_a) \theta \right] \alpha \theta^2}{g \underline{R}_u \rho_3 P^2} \qquad 4.28$$

## 4.6 Example of Clustered Rocket Flow

An example to show the variation of the downstream conditions with area ratio is given below. The exit conditions of the rocket are taken directly from Reference 1 for a small solid fueled rocket.

$C_3 = 0.65$ BTU/lb.$^\circ$R

$C_a = 0.240$ BTU/lb.$^\circ$R

$m_a = 29$

$m_3 = 26$

$U_3 = 8600$ ft/sec.

$J = 778$ ft. lb./BTU

$p_a = 14.7$ lb./in.$^2$

$p_3 = 9.4$ lb./in.$^2$

$\rho_3 = 0.0065$ lb./ft.$^3$

$T_3 = 3600^\circ$ R

$T_a = 520^\circ$ R

$$R_u = 1545 \frac{\text{ft. lb.}}{^\circ\text{R. lb. mole}}$$

Mach number of exit flow = 3.12

Then equation 4.25 becomes

$$-303.5\,\theta^4\,\alpha + 2620\,\theta^3\,\alpha + 1560\,\theta^2\,\alpha + 1478\,\theta^2 - 3890\,\theta - 125 = 0 \qquad 4.29$$

Chosing the area ratio $\alpha$ so the velocity ratio $\theta$ may vary between 0.0 and 1.0, the relationship shown in Figure 39 is obtained. It will be seen that for values of $\theta$ greater than 0.81, the area ratio, is found to be less than 1.0. This, in effect, describes completely the contraction that would occur due to the pressure rise of the exhaust gas from 9.4 psia to the atmospheric pressure. When $\theta$ is near 1.0, station 5 will be very close to the exit station 3, and in order that the pressure may become atmospheric at 14.7 psia, a contraction must take place since insufficient mass is drawn into the flow to keep the area constant. The way that this occurs is better examined by study of the other expressions. Figure 40 is a plot of the density ratio, $\beta$, against the area ratio, $\alpha$, and Figure 41 is the variation of temperature at station 5 with area ratio. Both these graphs show the contraction effect at values of $\theta$ near 1.0. Here, where $\alpha$ becomes less than 1.0, the density rise, which occurs as a jump, is accompanied by a temperature rise. Of course, these curves do not represent the actual conditions since this effect is caused by the assumption of pressure at station 5 equal to atmospheric. Also in the case of clustered nozzles, the station 4, to which 5 is related, is assumed to be at least a greater distance downstream than the core length

of an individual rocket, and the assumption that the pressure is atmospheric is then not unreasonable. This means that values of $a$ near 1.0 are not likely in physical flows. Figure 42 shows the mass flow at station 5 compared to the exit mass flow with various area ratios. It shows that in the normal case a large amount of air has been induced into the mixing flow at the downstream station. Despite the large mass of ambient air drawn into the flow, the temperature of the downstream gas is still high, and this is due to the energy contained in the high velocity of the exit gas. Figure 43 shows the area ratio for various clusters, where $n$ is the number of nozzles in the cluster and $R_2$ is the radius of the perimeter containing the individual nozzles. For most practical examples, the area ratio will generally be well above 5.0 and so the effects encountered at small values of area ratio will not occur.

## 4.7 Example of Clustered Rocket Noise Production

A series of sixteen rockets, each of nozzle exit diameter of 0.097 feet, are considered and the other exit conditions are taken at the values used in previous examples and given in Reference 1. Using the results of Figures 39, 40, and 41, the conditions of the apparent flow from station 5 are calculated for various nozzle separations. The spacing ratios are indicated by the value of $R_2/R_1$. When $R_2/R_1$ equals 4, then the nozzles must be distorted from their circular shape so that they all fit together to form one large circular nozzle. When $R_2/R_1$ is equal to infinity, the individual nozzles are so far apart that the exhaust flows do not interfere and so the resultant noise field produced is sixteen times that of a single rocket. At the intermediate values of $R_2/R_1$, the downstream flow is calculated, and the total sound formed by the configuration is obtained by adding the estimated sound from the two parts of the flow. For the upstream individual rockets only a certain number of the nozzles are considered as acting, to allow for the shielding effects and the reduction of the intensity of the turbulence in the inner mixing regions. The number of nozzles is estimated using the empirical expression given in Reference 18.

$$\text{Number of rockets acting} = \frac{R_2}{R_1} + 0.18\, n_p - 1 \qquad 4.30$$

where $n_p$ is the number of rockets in the outer region of the cluster.

Examination of various clustered configurations suggests that this equation is sufficient to indicate the amount of perimeter of the nozzles that generates the sound.

In calculating the sound from these individual rocket streams only that length of the exhaust stream up to the combined flow is considered. The generalized expressions for overall sound and spectra, devised in the previous sections of this report, are used. The final spectrum is then obtained by adding together the calculated values for the two flow portions, and converting to spectral density values by dividing by the bandwidth. The results obtained are plotted in Figure 44, which shows well the transfer of power from the low to the higher frequencies as the spacing increases. Figure 45 shows how, for one spacing ratio, the sound from the two flow regions combine to produce the total spectrum.

Figure 46 shows the effect of the number of nozzles on the resultant spectrum of total noise produced. The exit conditions and the total nozzle exit area have been kept constant at the previously used values. The area ratio, $a$, is also kept at the same value, which means that the overall radius, $R_2$, varies slightly with different numbers of nozzles. However this enables the calculations to be simplified since the downstream combined flow, and its associated noise, remain constant in all cases. The noise generated by the individual rockets up to the mixing plane is calculated using the generalized results and equation 4.30 as before. The final results for the spectral density of the noise formed are obtained by adding the two spectra as before.

These results show the way the low frequencies dominate the spectra as soon as the individual rocket flows interfere. Because the final curve is the result of adding two other spectra, it shows a two humped profile. However the effect shown is nowhere as great as was calculated for clusters of turbojet engines in Reference 18. Figure 47 shows a set of typical results calculated for a cluster of jets, based on measurements of a J57 engine, and is Figure 82 of Reference 18. Here it will be seen that two definite peaks are formed and that as the spacing ratio increases, the low frequency peak rapidly reduces. Comparison of Figures 44 and 46 with 47 shows the large differences in the acoustic power produced between clusters of rocket and jet engines and helps to point out the saliant features of clustered nozzle rocket noise.

The results in Figure 44 show that, when the spacing is increased, there is a reduction in the low frequency noise, but nowhere to the extent of the change in the jet engine spectra Figure 47. Until the spacing becomes quite large the spectra persist in peaking at the lower frequencies and this is because in rocket flow, the downstream region is the major noise producing region. The noise produced by this downstream region will peak at a low frequency on account of the larger width of the mixing region in comparison to the single rockets. Also the sound produced by this downstream flow will be considerable, compared to the sound formed in the less efficient noise producing regions of the individual rocket flows. The results of Figure 46

also show how the peak of the spectral density curve remains at a relatively low frequency as the number of nozzles is increased. This is because at the close spacing of the rockets used here, a similar downstream combined flow is produced in all cases. The changes in the spectra of sound generated are due only to the sound produced by the individual rocket flows before they interfere.

Experimental measurements confirm these results, especially concerning the predominant low frequency peak to the spectrum. Measurements of the noise field and the total acoustic power radiated from a cluster of four solid fueled rockets and an equivalent thrust cluster of sixteen smaller rockets are reported in Reference 28. These results show an almost identical spectrum of sound from the two configurations and the spectra peak at a lower frequency than the value obtained from measurements of a single nozzle equal to those of the four rocket cluster. This illustrates that for the rocket cluster the downstream interfering airflow is the dominant noise producing region and, except for a very large spacing ratio, it will determine the shape of the spectrum formed. These results also suggest that the major acoustic sources of a rocket are situated at a relatively greater distance downstream compared to the slower jet engine exhaust flow.

## 4.8 Comparison of Calculated and Measured Results

Boeing Report No. T2-2574 (Reference 28) gives detailed measurements of the acoustic field for clusters of four and sixteen model rockets. It was confirmed that these clusters are based on similar rockets to those used by Morgan in Reference 1, and so the calculated exit and flow conditions apply. The spectrum of the total noise power is calculated for these two examples and compared to the measured results.

For the four rocket cluster, the individual rockets are each of 0.097 feet radius and they are grouped together so that $R_2$ is 0.29 feet. The downstream combined rocket flow is calculated to be equivalent to that produced by a rocket of exit radius equal to 0.385 feet and exhaust velocity of 3220 ft/sec. The computed gas conditions are: density 0.0112 lb /ft$^3$, temperature 3390$^\circ$ R, and the pressure is assumed to be 14.7 lb /in.$^2$. The noise power and spectra are calculated for the two portions of the flow and the resultant total spectrum is shown in Figure 48, where it is compared to the measured value of Reference 28. This process is repeated for the sixteen nozzle clusters and the calculated and measured results are shown in Figure 49. In both figures the agreement is fair, the latter figure showing well the twin humps of the calculated curve produced by addition of the sound from the two parts of the flow. Both calculated curves tend to overestimate the lower frequencies, and this effect is the result of the generalized replacement of the downstream flow by a single large jet flow. However without making

an approximation of this kind, it is very difficult to apply basic prediction methods to the complicated flow patterns formed from clusters of rockets. The two flow region prediction method must also necessarily result in underestimation of the central part of the spectrum and the results show that the greatest difference is found here.

When a group of rockets is replaced by a greater number of smaller rockets but with the same total exit area and flow conditions, the prediction technique will calculate less total acoustic power for the cluster. (The calculated values for the Boeing nozzles gives 178.0 db for the four nozzle cluster and 176.4 db for the sixteen nozzle cluster.) However the results, as reported in Reference 28, show almost identical values for the overall levels and for the spectrum of both configurations. In fact, the reported values for the sixteen nozzle example are slightly greater than for the four nozzle set up. Analytical study and experience from jet-engine cluster mixing flows would suggest that a greater number of nozzles with interfering airflows should generate slightly less noise than a smaller number equivalent cluster. But the difference in the experimental results is less than one decibel and so no definite trend can be determined. The method of calculating the noise tends to overemphasize the interference effects.

Recognizing that these limitations will exist, the results presented here show that the proposed method of calculating the noise from a cluster of rockets produces reasonably good answers. Also the analysis explains the experimental results of noise spectra dominated by the lower frequencies, by indicating the importance of the downstream mixing flow in the generation of noise.

# 5.0 THE DEFLECTED ROCKET EXHAUST

## 5.1 Introduction

In order to predict the noise produced by a deflected rocket exhaust, it is useful to be able to predict the flow pattern formed. Then, the basic prediction techniques based on the flow parameters can be used fo determine the sound field produced. As the rocket rises above the deflector, changes in the flow will show how the noise generating mechanism is altered. The practical alternative to this approach is the study of the noise generated by a series of similar flow patterns.

A simple solution for deflected flow is obtained in the case of the two dimensional subsonic incompressible impingement of a constant velocity stream onto an inclined plane. Here the solution is that there are two streams of fluid, one up and the other down and both parallel to the surface of the plane. By using the equations of conservation of mass, momentum and energy, the solution is found that the velocity of both streams is the same as the impinging flow and the thickness of the streams is given in terms of the angle of incidence of the flow onto the plane.

$$h_1 = \frac{d}{2}(1 + \cos \delta) \qquad \text{Flow down the plane}$$

$$h_2 = \frac{d}{2}(1 - \cos \delta) \qquad \text{Flow up the plane}$$

$\delta$ is the angle of incidence
d is the width of the impinging flow

The two-dimensional incompressible case can be extended to three-dimensions. The deflected velocity is again found to be equal to the velocity before impingement, but the thickness of the deflected jet is now inversely proportional to the distance from the point of impingement. Experimental results for deflected flow show that most of the gas is turned down the plane and only a little escapes up and to the sides, provided that the deflection angle is not too great. This problem of back-flow is discussed in the case of a compressible deflected stream in Appendix B.

The problem is greatly complicated when the impinging jet is supersonic and of a radically different density and chemical composition from the surrounding atmosphere. Also recombustion of the gas in the exhaust stream can take place, which will cause the energy of the stream to be increased. This additional effect will not be considered in the following analysis.

The basis of the approach in this chapter, to determine the deflected flow conditions, is similar to that used in the solution of the clustered nozzles; a representative velocity, temperature and composition being used to describe a given point in the stream. The equations of momentum and heat are used to obtain relationships as the rocket flow mixes and spreads. In the study of the development of the flow from the rocket nozzle to the deflector and in the flow down the plane, the effect of air entrainment into the flow must be allowed for.

Once the solution for the flow has been obtained, the noise generated by the system is found by a method similar to that used for the clustered nozzles in the last chapter. The flow is considered in two parts, that up to the deflector and that downstream of the deflection. The noise generated by these two flow regions is estimated and the total power level obtained by summing the two separate parts.

## 5.2 Flow from the Nozzle to the Deflector

For some distance downstream of the rocket nozzle, the exhaust flow before it reaches the deflector is supersonic and so is unaffected by the deflector. Therefore the flow can be treated as undisturbed and the normal expressions for the sound produced by the initial regions of a rocket stream used. The outer portions of the initial mixing region are subsonic and will be affected by the deflector but Schlieren photographs of deflected flows show that this disturbance is slight.

Let the flow conditions at the nozzle be represented by the suffix e and the flow just before the deflection surface, be represented by the suffix 1. A certain mass of the atmosphere into which the rocket is mixing will be entrained into the exhaust. The conditions of the atmosphere are labelled 'a'. A representative velocity, density and area are assigned to the flow at each point, and these are similar to the maximum velocity and width parameters used in classical jet mixing theories. They are defined by,

$$\text{Total Mass Flow} = \rho A V = \dot{m}$$
$$\text{Total Momentum} = \rho A V^2$$

and the density is representative of the mixture of gases in the stream at that point.

Then for the flow from the nozzle to the deflection:
Continuity of Mass Flow

$$\dot{m}_1 = \dot{m}_e + \dot{m}_a \qquad 5.1$$

or

$$\rho_1 A_1 V_1 = \rho_e A_e V_e + \dot{m}_a \qquad 5.2$$

Conservation of Momentum

$$\rho_1 A_1 V_1^2 - \rho_e A_e V_e^2 = A_e p_e + (A_1 - A_e) p_a - A_1 p_1 \qquad 5.3$$

and if it is assumed that the station 1 is sufficiently far enough downstream for the static pressure $p_1$ to be atmospheric,

$$\rho_1 A_1 V_1^2 - \rho_e A_e V_e^2 = A_e (p_e - p_a) \qquad 5.4$$

Further the conservation of heat may be applied to the flow through the system; all heat transferred from the rocket stream is assumed to be to the entrained air:

$$\dot{m}_1 \bar{T}_1 C_1 = \dot{m}_e \bar{T}_e C_e + \dot{m}_a \bar{T}_a C_a \qquad 5.5$$

where $\bar{T}$ is the total temperature of the gas and
C is the specific heat at constant pressure.

For a perfect gas, the total temperature is related to the static temperature by:

$$\bar{T}C = TC + \frac{V^2}{2gJ} \qquad 5.6$$

where T is the static temperature

Then equation 5.5 becomes

$$\dot{m}_1 \left[ T_1 C_1 + \frac{V_1^2}{2gJ} - T_a C_a \right] = \dot{m}_e \left[ T_e C_e + \frac{V_e^2}{2gJ} - T_a C_a \right] \qquad 5.7$$

This equation is seen to be identical in form to the equations derived in the solution of the Flow of the Clustered Rockets in chapter 4.

But $T_1$ is unknown. If the gas constants (R) for air and rocket gas are approximately equal it is reasonable to write:

$$T_1 = \frac{p_1}{p_e} \cdot \frac{\rho_e}{\rho_1} \cdot T_e \qquad 5.8$$

Thus combining equations 5.7 and 5.8:

$$\dot{m}_1 \left[ C_1 T_e \cdot \frac{p_1 \rho_e}{p_e \rho_1} + \frac{V_1^2}{2gJ} \right] = \dot{m}_e \left[ T_e C_e + \frac{V_e^2}{2gJ} \right] + \dot{m}_a C_a T_a \qquad 5.9$$

$C_1$, the specific heat at constant pressure, for the mixture of air and rocket gas is unknown and is determined from:

$$C_1 = \frac{\dot{m}_e C_e + \dot{m}_a C_a}{\dot{m}_1} \qquad 5.10$$

Thus equations 5.9 and 5.10 give:

$$\rho_1 = \frac{p_1 \rho_e T_e}{p_e} \cdot \frac{\left( \dot{m}_e C_e + \dot{m}_a C_a \right)}{\left\{ \dot{m}_e \left[ C_e T_e + \frac{V_e^2}{2gJ} - \frac{V_1^2}{2gJ} \right] + \dot{m}_a \left[ C_a T_a - \frac{V_1^2}{2gJ} \right] \right\}} \qquad 5.11$$

However if the gas constants for air and rocket gas are unequal, it is necessary to calculate the gas constant at station 1, $\underline{R}_1$.

The gas constant $\underline{R}_1$ may be calculated from the atmospheric air $\dot{m}_a$ added to the rocket flow in its passage from the nozzle exit, the molecular weight at station 1, and the universal gas constant $\underline{R}_u$:

$$\text{Thus } \underline{R}_1 = \underline{R}_u \frac{\left( \dot{m}_a + \dot{m}_e \right)}{m_a \dot{m}_a + m_e \dot{m}_e} \qquad 5.12$$

On substituting, equation 5.11 becomes

$$\rho_1 = \frac{p_1 \left( \dot{m}_e C_e + \dot{m}_a C_a \right)}{\underline{R}_1 \left\{ \dot{m}_e \left[ C_e T_e + \frac{V_e^2}{2gJ} - \frac{V_1^2}{2gJ} \right] + \dot{m}_a \left[ C_a T_a - \frac{V_1^2}{2gJ} \right] \right\}} \qquad 5.13$$

Also it is possible to compute $V_1$ and $A_1$:

$$V_1 = \frac{\rho_e V_e^2 + p_e - p_a}{\rho_e V_e + \dot{m}_a / A_e} \qquad 5.2,\ 5.4 \qquad 5.14$$

$$A_1 = \frac{\rho_e A_e V_e + \dot{m}_a}{\rho_1 V_1} \qquad 5.2$$

Thus conditions at station 1, just before the deflector are related to conditions at the nozzle exit by the three equations 5.14, 5.2 and 5.11 or 5.13.

However there are four unknowns $\rho_1$, $A_1$, $V_1$ and $\dot{m}_a$. To solve for $\rho_1$, $A_1$ and $V_1$, one of these unknowns must be estimated. In Chapter 4, for the clustered rockets an estimated area was assumed, based on the cluster geometry. In this case it is not possible to obtain this value, and it is suggested that the mass of atmospheric air entrained is used.

Appendix A, presents the analysis of Eldred (Reference 18) for a constant density jet, extended to present the mass flow at various stations downstream. The mass flow entrained is given in terms of the core length of the jet. The expression for the region beyond the core tip reduces to a simple expression.

The analysis for the initial region involves certain approximations and it would appear that the downstream expression is also suitable for the initial region. Eldred has also found that the core length of a jet or rocket is given by the simple empirical expression:

$$\frac{x_t}{R} = 6.9\,(1 + 0.38\,M_e)^2 \qquad 4.2 \qquad 5.15$$

where $x_t$ is the downstream length to the core tip.

It is found experimentally that the core length of a hot low density jet is no more than 20 percent shorter than the core of a jet of the same Mach number which has a total temperature equal to ambient. Thus it would seem a good approximation to assume that the mass of air entrained by a hot low density jet is approximately equal to that entrained by a constant density jet.

Thus the fourth unknown $\dot{m}_a$ can be estimated and the problem solved for the flow conditions at station 1, by first estimating the core length $x_t$ from equation 5.15. From Appendix A the additional mass flow downstream of the core tip, is seen to be $(x/x_t)\,\dot{m}_e$ where $x$ is the distance downstream of the nozzle exit.

If the nozzle is very close to the deflector, a simpler solution may be obtained by assuming that no air is mixed into the flow. That is that $\dot{m}_a$ equals zero. This allows a rapid solution on the assumption that the static pressure at 1 is again atmospheric. The energy equation may be written as:

$$\frac{\gamma}{\gamma - 1} \cdot \frac{p_1}{\rho_1} + \frac{V_1^2}{2} = \frac{\gamma}{\gamma - 1} \cdot \frac{p_e}{\rho_e} + \frac{V_e^2}{2} \qquad 5.16$$

Then with the momentum and conservation of mass equations 5.2 and 5.4 a solution for $V_1$, $\rho_1$ and $A_1$ may be obtained. This, of course, is only an approximation which produces rapid solutions when the nozzle is close to the deflector. These results can then be used with the two dimensional shock relationships to solve the flow through the deflection. Since these relationships depend on an uniform velocity through the flow, they can only be used when the rocket is close to the deflector and a minimum of mixing occurs. This

simpler approach will therefore be strictly limited to the initial position of the rocket and then only if the nozzle exit is very close to the deflector surface.

## 5.3 Flow Through the Deflection

### 5.3.1 Nozzle Close to the Deflector

The order of Section 5.2 is reversed here and the flow striking the deflector when the nozzle deflector separation is very small is considered first. The conditions $V_1$, $A_1$ and $\rho_1$ at station 1 may be calculated using equations 5.2 5.13 and 5.14 from Section 5.2. Then the Mach number of the flow is given by:

$$M_1 = \frac{V_1}{a_1} \qquad 5.17$$

where $$a_1 = \sqrt{\frac{\gamma p_1}{\rho_1}} \qquad 5.18$$

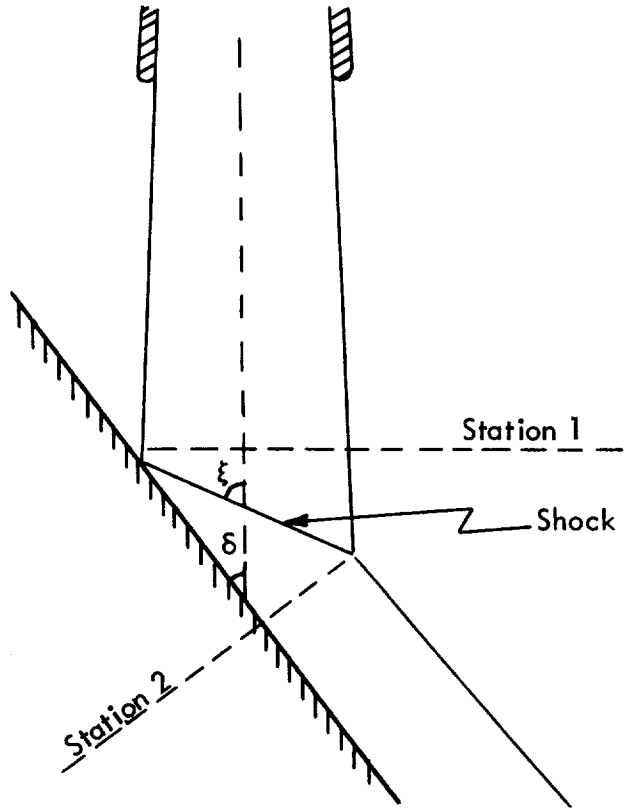


Figure 50 Deflected Jet Showing Shock Angles

Then using the shock relationships, (References 29 and 30)

$$M_2^2 = \frac{1 + \frac{\gamma - 1}{2} M_1^2}{\gamma M_1^2 \sin_\xi^2 - \frac{\gamma - 1}{2}} + \frac{M_1^2 \cos_\xi^2}{1 + \frac{\gamma - 1}{2} M_1^2 \sin_\xi^2} \qquad 5.19$$

$$\frac{p_2}{p_1} = \frac{1}{\gamma + 1}\left[2\gamma M_1^2 \sin_\xi^2 - (\gamma - 1)\right] \qquad 5.20$$

$$\frac{\rho_2}{\rho_1} = \frac{(\gamma + 1) M_1^2 \sin_\xi^2}{(\gamma - 1) M_1^2 \sin_\xi^2 + 2} \qquad 5.21$$

Continuity is assumed between stations (1) and (2), and no mass addition is assumed.

Then

$$\rho_2 A_2 V_2 = \rho_1 A_1 V_1 \qquad 5.22$$

and

$$a_2 = \sqrt{\frac{\gamma p_2}{\rho_2}} \qquad 5.23$$

and

$$V_2 = M_2 a_2 \qquad 5.24$$

In the numerical example in section 5.5, $\xi$ was measured from a Schlieren photograph of a model rocket firing with the deflection angle $\delta$.

However if $\xi$ is unknown and it is required to calculate $\xi$ for an arbitrary deflection angle $\delta$, it may be computed from the following equation (see Reference 31)

$$\sin^6\xi + a\sin^2\xi + b = 0 \qquad 5.25$$

where

$$a = \frac{2M^2+1}{M^4} + \left[\frac{(\gamma+1)^2}{4} + \frac{\gamma-1}{M^2}\right]\sin^2\delta - \frac{k^2}{3}$$

$$b = -\frac{2}{27}k^3 + \frac{k}{3}\left\{\frac{2M^2+1}{M^4} + \left[\frac{(\gamma+1)^2}{4} + \frac{\gamma-1}{M^2}\right]\sin^2\delta\right\} - \frac{\cos^2\delta}{M^4}$$

$$k = \frac{M^2+2}{M^2} + \gamma\sin^2\delta$$

and $M = M_1$, the upstream Mach number.

In reference 31, Briggs gives a complete solution to this equation and, noting that the smallest root represents an entropy decrease and is therefore not applicable to real flows, gives the equation for a strong shock and a weak shock.

For a small deflection a weak shock wave will invariably be formed and the value for $\xi$ is given by

$$\sin^2\xi = \frac{k}{3} - 2\left(-\frac{a}{3}\right)^{1/2} \cdot \cos\left[60^\circ + \frac{\tan^{-1}(-2h/b)}{3}\right]$$

While the solution for a strong shock is given by

$$\sin^2\xi = \frac{k}{3} + 2\left(-\frac{a}{3}\right)^{1/2} \cos\left[\frac{\tan^{-1}(-2h/b)}{3}\right]$$

where $h = \left[(-b^2/4) - (a^3/27)\right]^{1/2}$ in both cases

As the angle of deflection is increased, a critical angle is reached for each impingement Mach number at which this relationship breaks down. For a Mach 3 airstream which has a ratio of specific heats equal to 1.4, the critical angle is 34 degrees. Above the critical angle the shock can not remain attached to the surface and becomes curved and detached from the surface. Some gas flow back up the plane can then be expected. However, it must be remembered that the flow striking the deflector in the case of a rocket exhaust is not a uniform flow and cannot really be approximated to the one dimensional flow case, except when the rocket is very close to the deflector.

If the deflection angle, or initial deflection of the flow is greater than the critical angle, care in determining the solution for the flow must be taken. In this case the strong shock relationship is suitable for determining the flow relationships, but this results in a greater pressure rise. This complicates the exact determination of the downstream flow after the shock wave. Appendix B contains the method for calculation of the critical angle.

Values of the conditions after an oblique shock wave are given in various tables, for example Reference 29. These are for a specified ratio of specific heats. The equations here allow the exact solution to be obtained if the value of $\gamma$ for the rocket gas is much different from those listed in the tables and simple interpolation is not possible.

The next problem is determining the starting conditions for the flow down the deflector. It would seem appropriate to assume that the excess pressure formed at station 2 returns to atmospheric conditions and the jet stream consequently accelerates, but this results in very high velocities. The equations (5.2, 5.14 and 5.16) for the initial part of the flow from the nozzle to the deflector when the rocket is close to the jet are used, and again no mass addition is considered. However not all this pressure drop will be used to accelerate the jet stream since it will also help to spread the flow away from the plane.

Therefore except when the rocket is very close to the deflector, this method of calculating the flow is not likely to produce really accurate results, although it will help to pinpoint the shock patterns formed. The detached shock wave can be a very potent noise source and so an examination of the initial deflection angle is important to determine whether such a shock will occur. It is suggested that the method of section 5.3.2 is more suitable for determining the initial flow parameters for the deflected flow down the deflecting surface.

### 5.3.2 Nozzle Far from the Deflector

If there is a large velocity variation in the jet when it strikes the deflector, it is no longer possible to use the simple two-dimensional shock relationships for the flow through the impingement shocks which will occur at the deflector. However the general equations of momentum conserved in the direction parallel to the plane, continuity of flow, and conservation of energy may be used, since these properties are normally considered as conserved through shock waves. There will be some energy loss due to heat transfer to the deflector and with suitable experimental results some allowance could be made for this; but with no suitable results, the loss has been assumed to be zero.

Since the four flow conditions after the shock $\rho_2$, $A_2$, $V_2$ and $p_2$ are unknown and there are only three equations, it is again necessary to make some assumption in order to solve the flow.

The first assumption that the area:

$$A_2 = A_1 \cos \delta,$$ results in imaginary values for $V_2$.

Likewise the assumption that the pressure:

$p_2 = p_a + \rho_1 V_1^2 \sin^2 \delta$, that is that the mean pressure $p_2$ can be obtained by considering the momentum destroyed per second perpendicular to

the plane also gives imaginary values for the velocity. Without an accurate description of the pressure pattern in the jet stream after the impingement shock, this assumption is thus invalid.

Both the above assumptions are seen to be invalid. The assumption that is finally used to obtain the flow conditions after the impingement shock is that the station 2 is taken sufficiently far downstream so that the pressure at this station, $p_2$ may be assumed to be atmospheric. The pressure drop to atmospheric is assumed to occur in a short distance and it is thus valid to assume no air entrainment from the atmosphere. It is also assumed that all the flow is deflected down the deflector in a parallel stream. Then the following equations may be formulated.

Continuity:

$$\rho_1 V_1 A_1 = \rho_2 V_2 A_2 \qquad 5.26$$

Conservation of momentum parallel to the plane:

$$\rho_1 V_1^2 A_1 \cos \delta = \rho_2 V_2^2 A_2 + A_2 (p_2 - p_1)$$

and since $p_2 = p_a = p_1$

$$\rho_1 A_1 V_1^2 \cos \delta = \rho_2 A_2 V_2^2 \qquad 5.27$$

Thus $V_2 = V_1 \cos \delta$ 5.26 and 5.27 5.28

Conservation of Energy

This can be written as

$$\frac{\gamma}{\gamma - 1} \frac{p_1}{\rho_1} + \frac{V_1^2}{2} = \frac{\gamma}{\gamma - 1} \frac{p_2}{\rho_2} + \frac{V_2^2}{2} \qquad 5.29$$

The values for $\gamma$, $\underline{R}$ and C at station 2 are assumed constant through the deflection at those calculated for the station 1. (see equations 5.10 and 5.12) The ratio of specific heats of the gas flow at station 1 is given by:

$$\gamma_1 = \frac{C_1}{C_1 - \underline{R}_1} \qquad 5.30$$

5.28 and 5.29 give

$$\rho_2 = \frac{\rho_1}{1 + \frac{\rho_1 V_1^2}{2p_1} \cdot \frac{\gamma - 1}{\gamma} (1 - \cos^2 \delta)} \qquad 5.31$$

Hence

$$A_2 = \frac{\rho_1 A_1 V_1}{\rho_2 V_2} \qquad 5.32$$

and the "mean" conditions $V_2$, $\rho_2$ and $A_2$ for station 2 may be found. The meaning of these "mean" values of density, area and velocity are discussed in Appendix D.

## 5.4 Flow Down Deflector

### 5.4.1 Theoretical Analysis

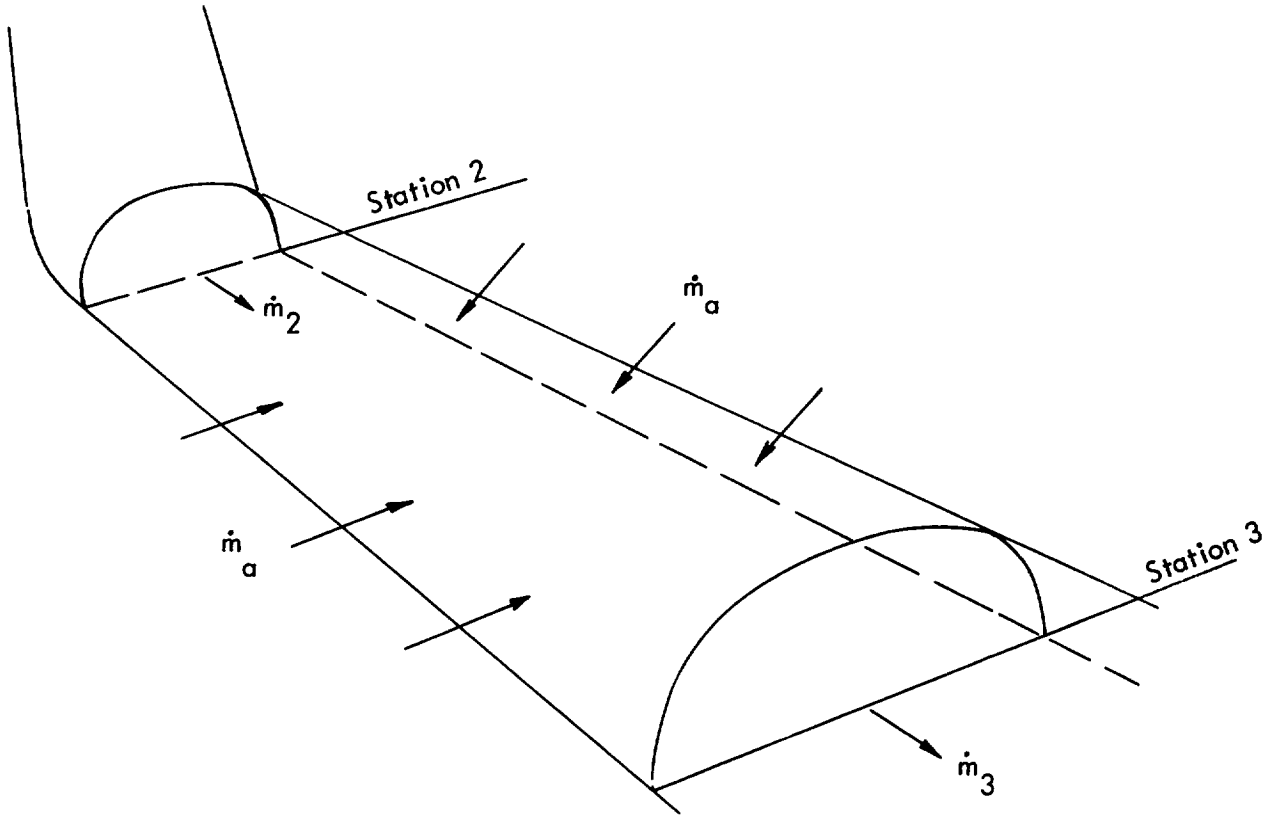


Figure 51 Flow Down the Deflector Plane

The flow is considered to be completely deflected down the deflection plane and to flow in a parallel stream, parallel to the surface. In Appendix B, it is shown that provided the angle of deflection $\delta$ is not two large, the shock wave does not separate and no back flow up the deflector need be considered. Viscosity is neglected and this seems a reasonable assumption since experimental results (Reference 32) show that the boundary-layer thickness of the flow on the deflector is of a lower order of magnitude compared with the thickness of the boundary between the deflected jet and the atmosphere.

If the deflector is short or it deflects the stream up into the atmosphere, the stream is then considered to be a simple rocket mixing into the atmosphere. However the same basic equations presented here still apply and only the analysis of the cross-sectional area changes.

With the above assumptions and the assumption that all heat transferred from the stream is to the entrained air, then the following analysis is derived. Representative mean flow conditions are used as before.

Continuity:

$$\rho_3 A_3 V_3 = \rho_2 A_2 V_2 + \dot{m}_a \qquad 5.33$$

where 3 is the downstream station and $\dot{m}_a$ is the rate of air entrainment between stations 2 and 3.

Conservation of momentum:

$$\rho_3 A_3 V_3^2 - \rho_2 A_2 V_2^2 = A_2 p_2 - A_3 p_3 + (A_3 - A_2) p_a$$

$$\rho_3 A_3 V_3^2 = \rho_2 A_2 V_2^2 \qquad 5.34$$

provided $p_3 = p_2 = p_a$ the atmospheric pressure.

Conservation of heat:

$$\dot{m}_3 \bar{T}_3 C_3 = \dot{m}_2 \bar{T}_2 C_2 + \dot{m} \bar{T}_a C_a \qquad 5.35$$

It is seen that the above three equations are similar to the three basic equations derived in Section 5.2 for the flow from the nozzle exit to the deflector. Compare equations 5.33, 5.34, and 5.35 with 5.2 , 5.4 , and 5.5 .

Using static temperatures 5.35 becomes:

$$\rho_3 A_3 V_3 \left[ C_3 T_3 + \frac{V_3^2}{2gJ} - C_a T_a \right] = \rho_2 A_2 V_2 \left[ C_2 T_2 + \frac{V_2^2}{2gJ} - C_a T_a \right] \qquad 5.36$$

The use of the gas equation:

$$\frac{p_3}{\rho_3 T_3} = \frac{p_2}{\rho_2 T_2} \qquad 5.37$$

and the equations for the coefficient of specific heat at constant pressure and for the gas constant at station 3

$$C_3 = \frac{\dot{m}_2 C_2 + \dot{m}_a C_a}{\dot{m}_3} \qquad 5.38$$

and $$\underline{R}_3 = \frac{\underline{R}_u (\dot{m}_a + \dot{m}_2)}{m_a \dot{m}_a + m_2 \dot{m}_2} \qquad 5.39$$

enable a solution to be obtained for the flow properties at station 3, once one of them has been determined empirically.

It should prove possible to use the approach of Section 5.2 and to estimate the mass entrained into the flow. However the results of Anderson and Johns (Reference 32) allow an estimate of the velocity at station 3 to be obtained. They made a series of experiments involving a hot air jet and three rockets impinging on a large plane surface. They present generalized curves for the total and static pressures and temperature decay in the flow down the plane after the deflection. Figure 52 shows their curves for dynamic pressure and velocity decay, and these enable an estimate of the velocity in the deflected flow to be obtained. The values are normalized against those values measured just before the impingement and the downstream distance is normalized against a representative diameter of the flow just before impingement. In Appendix D it is shown that the typical or "mean" velocity used here in this analysis is almost exactly one half the maximum velocity at any flow station, and so this generalized velocity curve is suitable to estimate $V_3$.

In the examples that follow in Section 5.5, the velocity $V_3$ is the property which is determined empirically so that the flow properties in the deflected flow may be determined. It is assumed that the ratio of mean velocity at station 3 to mean velocity just before impingement is the same as the ratio of maximum velocity at station 3 to maximum velocity just before impingement given in Figure 52. The value of $d_j$, used in Anderson and John's expressions, is that diameter of the flow just before the impingement that includes all the flow where q, the dynamic pressure, is greater than half the maximum q. The "mean" velocity at any downstream point may then be determined. This allows a solution for $A_3$ and $\rho_3$ to be found. Thus the method used to solve the deflected flow is:

since $V_3 / V_2$ is known

$$\dot{m}_3 = \frac{\rho_3 A_3 V_3^2}{V_3} \cdot \frac{\rho_2 A_2 V_2^2}{V_3} \qquad 5.34$$

$$\rho_3 = \frac{C_3 T_2 \frac{P_3}{P_2} \rho_2}{\frac{\dot{m}_2}{\dot{m}_3}\left(C_2 T_2 + \frac{V_2^2}{2gJ} - T_a C_a\right) - \frac{V_3^2}{2gJ} + T_a C_a} \qquad 5.36,\ 5.37$$

and $$A_3 = \frac{\dot{m}_3}{\rho_3 V_3} \qquad 5.33$$

The value of $C_3$ is determined from equation 5.38.

## 5.4.2 Discussion of Experimental Results

Anderson and Johns give a series of non-dimensional curves for the growth of the flow down the deflector plane and these allow the true physical dimensions of the flow to be determined within certain limits. The width and height of the flow are normalized on distance to the 1/2 (q maximum) point at each station. Figure 53 shows the width to height of the flow ratio in terms of the normalizing values. The curve is plotted for the different deflection angles and should show an increasing aspect ratio with deflection angle. The decrease at the highest angles is due to the traversing gear, for the pressure measurements, operating along straight lines for experimental convenience rather than the constant radius circular arcs that truly should be used. These results show the very high aspect ratio flow which is formed and persists for some distance down the plane. The generalized curves enable the momentum of the flow before and after the deflection to be compared and to compare these values with the values predicted by the equations used here.

Figure 54 presents a representation of the flow at a downstream station and the notation used in the following analysis. Figures 55, 56 and 57 show the normalized functions for the growth of the mixing region. Figure 58 represents the dynamic pressure, q, in terms of the maximum value at the center and the value of y to half this maximum center value.

Then the momentum per second at the downstream station is given by integrating q across the whole cross-sectional area of the flow and doubling this value,

$$\overline{M} = 2 \int_A q \, d A \qquad 5.40$$

Thus the momentum per second

$$\overline{M} = 4 \int_{h=0}^{\infty} \int_{y=0}^{\infty} q_{yh} \, dy \, dh$$

$$\overline{M} = 4 \int_{h=0}^{\infty} \left[ \int_{\frac{y}{y_h}=0}^{\infty} q_{max\ h} \cdot f_1\left(\frac{y}{y_h}\right) y_h \, d\left(\frac{y}{y_h}\right) \right] dh$$

$$\overline{M} = 4 \int_{\frac{h}{h_0}=0}^{\infty} \int_{\frac{y}{y_h}=0}^{\infty} q_{max\ 0} \cdot f_2\left(\frac{h}{h_0}\right) f_1\left(\frac{y}{y_h}\right) y_0 \, f_3\left(\frac{h}{h_0}\right) d\left(\frac{y}{y_h}\right) h_0 \, d\left(\frac{h}{h_0}\right)$$

and if $f_1$ is assumed constant for any $h$ :

$$\int_{\frac{y}{y_h}=0}^{\infty} f_1\left(\frac{y}{y_h}\right) d\left(\frac{y}{y_h}\right) = \int_{\frac{y}{y_0}=0}^{\infty} f_1\left(\frac{y}{y_0}\right) d\left(\frac{y}{y_0}\right)$$

Then $$\overline{M} = 4 \int_0^{\infty} \int_0^{\infty} q_{max\ 0} \; y_0 \, h_0 \, f_1\left(\frac{y}{y_0}\right) f_2\left(\frac{h}{h_0}\right) f_3\left(\frac{h}{h_0}\right) d\left(\frac{y}{y_0}\right) d\left(\frac{h}{h_0}\right)$$

$$\overline{M} = 4.5 \; y_0 \, h_0 \, q_{max\ 0} \qquad 5.41$$

The notation used in the above analysis is explained in Figure 54, it is similar to, but different from that used in reference 32. The symbol $y_h$ represents the distance $y$ for $q_{yh}$ to be $\frac{1}{2} q_{max\ h}$; $y_0$ represents the distance $y$ for $q_{y0}$ to be $\frac{1}{2} q_{max\ 0}$, at $h = 0$; and $h_0$ represents the height on the center line of the deflected jet for $q_{max\ h}$ to be $\frac{1}{2} q_{max\ 0}$. The functions $f_1\left(\frac{y}{y_0}\right)$, $f_2\left(\frac{h}{h_0}\right)$ and $f_3\left(\frac{h}{h_0}\right)$ are given in Figures 58, 56 and 59 respectively and were used to give the result presented in equation 5.41.

Anderson and Johns give values for the growth of these parameters with distance downstream. In the case of the width and height parameters, they are separate curves for each angle of deflection, but they suggest that one curve for all deflection angles is suitable for the dynamic pressure decay.

The dimensions are all normalized in terms of the representative diameter of the impinging jet. By applying equation 5.41, the longitudinal momentum of the deflected flow at various distances down the plane may be calculated and compared with the incident flow of the rocket exhaust. These calculations are then compared to the results calculated from the expressions given here for the momentum change through the deflection.

The results are given in Figure 60 and are presented on the normalized downstream distance of Anderson and Johns. The straight line represents the constant momentum suggested by the analysis in Section 5.4.1, which is (cos $\delta$) times the momentum of the incident flow. However the results of the measurements of Anderson and Johns show the momentum is increasing rapidly with distance down the plane and this is contrary to what is expected.

This analysis suggests that certain results are suspect and that which most obviously could be in error is the completely normalized curve for maximum dynamic pressure decay. It should be noted that Anderson and Johns did not measure static pressures in the flow and the dynamic pressures are given with the assumption that the static pressure everywhere is atmospheric. This will produce an appreciable error in values of dynamic pressure a short distance after impingement where the static pressure may be appreciably above atmospheric. The dynamic pressures given by Anderson and Johns for the deflected flow have not been reduced tc true dynamic pressures by removal of the compressibility factor $\left(1 + \frac{M^2}{4} + \frac{M^4}{40} \text{ etc.}\right)$. This will have the biggest effect where the flow velocity is highest. That is immediately after the deflector. Recognizing that the aspect ratio of the deflected flow is greatly affected by the deflection angle, it seems likely that the curves for decay of dynamic pressure and velocity will be different for different deflection angles. Figure 61shows the curve of dynamic pressure decay, with the calculated curves added for the various deflection angles, so calculated that the downstream momentum is preserved constant. The figure is plotted on the logarithmic scale of the original results and also the measurements of Anderson and Johns are shown. It is seen that only a slight variation in the curves is necessary to produce constant momentum and these calculated curves still fall fairly well within the scatter of the experimental points. It is recognized that the whole problem will be more complicated than has been represented, these curves can only be general approximations, since they take no account of the way that the exhaust gas can change its composition and thermal properties for different rockets and as more air is entrained into the flow. The validity of this momentum approach was checked by analyzing the results of Pitkin and Glassman (Reference 33). They produce results for the total and static pressure at the exit, 20 and 30 nozzle radii downstream for a Mach 2.6 air jet. The momentum per second at each station was calculated from their results and is plotted in Figure 62. These values

show a decreasing momentum with distance downstream, an opposite effect to that derived from Anderson and Johns results. This helps to show how critical the accuracy of the experiment is when making measurements in jet flows. The probable error in the Anderson and Johns results is that one generalized curve for dynamic pressure decay is not suitable. The various rocket measurement points are not identified as to deflection angle and it cannot be stated as to whether the calculated trend with deflection angle was observed. If the results in Figure 60 are interpolated back to $x/D_i = 0$, they agree fairly well with the calculated values of this analysis. In determining the characteristics of the downstream flow it is suggested that the basic results of Anderson and Johns will give some idea of the flow characteristics.

Examination of the width and height parameters (Figures 57 , 55 ) suggests that the aspect ratio of the deflected jet does not change very greatly with downstream distance. The rate of growth of both the parameters $y_0$ and the $h_0$ is given as a straight line, which means the high aspect ratio of the flow persists down the plane. Higgins and Wainwright (Reference 34) report a series of pressure measurements for jets of varying shape, and their results show how high aspect ratio rectangular jets quickly become circular. That is for nozzles with convergent mouths or slightly divergent. For example a 5:1 aspect ratio nozzle is almost completely circular by 20 nozzle equivalent exit diameters. However for the case of rectangular nozzles with $30^\circ$ divergent mouths, ( only the wider edge diverges, see Figure 63) they produce results that show the downstream flow remains at a high aspect ratio. This is equivalent to the deflected jet case, here the gas on striking the plate does flow outwards more easily than upwards and a greatly divergent jet of high aspect ratio is formed and persists down the plane.

However one point should be noted; the nozzles of Higgins and Wainwright show that for the divergent nozzles the maximum dynamic pressure falls off very rapidly and much faster than in the case of the straight mouth nozzle. Therefore it is suggested that the greater the deflection of the rocket exhaust the greater the tendency for the jet stream to spread out and for it to persist at a high aspect ratio, and also the quicker the maximum dynamic pressure can be expected to decay. Thus it would seem that Anderson and Johns results for the deflected flow dimensions are correct but that a graph of pressure decay similar to the calculated curves is more likely to be correct.

Therefore the results of the analysis using the curves of Figures 55, 56 and 57 allow a reasonable picture of the downstream deflected flow to be calculated.

## -5.5 Examples of Flow Calculations

### 5.5.1 Small Solid Fueled Rocket

In Reference 1 nozzle exit conditions for a 2.33 inch diameter solid fuel rocket are given. Also measured values of the far-field sound pressure levels on the ground when the rocket is deflected by a simple plane deflector are given. The flow pattern produced by this experimental set-up is calculated.

a) Nozzle close to deflector

$V_e$ = 8,600 ft/sec

$T_e$ = 3,600 $^{o}$R

$p_e$ = 9.4 x 144 lb/ft$^2$

$\rho_e$ = 0.0065 lb/ft$^3$

$\gamma$ = 1.12

$A_e$ = 0.0296 ft$^2$

Nozzle deflector separation = $2D_e$ = 4.66 inches

Impingement angle = 37$^{o}$

Shock angle = 60$^{o}$

Calculation of the flow conditions at 1 is completed by the method of section 5.2 by allowing the pressure to go to atmospheric value 14.7 psi and considering no mass entrained into the rocket exhaust flow. Use is made of equations 5.2, 5.4 and 5.16.

Then $V_1$ = 8160 ft/sec

$A_1$ = 0.02114 ft$^2$

$\rho_1$ = 0.0096 lb/ft$^3$

$p_1$ = 14.7 lb/in$^2$

which give

$a_1$ = 2770 ft/sec

$M_1$ = 2.94

The conditions immediately after the shock are calculated using the shock relationships: 5.19, 5.20, 5.21, 5.23 and 5.24.

Thus $V_2 = 1350$ ft/sec

$A_2 = 0.0241$ ft$^2$

$\rho_2 = 0.0508$ lb/ft$^3$

$p_2 = 100$ lb/in$^2$

Then letting $p_2$ go to the atmospheric value of 14.7 lb/in$^2$, the conditions at $2^1$ are found using the basic equations of continuity, momentum and energy.

$V_2^1 = 7110$ ft/sec

$A_2^1 = 0.0223$ ft$^3$

$p_2^1 = 14.7$ lb/in$^2$

$\rho_2^1 = 0.0104$ lb /ft$^3$

These are the starting conditions for solving the flow down the plane and also for determining the noise from this deflected flow.

b) Nozzle far from the deflector

In this case the rocket exhaust will mix with the air for some distance before it reaches the deflector. This means that the physical properties of the rocket exhaust gas will change as the air is entrained into the flow. Basically the three equations, continuity, momentum and heat or energy conservation are used and there are 4 unknowns. In determining the flow pattern just before the impingement, one of these quantities must be estimated. In this instance it is preferable to estimate the mass addition since the area will only be a representative area as will be the velocity and density. The pressure is assumed atmospheric and since the flow will be mainly supersonic, it is assumed that there is no back reaction on the flow from the deflector and the rocket flow is considered as forming normally for a free jet.

The determination of the mass addition is estimated from the constant density rocket curves as suggested in Section 5.2. The core length for the rocket exhaust is estimated by use of equation 5.15. In this example for the small solid rocket it is found to be 32.8 nozzle exit radii.

Calculation of the various "mean" value ratios are completed using the method outlined in Section 5.2 and in particular equations 5.2, 5.13 and 5.14, and the resultant values listed below and plotted in Figure 64.

| $\frac{x}{R}$ | $\frac{x}{x_t}$ | $\frac{\dot{m}_a}{\dot{m}_o}$ | $V_1$ $\frac{ft}{sec}$ | $\frac{V_1}{V_o}$ | $\rho_1$ $\frac{lb}{ft^3}$ | $\frac{\rho_1}{\rho_o}$ | $\frac{A_1}{A_o}$ |
|---|---|---|---|---|---|---|---|
| 0 | 0 | 0 | 8160 | | | | |
| 20 | 0.61 | 0.55 | 5280 | .614 | .00950 | 1.460 | 1.73 |
| 40 | 1.22 | 1.22 | 3690 | .429 | .01028 | 1.580 | 3.18 |
| 60 | 1.85 | 1.85 | 2870 | .334 | .01120 | 1.723 | 4.96 |
| 80 | 2.44 | 2.44 | 2380 | .277 | .01210 | 1.862 | 6.66 |
| 100 | 3.05 | 3.05 | 2020 | .235 | .01308 | 2.010 | 8.56 |

In this example, the distance from the nozzle to the deflector is taken as 40 nozzle exit radii, or 46.5 inches. The value for $V_1$ is read off the appropriate line of the table above and the conditions after the deflection calculated using equations 5.28, 5.31 and 5.32. These produced

$$V_2 = 2950 \text{ ft/sec}$$
$$A_2 = 0.1242 \text{ ft}^2$$
$$P_2 = 14.7 \text{ lb/in}^2$$
$$\rho_2 = 0.00968 \text{ lb/ft}^3$$
$$T_2 = 3780^{\circ}R$$
$$\underline{R}_2 = 1740 \frac{ft^2}{sec^2\ ^{\circ}R}$$

For the flow down the plane the relationships derived in Section 5.4.1 are used. Anderson and Johns give the ratio of maximum velocity in the deflected jet to the impingement flow maximum velocity, and in Appendix D it is shown that it is reasonable to assume the same ratios for the mean velocities of the jet. Therefore the velocity fall-off, for the "mean" values used in this calculation are given by Figure 52.

At $x/D_i$, where $D_i = 2\sqrt{A_1/\pi}$, equal to 5 then

$$V_3 = 0.5 \times V_1$$

$$= 0.5 \times 3690 = 1845 \text{ ft/sec}$$

This is the unknown estimated in this case and the flow can be solved for A, T, $\rho$ and mass flow, provided $p_3$ is assumed $= p_2 = p_a$.

Then using equations 5.34; 5.38; 5.36; 5.37; and 5.33:

$$\dot{m}_3 = \frac{\rho_3 A_3 V_3^2}{V_3} = \frac{1}{V_3}\left[\rho_2 A_2 V_2^2\right] = 5.67 \text{ lb/sec}$$

$C_3$ calculates at 0.362 BTU/lb$^\circ$R

$$\rho_3 = 0.01168 \text{ lb/ft}^3$$

$$A_3 = m_3 / \rho_3 V_3 = 0.263 \text{ ft}^2$$

Similarly at $x/D_i = 10$

$$V_3 = 1025 \text{ ft/sec}$$

$$\dot{m}_3 = 10.2 \text{ lb/sec}$$

$$C_3 = 7690 \frac{\text{ft}^2}{\text{sec}^2\,^\circ\text{R}}$$

$$\rho_3 = 0.01595 \text{ lb/ft}^3$$

$$A_3 = 0.624 \text{ ft}^2$$

From the basic Anderson and Johns results for a deflection angle of 37$^\circ$, the aspect ratio of the flow is found to be 22 at $x_i/D_i = 5$ and 20 at $x_i/D_i = 10$. This means that the resultant flow is very flat on the plane surface and is spreading sideways at a considerable rate.

## 5.5.2 Large Clustered Rocket

a) Nozzles close to the deflection:

In this example a typical cluster of eight engines similar to SA1 is taken. The exit conditions for each individual nozzle are taken as

$\rho_e = 0.00728$ lb/ft$^3$

$V_e = 8,100$ ft/sec

$p_e = 12.7$ lb/in$^2$

$D_e = 3.8$ ft.

$\gamma = 1.2$

$T_e = 3260^\circ R$

$m_e = 20$

The conditions for each nozzle are calculated on the basis of a separation of $5D_e = 19$ ft from a $30^\circ$ deflector, using equations 5.2, 5.13 and 5.14. The flow is then considered as swept around the deflector and unchanged for any other angle deflection. After the deflection, the flows are considered as having mixed together completely and a single flow representing the clustered nozzles is to be used. The calculation is therefore completed for one nozzle through the deflection using equations 5.28, 5.31 and 5.32, and then the representative area $A_2$ is multiplied by 8 to take account of the cluster.

The following are the results:

| Station | V ft/sec | p lb/in$^2$ | $\rho$ lb/ft$^3$ | A ft$^2$ |
|---|---|---|---|---|
| e | 8100 | 12.7 | 0.00728 | 10.4 |
| 1 | 6350 | 14.7 | 0.00861 | 15.3 |
| 2 | 5500 | 14.7 | 0.00775 | 19.6 |

The initial aspect ratio of the deflected flow is calculated from Anderson and Johns results as 14 to 1. This is for the flow continuing down the plane. In actual fact for a rocket this size, the exhaust will normally be deflected back into the atmosphere so that the aspect ratio will quickly approach 1 again.

b) Nozzles far from the deflector

A second example is computed where the rocket separation from the deflector is taken as 20 nozzle diameters equal to 76 feet. The mass admitted to the initial flow is estimated as 1.22 times the exit flow and the conditions through the deflection calculated using the same methods and equations as immediately above. The resulting flow conditions are presented below

| Station | V ft/sec | p lb/in$^2$ | ρ lb/ft$^3$ | A ft$^2$ |
|---|---|---|---|---|
| e | 8100 | 12.7 | 0.00728 | 10.4 |
| 1 | 3570 | 14.7 | 0.01060 | 39.2 |
| 2 | 3090 | 14.7 | 0.01009 | 47.5 |

## 5.6 Noise Prediction Technique and Examples

So that the noise produced by the deflected rocket exhaust can be calculated, the flow pattern is considered in two parts. The noise produced by the flow from the rocket exit to the deflector is calculated and added to the noise produced by the deflected flow down the plane.

### 5.6.1 The Flow Before the Deflection

The methods of Chapters 2 and 3 are used here. First the total overall power of the rocket is calculated as if no deflection is occurring. The exit conditions and nozzle dimensions are used to calculate the critical dimensions by the method of Appendix C and these are used with equation 2.3 to calculate the total noise produced. The rocket exhaust up to the deflection is then considered as a noise source and the generalized curves of Figures 30 and 33 are used to determine the sound field from the initial part of the exhaust. The directivity patterns of Figure 31 are applied if the sound pressure level at a specific point is required. Then the far field noise from this part of the flow may be computed from

$$SPL = PWL - 10 \log_{10} 2\pi R^2 \qquad 5.42$$

in db (re 0.0002 dyne/cm$^2$) where R is the distance in feet. This is assuming hemispherical radiation.

The flow is then calculated to find the conditions of the downstream deflected flow pattern.

### 5.6.2 The Deflected Flow

The "mean" flow conditions after the deflection are calculated, $V_2$, $\rho_2$ and $A_2$, and these values are used to determine an equivalent rocket flow. Some idea of the aspect ratio of the flow is determined, and also the likely changes in the aspect ratio as the flow precedes downstream. If it is unrestrained except by the deflector plane, then the results of Anderson and Johns (Reference 32) and Higgins and Wainwright (Reference 34) indicate that it will retain this high aspect ratio. However if it is restrained by a channel deflector with high walls and is then directed up into the air, the aspect ratio of the deflected flow mixing region will be nearer unity, and the simple circular jet radiation patterns can be used. The problem of the noise directivity of the deflected flow when it is a high aspect ratio flow is complicated by a gradual transition into a circular flow which results in different patterns for the different frequency bands.

Tyler, Sofrin and Davis (Reference 35) investigated the noise from a number of rectangular nozzles and obtained results which show a slight overall reduction in the sound power produced. Using a J57 engine with several rectangular nozzles they measured the sound field around the mixing flow. While they recorded some slight reduction in the overall sound field, the major result was the ellipticity of the sound field produced. Figure 65 presents their generalized results for attenuation of the overall signal measured by the microphones opposite to the short edges of the rectangular nozzles. These results show an attenuation rising to almost 15db. at aspect ratios of 50 to 1. They also report that the ellipticity of the higher frequencies is greater and this is obviously due to the mixing region nearest to the exit retaining its higher aspect ratio compared to the downstream region.

To see if this effect is observed with deflected rocket exhausts which, according to the present analysis should show a high aspect ratio deflected flow, the results of Cole, England and Powell (Reference 11) have been examined. Configuration D of their experiments consists of a curved plate deflector and a 2.60 inch exit diameter rocket spaced at 4.0 inches from the exit to the deflector. The rocket impinges on the deflector at approximately $30^\circ$ and is then swept through $90^\circ$ by the deflector. There are no restraining sides to the deflector plate and so this configuration would be expected to produce a high aspect ratio deflected flow. The rocket is fired horizontally and the jet deflected out at various angles, the microphones being arranged in a semicircle in the ground plane. Interpolating the results enable the overall and octave band levels to be obtained when the deflection is vertically upwards. These results are plotted in Figure 66 where the angle

$\theta$ is that angle the microphones make around the deflected flow, in a plane perpendicular to this direction of the deflected flow. Angle $0^{\circ}$ is back behind the rocket, $90^{\circ}$ is at right angles to the rocket casing and is therefore opposite the narrow side of the deflected flow. This figure shows the directivity expressed in db relative to the lowest sound pressure level measured in that octave band. Also shown is the overall level.

The results show that the smallest sound pressures are measured generally opposite the short side of the flow, and that the directivity is greatest for the higher frequencies. The lower values at $0^{\circ}$ are believed to be due to the shielding effect of the rocket and its mounting stand. These results both bear out the results of Tyler, Sofrin and Davis, and also the fact that the deflected flow has a high aspect ratio. This of course complicates estimating the noise from a high aspect ratio deflected flow. Fortunately for large rockets the deflected flow is well constrained by the deflector side walls so that when it is ejected out into the atmosphere, it is almost circular in cross-sectional area. The noise pattern produced is then similar to that for a circular rocket or jet flows.

The high aspect ratio of the deflected flow down the plane means that prediction techniques to give the spectrum of the noise power are notoriously weak, as is discussed by Eldred, et al, (Reference 18) when considering a slot jet. Experimental measurements from slot nozzles indicate a much higher low frequency sound content than expected, the spectrum being much broader than estimates based on the nozzle width as a critical dimension.

Eldred discusses the weakness of replacing a slot jet by a row of equivalent small diameter circular nozzles and suggests that this difference is due to the different mixing characteristics of slot and two dimensional jets. The center line maximum velocity decay is much slower for a slot jet and the relationships for power per unit axial length suggested for circular nozzles cannot be used. Figure 67 shows the results of Coles (Reference 36) for a 100:1 slot nozzle and the results for the standard J57 engine. Also shown is the results for overall sound pressure level measured by Boeing (Reference 1) for a deflected rocket based on ground plane measurements and this too shows a very wide and flat spectrum. Because of the slower fall off in center velocity of the slot mixing region, the rate of sound generation per unit axial length will not decay as fast as for the circular jet.

It is suggested that this low frequency effect can be predicted by choosing a characteristic dimension based on an equivalent circular nozzle and then broadening the spectrum by applying a frequency correction curve based on aspect ratio. In estimating the sound pressure level at any point, corrections must be applied for the ellipticity of the sound field produced. The additional low frequency is allowed for on a different normalized power level curve, which falls off at 3 db per octave instead of 6 db as for the

circular jet spectrum. The higher frequencies must be reduced to allow for this effect so that the overall level remains constant. The corrected curve for use when the aspect ratio of the flow is greater than 5:1 is shown in Figure 68, and the dimension used here is the equivalent diameter or diameter of the equal circular area. The frequency ellipticity is allowed for using the normalized curve in Figure 69, which is deduced from the results of Tyler, et al, (Reference 35) and Coles, et al, (Reference 11).

### 5.6.3 Examples of the Sound Generated by Deflected Rockets

The first example considered is that of the small rocket reported by Boeing (Reference 1). From the exit conditions the downstream flow conditions after the deflection are calculated in Section 5.5. Completing the calculations of Appendix D give the characteristic velocity as 3350 ft/ sec and the characteristic throat area as 0.073 $ft^2$, and characteristic diameter as 0.345 ft. The aspect ratio of the deflected flow is estimated as 20:1. This is for the half flow, giving a value of 10:1 for the whole flow. Taking half this value again, the characteristic dimension for determining the spectrum is taken as 1.725 ft. The overall sound power generated by the deflected flow is found to be 169.9 db relative to $10^{-12}$ watts. Taking half of this value, since the rocket flow was doubled gives 166.9 db.

The spectrum is calculated using the corrected result for the slot jet in Figure 68 and is compared to the measured value in Figure 70. The calculated curve overestimates the center band of frequency noise generated and also produces a less broad spectrum. The overall level is found to be approximately 5 db higher than the measured value. The exact details as to how the measured spectrum was obtained are not given. If, as believed, the measured spectrum was estimated from ground plane sound pressure level measurements only, with no correction for the different distribution around the deflected flow, then the agreement is considered fairly good. This effect would also allow for the discrepancies in the overall levels.

A second example with this smaller rocket considers the case when the nozzle to deflector distance is increased to 20 nozzle exit diameters. Here the sound pressure level at a position on the ground plane at $90^{\circ}$ to the deflected flow direction is calculated, and the full directivity and source distribution curves of Chapter 3 are used. The results are plotted in Figure 71 where the sound pressure calculated for the two parts and the overall spectrum obtained by addition are plotted. This value is compared to a curve for the sound pressure level at this point computed from the previous example when the nozzle was much nearer the deflector. Two points are illustrated.

a) the way in which the undeflected flow produces the high frequency sound

b) the way in which the spectrum alters, to include higher frequencies as the rocket rises from the deflector. This effect has been confirmed experimentally for near field noise, at least, as shown in Figure 74.

This latter effect shows how the deflector destroys a certain part of the high frequency sound and in turn shows the necessity for a good prediction technique. When the rocket is being tested early in its developement, on a static firing range, measurements of the sound field may give a false picture of the high frequency acoustic loading. When the rocket rises it is possible, under certain circumstances, that the high frequency loading on some critical components may increase and cause failure.

The final examples concern a large clustered rocket and the flow conditions are those of the flow examples of Section 5.5. The rocket here is considered close to the deflector, at 5 individual nozzle diameters distance for the first example and 20 nozzle diameters for the second example. The calculated flow conditions are used to obtain the sound pressure levels at 600 feet from the nozzles and at 90° to the deflected flow and the calculated spectra are compared with the measured values from Reference 39 in Figures 72 and 73. Examination of the two spectra shows that the predicted curve underestimates the center frequencies of the spectrum. This is in direct contrast to the results obtained for the small rocket, and so indicates the limitations of the prediction technique.

## 5.7 Discussion

The analysis presented in this chapter is only approximate in that "mean" values must be used to describe the flow. However until sufficient information is available to produce a more exact theory of hot rocket exhaust gas mixing, it is necessary to rely on such a method.

The basic idea of dividing the flow into two parts appears to be suitable and fairly accurate when the final predicted results are compared to the limited reported values for deflected rocket flow and noise. The main difficulty in the flow analysis is the determination of the flow through the deflection. If any part of the impinging jet is supersonic then shock waves will be formed. The simple two-dimensional shock relationships only truly apply if the whole flow is supersonic. The calculation of a three dimensional flow deflection will be very complex and so this shock calculation method is limited to when the rocket is very close to the deflector. Otherwise the use of the equations of continuity, momentum and energy are used, and this in turn involves an assumption that the pressure at the downstream station returns to atmospheric in a short distance.

The use of a normalized spectrum results in a consistent series of noise results, as shown in the examples. The major difficulty in the noise analysis is obtaining generalized curves that take account of the high aspect ratio flows produced by the deflection.

## 6.0 CONCLUSIONS

In this report, the problem of predicting the noise generated by rocket exhaust flows has been considered and a comparison has been made between the various published overall noise and sound field prediction techniques. The analysis has shown the manner in which certain experimental results may be normalized in terms of the rocket exhaust flow parameters, the nozzle and missile geometry and the atmospheric conditions, to provide generalized curves for rocket noise. In Chapters 4 and 5, these results have been applied to the study of clustered rockets and deflected rocket exhausts.

To calculate the overall noise power produced by a rocket, the expression given in equation 2.3 is recommended, and the spectrum of this overall noise power is obtained from Figure 8. These expressions are in terms of a characteristic velocity and diameter, which are calculated from the exhaust flow parameters by the method given in Appendix C. The directivity of noise radiation is given by the curves of Figures 9 through 16, and it is recognized that some difficulty may arise in the application of these curves. The limited published results cannot be normalized easily and the physical dimensions of the rocket flow appear to have a definite bearing on the directivity pattern.

Noise estimation from the near field measurements on the 10 degree boundary shows more promise. A normalized source spectrum given in Figure 30 allows the allocation of a spectrum of sources at each position in the exhaust flow. This, when combined with the directivity patterns of Figure 31, produces the sound pressure level at the required point. However it is noted that these directivity curves were computed on the basis of turbojet results and not rocket flows. They are presented here since sufficient near field correlation measurements for rocket exhaust flows are not available. The only justification for their use is the accuracy of the predicted levels when compared to actual measurements of rocket noise.

The allocation of overall sound sources down the exhaust flow is not such a clear cut procedure. The various reported results cannot be simply normalized and the resultant mean curve, given in Figure 33, cannot be considered too accurate or the best available result. Further work concerning this point, including a full set of near field measurements on various rocket exhaust flows, is required. This would also include correlation measurements to allow a full examination of the near field directivity of the noise sources.

The clustered nozzles and deflected rocket exhaust noise fields are determined by first obtaining a mean value for the exhaust flow at each

downstream station. The prediction techniques of Chapter 3 are then applied to the individual parts of the flow, to give the required sound pressure levels.

In the case of the deflected rocket stream, the flow and noise fields before and after deflection are considered separately. Figures 30 and 33 are used again to calculate the noise power produced by the undeflected flow. The flow conditions after deflection ( at Station 2 ) are calculated as described in Section 5.3.2 and these used to determine an equivalent rocket flow and the noise power produced by this flow determined. Some consideration is given to the flow down the deflector so that corrections to the spectrum shape, due to the aspect ratio of the particular flow can be made from figures 68 and 69.

The deflected rocket noise examples, presented in this report show good agreement with measured values. In particular the prediction method shows how the deflector destroys part of the high frequency noise when a vehicle is on the launch pad and it also shows the way in which the noise spectrum shifts to include these higher frequencies as a vehicle rises from the deflector.

Published measurements of deflected rocket exhaust flow parameters are presently very limited, and the analysis of these measurements in Chapter 5 suggests some inconsistencies in the results. Further measurements of deflected flow parameters, including measurements of the various profiles and static pressure in the deflector region are desirable.

APPENDIX A

## Calculation of the Mass Flow at Various Stations Downstream in a Constant Density Jet with No External Velocity

In order to obtain some idea of the mass entrained into a jet when it mixes turbulently with the atmosphere the following brief calculation for a constant density jet is presented. Naturally it is not sufficient to directly estimate rocket mass flows from this result and the full calculations as indicated in Chapters 4 and 5 must be used, but it is instructive to be able to visualize the large mass of the entrained air.

Representing the jet velocity profile by the expression used by Eldred, et al. (Reference 18)

$$u = U \cdot e^{-\eta^2/2} \qquad A.1$$

where $U$ is the maximum velocity and
$\eta = (r - a) / b$
$a$ is the width of the core and
$b$ is the width parameter of the mixing region as defined in Reference 18, and used in Chapters 4 and 5 and
$r$ is the radial distance from the center line to the point considered

Between the nozzle exit and the tip of the core, approximate expressions for a and b are

$$b = R \frac{x}{x_t} \qquad A.2$$

$$a = R \left( 1 - \frac{x}{x_t} \right) \qquad A.3$$

where $x_t$ is the distance to the tip of the core and
$x$ is the distance downstream to the station under consideration and
$R$ is the exit radius.

The maximum velocity is the nozzle exit velocity

$$U = U_e \qquad \text{A.4}$$

The expressions for a and b are only approximate, but calculations in Reference 18 indicate that they are within 3 per cent of the exact solutions.

Downstream of the tip of the core the expressions for a, b and U become

$$b = 0.5\ R \left[1 + \frac{x}{x_t}\right] \qquad \text{A.5}$$

$$a = 0 \qquad \text{A.6}$$

$$U = \frac{2\ U_e}{1 + \frac{x}{x_t}} \qquad \text{A.7}$$

1) At a station up to the core tip, the mass flow is

$$\dot{m}_x = \rho \int_o^{R_o} 2\pi r\ u\ dr \qquad \text{where } u = 0, \text{ at } r = R_o$$

Thus $\dot{m}_x = 2\pi\rho \int_o^a U_e\, r\, dr + 2\pi\rho \int_a^{R_o} r\, U_e\, e^{-\eta^2/2}\, dr$

But $\eta = (r - a)/b$, thus $r = b\eta + a$ and $dr = b\, d\eta$ ;

now when $r = a$, $\eta = o$.

and when $r = R_o$, $\eta = \infty$.

Then $\dot{m}_x = 2\pi\rho\, U_e \left[\frac{r^2}{2}\right]_o^a + 2\pi\rho\, U_e \int_o^\infty (b\eta + a)\, b\, e^{-\eta^2/2}\, d\eta$

$$= \pi\rho\, U_e \left[a^2 + 2\int_o^\infty b^2\, \eta\, e^{-\eta^2/2}\, d\eta + 2\int_o^\infty ab\, e^{-\eta^2/2}\, d\eta\right]$$

$$= \pi\rho\, U_e \left[a^2 + 2b^2 + 2ab\sqrt{\frac{\pi}{2}}\right]$$

$$\dot{m}_x = \pi\rho U_e \left[ a^2 + \sqrt{\pi}\, ab + b^2 + b^2 + \left(\sqrt{2} - 1\right)\sqrt{\pi}\, ab \right]$$

$$= \pi\rho U_e \left[ R^2 + b^2 + \left(\sqrt{2} - 1\right) \sqrt{\pi}\, ab \right]$$

since $a^2 + \sqrt{\pi}\, ab + b^2 = R^2$ (See Ref. 18)

Substitute for a and b from equations A2 and A3; then the mass flow at downstream station x, compared to the mass flow at the nozzle exit, is

$$\frac{\dot{m}_x}{\dot{m}_e} = \left[ 1 + \left(\frac{x}{x_t}\right)^2 + \left(\sqrt{2} - 1\right) \sqrt{\pi} \left(1 - \frac{x}{x_t}\right) \frac{x}{x_t} \right] \qquad \text{A.8}$$

At the core tip $x = x_t$ and

$$\frac{\dot{m}_{x_t}}{\dot{m}_e} = 2$$

2) At a station after the core tip the mass flow is

$$\dot{m}_x = \rho \int_o^{R_o} 2\pi r \; u \; dr \qquad \text{where } u = 0, \text{ at } r = R_o$$

$$= 2\pi\rho \; U \int_o^{\infty} b^2 \; \eta \; e^{-\eta^2/2} \; d\eta$$

$$= 2\pi\rho \; U \; b^2$$

Substitute for b and U from equations A.5 and A.7

$$\dot{m}_x = \pi \rho U_e \; r_e^2 \left[1 + \frac{x}{x_t}\right]$$

So

$$\frac{\dot{m}_x}{\dot{m}_e} = \left[1 + \frac{x}{x_t}\right] \qquad \text{A.9}$$

and at $x = x_t$, $\dot{m}_x / \dot{m}_e = 2$

Equations A.8 and A.9 are plotted in Figure A.1 and show the rapid increase of the mass flow of the mixing region.

APPENDIX B

Determination of Deflection Angle for Impingement Shock Wave Separation for a Uniform Supersonic Deflected Jet

When a supersonic jet impinges on a deflecting surface, normally a shock wave is formed which is attached to the surface. However as the deflection angle is increased, a stage is reached where the shock wave becomes detached from the surface and some back-flow up the deflector occurs. Since damage to the vehicle can be caused if too much back flow occurs, this condition and the deflection angle at which it first occurs, is of interest in deflector design.

Consider the case of a uniform supersonic jet impinging on an inclined plane. After deflection, the flow is assumed to be parallel and the effects of jet mixing with the surrounding air are neglected.

If the deflection angle is $\delta$, the shock angle $\alpha$ and denoting the conditions before the shock by subscript 1 and after the shock by subscript 2, then the flow may be represented by Figure B 1:

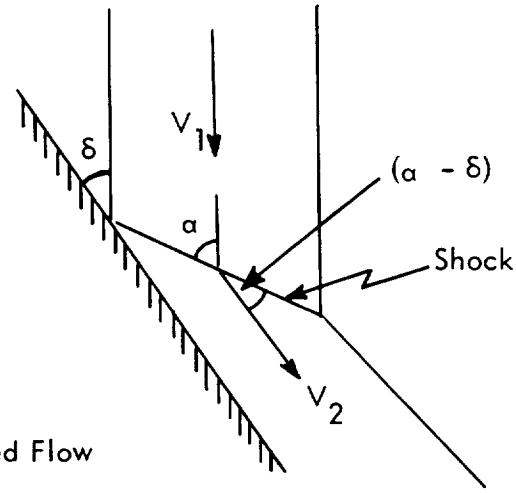


Figure B1. Shock Angles of Deflected Flow

Mass flow, momentum and energy are all assumed to be conserved through a shock wave.

Conservation of mass flow across the shock front gives:

$$\rho_1 V_1 \sin \alpha = \rho_2 V_2 \sin (\alpha - \delta) \qquad (B\ 1)$$

Conservation of momentum normal to the shock, gives:

$$p_1 + \rho_1 V_1^2 \sin^2 \alpha = p_2 + \rho_2 V_2^2 \sin^2 (\alpha - \delta) \qquad (B\ 2)$$

Also conservation of momentum parallel to the shock front gives:

$$\rho_1 V_1^2 \sin \alpha \cdot \cos \alpha = \rho_2 V_2^2 \sin (\alpha - \delta) \cdot \cos (\alpha - \delta) \quad \text{(B 3)}$$

The effects of heat-transfer to the deflector surface and air entrainment are assumed to be small, in the region of impingement, and thus conservation of energy through the shock gives:

$$\frac{\gamma}{\gamma - 1} \cdot \frac{p_1}{\rho_1} + \frac{V_1^2}{2} = \frac{\gamma}{\gamma - 1} \cdot \frac{p_2}{\rho_2} + \frac{V_2^2}{2} \quad \text{(B 4)}$$

Combinations of the above equations yield the following results:

$$V_2 = V_1 \frac{\cos \alpha}{\cos (\alpha - \delta)} \quad \text{(B 1) and (B 3)} \quad \text{(B 5)}$$

$$p_2 = p_1 + \rho_1 V_1 \sin \alpha \left[ V_1 \sin \alpha - V_2 \sin (\alpha - \delta) \right] \quad \text{(B 1) and (B 2)} \quad \text{(B 6)}$$

thus

$$p_2 = p_1 + \rho_1 V_1^2 \left[ 1 - \frac{\tan (\alpha - \delta)}{\tan \alpha} \right] \sin^2 \alpha \quad \text{(B 6) and (B 5)} \quad \text{(B 7)}$$

$$\rho_2 = \rho_1 \frac{\tan\alpha}{\tan(\alpha - \delta)} \qquad \text{(B 1) and (B 5)} \qquad \text{(B 8)}$$

If these expressions for $V_2$, $p_2$ and $\rho_2$, (equations B5, B7, and B8), are substituted into equation B4, together with the relations for speed of sound and Mach number,

$$a_1^2 = \frac{\gamma p_1}{\rho_1} \qquad \text{(B 9)}$$

and

$$M_1 = \frac{V_1}{a_1} \qquad \text{(B 10)}$$

then equation B4, after some manipulation may now be rewritten:

$$\frac{1}{M_1^2} = \sin^2 \alpha - \frac{\gamma + 1}{2} \cdot \frac{\sin\alpha \sin\delta}{\cos(\alpha - \delta)} \qquad \text{(B 11)}$$

For specific values of Mach number $M_1$, and the ratio of specific heats for the exhaust gas, $\gamma$, as the deflection angle $\delta$ is increased, this equation becomes indeterminate at a certain critical shock wave angle $\alpha$ and deflection angle $\delta$. In the physical case, this represents a deflection angle $\delta$, at which the shock wave will separate and back flow will occur up the deflector plane.

In practice, of course, some back flow will occur at smaller angles of $\delta$, since the impinging jet will not be of uniform velocity and the flow in the boundary of the jet will not have sufficient energy to negotiate the shock wave.

For a Mach number of 3.12 and $\gamma$ of 1.2, the critical angle occurs at a deflection angle $\delta$ of approximately $42^\circ$ (reference 37).

APPENDIX C

Solution of the Rocket Exhaust Gas Flow at the Nozzle Throat, from the Exit Conditions, and the Calculation of the Characteristic Diameter and Velocity.

In order to use the generalized formulae for total acoustic power and spectrum of total acoustic power generated, it is necessary to determine a certain characteristic velocity and diameter. In the expressions given by Eldred, Roberts and White (Reference 8 ), these characteristic values are based on the throat conditions of the flow. If these values are not known, they can be quickly calculated from the exit conditions of the gas on the assumption of isentropic flow.

Given the exit pressure, density, velocity, temperature and ratio of specific heats for the exit gas, the throat conditions are obtained by calculating the critical values for the defined fluid. Because the rocket will operate at pressure ratios much greater than the critical values and since the nozzle will be of the convergent-divergent type, the flow conditions at the throat of the nozzle will be the critical values. The velocity, for example, will equal the critical speed of sound in the gas, $a_*$ , since the Mach number must be 1 at this point. A full description of supersonic nozzle flow is given by Miles in Chapter 1 of his book (Reference 38), and for the design of actual nozzle contours see Handbook of Astronautical Engineering, Chapter 20, (Reference 37). The basic equations for determining the characteristic values of velocity and diameter are given in the following paragraphs.

Starting from the exit conditions of the exhaust gas, the speed of sound at the exit is given by,

$$a_e = \sqrt{\frac{\gamma p_e}{\rho_e}} \qquad C.1$$

where $\gamma$ is the ratio of specific heats of the fluid
$p$ is the pressure
$\rho$ is the density and
subscript e denotes the exit conditions

The "maximum" velocity is obtained when the fluid exhausts into a vacuum and is,

$$V_{max} = \left(V_e^2 + \frac{2}{\gamma - 1} a_e^2\right)^{1/2} \qquad C.2$$

where $V_e$ is the gas exit velocity.

The critical speed of sound for the gas, (the velocity at the throat) is then obtained from

$$a_* = \left(\frac{\gamma - 1}{\gamma + 1}\right)^{1/2} \cdot \quad V \text{ max} \qquad \text{C.3}$$

The exit Mach No. is given by

$$M_e = \frac{V_e}{a_e} \qquad \text{C.4}$$

Then the total pressure and density are,

$$p_o = p_e \left[1 + \frac{\gamma - 1}{2} M_e^2\right]^{\frac{\gamma}{\gamma - 1}} \qquad \text{C.5}$$

$$\rho_o = \rho_e \left[1 + \frac{\gamma - 1}{2} M_e^2\right]^{\frac{1}{\gamma - 1}} \qquad \text{C.6}$$

and the total conditions are related to the critical conditions by

$$p_* = p_o \left[\frac{2}{\gamma + 1}\right]^{\frac{\gamma}{\gamma - 1}} \qquad \text{C.7}$$

$$\rho_* = \rho_o \left[\frac{2}{\gamma + 1}\right]^{\frac{1}{\gamma - 1}}$$

Hence, the critical conditions, or the values at the the throat, are,

$$p_* = p_e \left[ \frac{2}{\gamma + 1} + \frac{\gamma - 1}{\gamma + 1} \cdot M_e^2 \right]^{\frac{\gamma}{\gamma - 1}} \qquad C.9$$

$$\rho_* = \rho_e \left[ \frac{2}{\gamma + 1} + \frac{\gamma - 1}{\gamma + 1} \cdot M_e^2 \right]^{\frac{1}{\gamma - 1}} \qquad C.10$$

The diameter of the throat is then given by

$$D_t^2 = D_e^2 \cdot \frac{\rho_e \, V_e}{\rho_t \, V_t} \qquad C.11$$

Where suffix t indicates the throat conditions, and is equal to the critical conditions.

Hence,

$$D_t = D_e \sqrt{\frac{\rho_e \, V_e}{\rho_* \, a_*}} \qquad C.12$$

The characteristic velocity and diameter.

The characteristic velocity used in the generalized formulae of Eldred et al. (Reference 8 ) is the throat velocity

$$V_c = V_t = a_* \qquad \text{C.13}$$

The characteristic diameter which best fits the experimental results, as suggested by Eldred, Roberts, and White (Reference 8 ), is based on an isothermal expansion of the throat gas to atmospheric conditions. This derivation was determined by comparison with the results of sonic jets and is based on a continuity of the flow in the rocket stream. By using these characteristic values, the basic Area x Velocity to the eighth law may be retained for supersonic jets and rockets. Then the characteristic diameter:

$$D_c = D_t\left(\frac{p_t}{p_a}\right)^{1/2} \qquad \text{C.14}$$

where $p_a$ is the atmospheric pressure of the air with which the rocket gas is mixing.

$$D_c^2 = D_e^2 \cdot \frac{\rho_e}{\rho_*} \cdot \frac{p_*}{p_e} \cdot \frac{V_e}{V_t} \cdot \frac{p_e}{p_a} \qquad \text{C.15}$$

$$= D_e^2 \left[\frac{2}{\gamma+1} + \frac{\gamma-1}{\gamma+1} M_e^2\right]^{\gamma} \cdot \frac{V_e}{a_*} \cdot \frac{p_e}{p_a}$$

The generalized expressions for acoustic power generation also include a term which is a function of the temperature of the gas. The temperature normally is the exit gas temperature but the nozzle throat temperature can be quickly calculated.

The gas constant for the gas is

$$\underline{R} = \frac{p_e}{g\rho_e T_e} \qquad \text{C.16}$$

and the total temperature is given by

$$T_o = a_*^2 \, (\gamma + 1) \, / \, 2 \gamma g \underline{R} \qquad \text{C.17}$$

Then $T_*$ , the temperature at the throat, is given by

$$T_* = \frac{T_o \rho_o p_*}{p_o \rho_*} \qquad \text{C.18}$$

For most rocket gas flows from existing rockets $T_* = T_t$ is very near $T_e$.

Procedure for Determining the Characteristic Diameter and Velocity

Starting with the exit values for velocity, density, pressure and the ratio of specific heats $V_e$, $\rho_e$, $p_e$, $\gamma$

1) $$a_e^2 = \frac{\gamma p_e}{\rho_e} \qquad \text{C.1}$$

2) $$V_{max} = \left( V_e^2 + \frac{2}{\gamma - 1} a_e^2 \right)^{1/2} \qquad \text{C.2}$$

3) $$M_e = \frac{V_e}{a_e} \qquad \text{C.4}$$

4) The characteristic velocity

$$V_c = a_* = \left( \frac{\gamma - 1}{\gamma + 1} \right)^{1/2} V_{max} \qquad \text{C.3}$$

5) The characteristic diameter

$$D_c = D_e \left[ \frac{2}{\gamma + 1} + \frac{\gamma - 1}{\gamma + 1} M_e^2 \right]^{\gamma/2} \left( \frac{V_e}{a_*} \cdot \frac{p_e}{p_a} \right)^{1/2} \qquad \text{C.15}$$

APPENDIX D

## The Meaning of the Use of a Representative "Mean" Velocity for a Non-Uniform Velocity Jet Flow

In Chapter 5, the problem of deflected supersonic jets is approached by considering mean jet properties for the jet before and after impingement; that is that the flow may be considered to be uniform or two dimensional at any downstream station. It is shown here, that this approach is valid at least in the case of the undeflected part of the jet.

For a constant density jet, see Figure D1, with no external velocity, Eldred (Ref. 18) has shown that downstream of the core tip, where the turbulent flow is fully developed, the center line velocity is given by:

$$U = \frac{U_e}{1 + 1.56 \frac{k c^2}{R} (x - x_t)} \quad \text{for } x > x_t \qquad \text{(D 1)}$$

where $$k c^2 = 0.32 \frac{R}{x_t} \qquad \text{(D 2)}$$

thus $$U = \frac{U_e}{1 + 1.56 \times 0.32 \frac{R}{x_t} \cdot \frac{(x - x_t)}{R}} = \frac{2 U_e}{1 + \frac{x}{x_t}} \qquad \text{(D 3)}$$

Now, Eldred has also shown that experimental data indicate that the velocity profile downstream of the core tip $(x > x_t)$ is well represented by:

$$u = U e^{-\eta^2/2}$$

where $$\eta = \frac{r}{b}$$

b is a momentum width parameter

and r is the radial distance from the center line to the point considered.

. Thus mass flow at any station

$$\dot{m} = \rho \int_0^\infty u \cdot 2\pi r \cdot dr$$

$$= \rho U \int_0^\infty e^{-\eta^2/2} \cdot 2\pi r \, dr$$

$$= 2\pi \rho b^2 U \qquad \text{(D4)}$$

$$\text{Momentum} = \rho \int_0^\infty u^2 \cdot 2\pi r \cdot dr$$

$$= \rho U^2 \int_0^\infty e^{-\eta^2/2} \, 2\pi r \cdot dr$$

$$= \pi \rho b^2 U^2 \qquad \text{(D5)}$$

If a mean velocity $\bar{U}$, at any station is defined as:

$$\bar{U} = \frac{\text{total momentum}}{\text{total mass flow}}$$

$$\bar{U} = \frac{\pi \rho b^2 U^2}{2\pi \rho b^2 U} = \frac{U}{2} \qquad \text{(D6)}$$

$$\text{Thus} \quad \bar{U} = \frac{U_e}{1 + x/x_t} \qquad \text{(D3) and (D6)} \qquad \text{(D7)}$$

Thus the "mean" velocity at any station downstream of the core tip, in a constant density free jet is seen to be half the center line velocity at that station. The "mean" velocity at any station, downstream of the core tip, is related to the exit velocity by equation (D7).

In the prediction method described in chapter 5, although allowance was made for air entrainment from the atmosphere, when considering the free part of the rocket exhaust before impingement, the flow was still considered to be uniform at any station downstream and thus two-dimensional.

The equations used to describe the flow of the "uniform" free jet before impingement, (see Figure D 2), are:

$$\rho_1 A_1 V_1^2 = \rho_o A_o V_o^2 + A_o (p_o - p_a) \qquad (D7)$$

$$\rho_1 A_1 V_1 = \rho_o A_o V_o + \dot{m}_a \qquad (D8)$$

$$\dot{m}_a = \dot{m}_o \cdot x/x_t \qquad (x > x_t) \qquad (D9)$$

and thus

$$V_1 = \frac{\rho_o A_o V_o^2 + A_o (p_o - p_a)}{\rho_o A_o V_o (1 + x/x_t)} \qquad (D10)$$

and provided $p_o = p_a$,

$$V_1 = \frac{V_o}{1 + x/x_t} \qquad (D11)$$

Comparing equations D(7) and D(11), it is seen that $V_1 = \overline{U}$.

Thus if the free jet is assumed to be "uniform" at any station downstream of the exit, then the velocity computed by the use of equations (D7), (D8) and (D9) will be identical to the "mean" velocity defined in equation (D6) for a constant density free jet, downstream of the core tip.

This velocity will also be half the center line velocity for the constant density free jet at the same station.

It is of interest to note that in the case of the deflected jet, a value of $\bar{U} = 0.486\ U$ was obtained by integrating graphically experimental results of Anderson and Johns (Reference 32).

Values of $2V_1/V_o$ for a small solid fuel rocket have been plotted with values of $\frac{2}{1 + x/x_t}$ against $x/x_t$ in Figure (D3). The reason that the values of $2V_1/V_o$ do not lie exactly on the curve is that $p_o \neq p_a$ for the rocket used in this example.

REFERENCES


1. Morgan, W. V. and Young, K. J. "Studies of Rocket Noise Simulation with Substitute Gas Jets, and the Effects of Vehicle Motion on Jet Noise." Wright Patterson, ASD-TDR-62-787, 1962

2. Morgan, W. V.; Sutherland, L. C. and Young, K. J. "The Use of Acoustic Scale Models for Investigating Near Field Noise of Jet and Rocket Engines." WADD TR 61-178, 1961

3. Cole, J. N.; Von Gierke, H. E.; Kyrazis, D. T.; Eldred, K. M. and Humphrey, A. J. "Noise Radiation from Fourteen Types of Rocket in the 1000 to 130,000 Pounds Thrust Range." WADC, TR 57-354, 1957

4. Zucrow, M. J. "Aircraft and Missile Propulsion." John Wiley and Sons Ltd., 1958

5. Lighthill, M. J. "On Sound Generated Aerodynamically." Part I "General Theory." Proc. Roy. Soc. A. Vol 211, 1952

6. Dyer, I. "Estimation of Sound Induced Missile Vibration." Chapter 9, edited Crandall, S. H. "Random Vibration." Tech. Press. M.I.T., 1958

7. Wilhold, G. A. "Vehicle Environment Prediction Technique." (M-P and Ve ST) MSFC, Huntsville, Alabama, 1962

8. Eldred, K.; Roberts, W. M. and White, R. "Structural Vibrations in Space Vehicles," WADD TR 61-62, 1961

9. Von Gierke, H. E. "Aircraft Noise Sources" Chapter 33 edited Harris, C. M. "Handbook of Noise Control" McGraw Book Co., Inc., 1957.

10. Mayes, W. H.; Lanford, W. E. and Hubbard, H. H. "Near Field and Far Field Noise Surveys of Solid Fuel Rocket Engines for a Range of Nozzle Exit Pressures." NASA TN D-21, 1959

11. Cole, J. N.; England, R. T. and Powell, R. G. "Effects of Various Exhaust Blast Deflectors on the Acoustic Noise Characteristics of 1000 Pound Thrust Rockets." WADD TR 60-6, 1960

12. Lassiter, L. W. and Heitkotter, R. H. "Some Measurements of Noise from Three Solid-fuel Rocket Engines." NACA TN 3316, 1954

13. Bolt, Beranek and Newman, Inc. "100FW3 Solid Fuel Motor Static Firing - Acoustic and Vibration Spectra." Report No. 822, 1962.

14. Bolt, Beranek and Newman, Inc. "DVXL 5-1 Solid Fuel Motor Static Firing - Acoustic and Vibration Spectra" Report No. 1035, 1963

15. Cole, J. N. and Thomas, C. E. "Far Field Noise and Vibration Levels Produced During the Saturn SA-1 Launch" Wright Patterson AFB, ASD TR 61-607, 1961

16. Wilhold, G. A., Guest, S. H. and Jones , J. H. "A Technique for Predicting Far Field Acoustic Environments Due to a Moving Rocket Sound Source." NASA TN D-1832, 1963

17. Lighthill, M. J. "Jet Noise" Wright Brothers Memorial Lecture, AIAA Journal, Vol 1, Part 7, 1963

18. Eldred, K. E.; White, R.; Mann, M. and Cottis, M. "Suppression of Jet Noise, with Emphasis on the Near Field." Wright Patterson AFB, ASD-TDR-62-578, 1963

19. Cole, J. N.; Powell, R. G. and Hille, H. K. "Noise and Vibration Studies at Cape Canaveral Missile Test Annex, Atlantic Missile Range, Vol. 1, Acoustic Noise, " Wright Patterson AFB, ASD TR 61-608 (1), 1962

20. Dorland, W. D. "Far Field Noise Characteristics of Saturn Static Tests." NASA TN D-611, 1961

21. Mull, H. R. and Erickson, J. C. Jr. "Survey of the Acoustic Near Field of Three Nozzles at a Pressure Ratio of 30." NACA TN 3978, 1957

22. Franken, P. A. "Methods of Space Vehicle Noise Prediction" WADC TR 58-343, Vol II, 1960

23. Howes, W. L. and Mull, H. R. "Near Noise Field of a Jet Engine Exhaust, I-Sound Pressures." NACA TN 3763, 1956

24. Cummings, N.; Tedrick, R. N. and Dorland, W. D. "Results of Acoustical Survey of SA-3 Launch" MSFC, MTP-TEST-63-2, 1963

25. Tedrick, R. N. and Thornton, C. C. "Results of the Far Field Acoustical Survey of the SA-4 Launch" MSFC, MTP-TEST-63-5, 1963

26. Laurence, J. C. "Intensity, Scale and Spectra of Turbulence in Mixing Region of Free Subsonic Jet." NACA Report 1292, 1956

27. Squire, H. B. and Trouncer, J. "Round Jets in a General Stream." British ARC, R and M No. 1974, 1944

28. Boeing Company, Seattle, Washington. "Clustered Model Rocket Acoustics Test." Report No. T2-2574, 1964

29. Ames Research Staff "Equations, Tables and Charts for Compressible Flows." NACA Report 1135, 1953

30. Duncan, W. J.; Thom, A. S. and Young A. D. "The Mechanics of Fluids." p. 492. Edward Arnold (Publishers) Ltd., London. 1960

31. Briggs, J. L. "Comment on Calculation of Oblique Shock Waves." AIAA Journal, Vol. 2, No. 5, p. 974, 1963

32. Anderson, A. R. and Johns, F. R. "Nondimensional Characteristics of Free and Deflected Supersonic Jets Exhausting into Quiescent Air" Report NADC-ED-5401, 1954

33. Pitkin, E. T. and Glassman, I. "Experimental Mixing Profiles of a Mach 2.6 Free Jet." Journal of the Aero/Space Sciences, Vol. 25, p. 791, 1958

34. Higgins, C. C. and Wainwright, T. W. "Dynamic Pressure and Thrust Characteristics of Cold Jets Discharging from Several Exhaust Nozzles Designed for V.T.O.L. Downwash Suppression." NASA TN D-2263, 1964

35. Tyler, J.; Sofrin, T. and Davis, J. "Rectangular Nozzles for Jet Noise Suppression" S.A.E. Journal Vol. 67, 1959

36. Coles, W. D. "Jet Engine Exhaust Noise from Slot Nozzles." NASA TN D-60, 1959

37. Koelle, H. H. editor "Handbook of Astronautical Engineering" p. 28-44 McGraw Hill Book Co., Inc. 1961

38. Miles, E. R. C. "Supersonic Aerodynamics." Dover Publications, Inc. 1961

39. Dorland, W. D. and Tedrick, R. N. "Results of Acoustical Survey of SA-1 Launch" MSFC MTP-TEST-62-2, 1962.

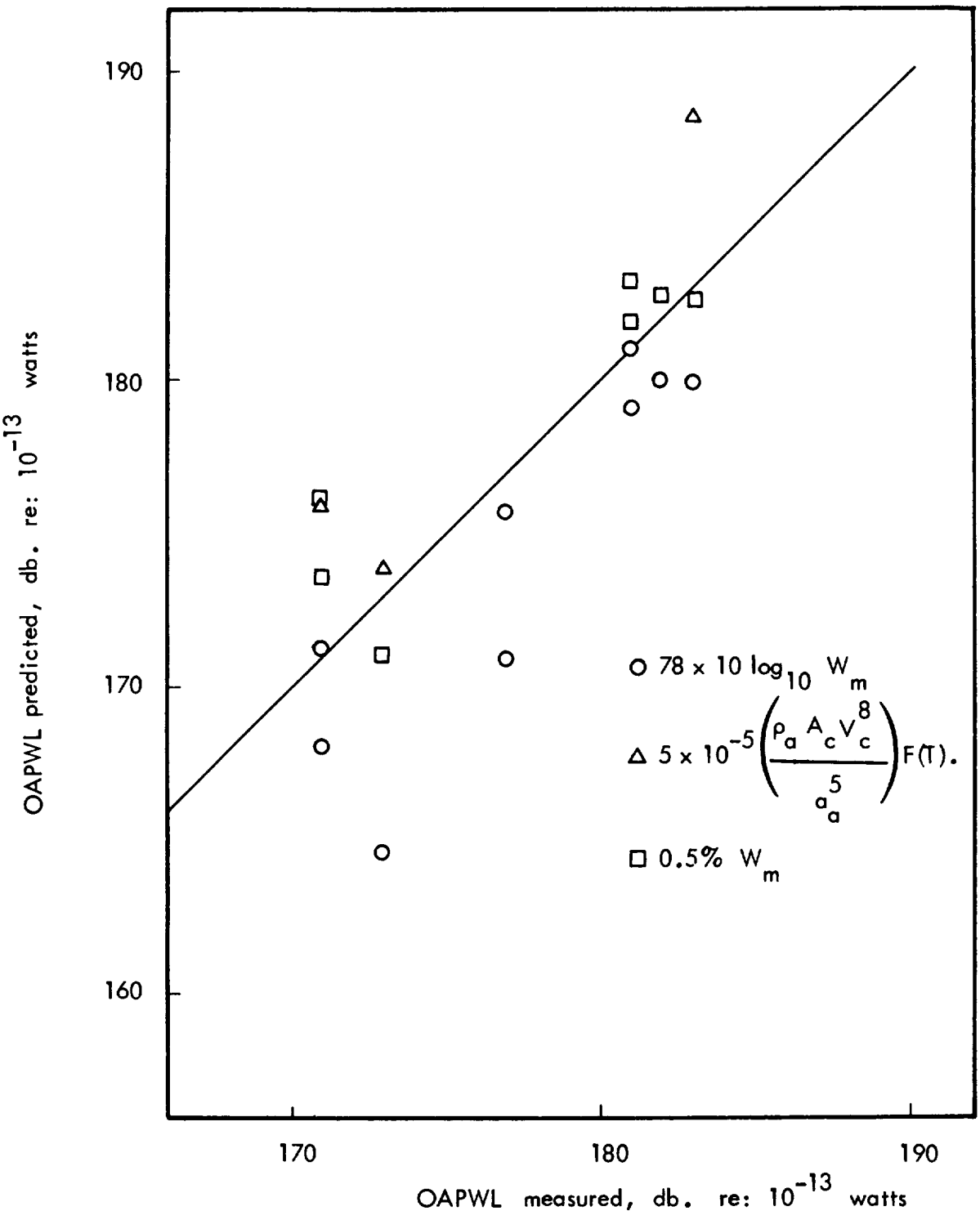


Figure 1: Total Acoustic Power Produced by Rockets

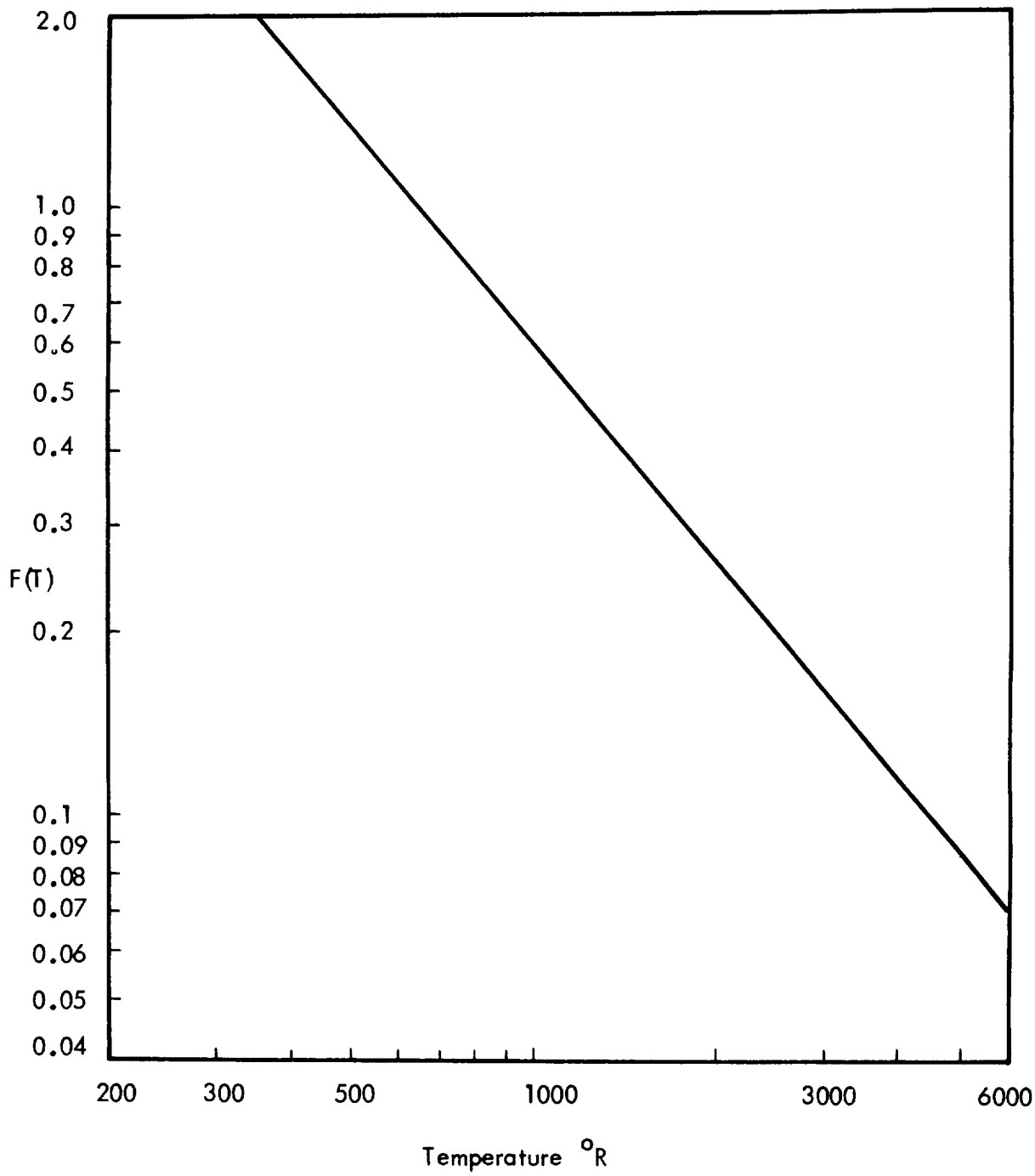


Figure 2 : Temperature Correction for Generalized Overall Power

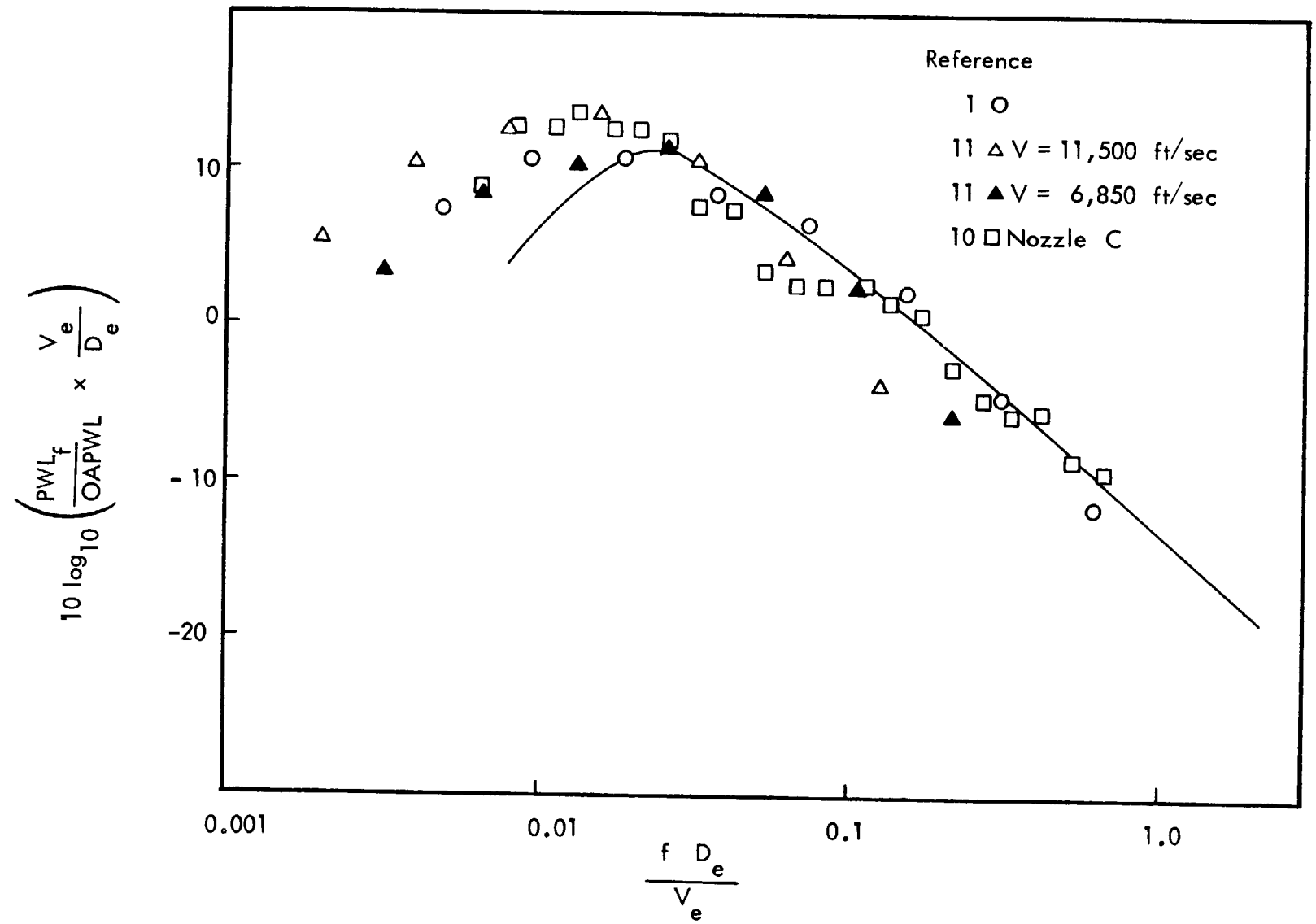


Figure 3 : Normalized Power Spectra of Rocket Noise

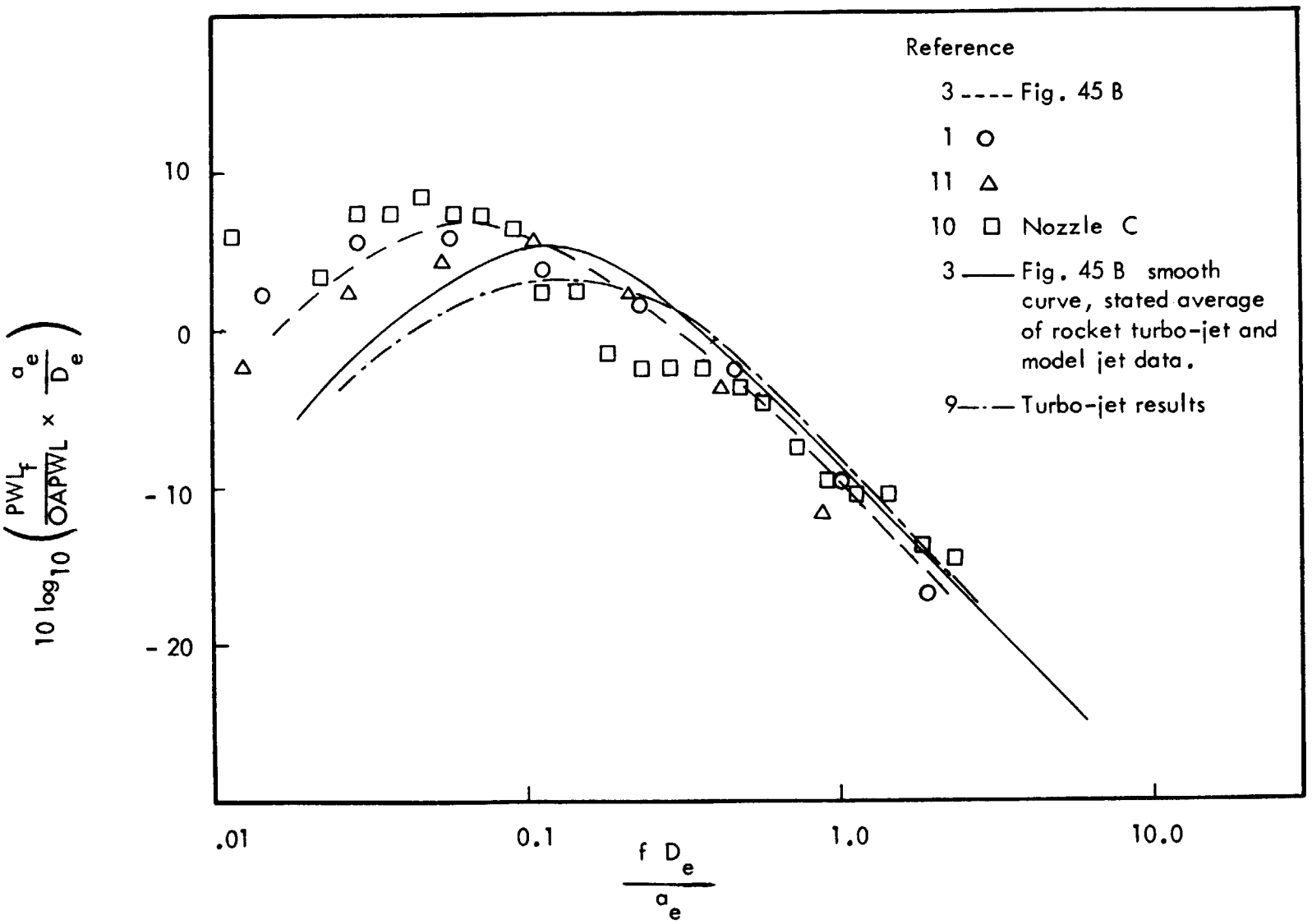


Figure 4 : Normalized Power Spectrum of Rocket Noise

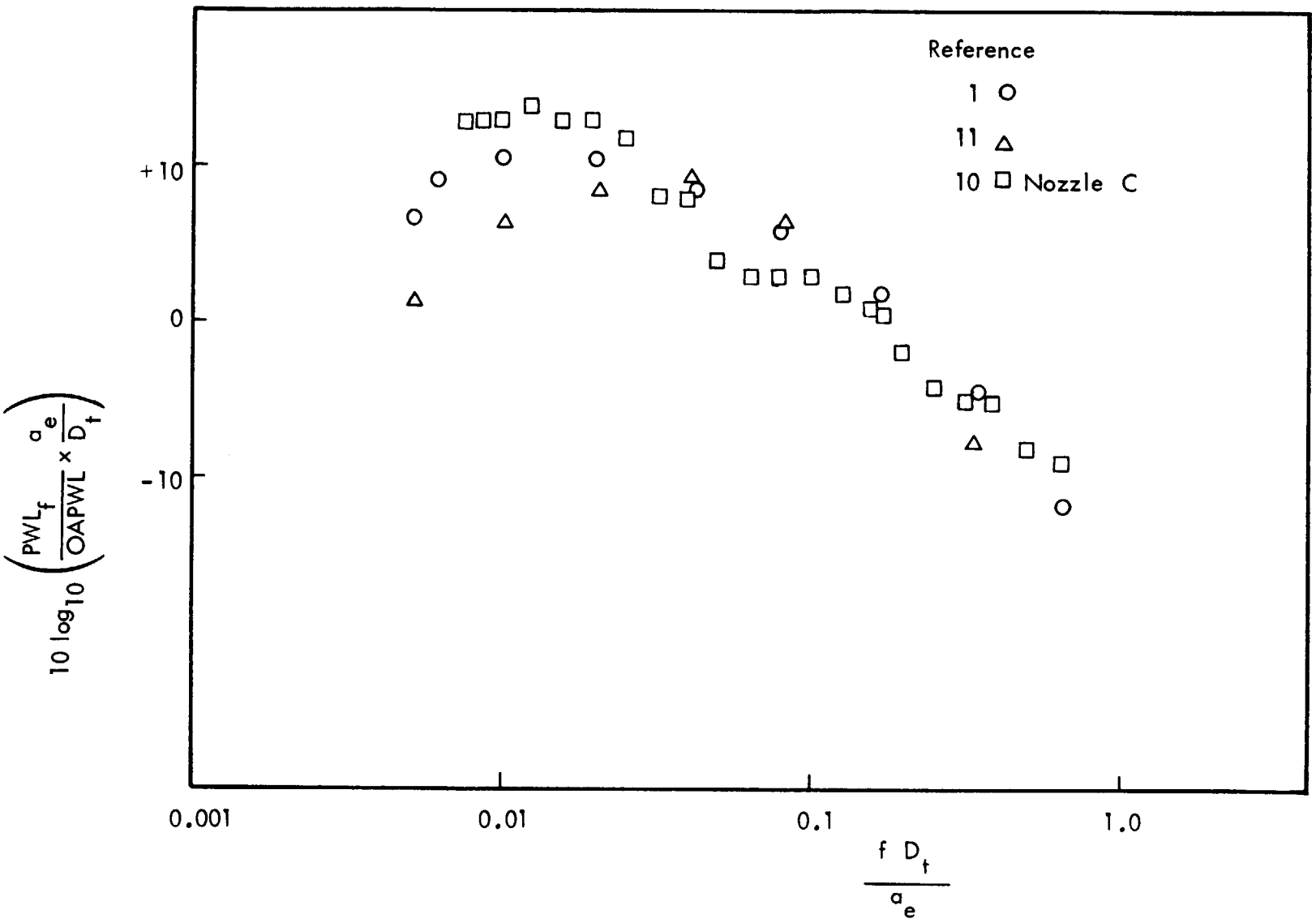


Figure 5 : Normalized Power Spectra of Rocket Noise

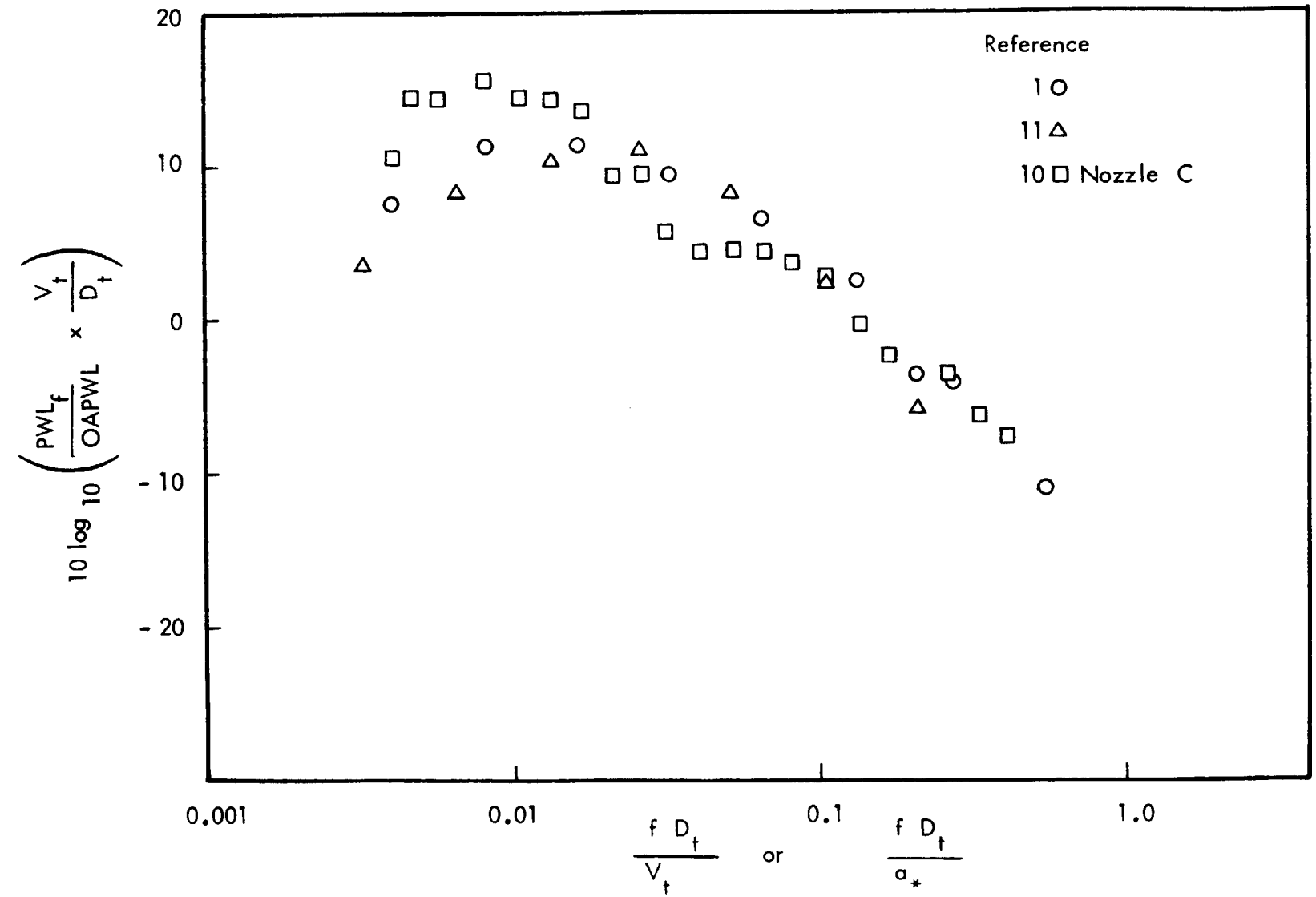


Figure 6 : Normalized Power Spectra of Rocket Noise

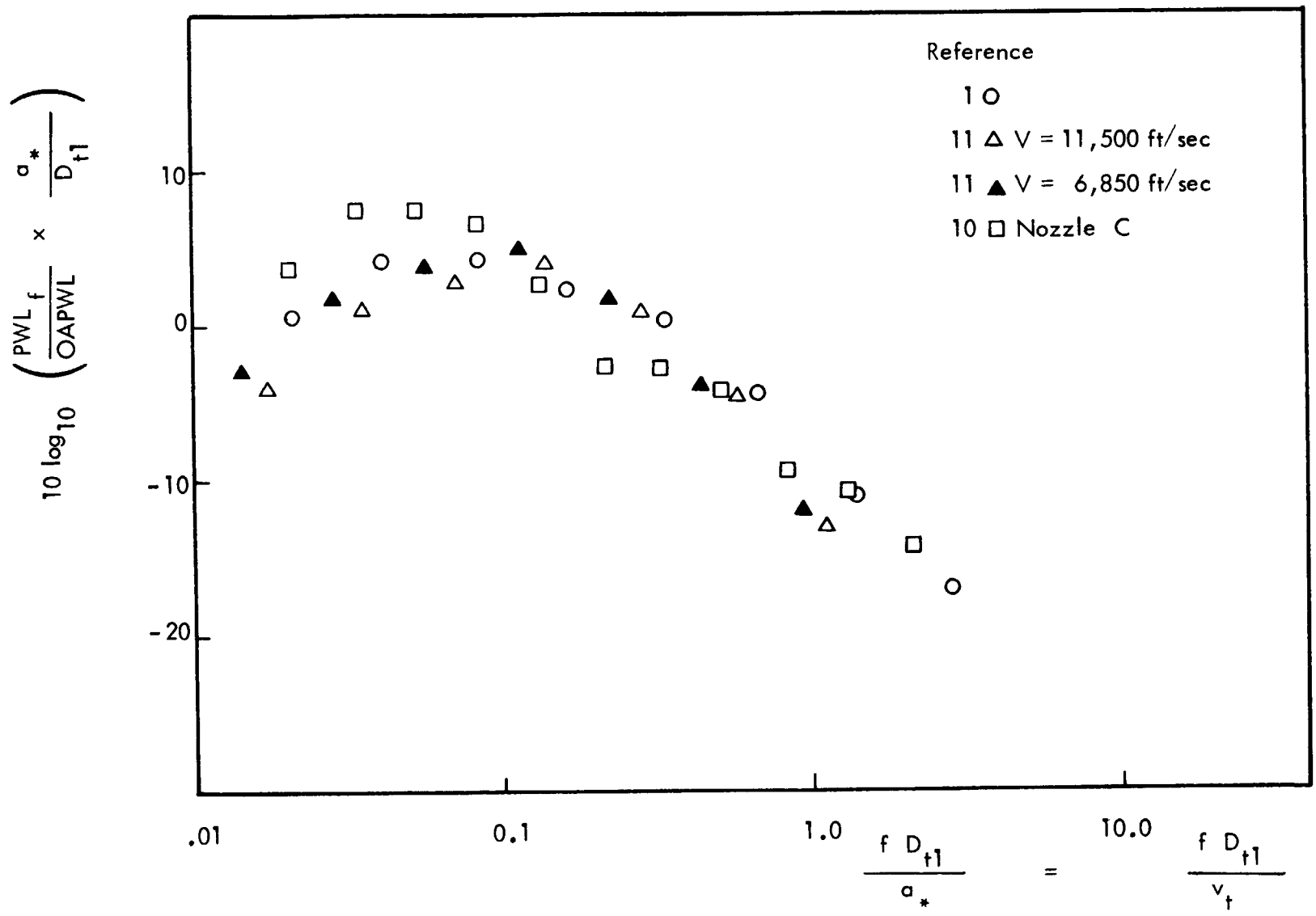


Figure 7 : Normalized Power Spectra of Rocket Noise

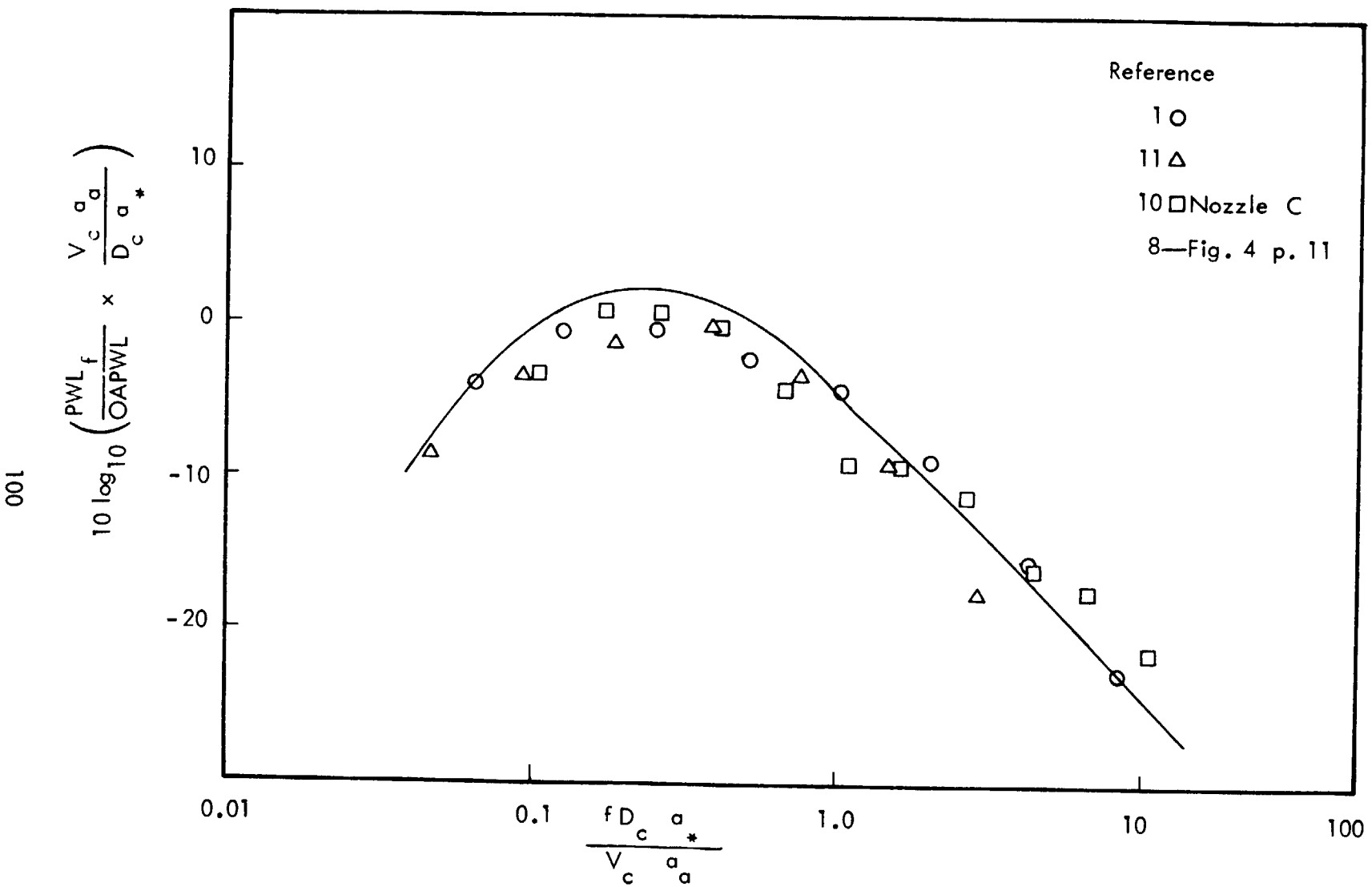


Figure 8: Normalized Power Spectra of Rocket Noise

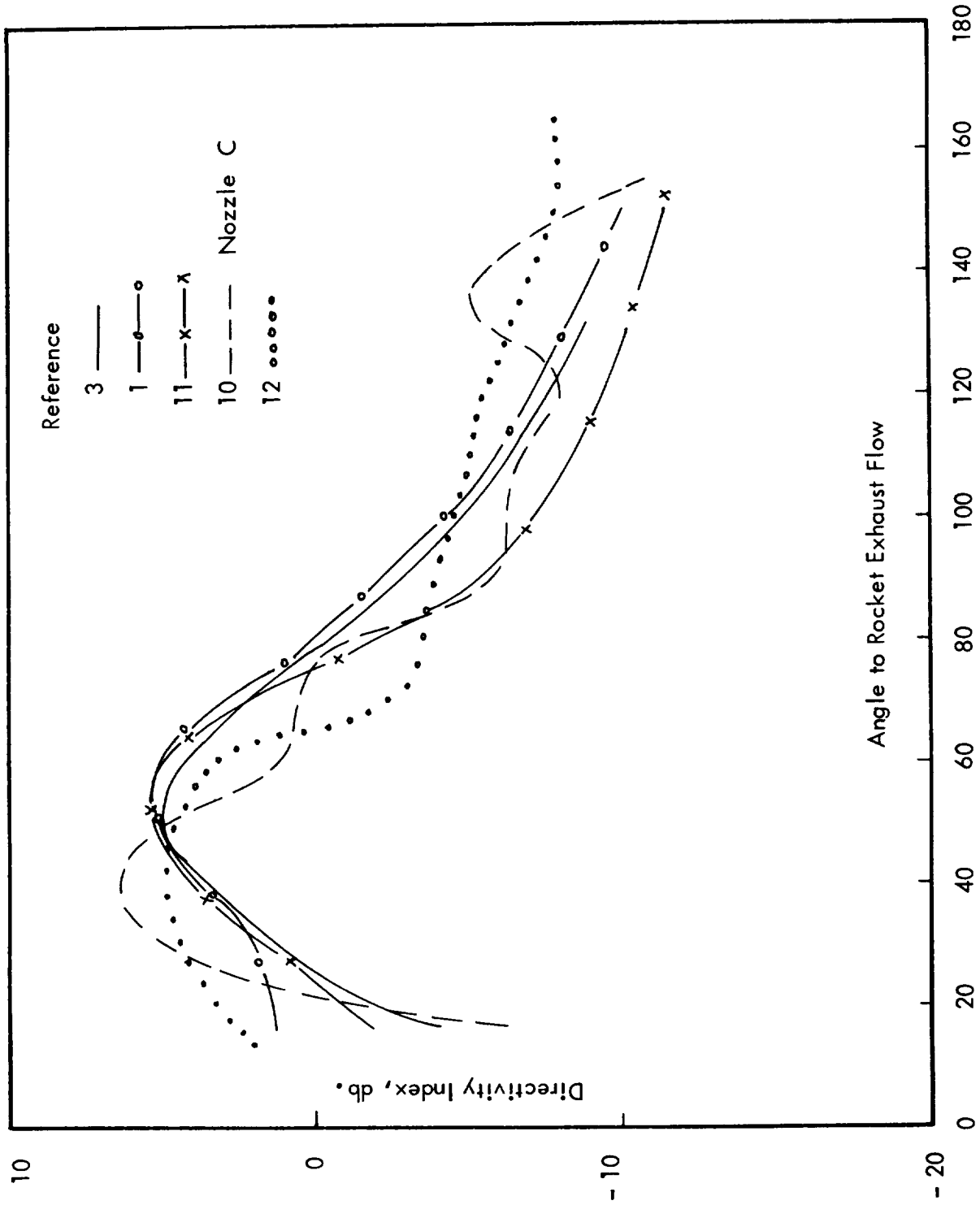


Figure 9 : Directivity Indices of Rocket Noise, Overall Bandwidth

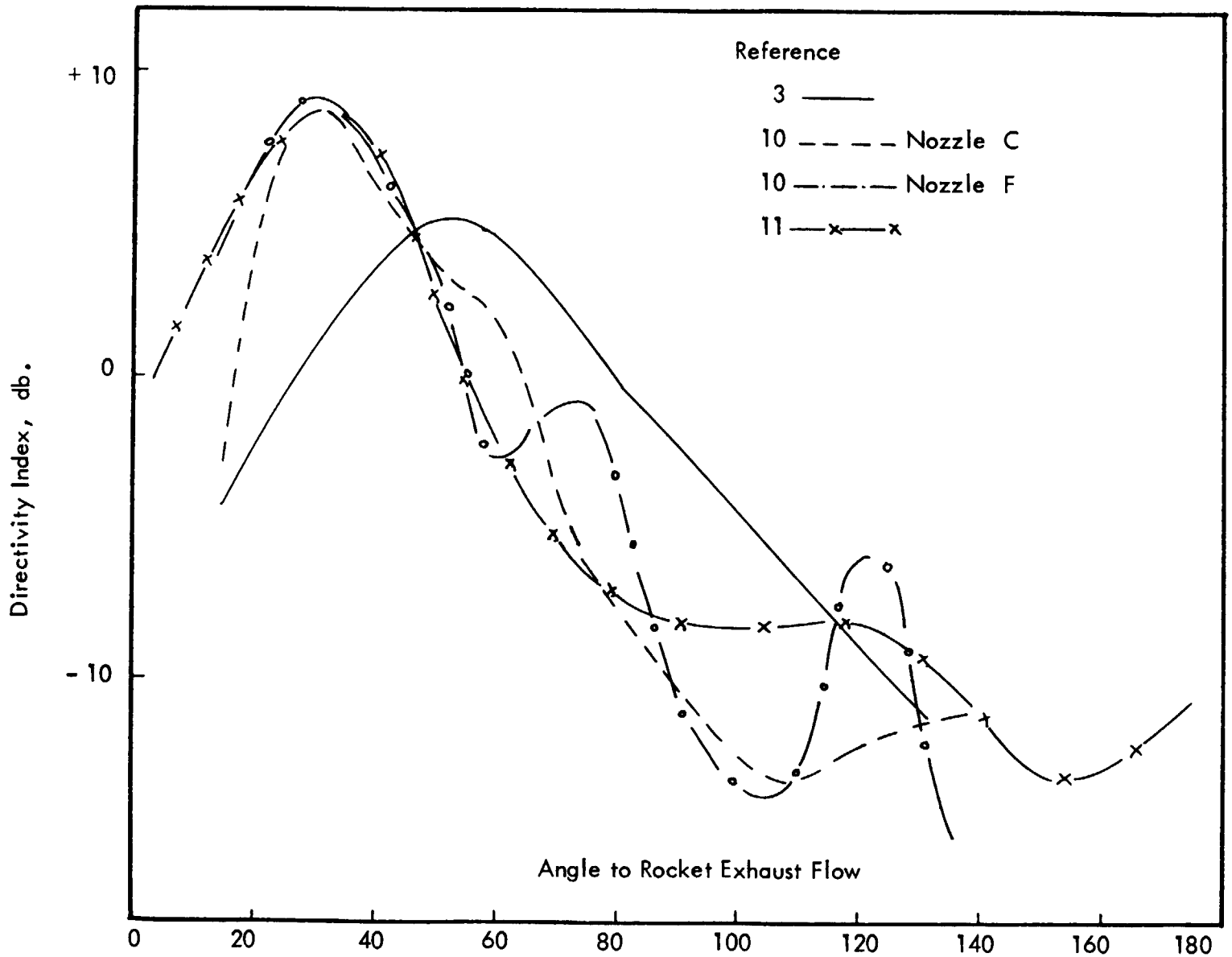


Figure 10: Directivity Indices of Rocket Noise 75 - 150 cps

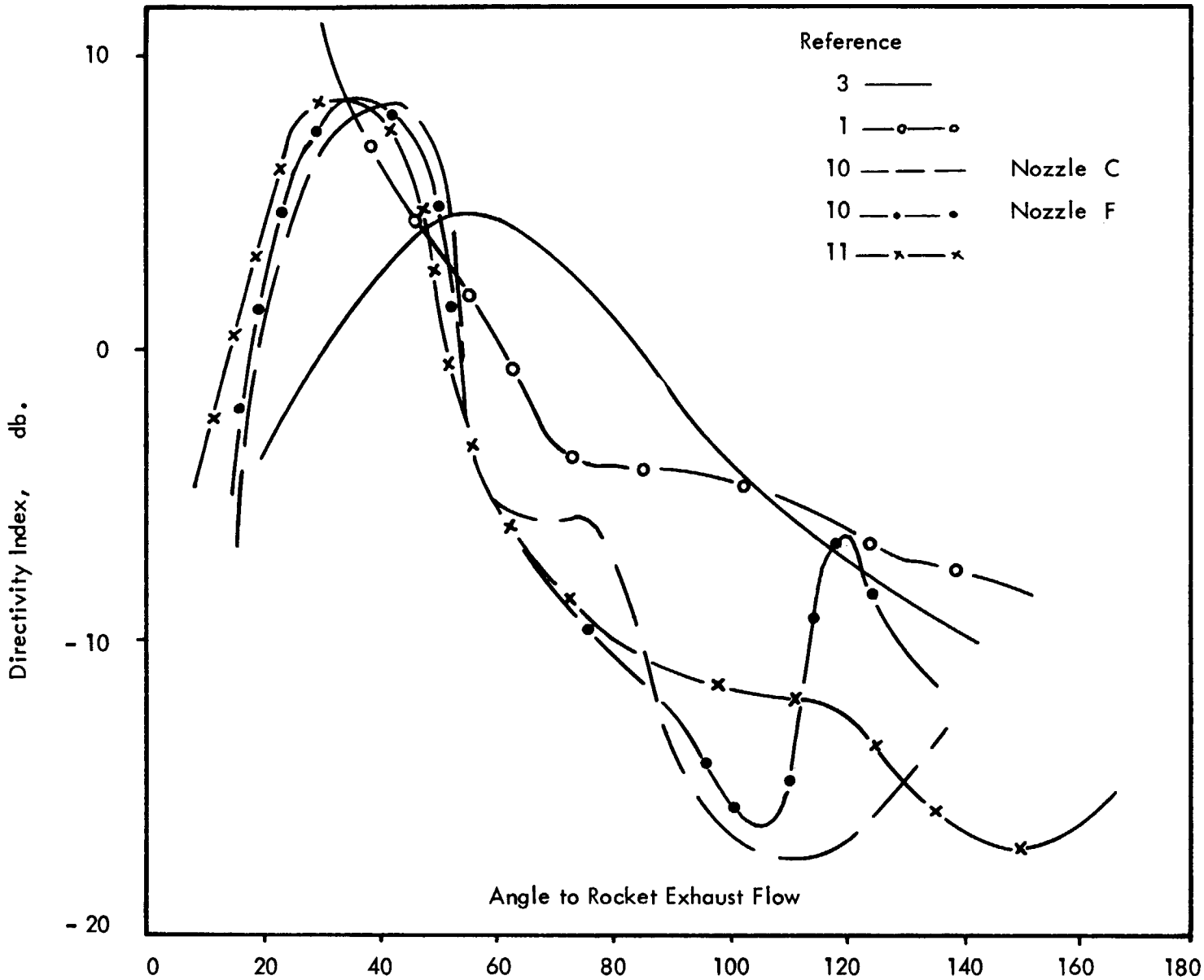


Figure 11 : Directivity Indices of Rocket Noise 150 - 300 cps

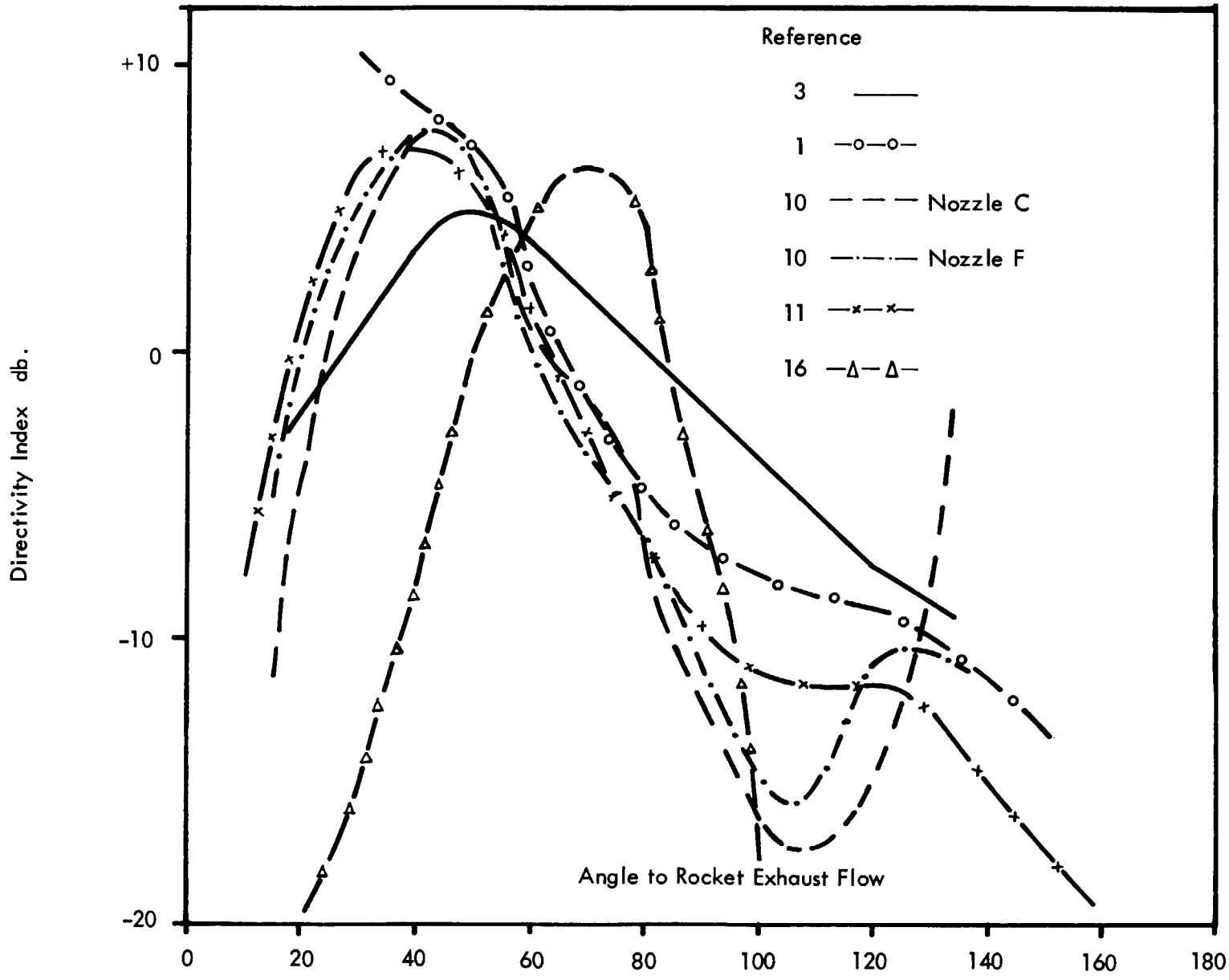


Figure 12: Directivity Indices of Rocket Noise 300 - 600 cps

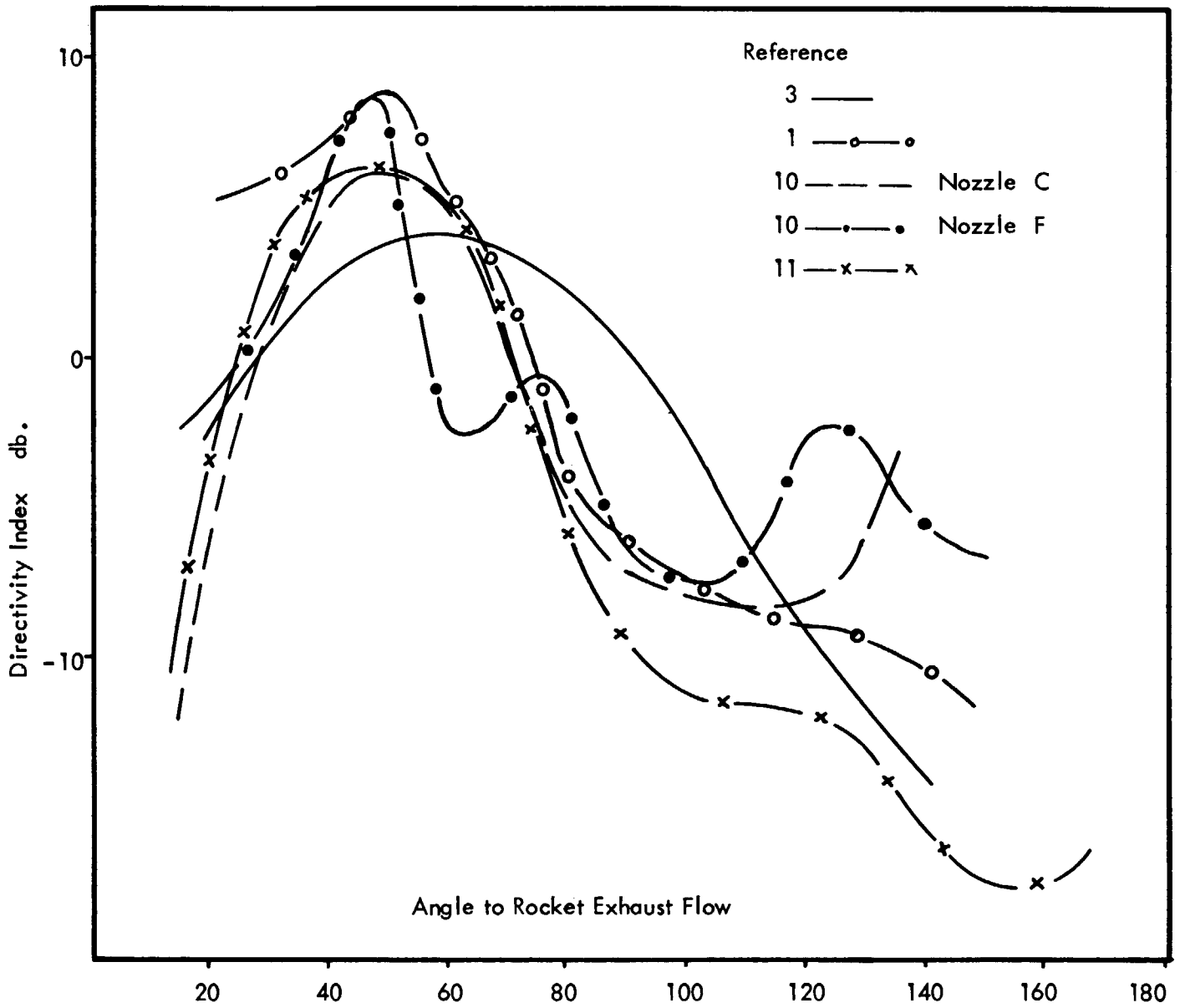


Figure 13: Directivity Indices of Rocket Noise 600 - 1200 cps

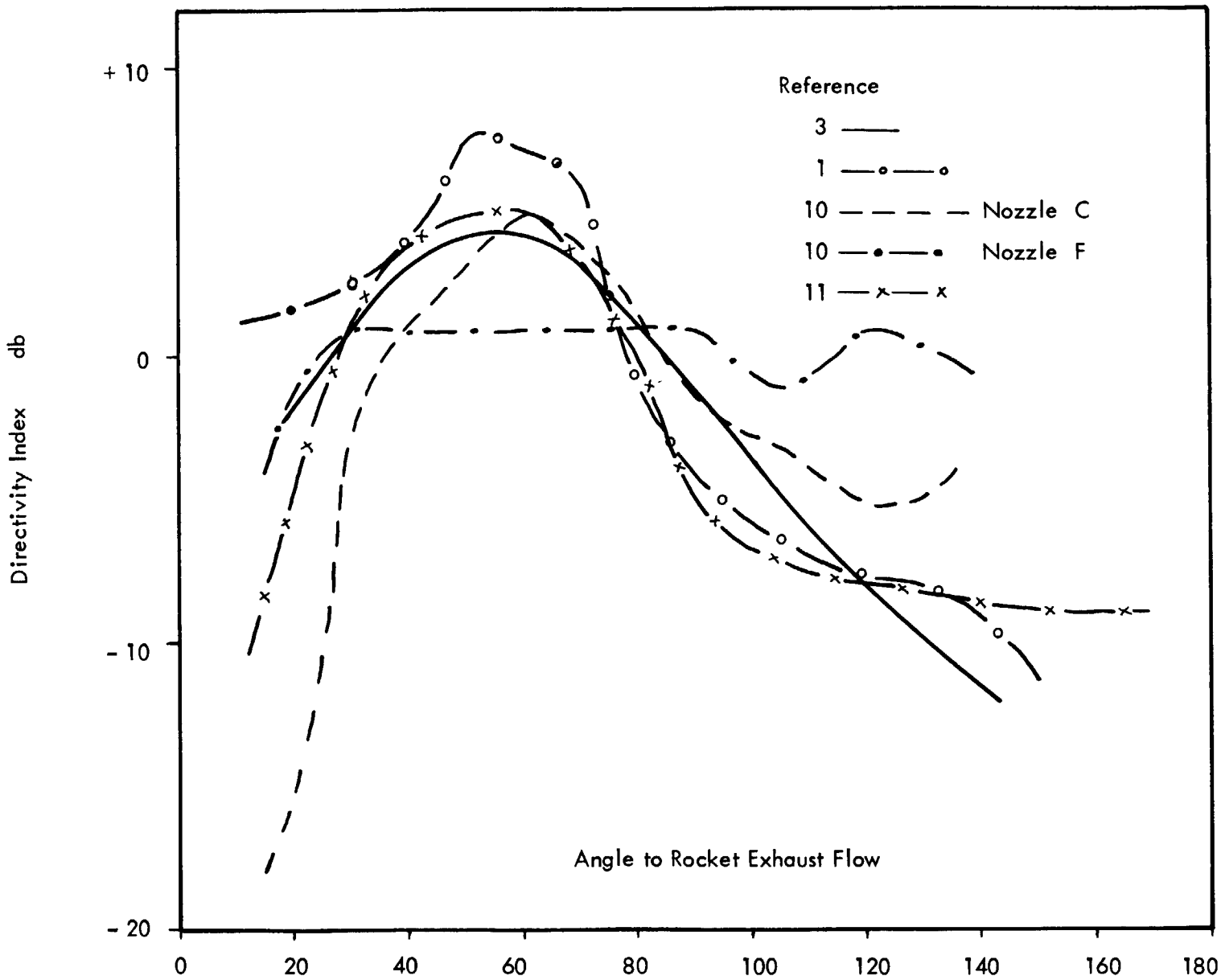


Figure 14: Directivity Indices of Rocket Noise 1200 - 2400 cps

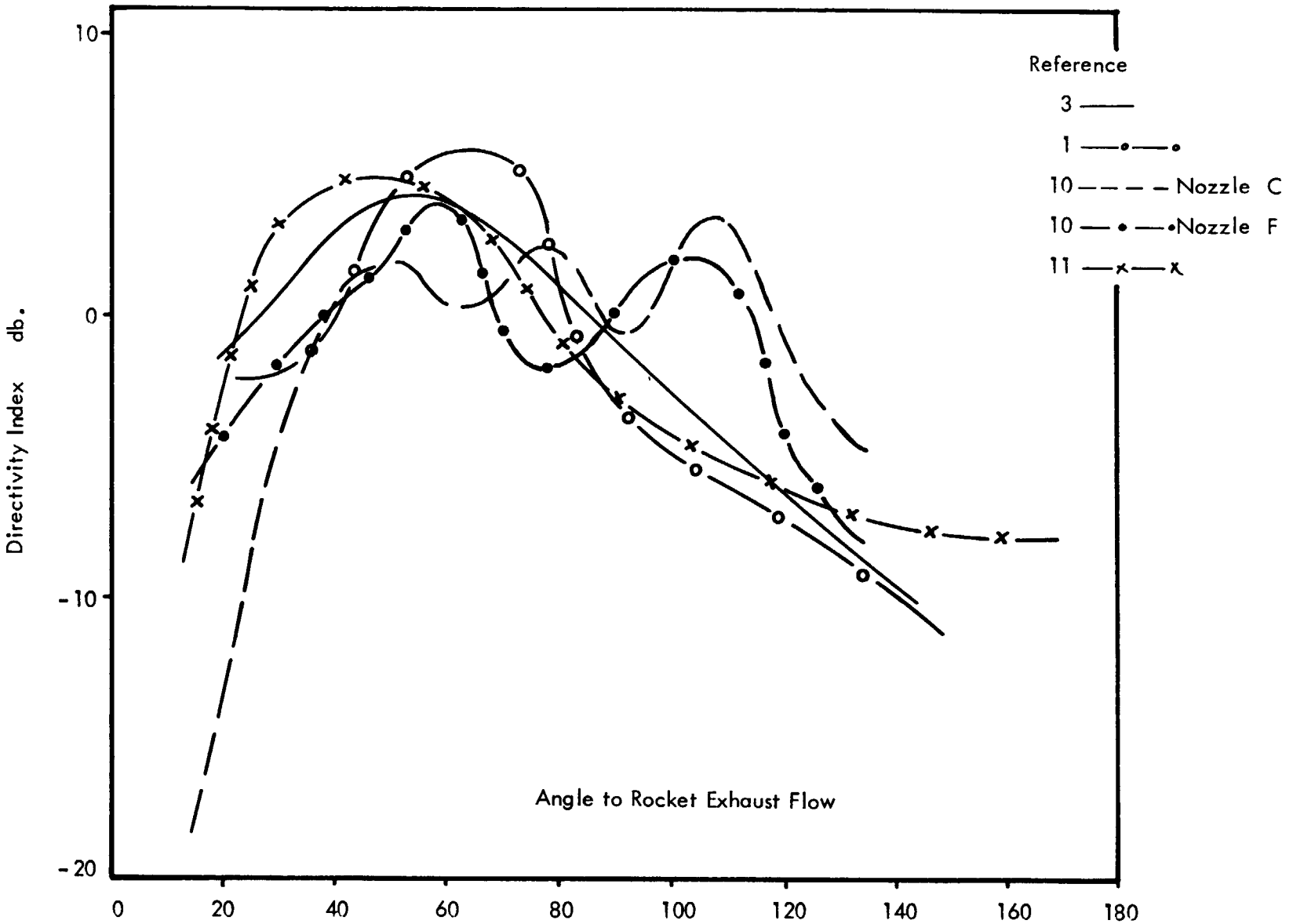


Figure 15: Directivity Index of Rocket Noise 2400 - 4800 cps

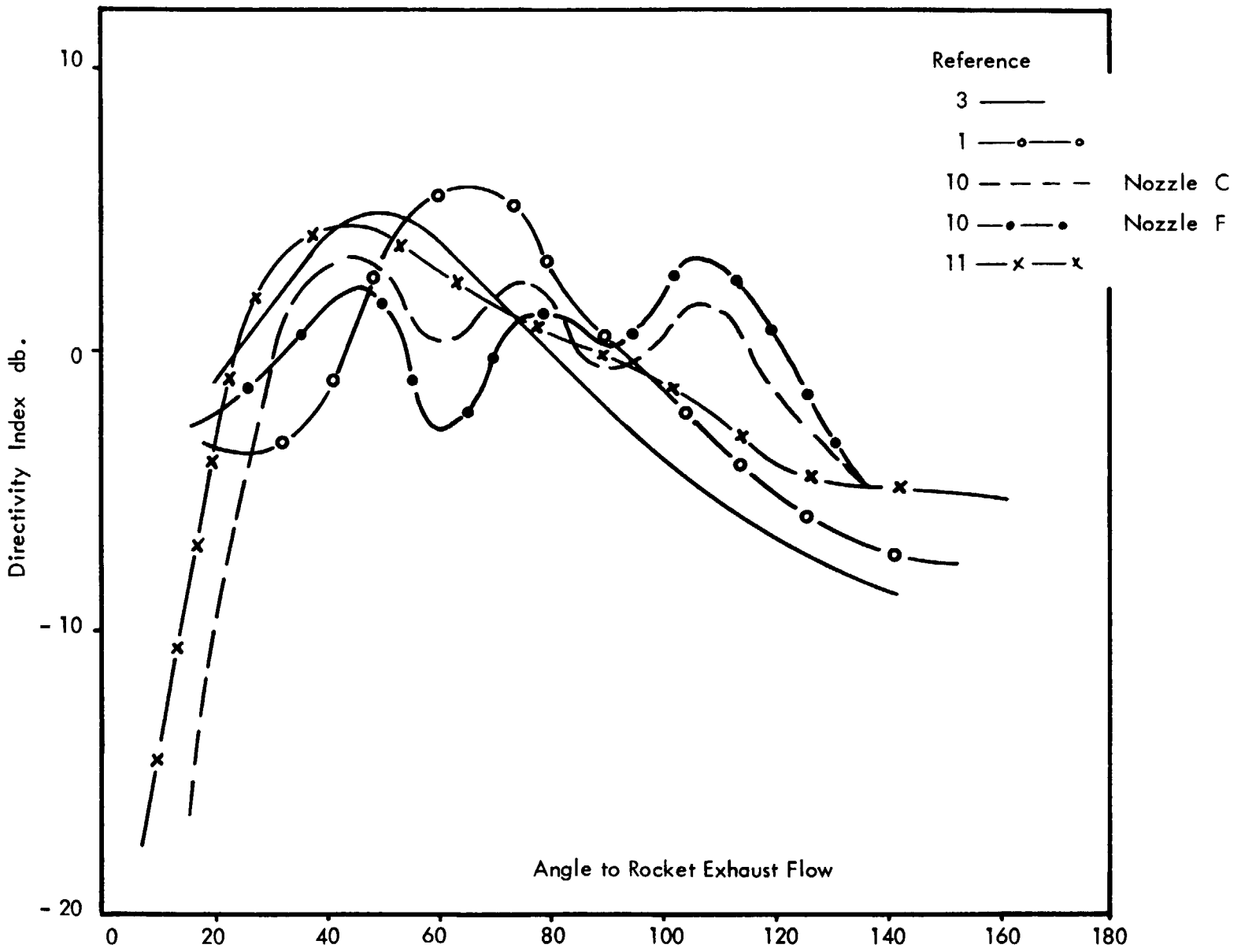


Figure 16: Directivity Indices of Rocket Noise 4800 - 9600 cps

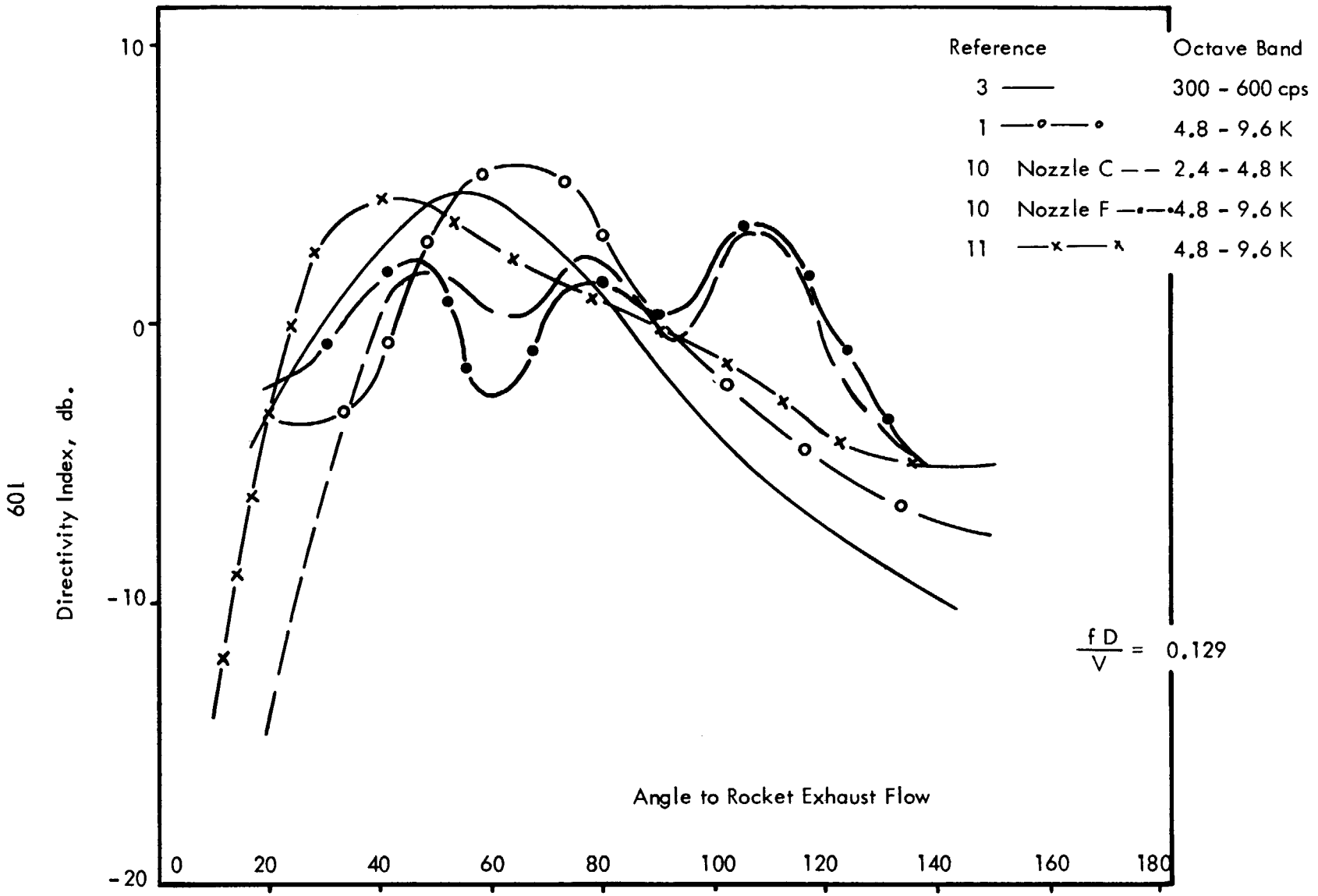


Figure 17: Directivity Indices - at Same Exit Strouhal Number

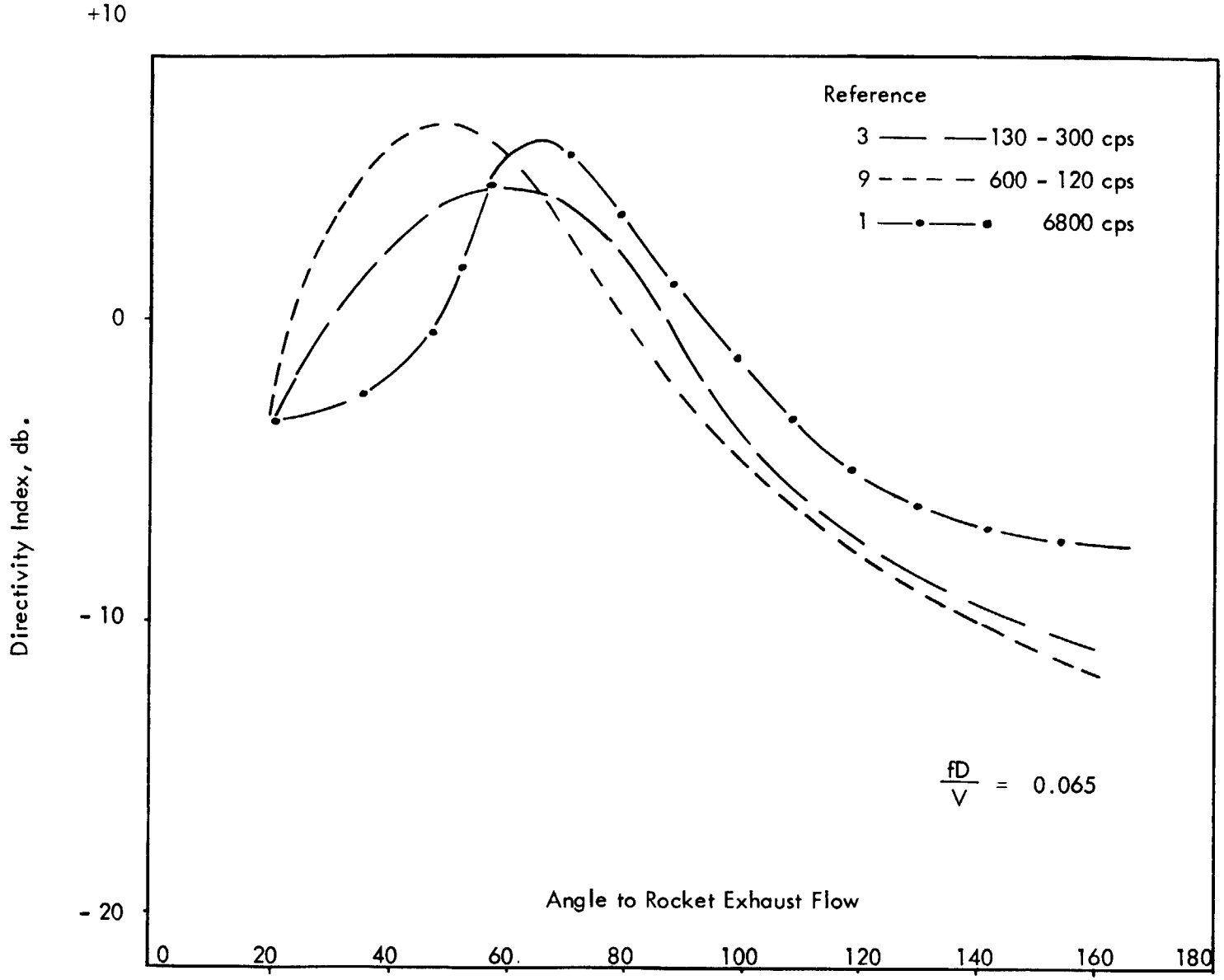


Figure 18: Directivity Indices at Same Exit Strouhal Number

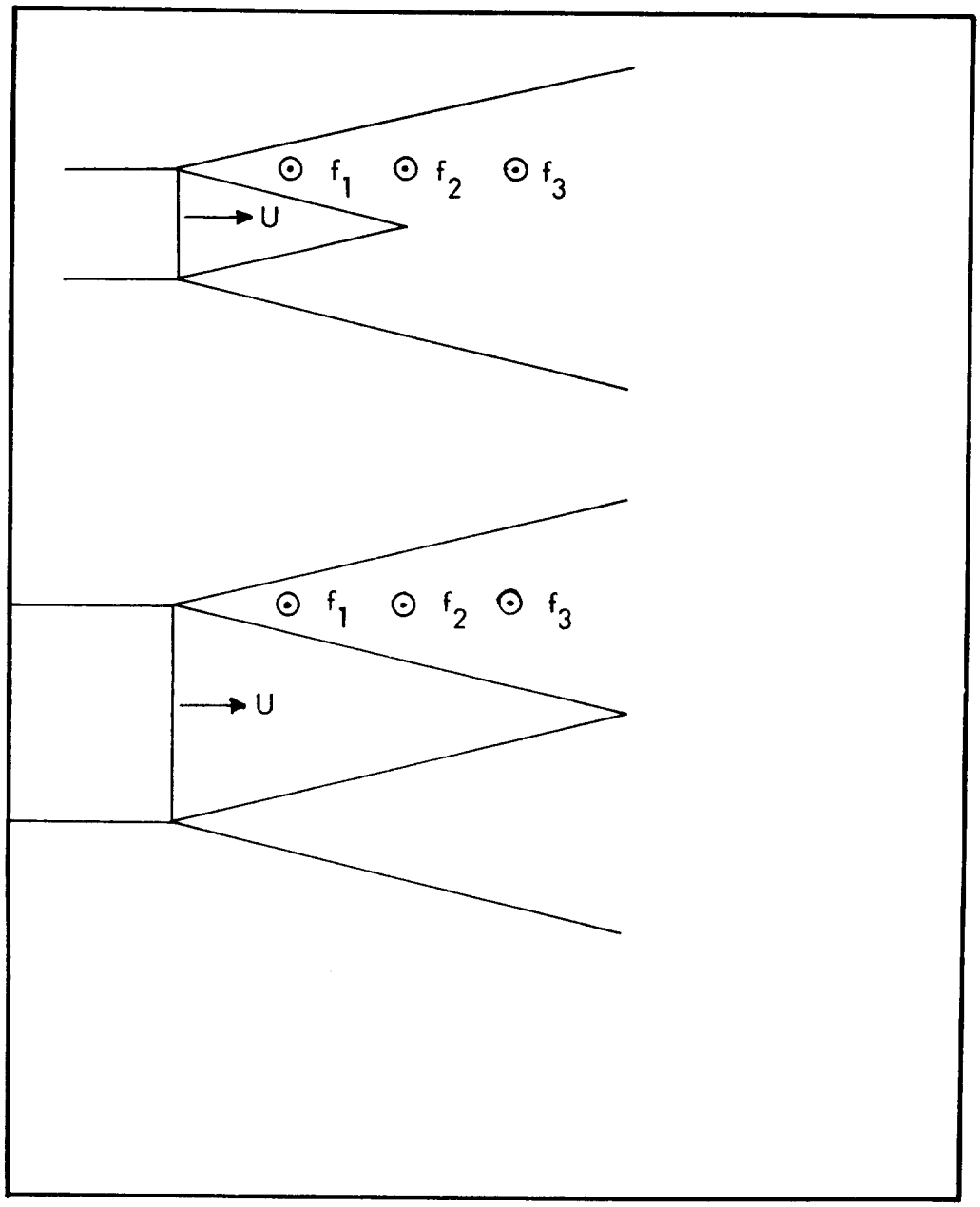


Figure 19: Source Allocation in Mixing Region of Rocket Exhaust

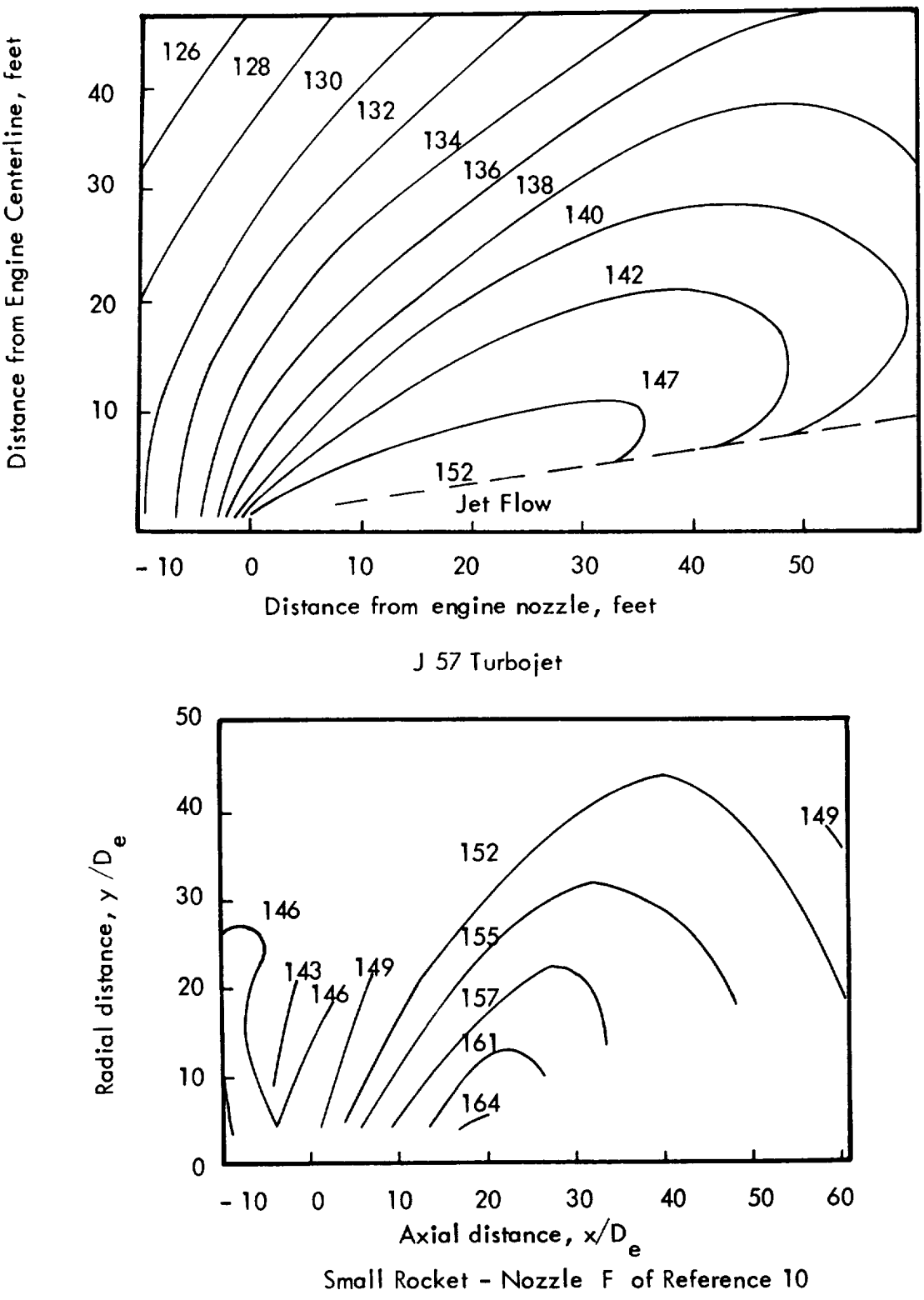


Figure 20: Near Field Noise Pattern of a Jet and a Rocket, SPL in Decibels re: 0.0002 dynes/cms$^2$

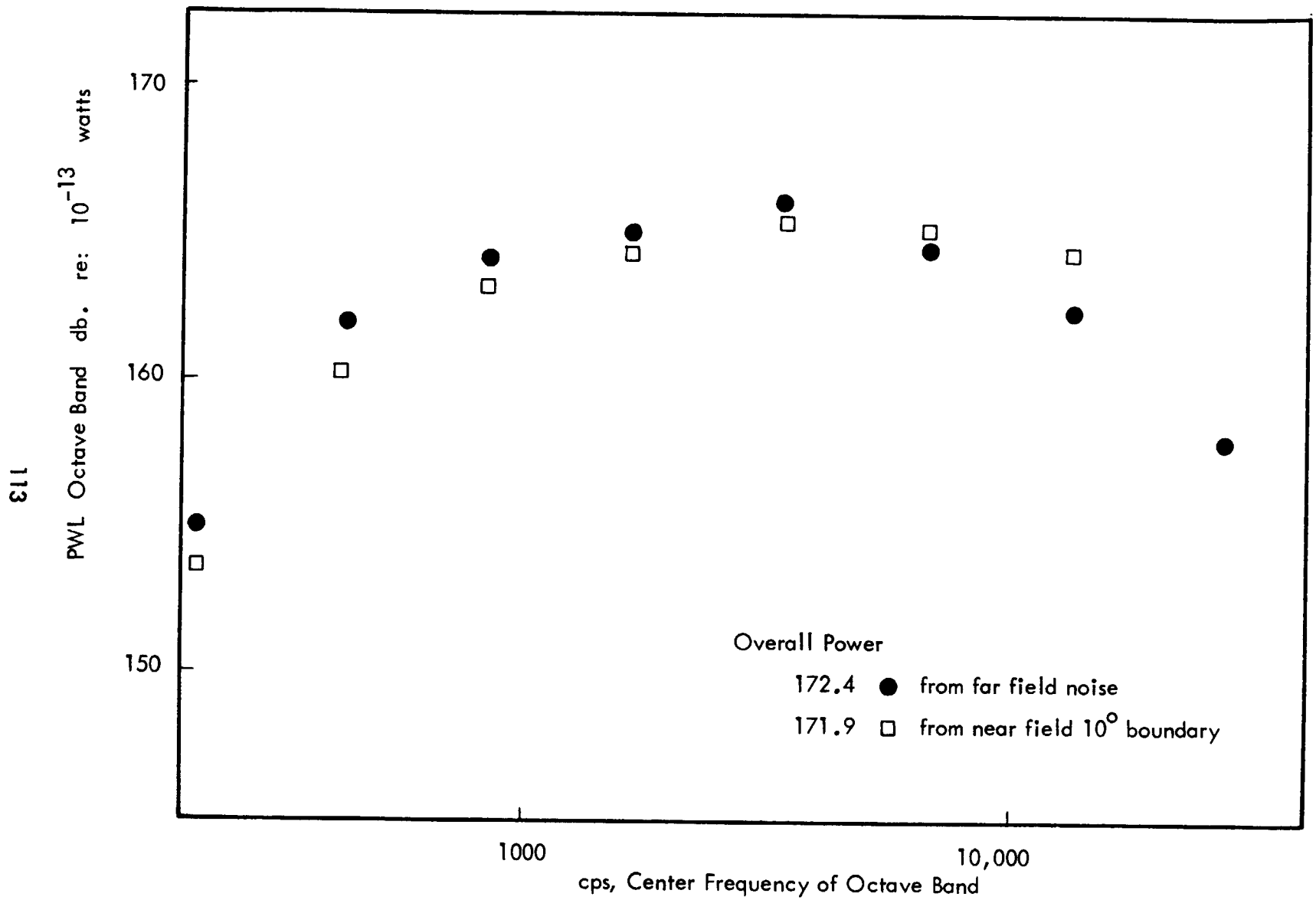


Figure 21: Comparison of Power Produced by Rocket, Calculated From the Far Field and the Near Field Results

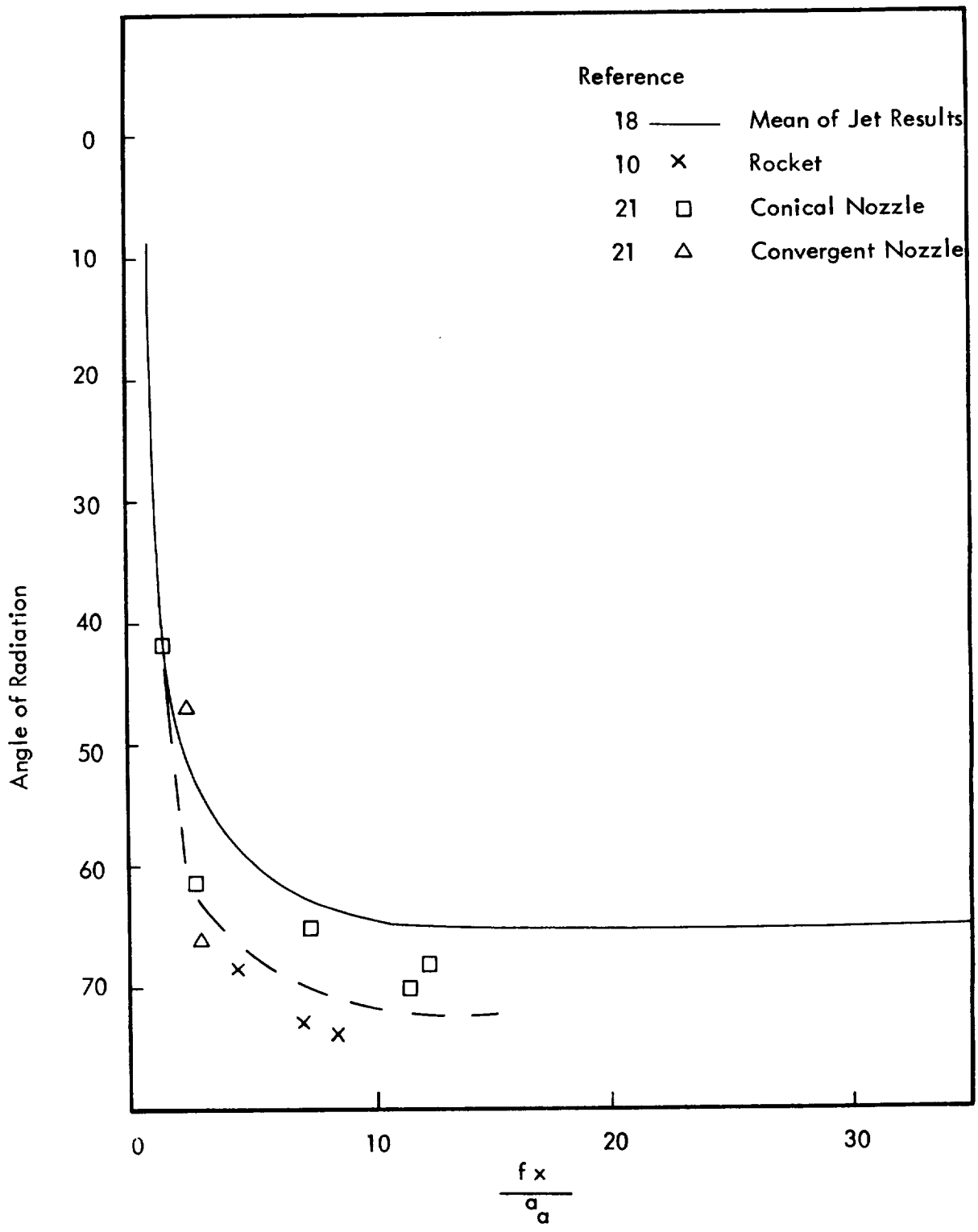


Figure 22: Variation of Predominant Propagation Angle for Various Frequencies from Measurement Along the 10° Boundary as a Function of a Non-Dimensional Axial Frequency Parameter

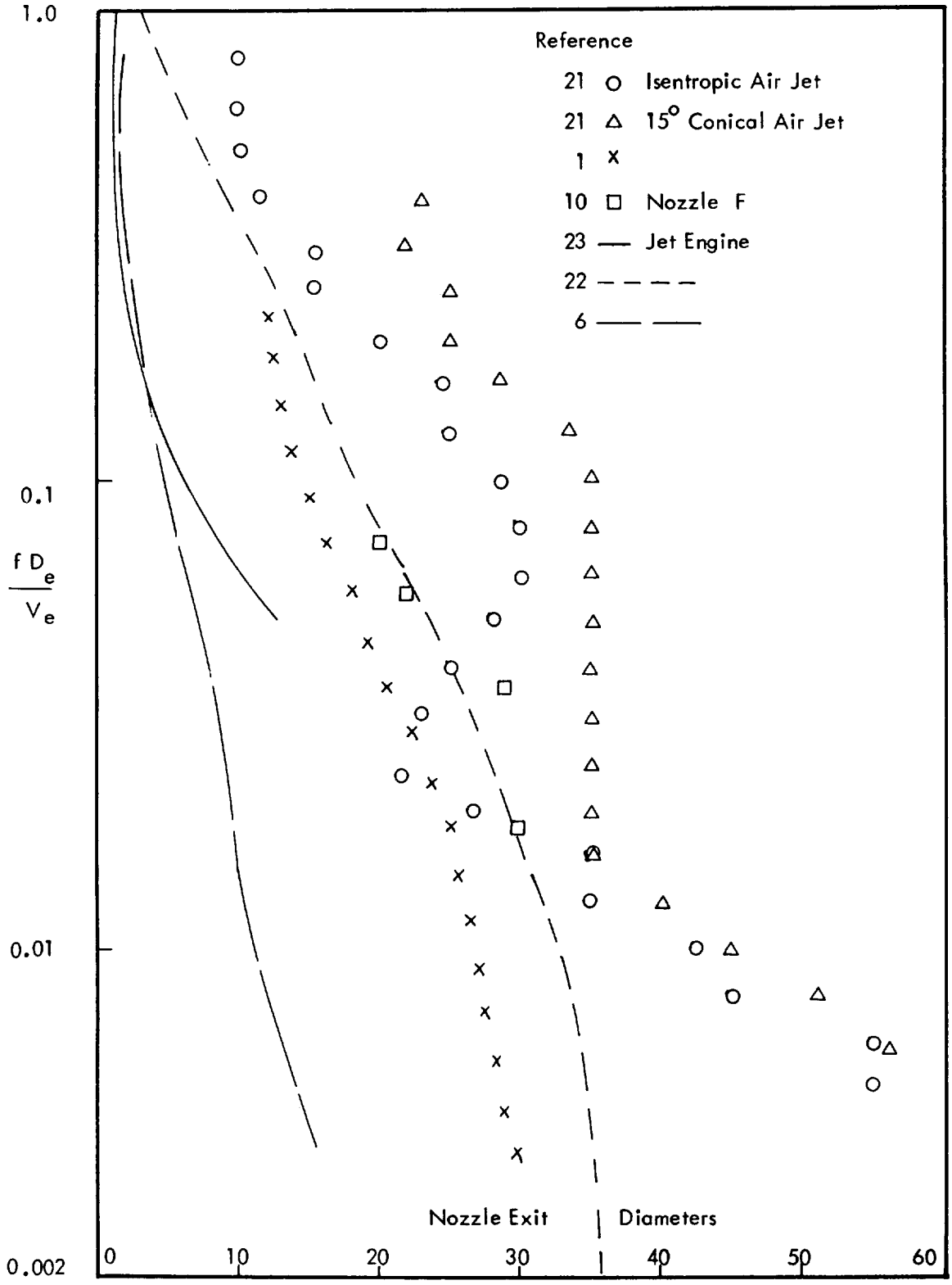


Figure 23: Source Location in High Speed Flows

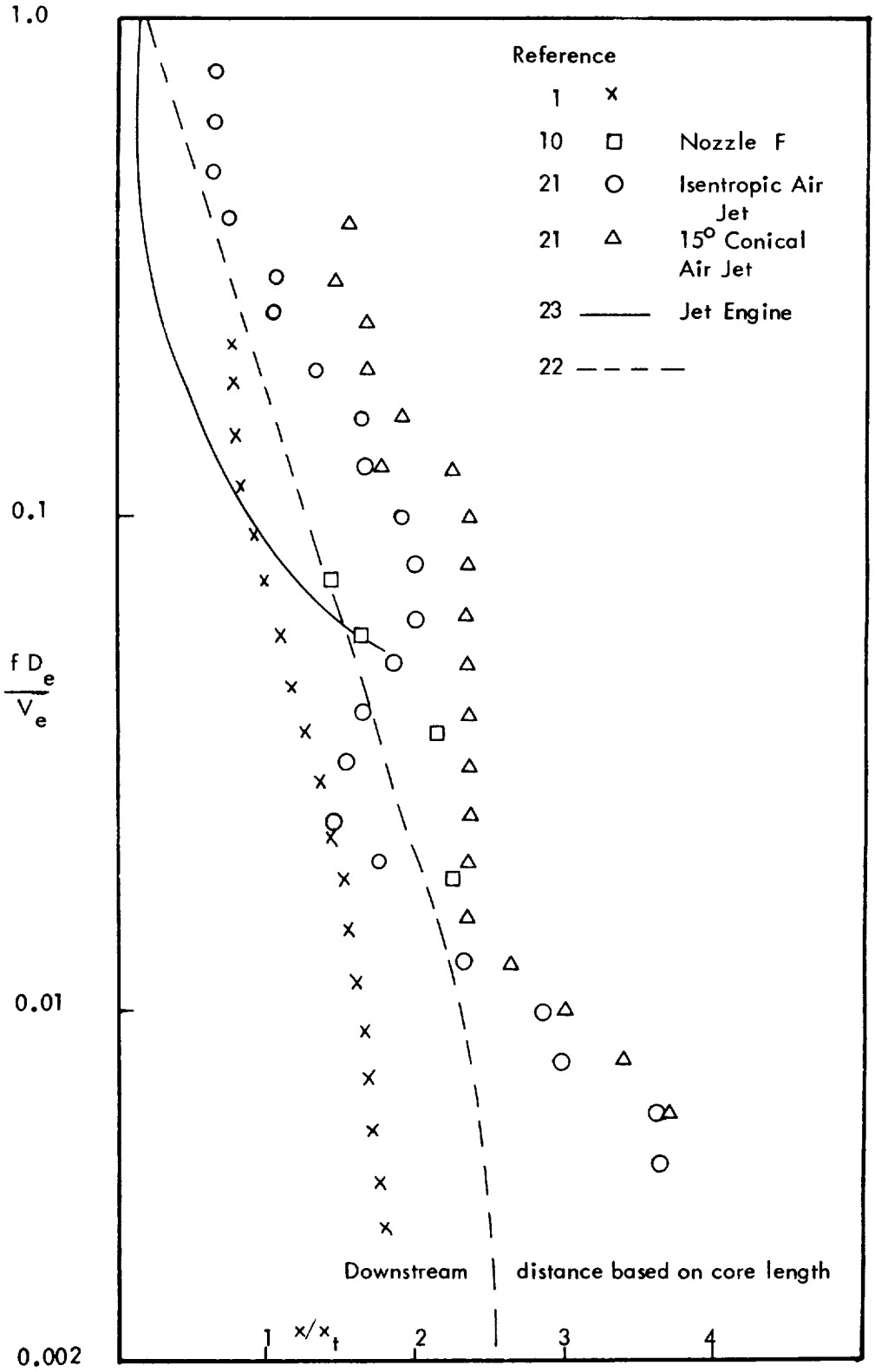


Figure 24: Normalized Source Location in High Speed Flow

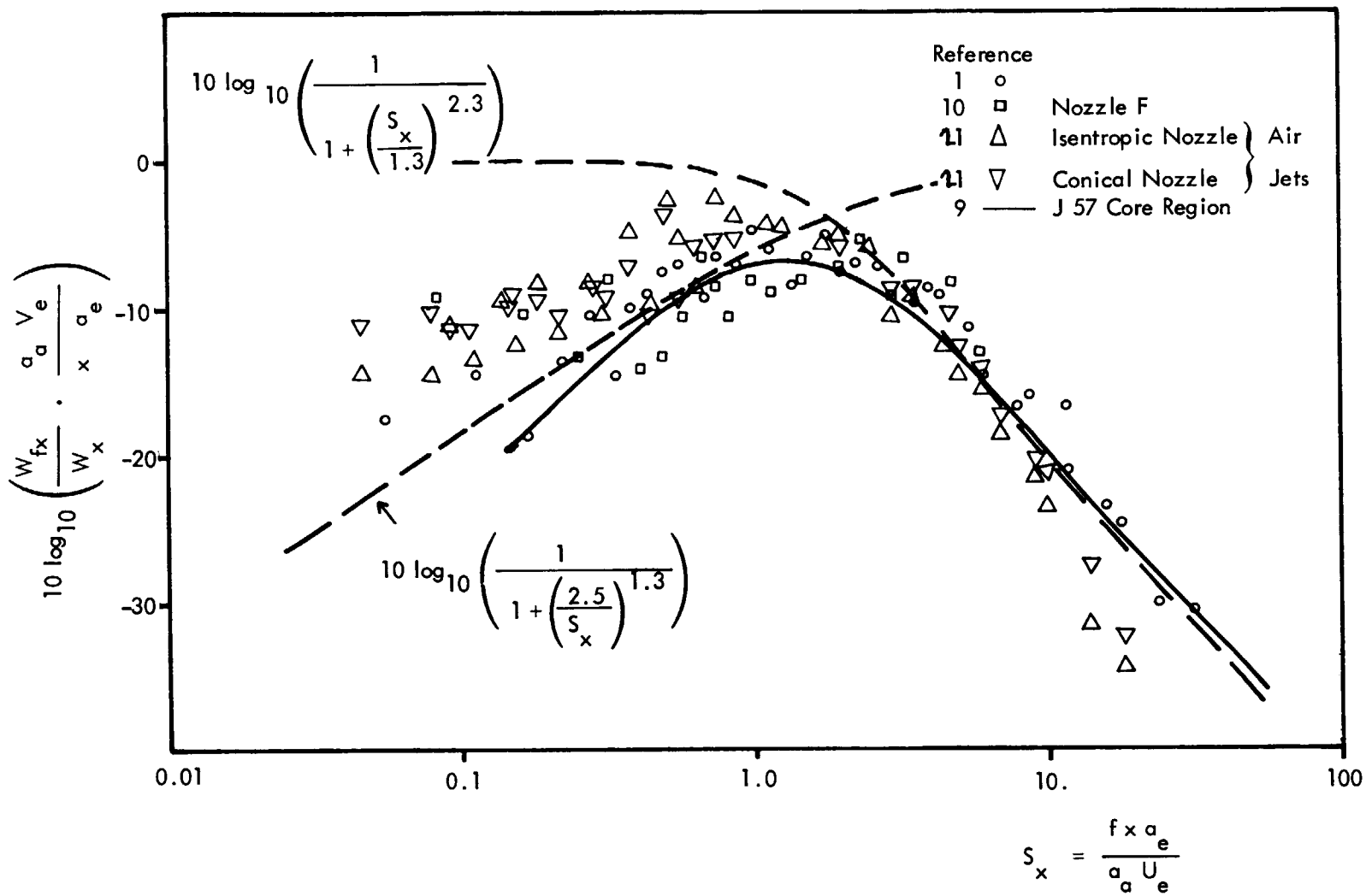


Figure 25: Normalized Source Spectrum of Rockets

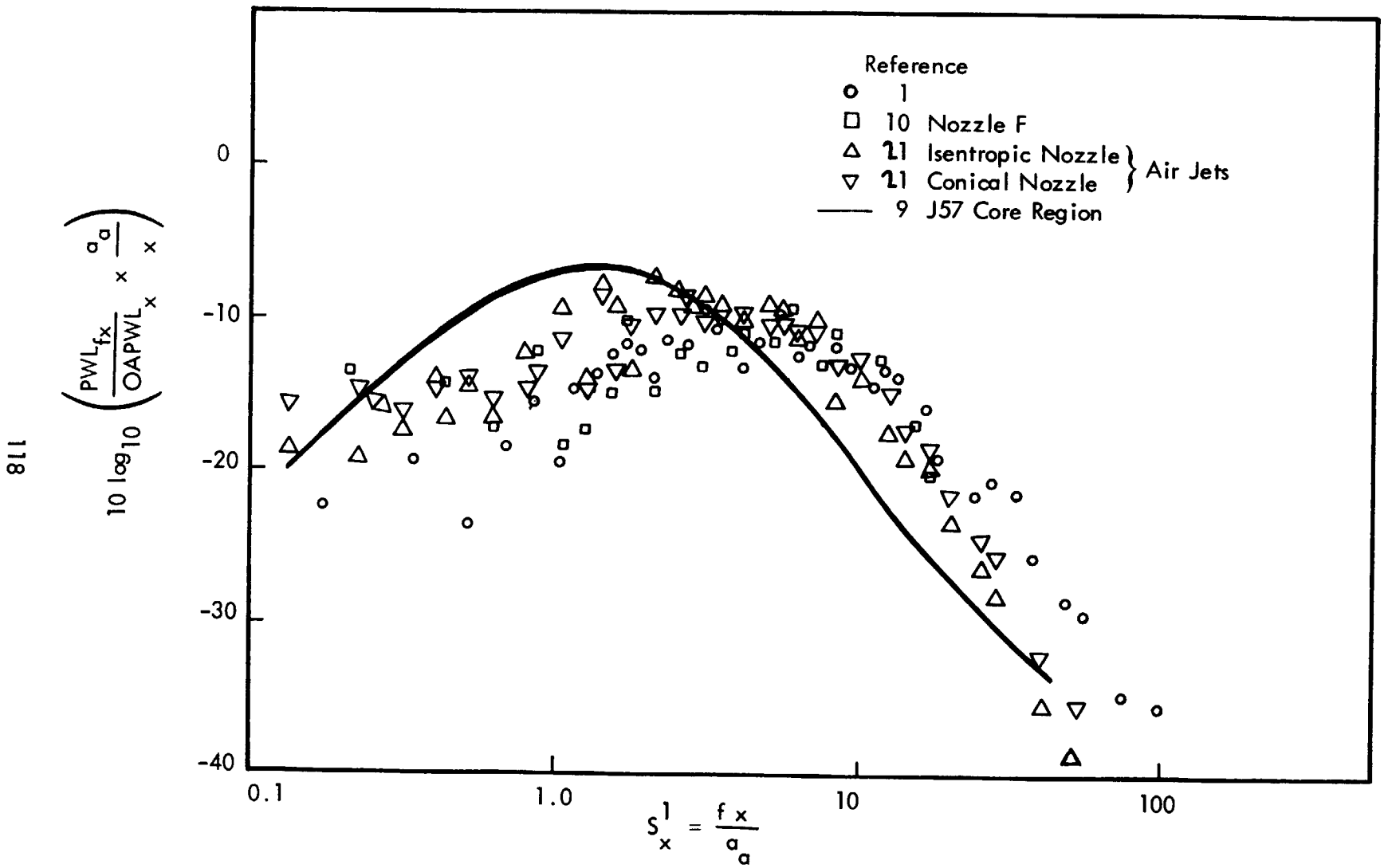


Figure 26: Normalized Source Spectrum of Rockets

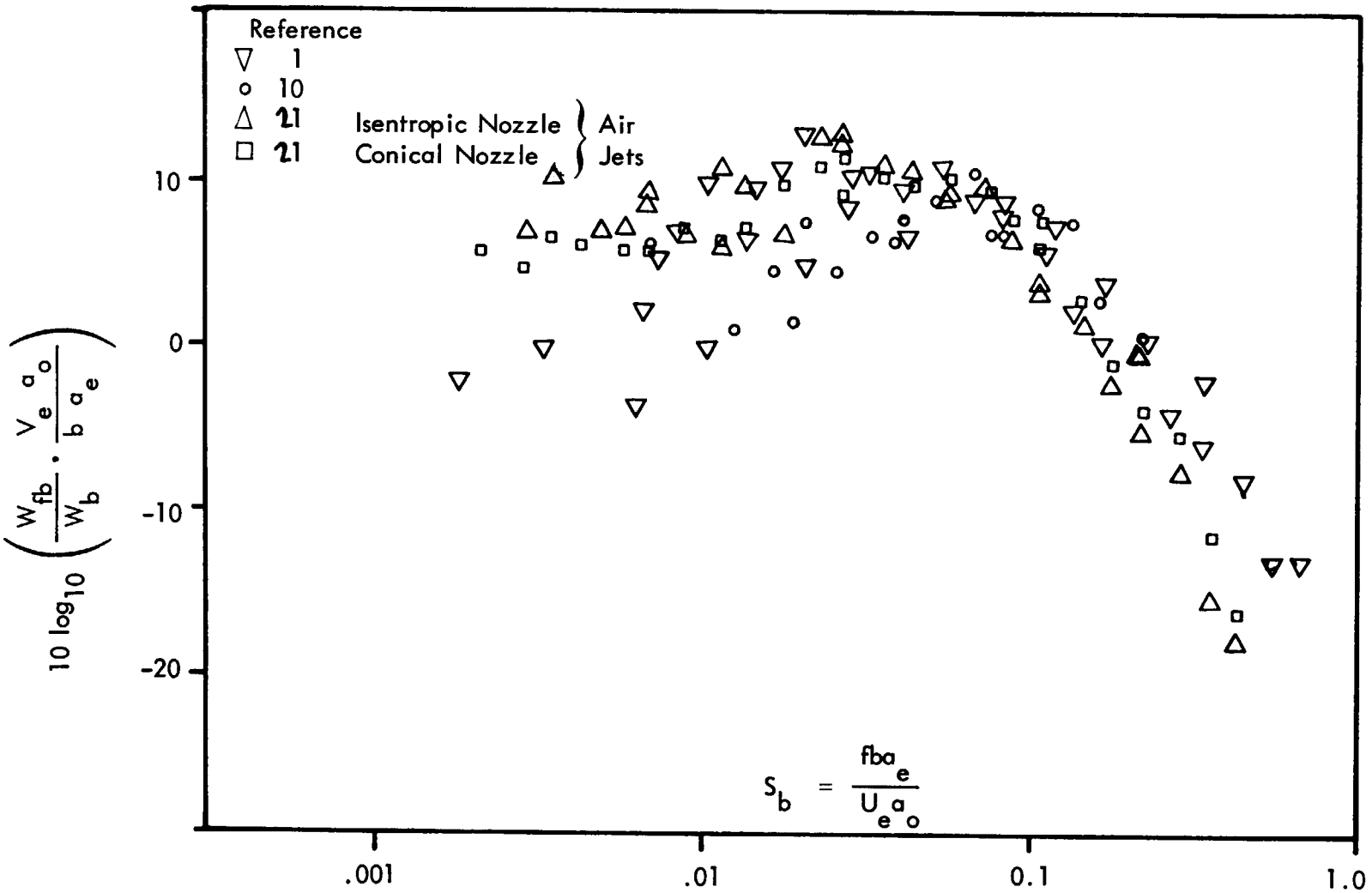


Figure 27: Normalized Source Spectrum of Rocket

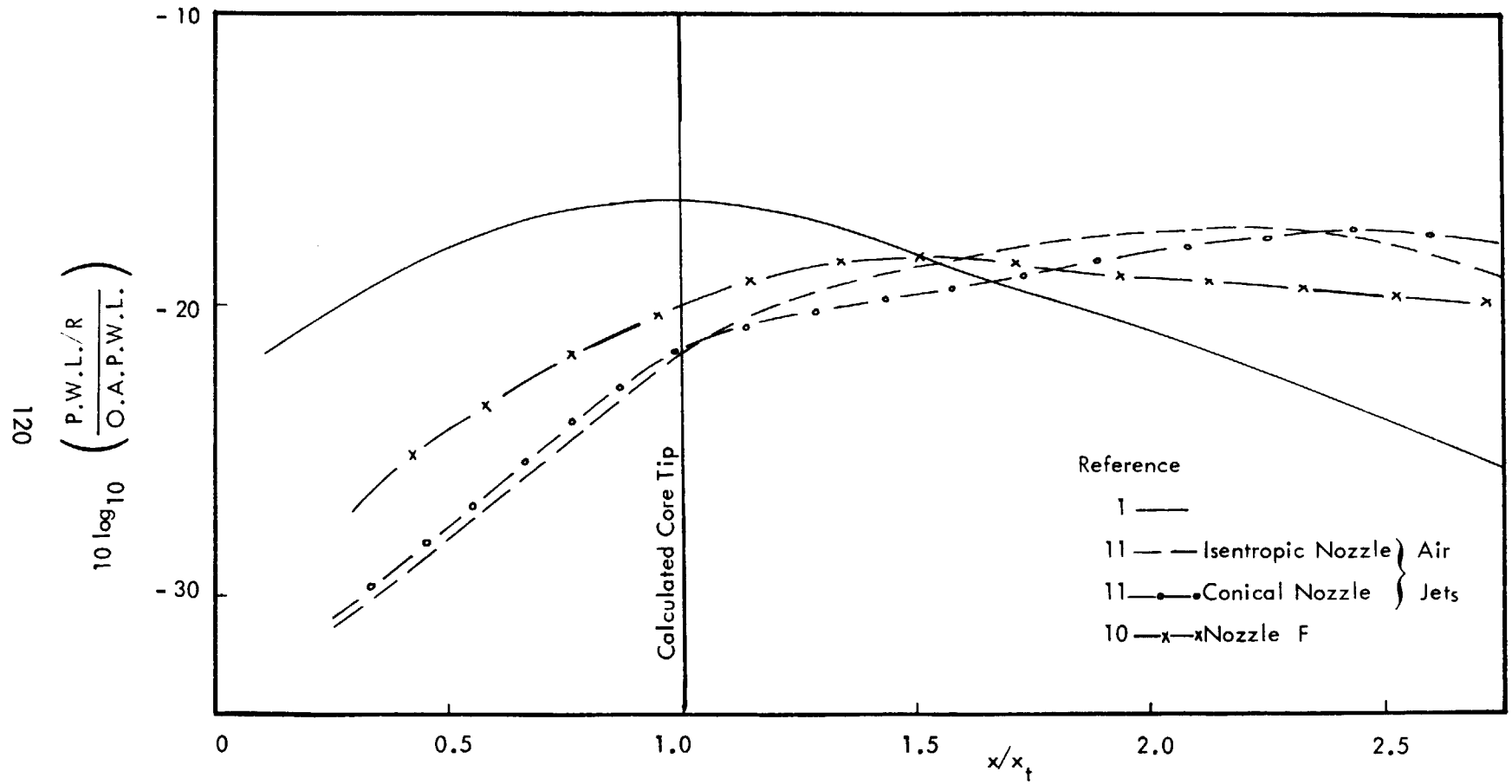


Figure 28: Overall Sound Power Produced by Downstream Segments of High Speed Flows

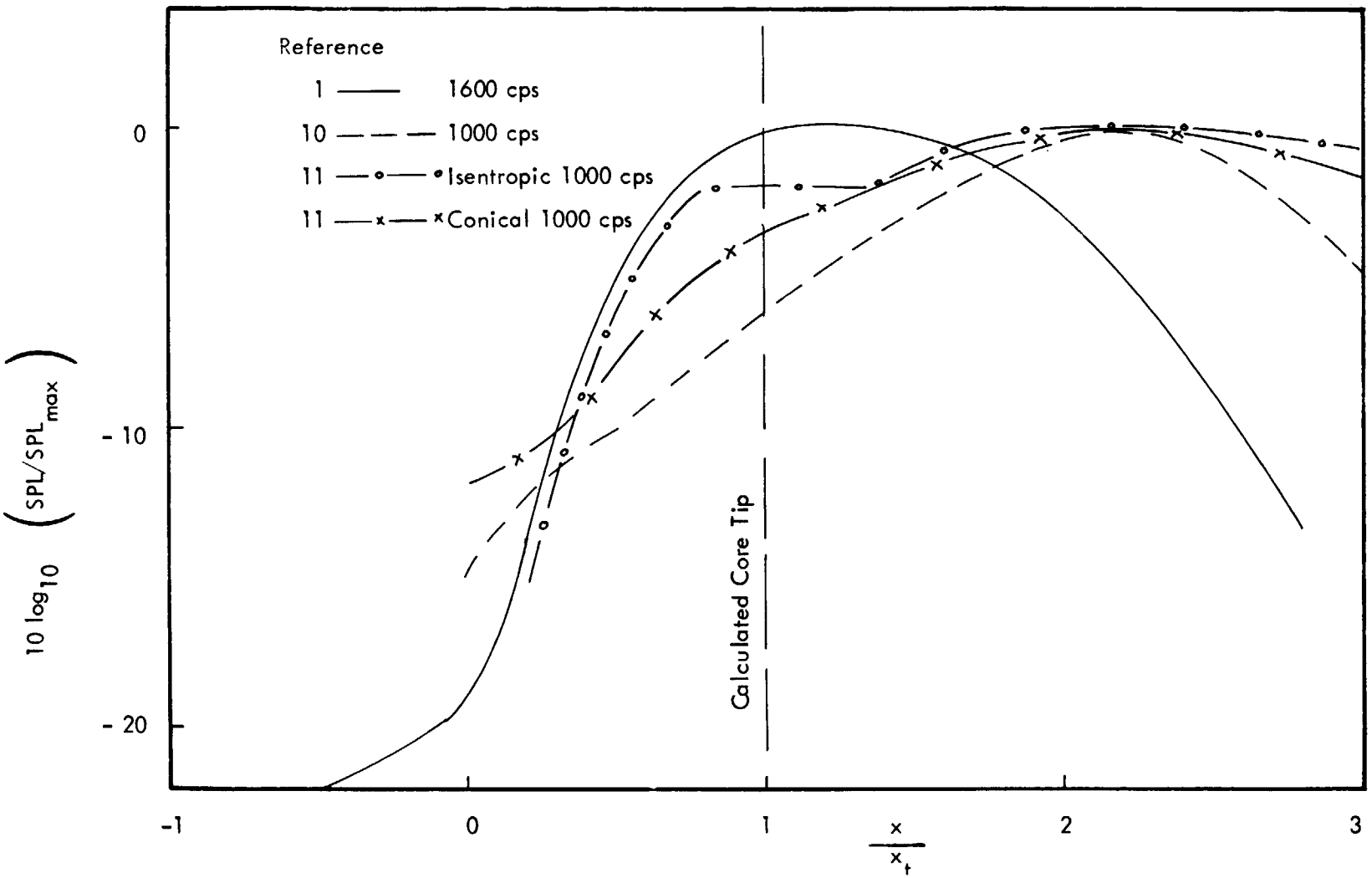


Figure 29 : Sound Pressure Levels Measured on the 10 Degree Boundary

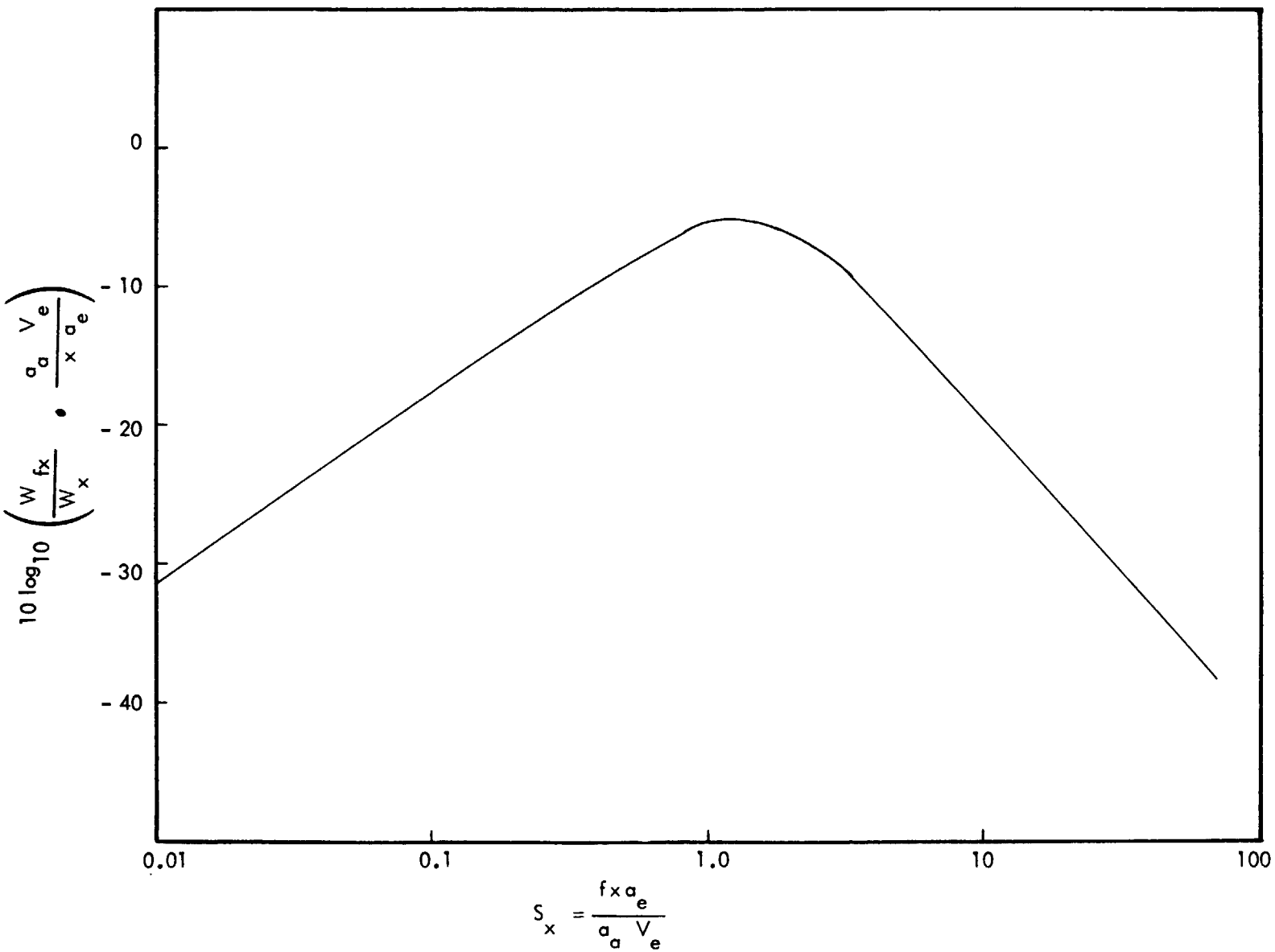


Figure 30: Normalized Power Spectrum with Distance Downstream, Mean of all Results

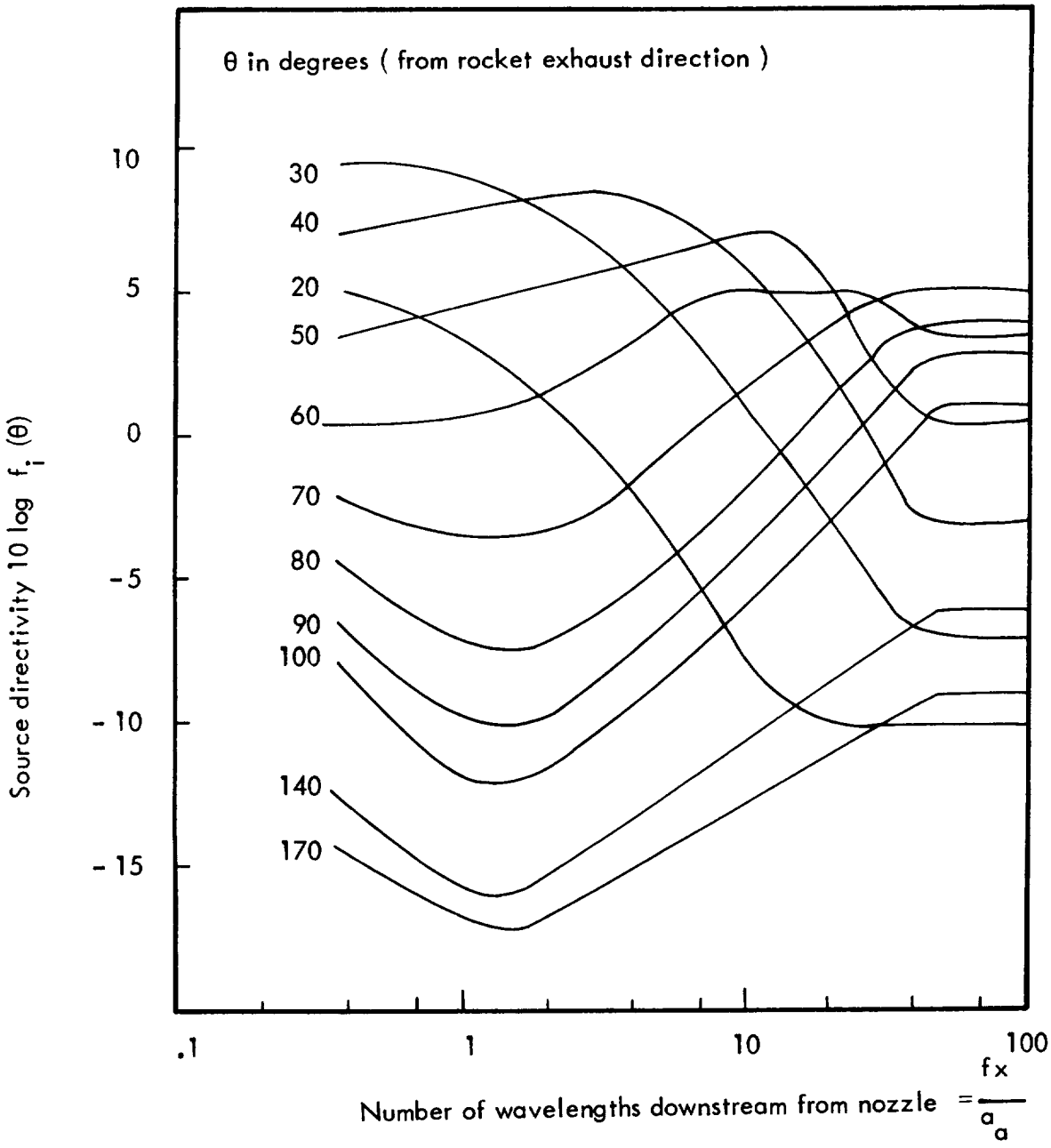


Figure 31: Calculated Directivity as a Function of Position in the Jet (From Ref. 18)

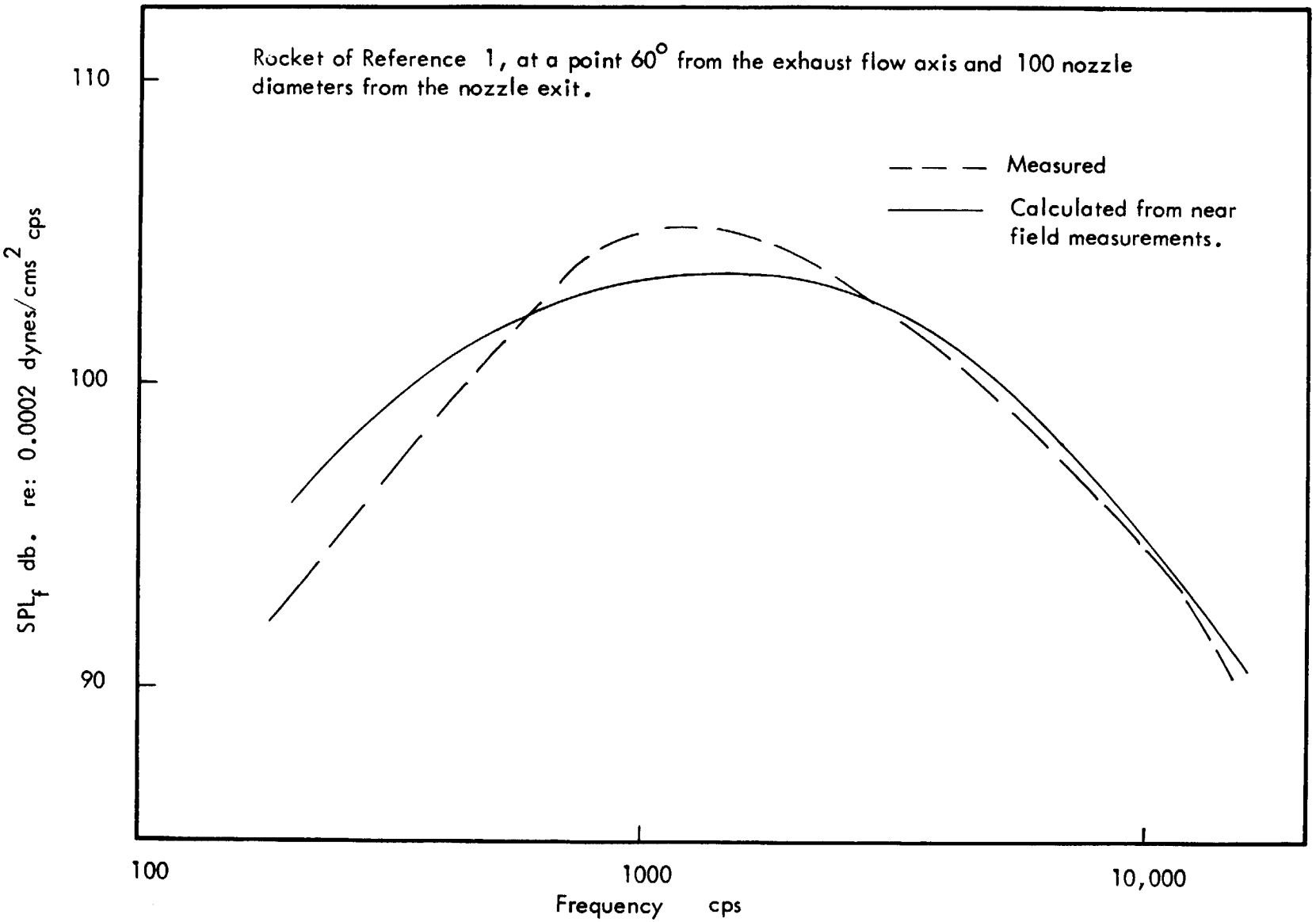


Figure 32: Calculated and Measured Spectrum of Sound Pressure Level For Small Solid Fueled Rocket

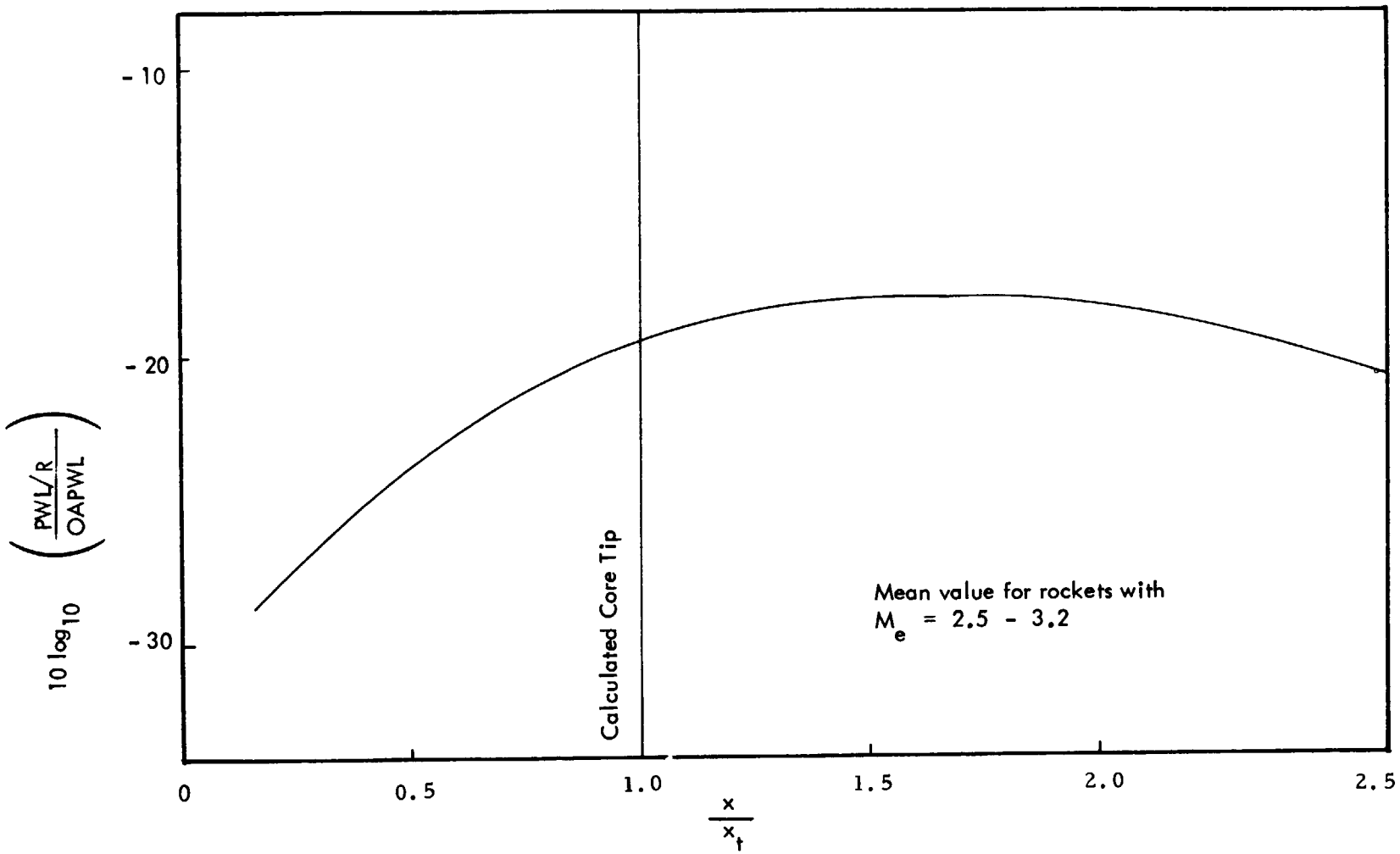


Figure 33: Mean Result of Sound Power Produced by Downstream Segments of Rocket Exhaust

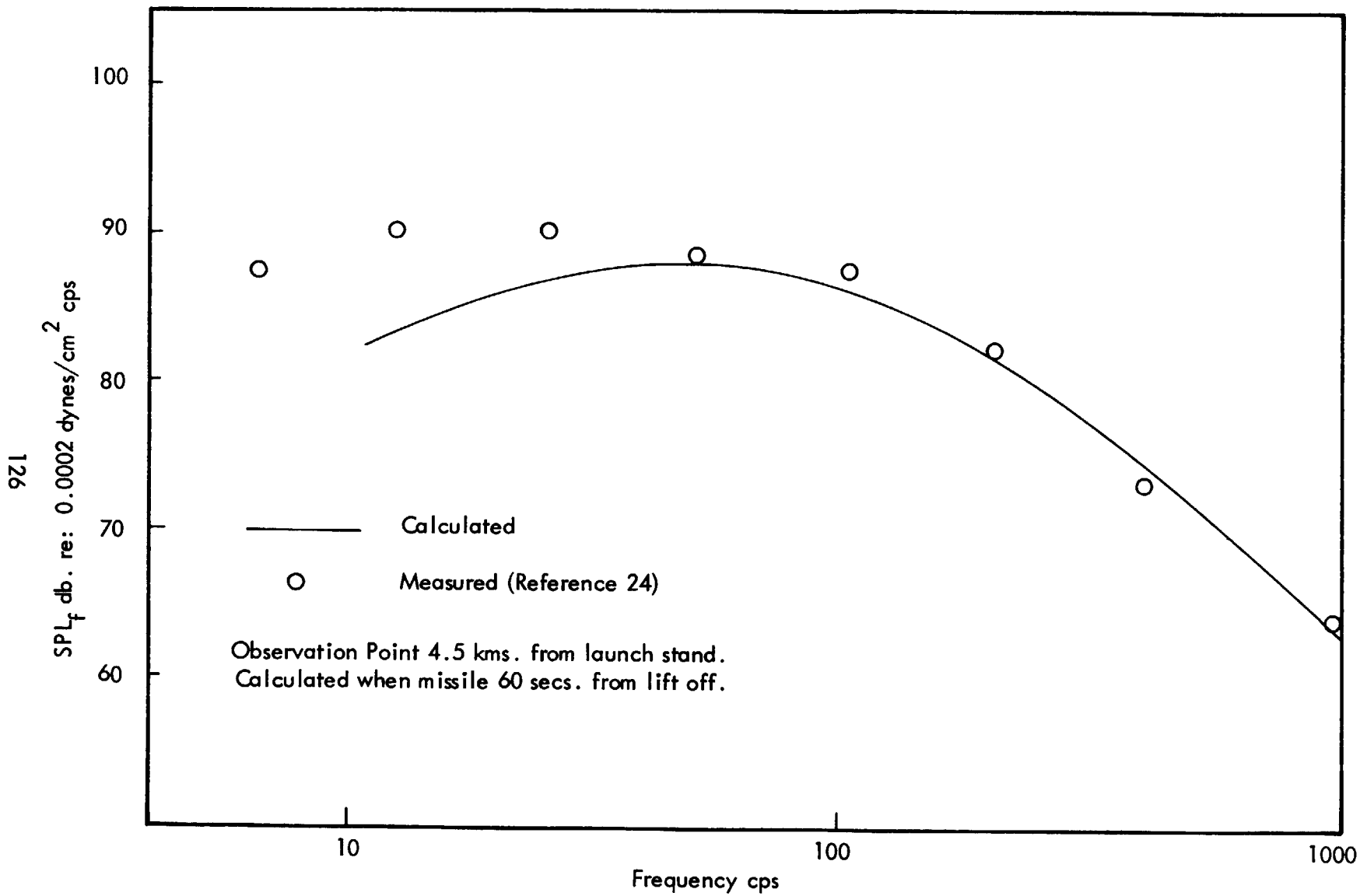


Figure 34: Calculated and Measured Spectra of Far Field Sound Pressure Level for Saturn SA3.

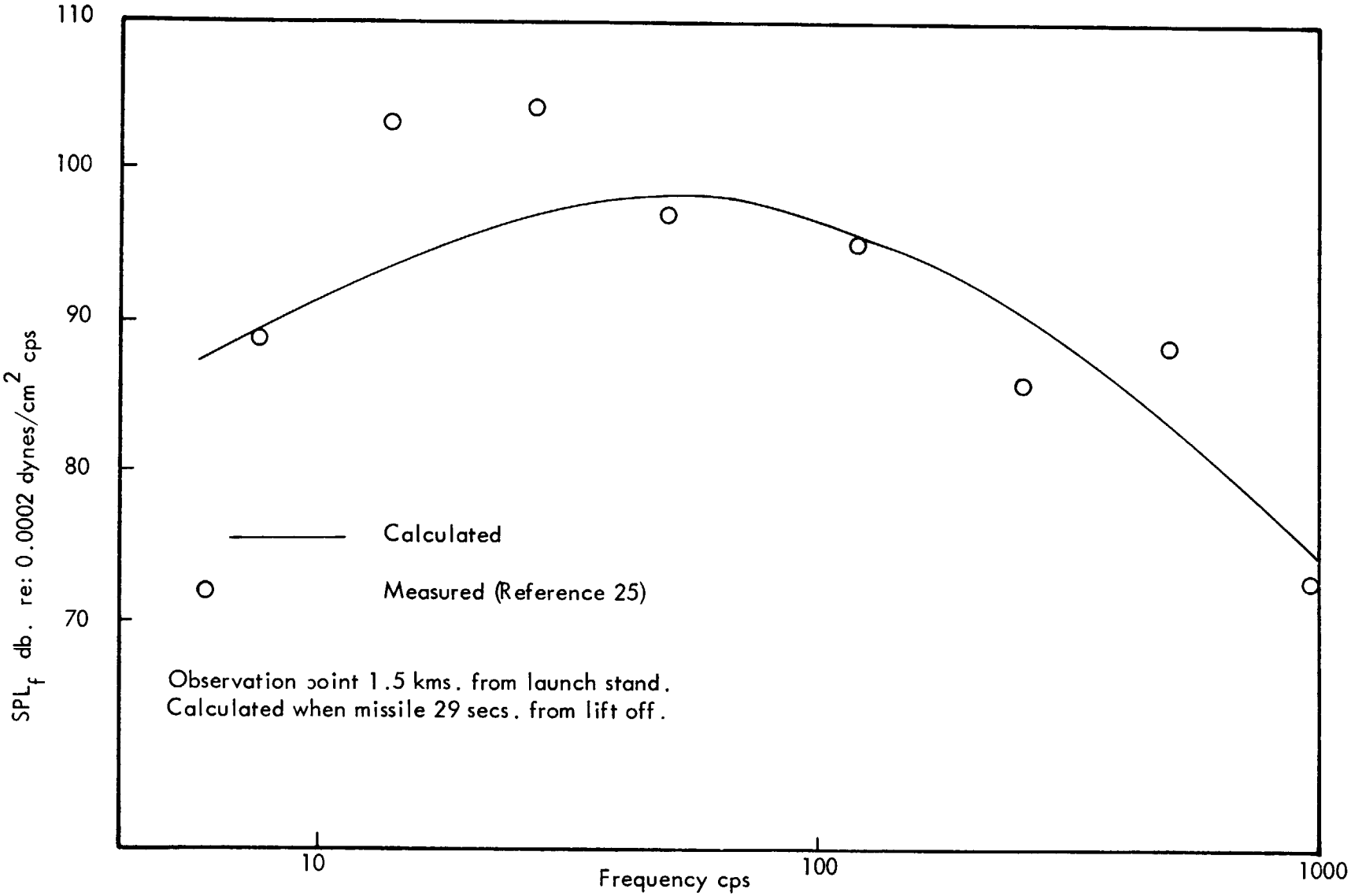


Figure 35: Calculated and Measured Spectra of Far Field Sound Pressure Level for Saturn SA4

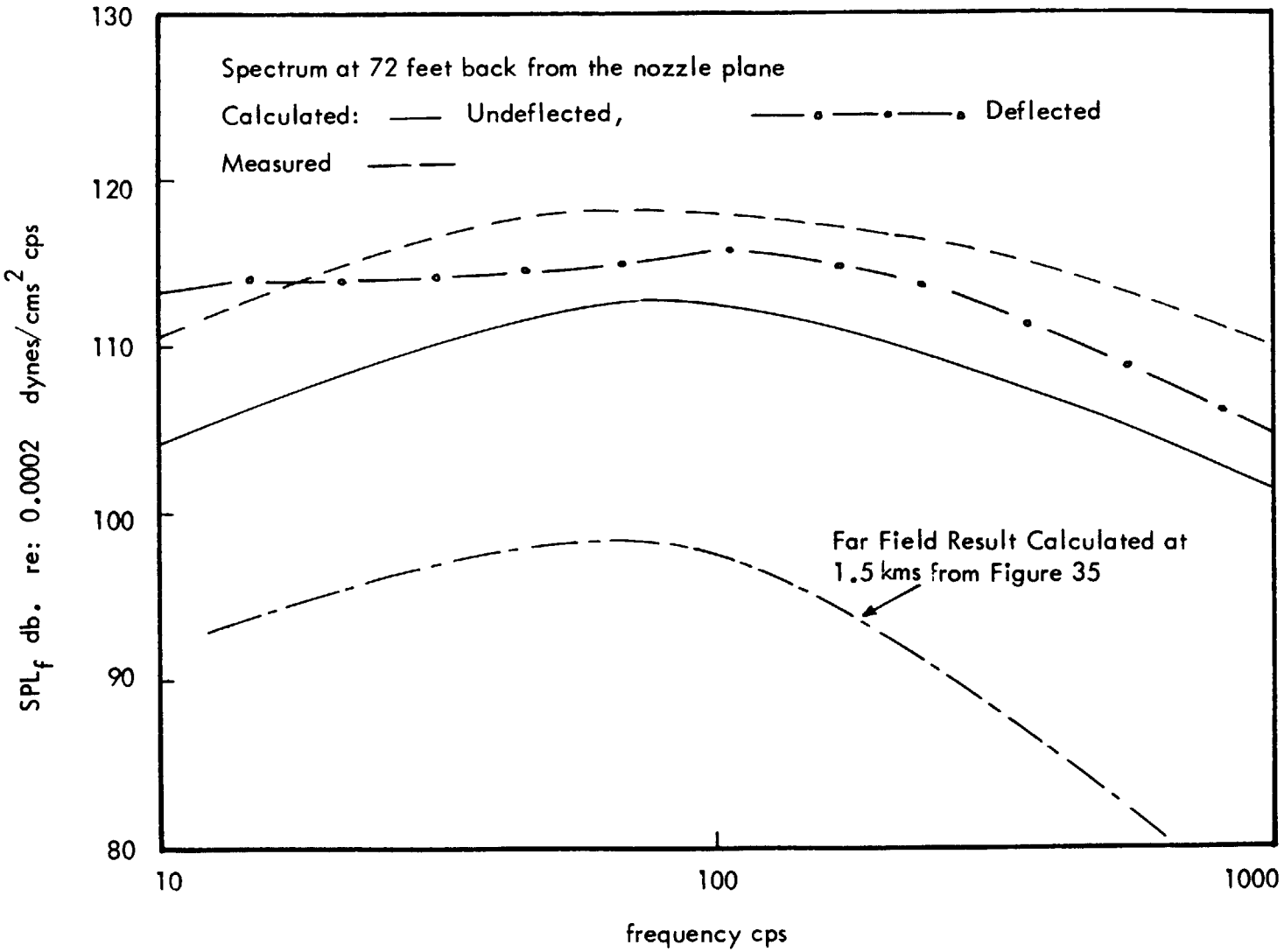


Figure 36 : Calculated and Measured Spectra of Sound Pressure Level on Rocket Body for Saturn and Comparison of Near and Far Field Results

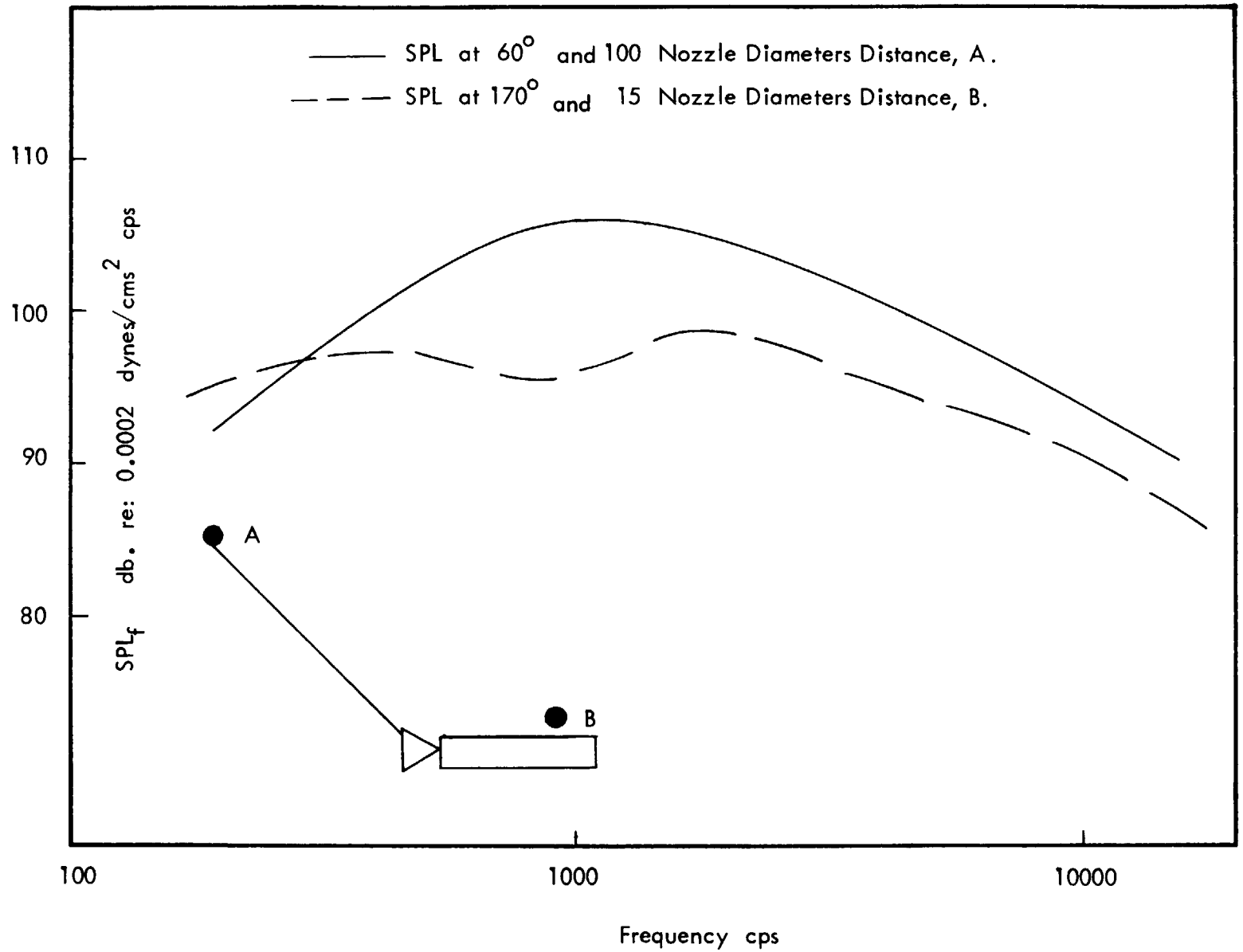


Figure 37: Comparison of Spectra of Sound Pressure Level for Small Solid Fueled Rocket (Reference 1)

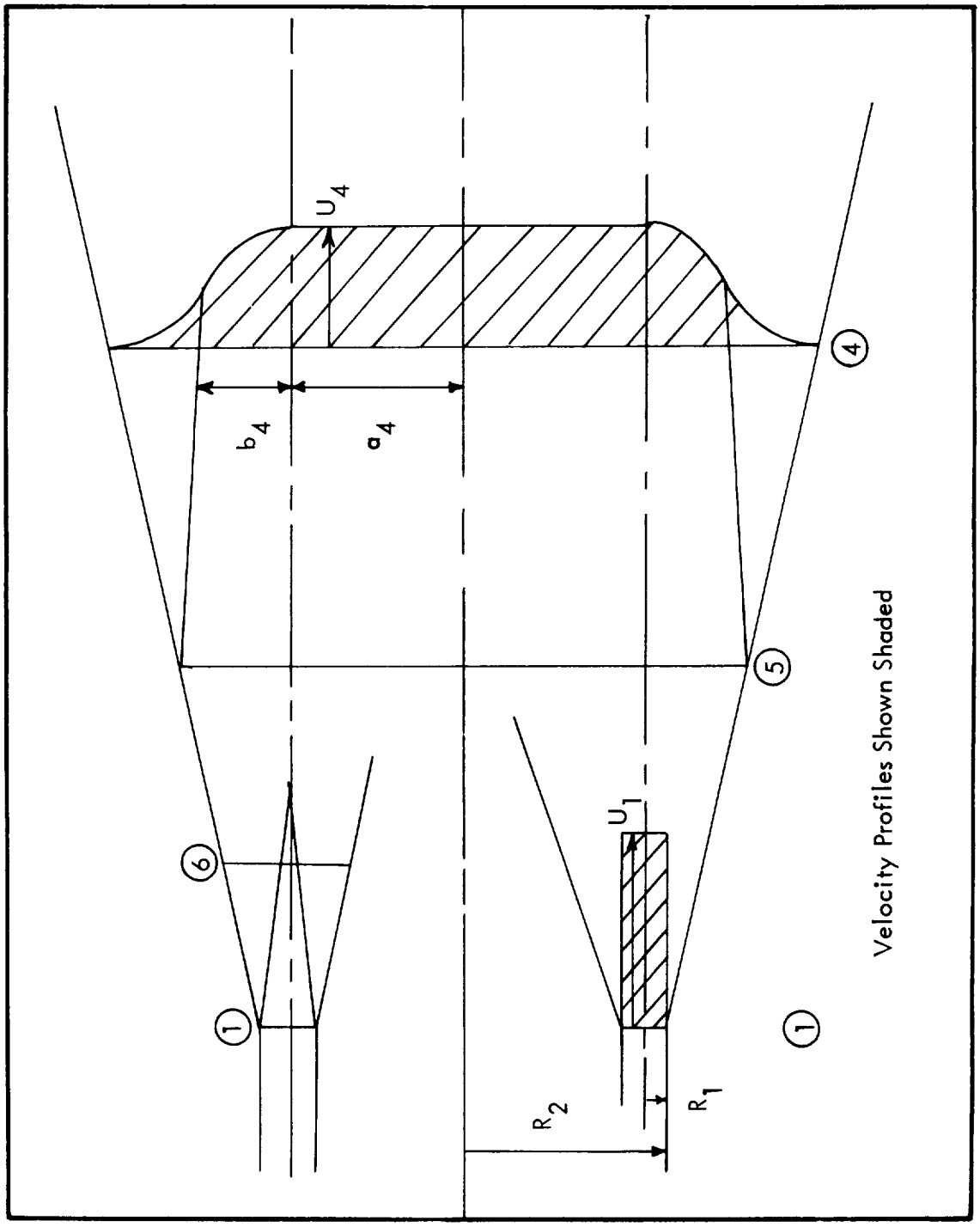


Figure 38: Multiple Rocket Nozzles

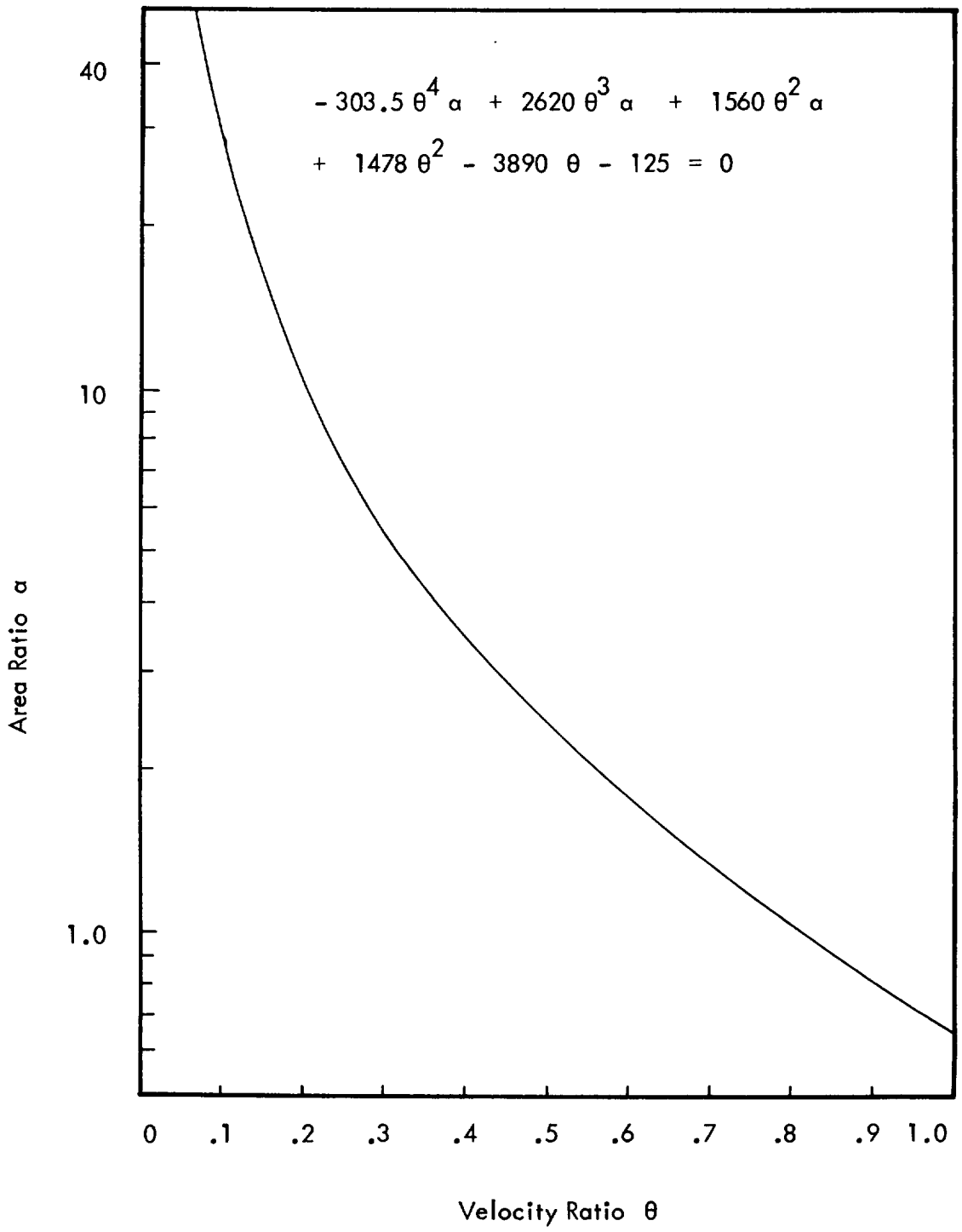


Figure 39: Velocity Ratio at the Downstream Fully Mixed Flow Position of Rocket Cluster Example

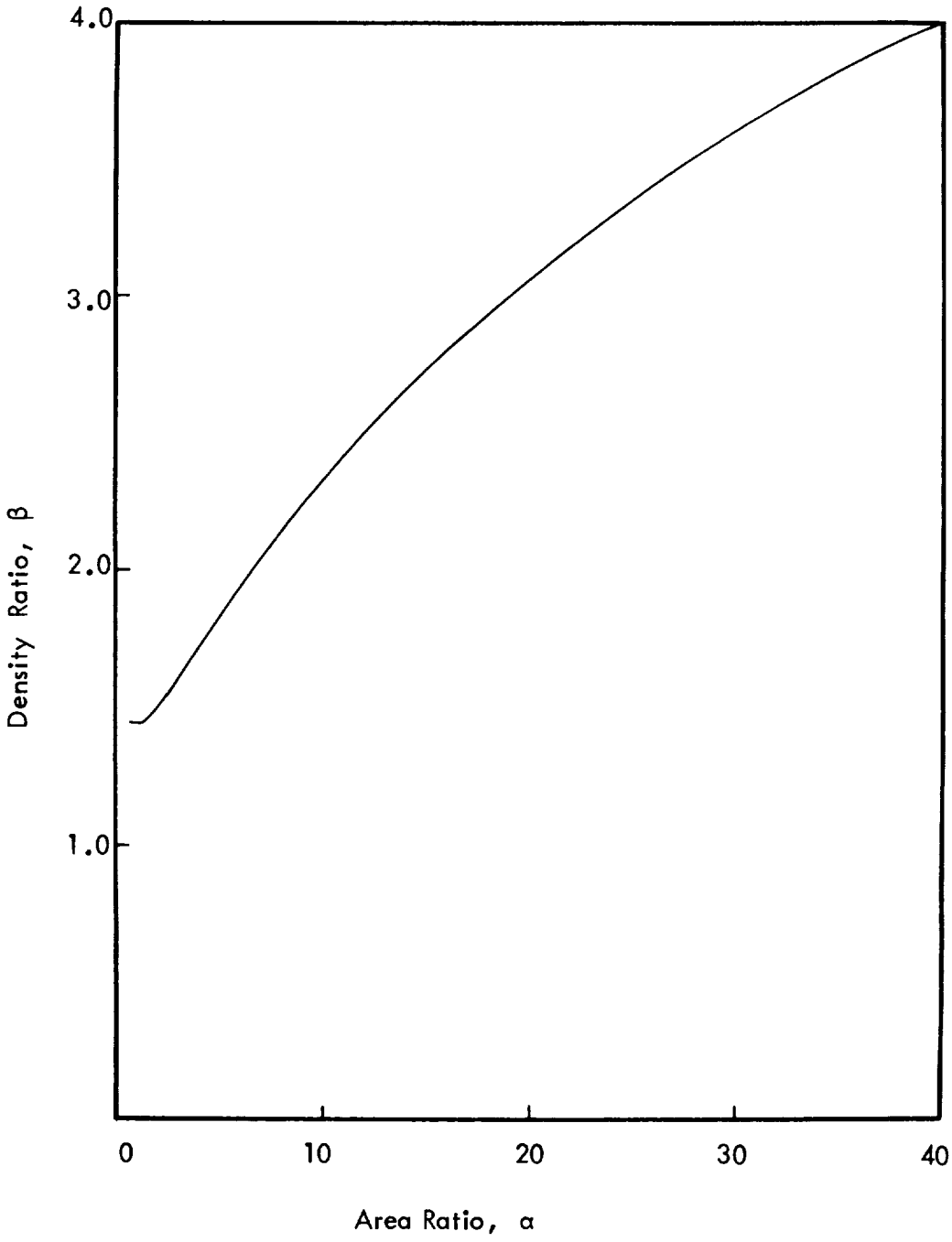


Figure 40: Density Ratio at the Downstream Fully Mixed Flow Position of Rocket Cluster Example

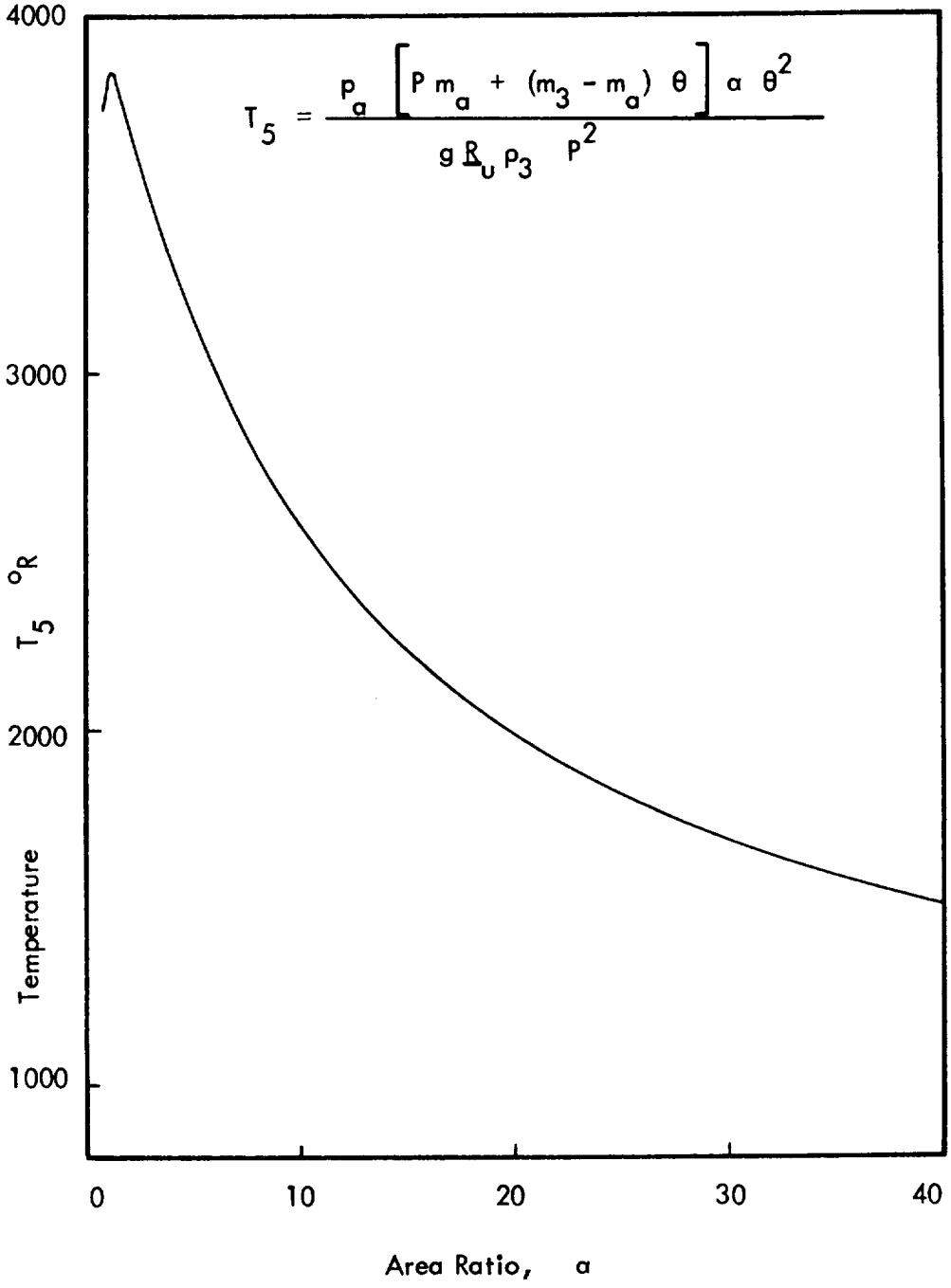


Figure 41: Temperature at the Downstream Fully Mixed Flow Position of the Rocket Cluster Example

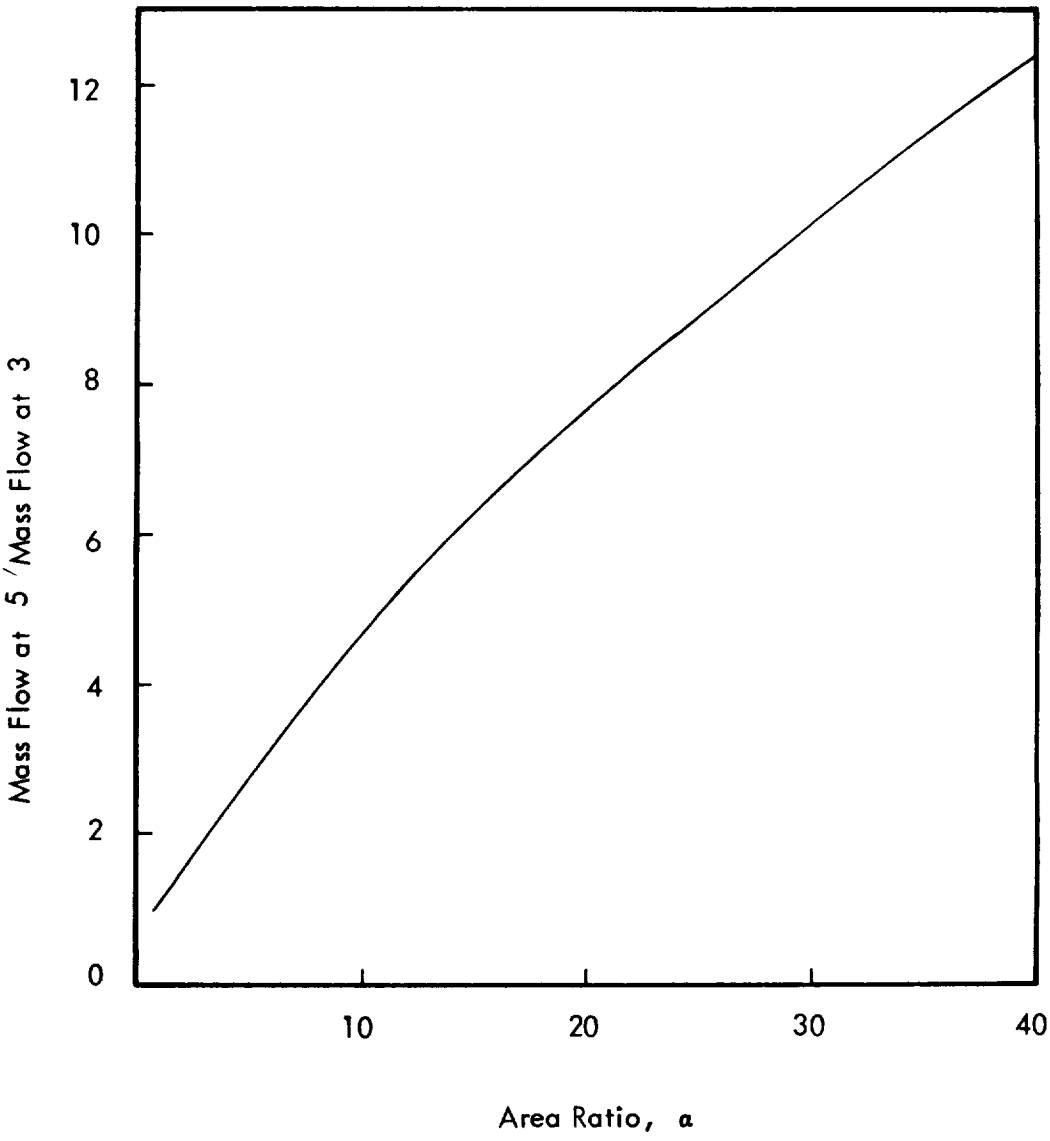


Figure 42: Mass Flow Ratio at the Downstream Fully Mixed Flow Position of Rocket Cluster Example

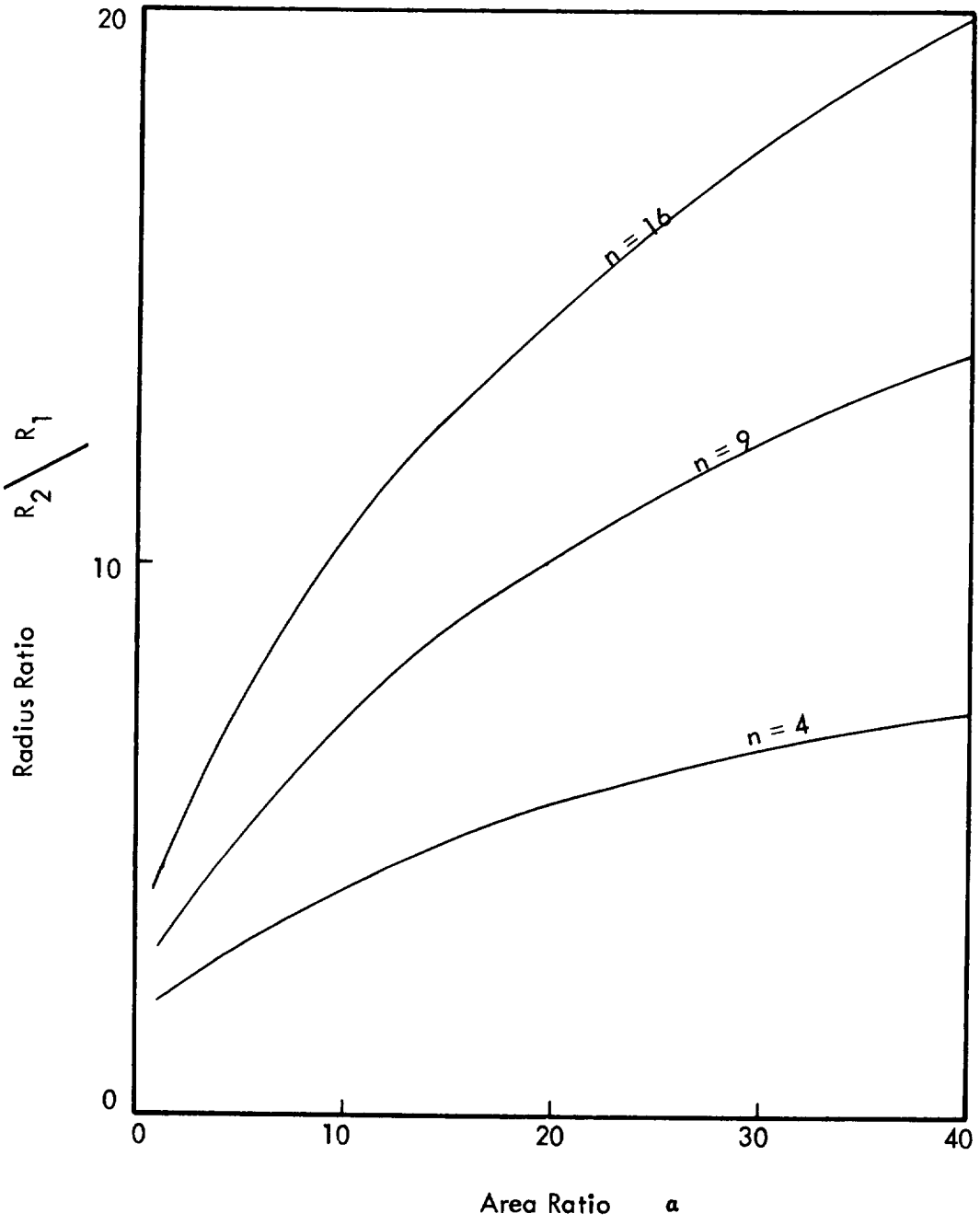


Figure 43: Area Ratio for the Downstream Fully Mixed Flow for Various Clusters

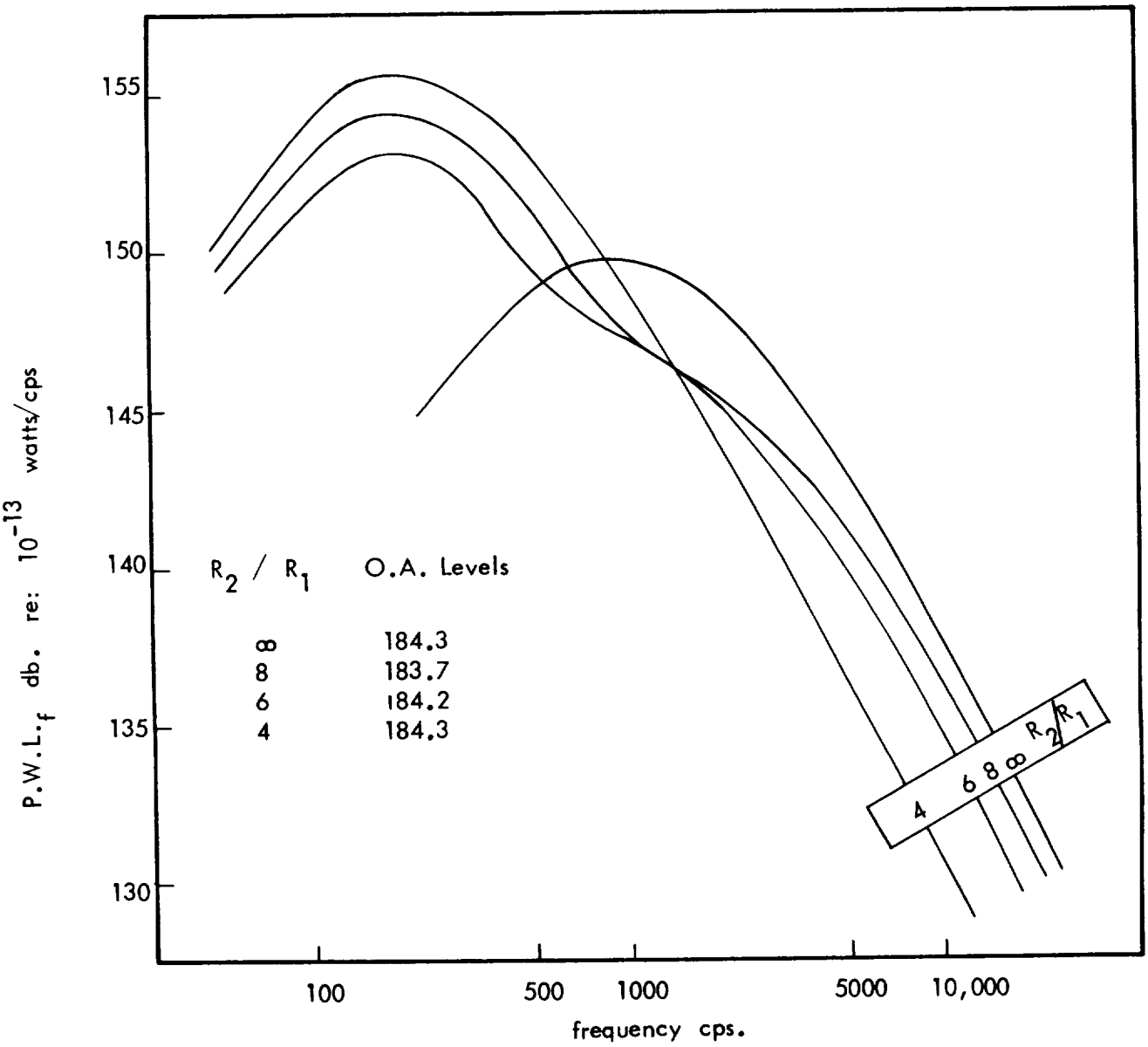


Figure 44: Calculated Spectra of Noise Power for 16 Rocket Cluster

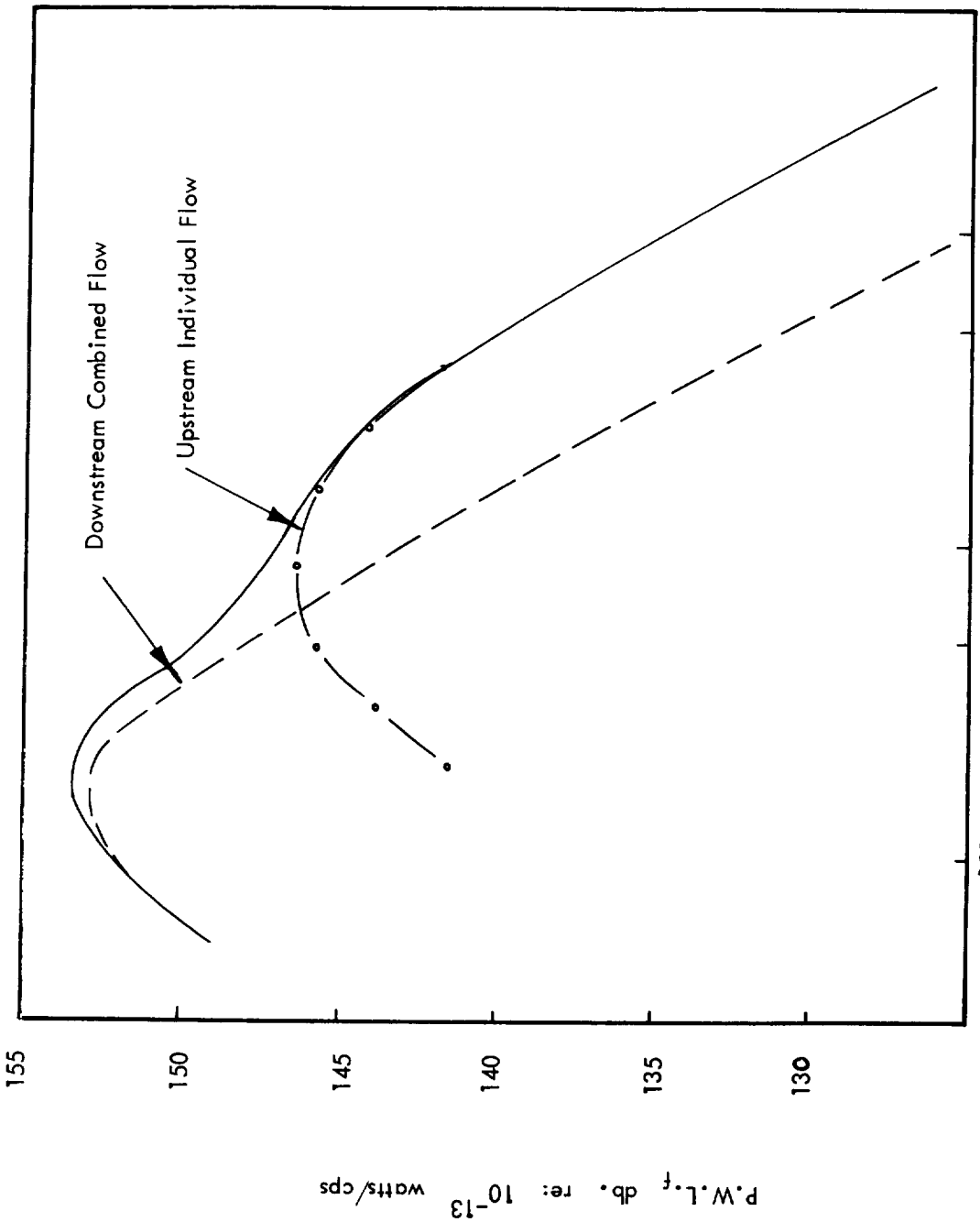


Figure 45: Calculated Spectrum of Noise Power for 16 Rocket Cluster Showing Sound Generated by the two Parts of the Flow.

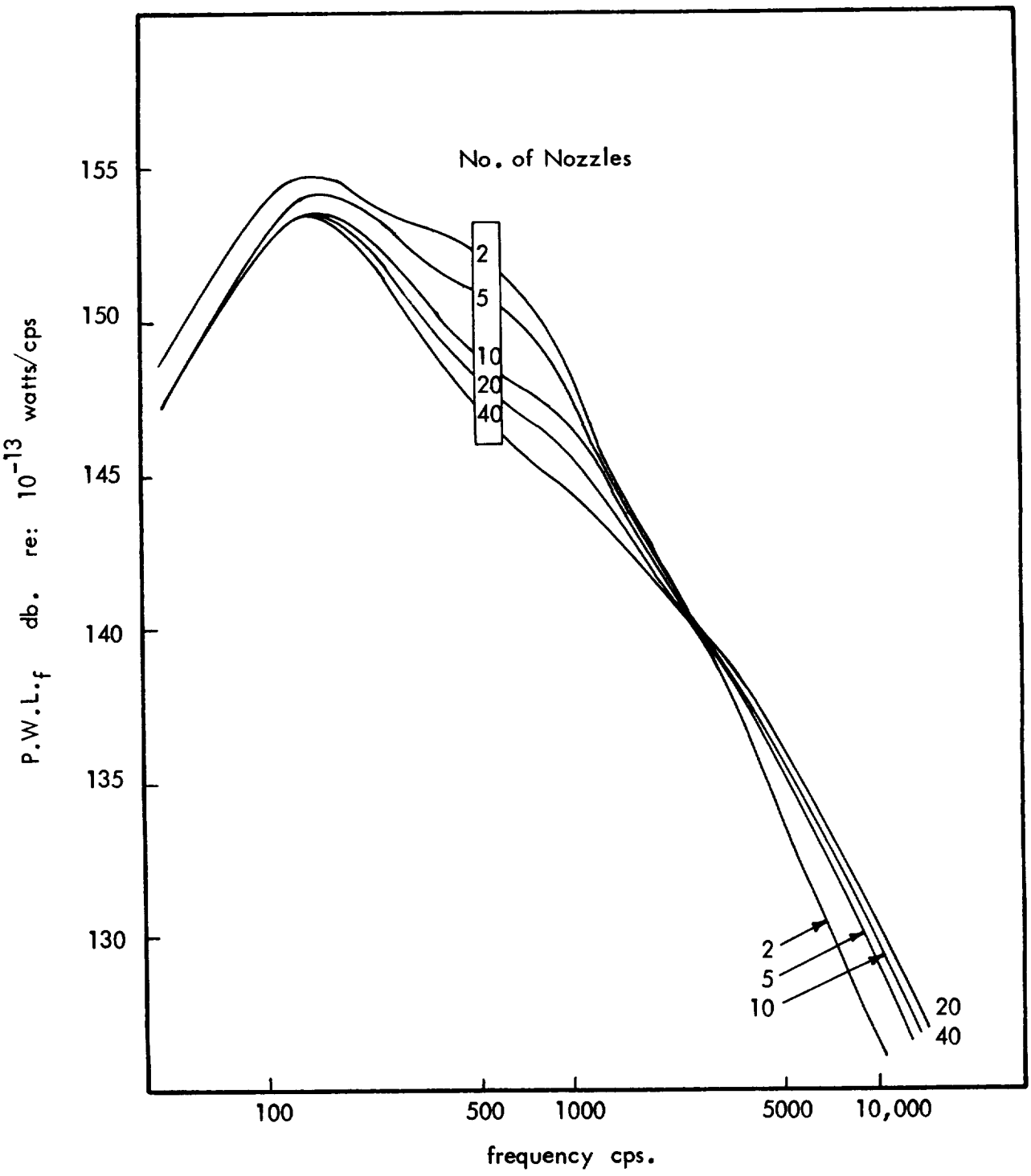


Figure 46: Effect of Number of Nozzles on the Calculated Resultant Power Spectrum of a Rocket Cluster

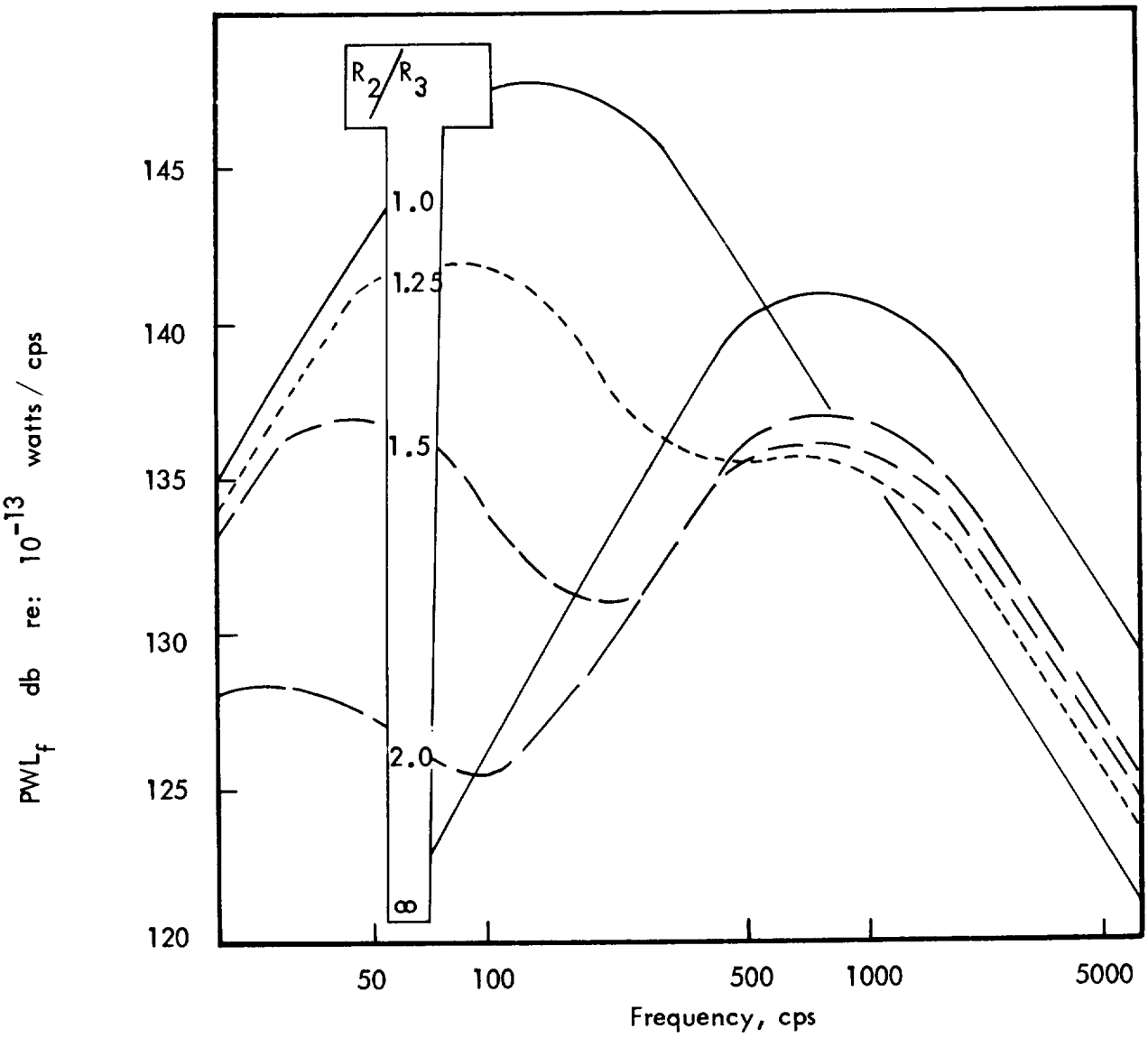


Figure 47: Calculated Power Spectra for Clusters of Turbojet Nozzles
( from Reference 18 )

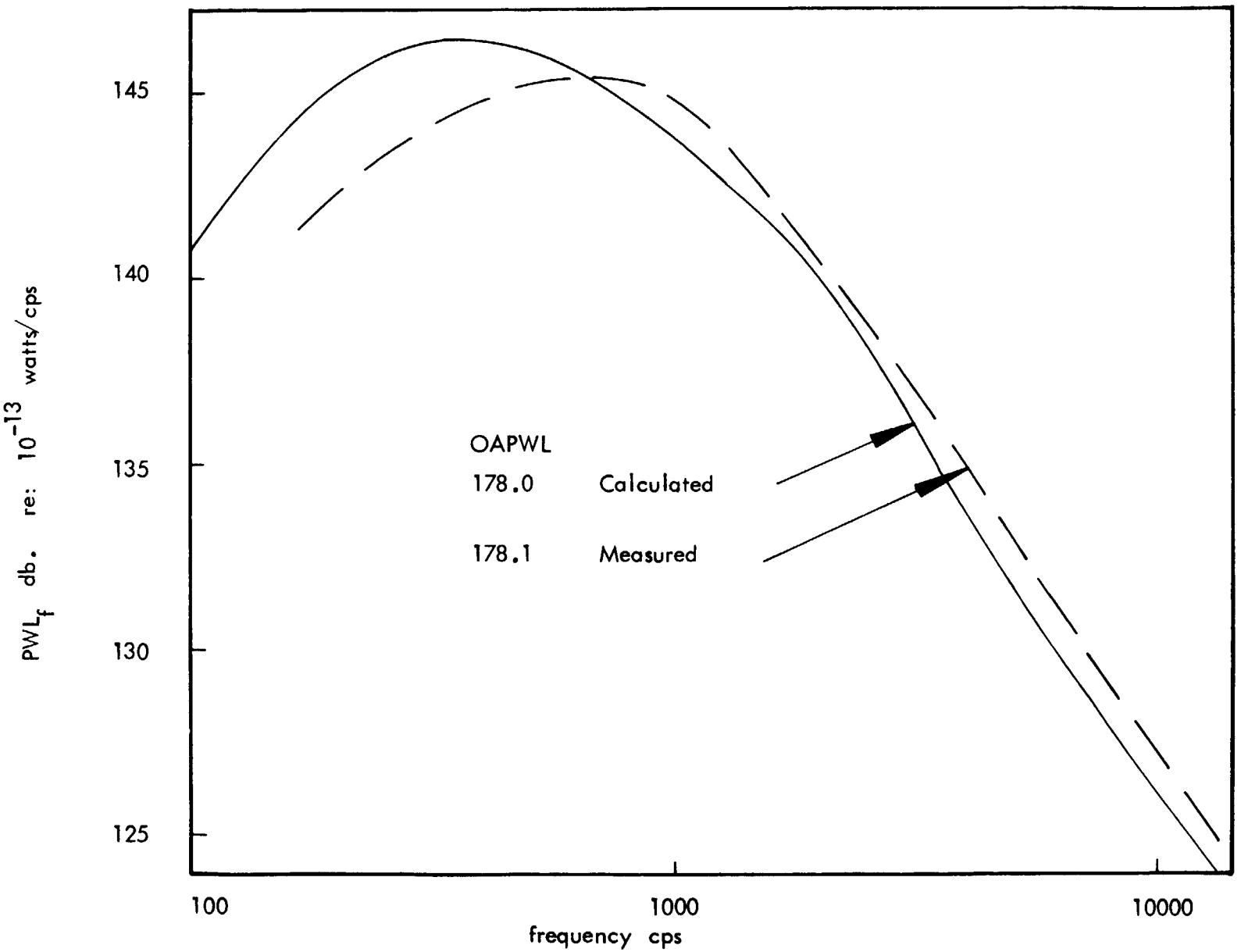


Figure 48: Boeing 4 Nozzle Cluster Calculated and Measured Spectra of Noise Produced

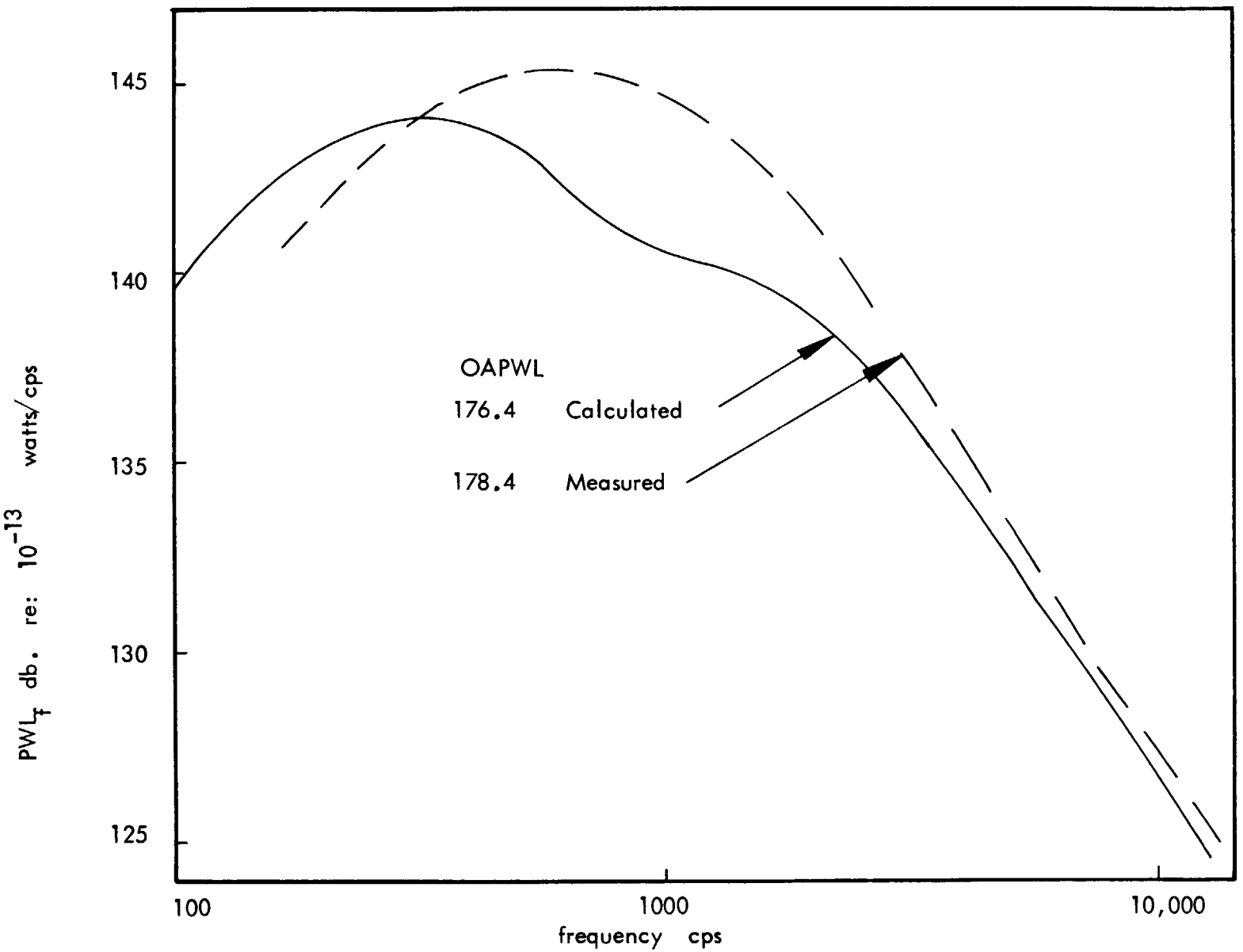


Figure 49: Boeing 16 Nozzle Cluster, Calculated and Measured Spectra of Noise Produced

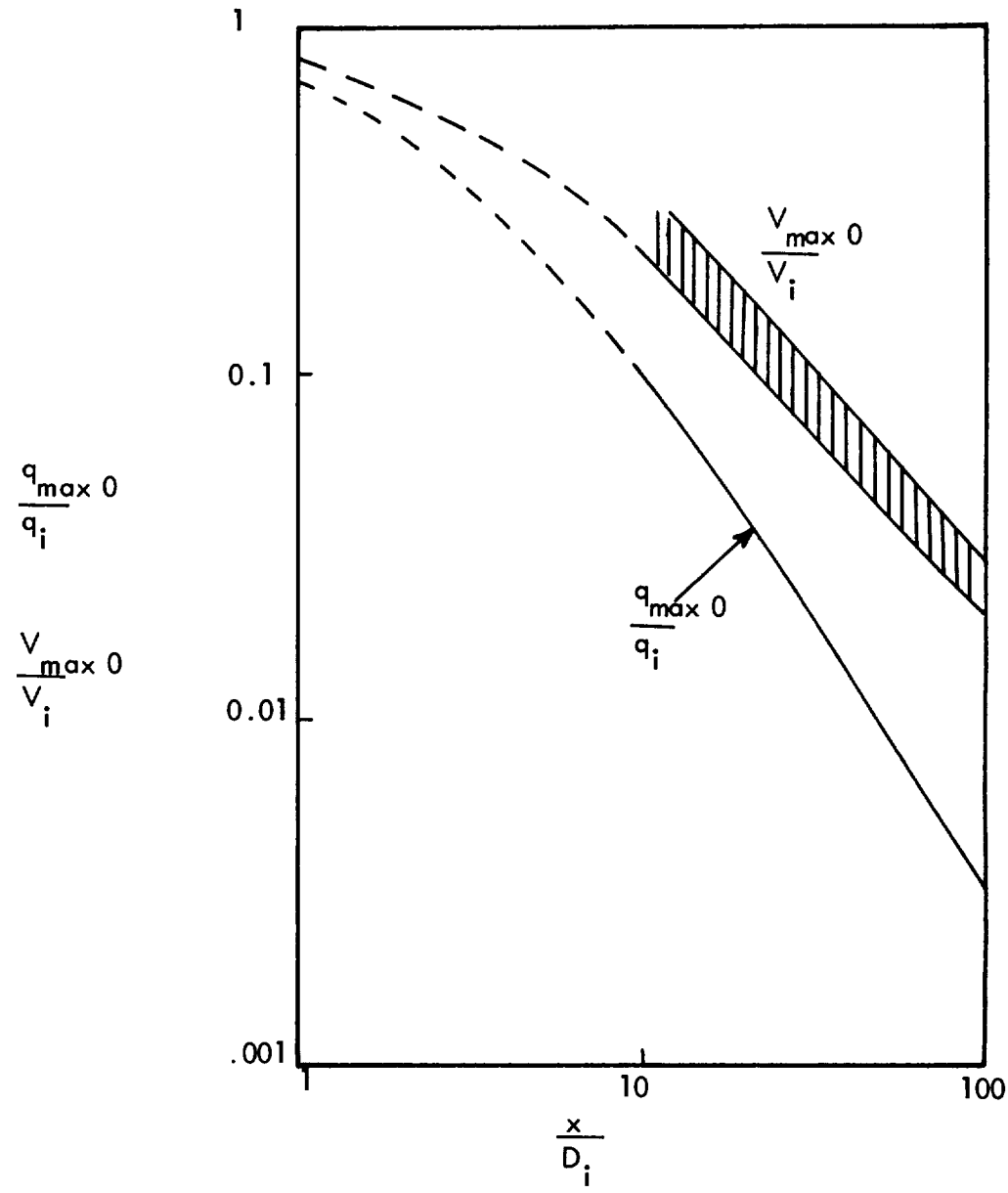


Figure 52, Decay of Dynamic Pressure and Velocity Down Deflector, (from Reference 32)

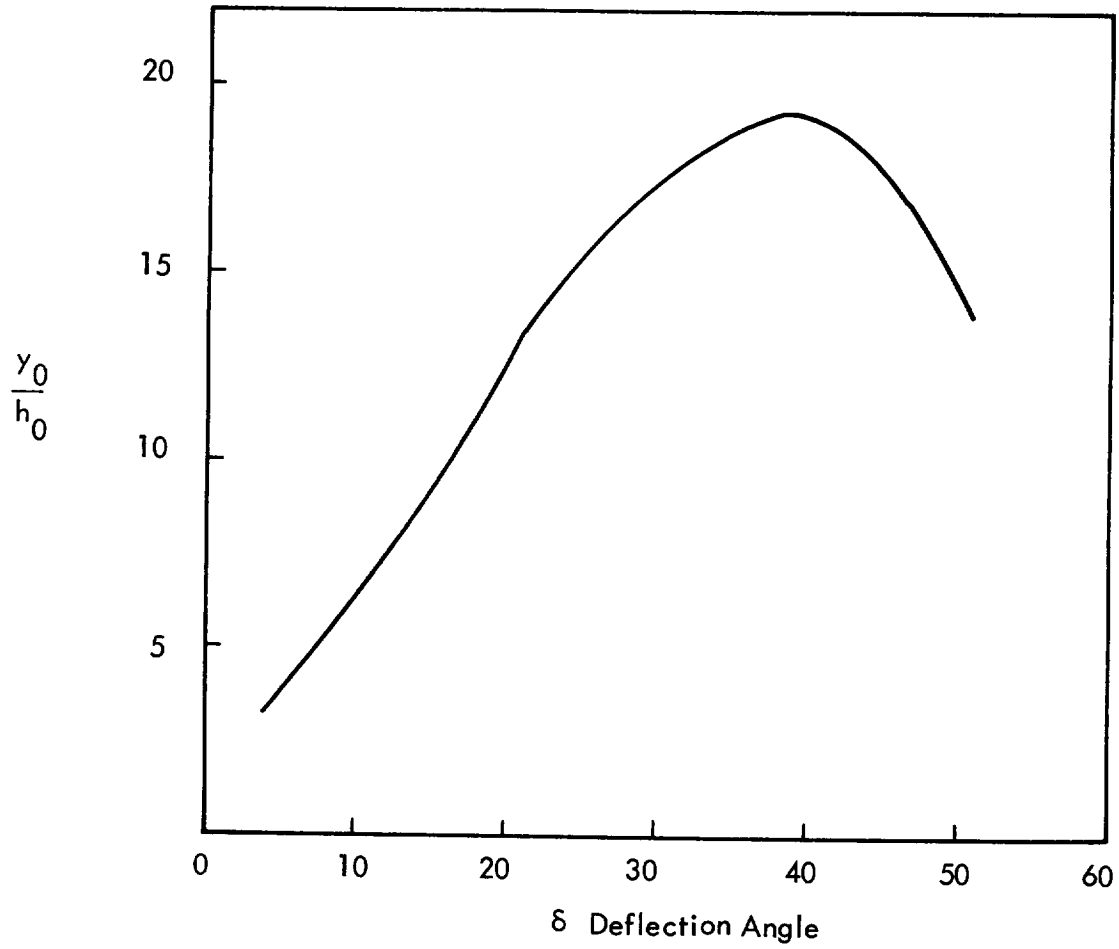


Figure 53: Width to Height Ratio of Deflected Flow (from Reference 32)

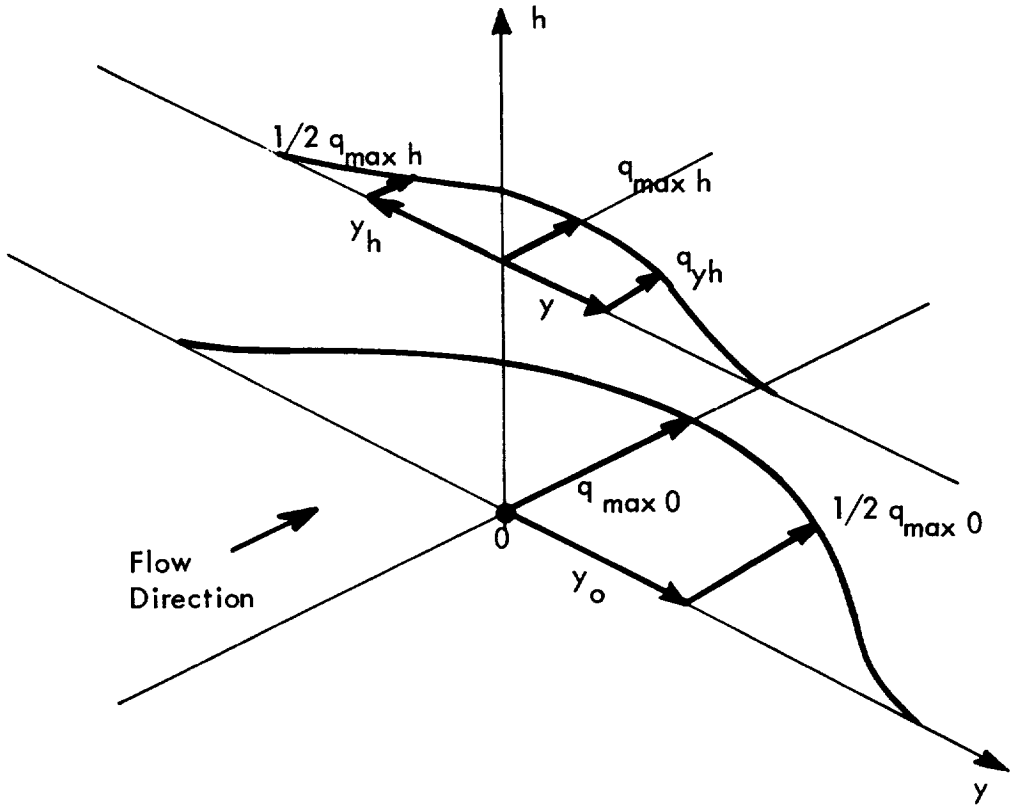


Figure 54: Representation of Deflected Flow

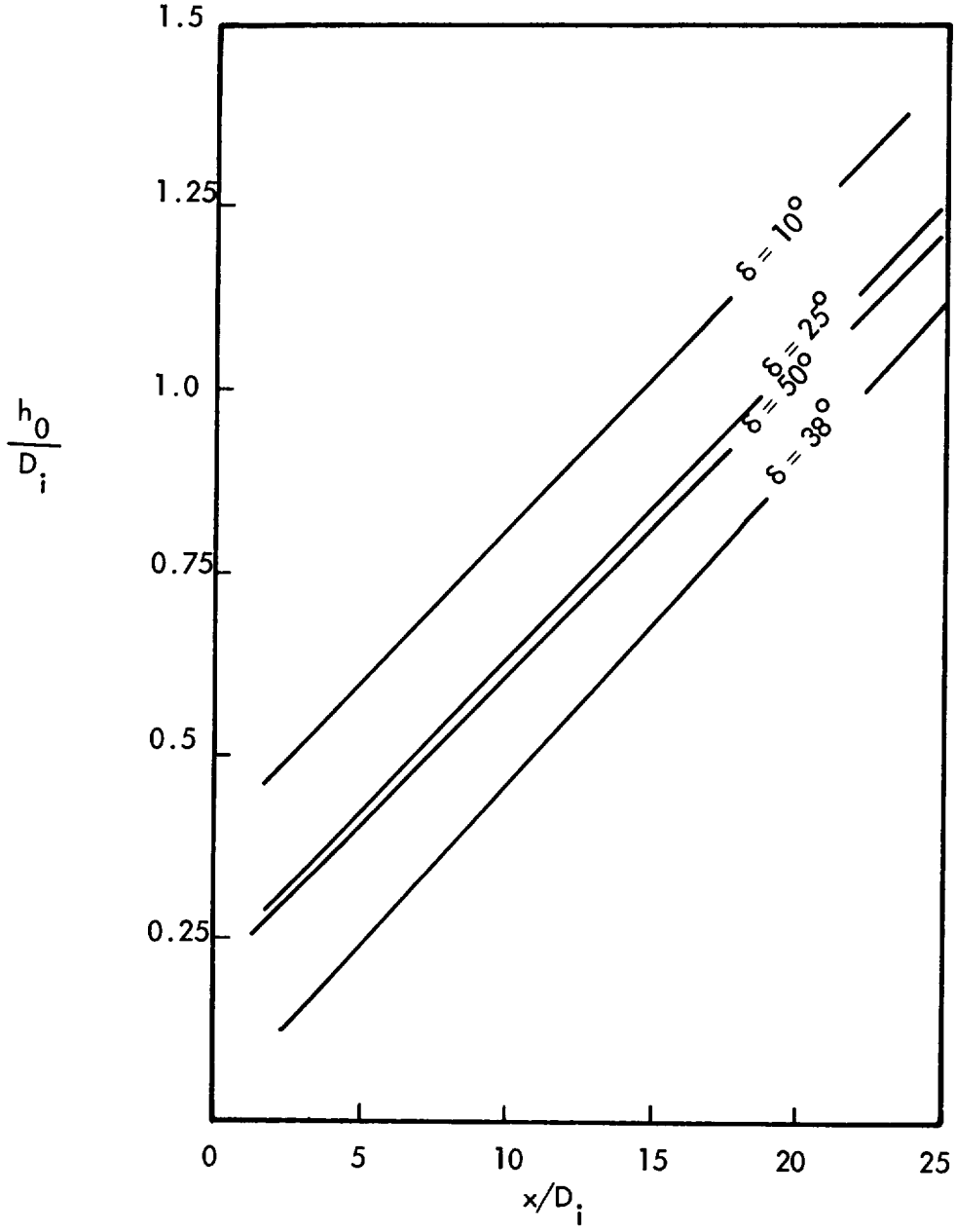


Figure 55: Vertical Rise of Deflected Jet (from Reference 32)

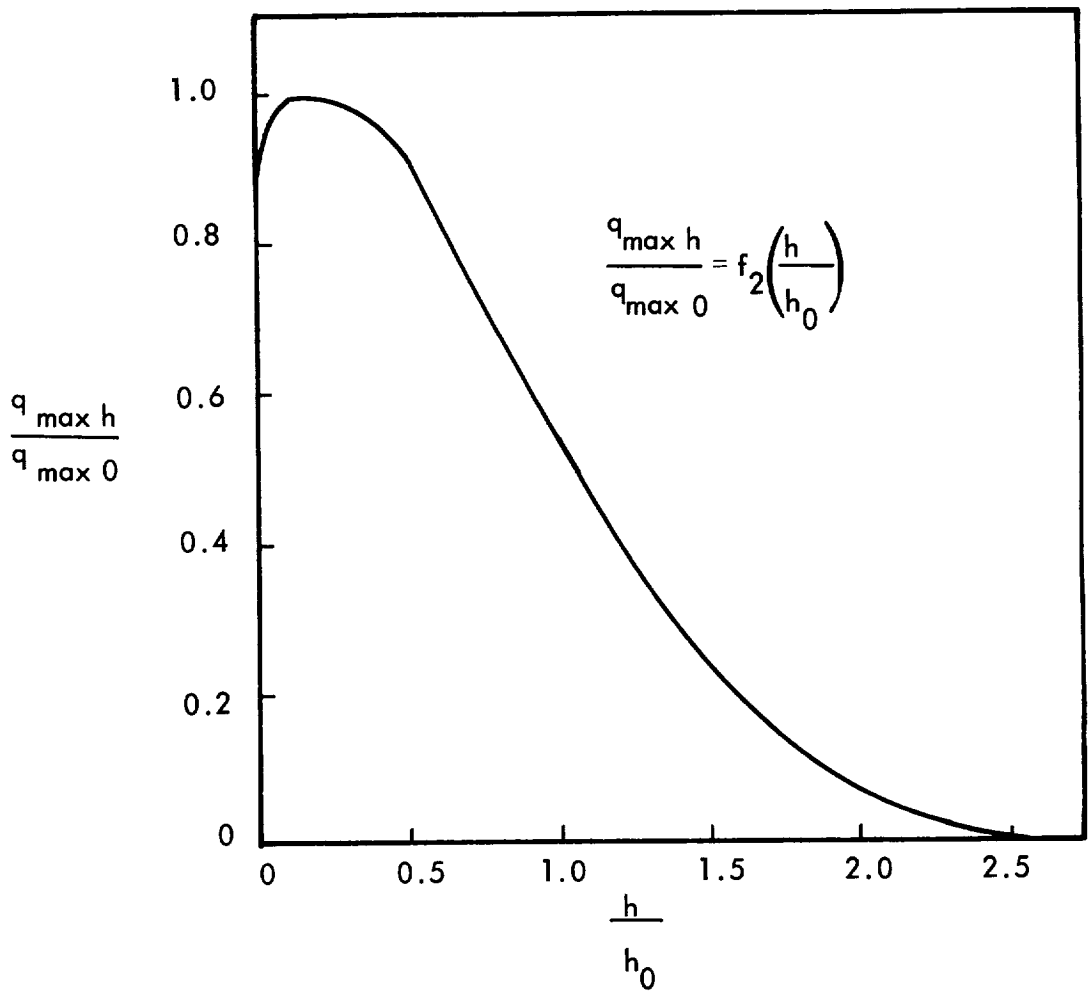


Figure 56: Deflected Jet, Vertical Total Pressure Profile (from Reference 32)

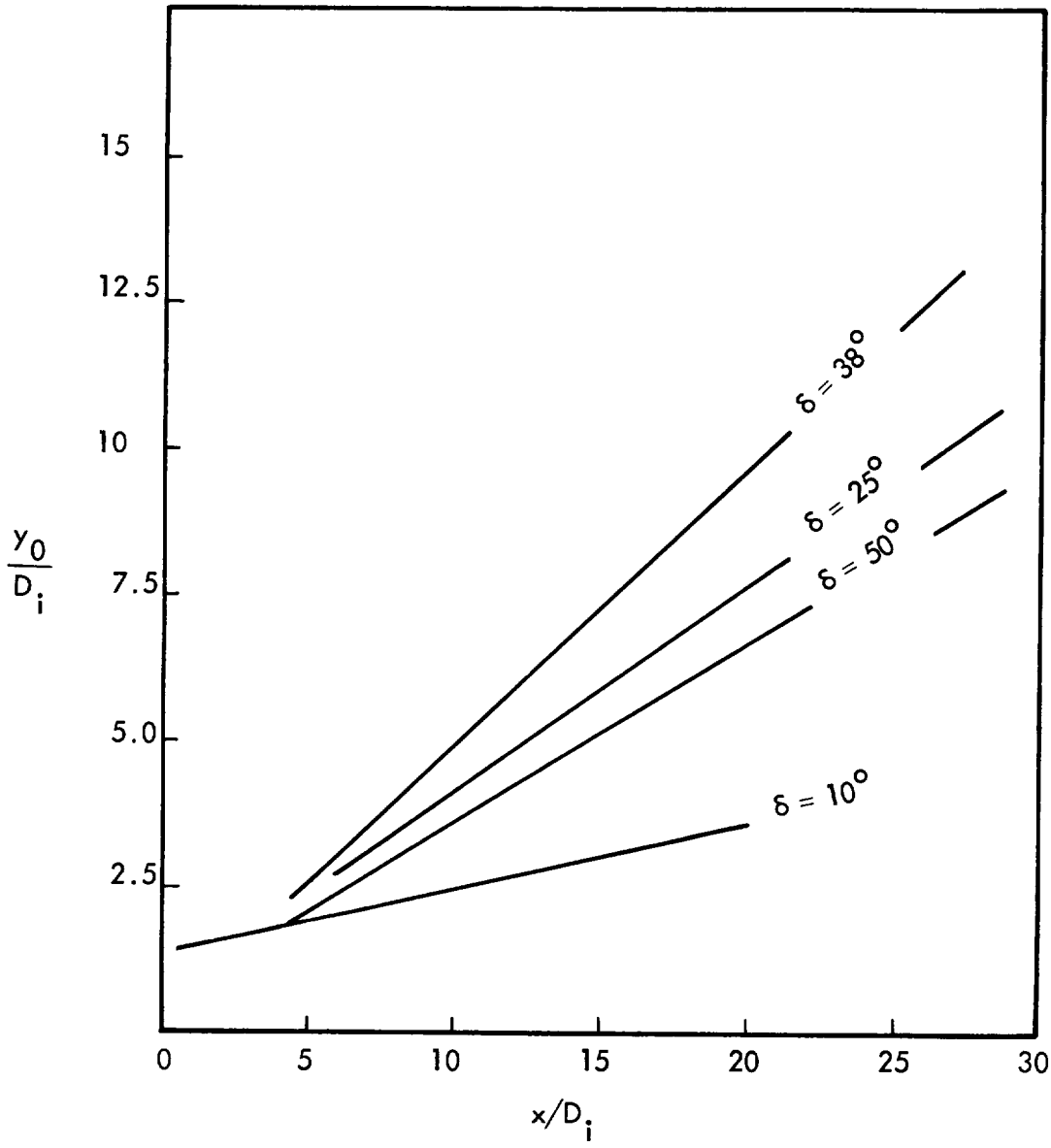


Figure 57: Horizontal Spreading of Deflected Jet (from Reference 32)

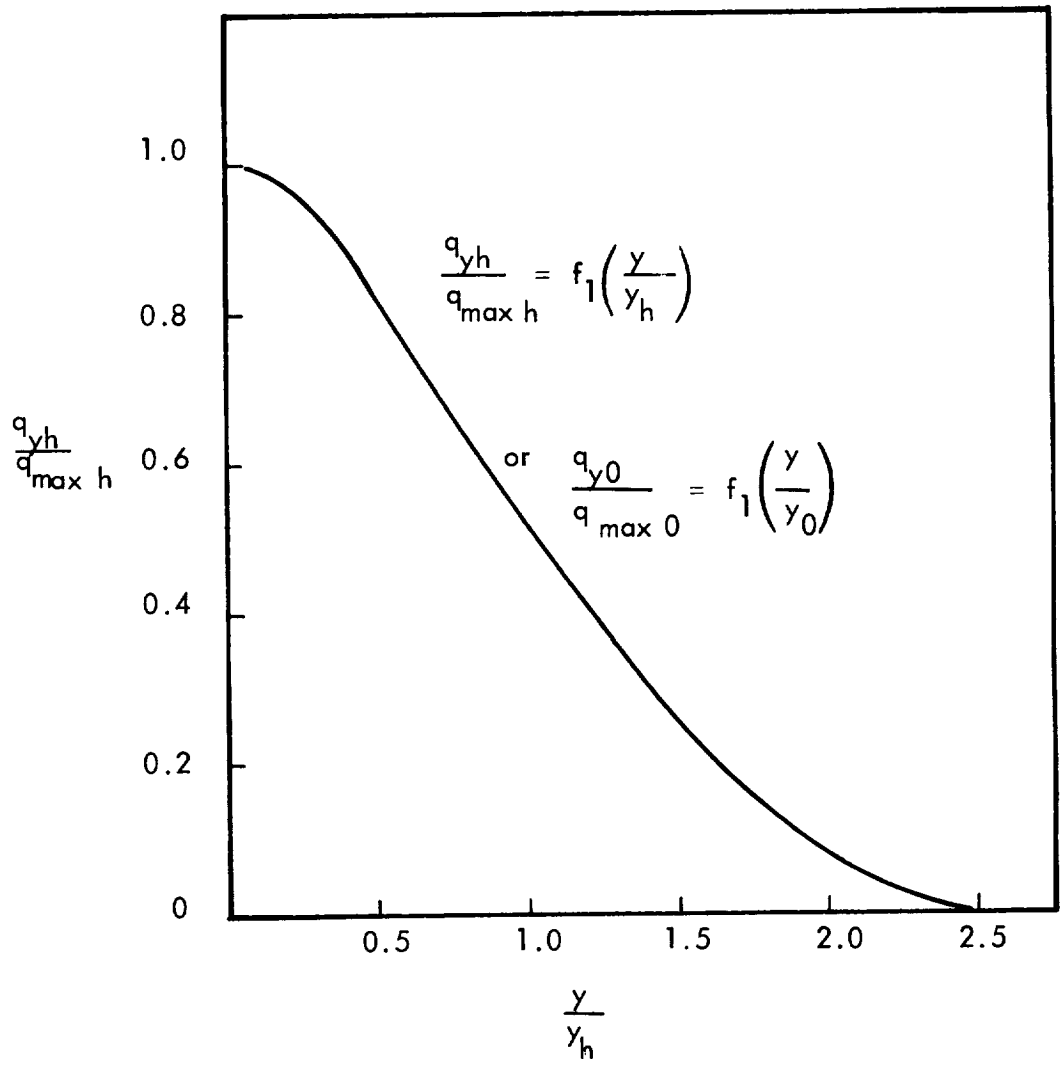


Figure 58: Deflected - Jet, Total Pressure Profile (from Reference 32)

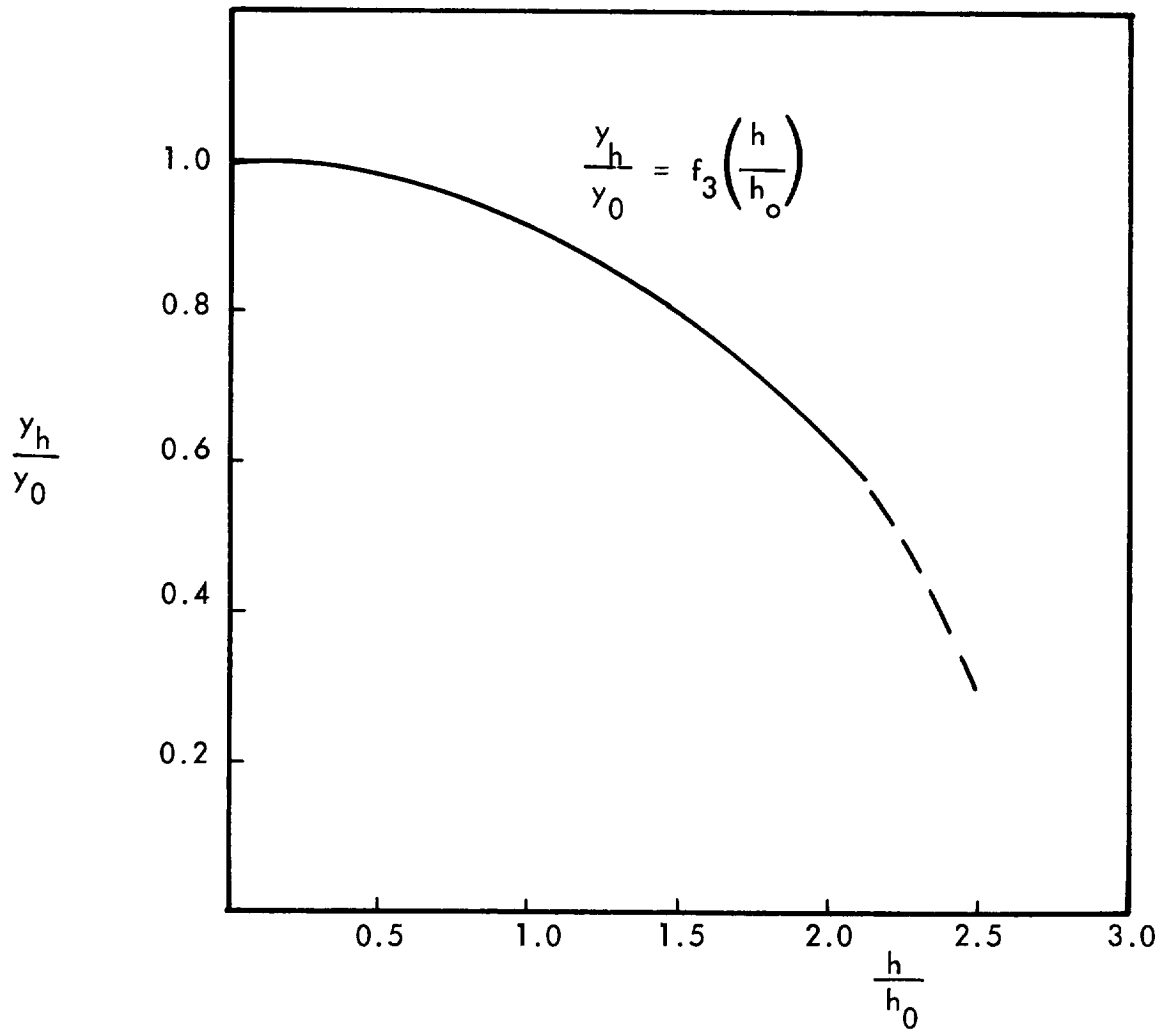


Figure 59: Decay Curve of $y_h$ with Height of Deflected Jet
$\delta = 10^o$ to $50^o$ (from Reference 32)

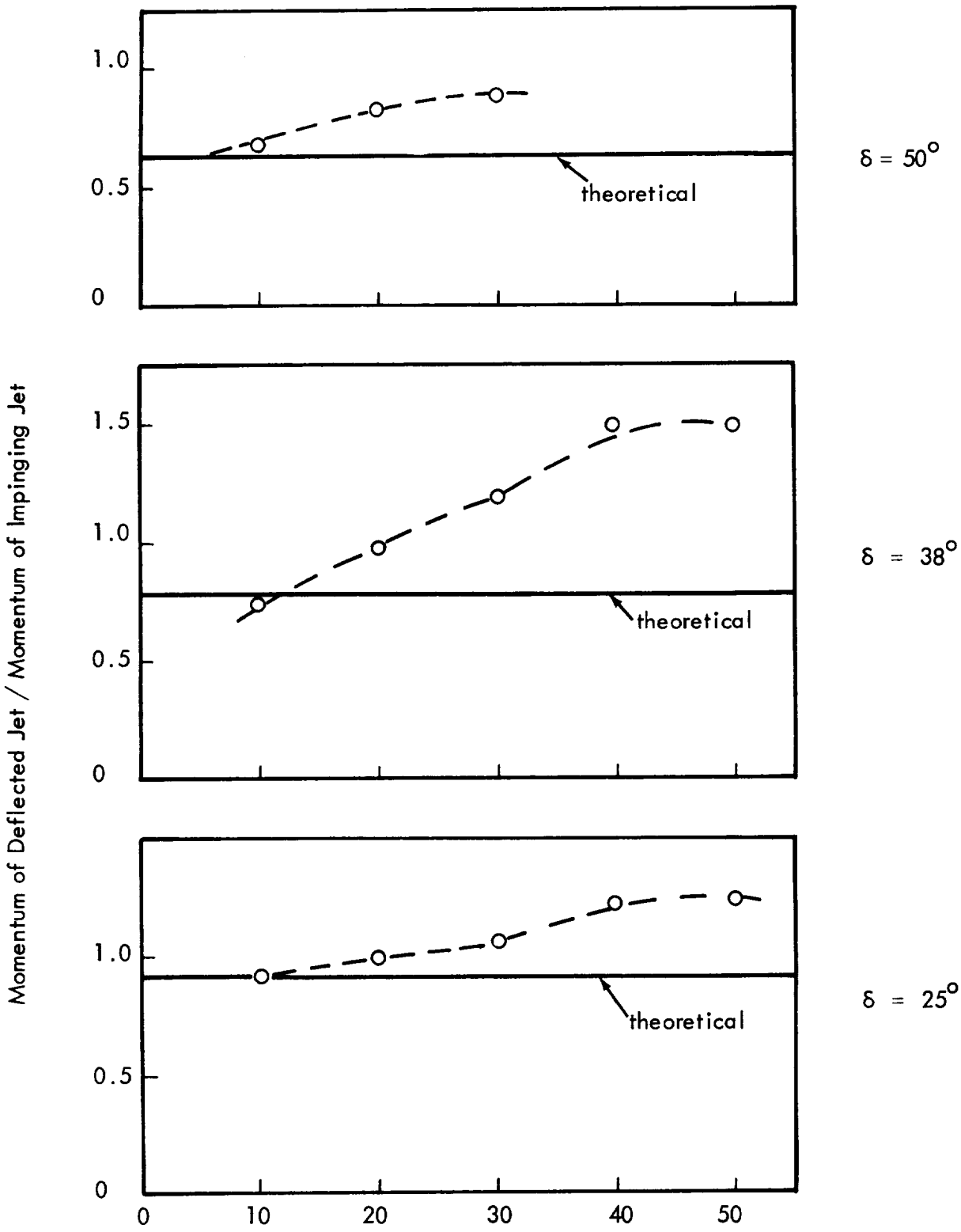


Figure 60: Momentum for a Deflected Jet Compared with Theoretical Value of cos δ Times Incident Momentum (from the Results of Reference 32)

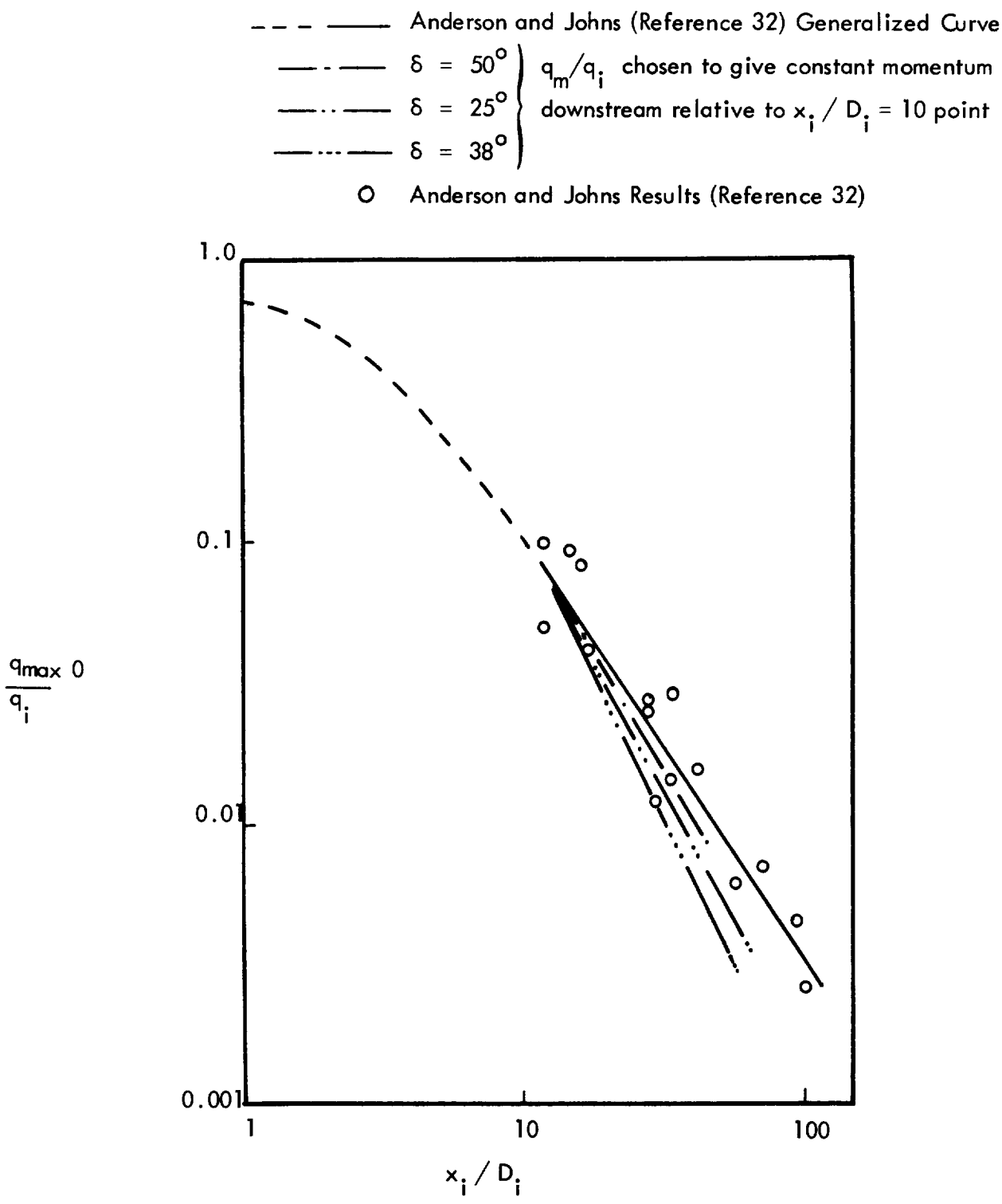


Figure 61: Corrected Dynamic Pressure Decay for Deflected Jet

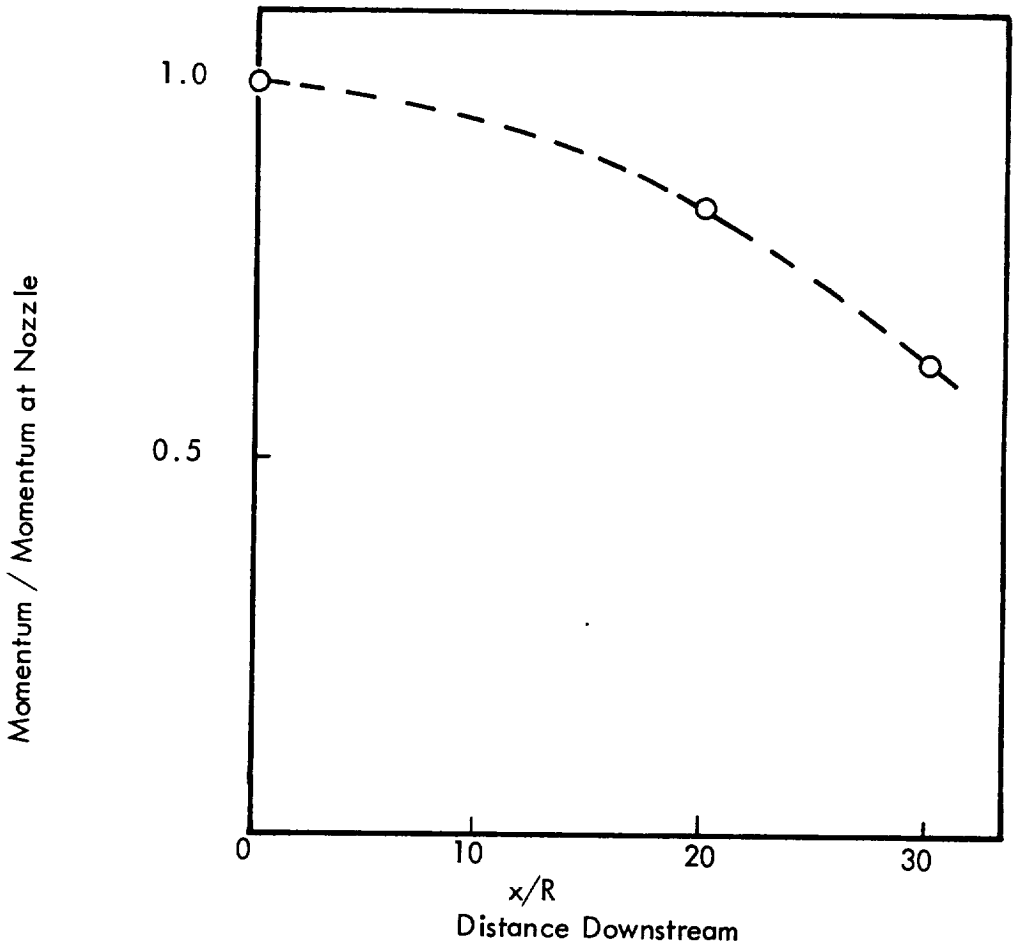


Figure 62: Momentum of Rocket Exhaust (from Reference 33)

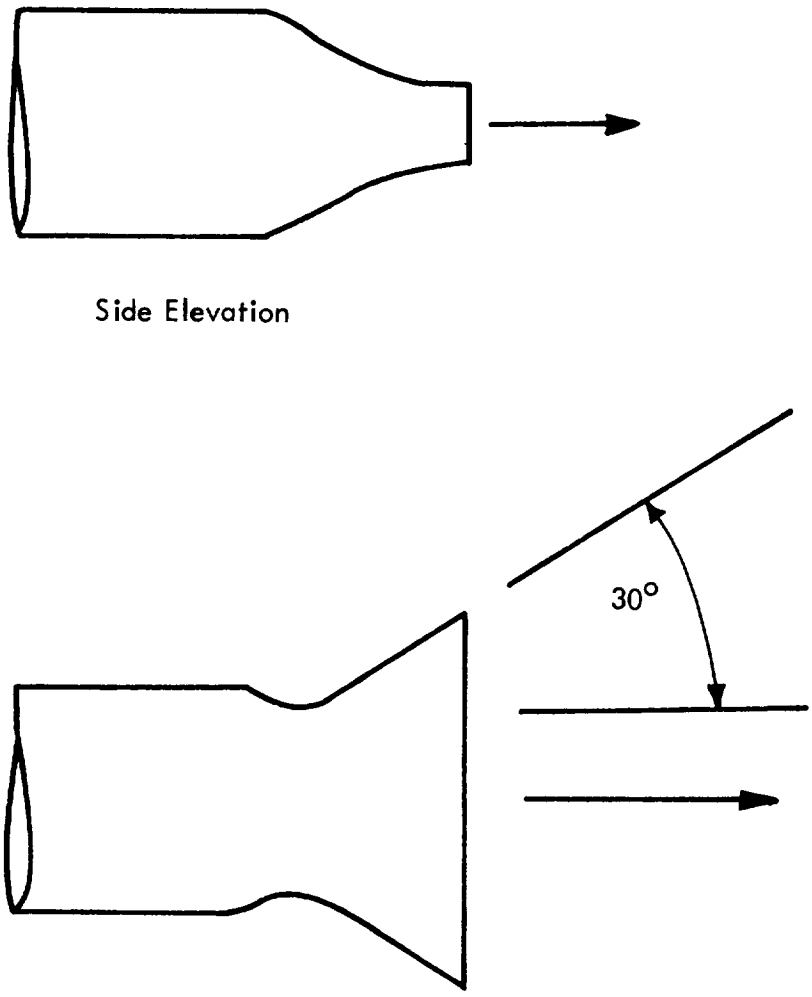


Figure 63: Divergent Nozzles (from Reference 34)

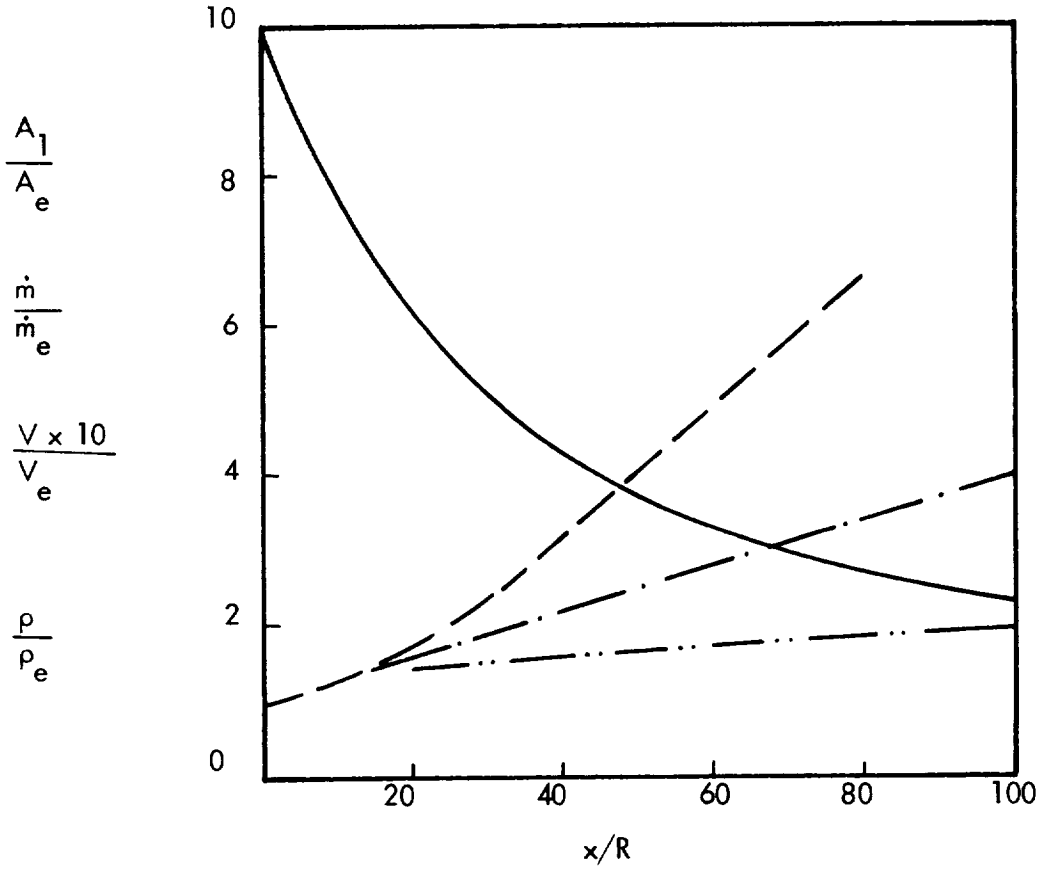


Figure 64: Growth of Flow Parameters for Small Rocket Example

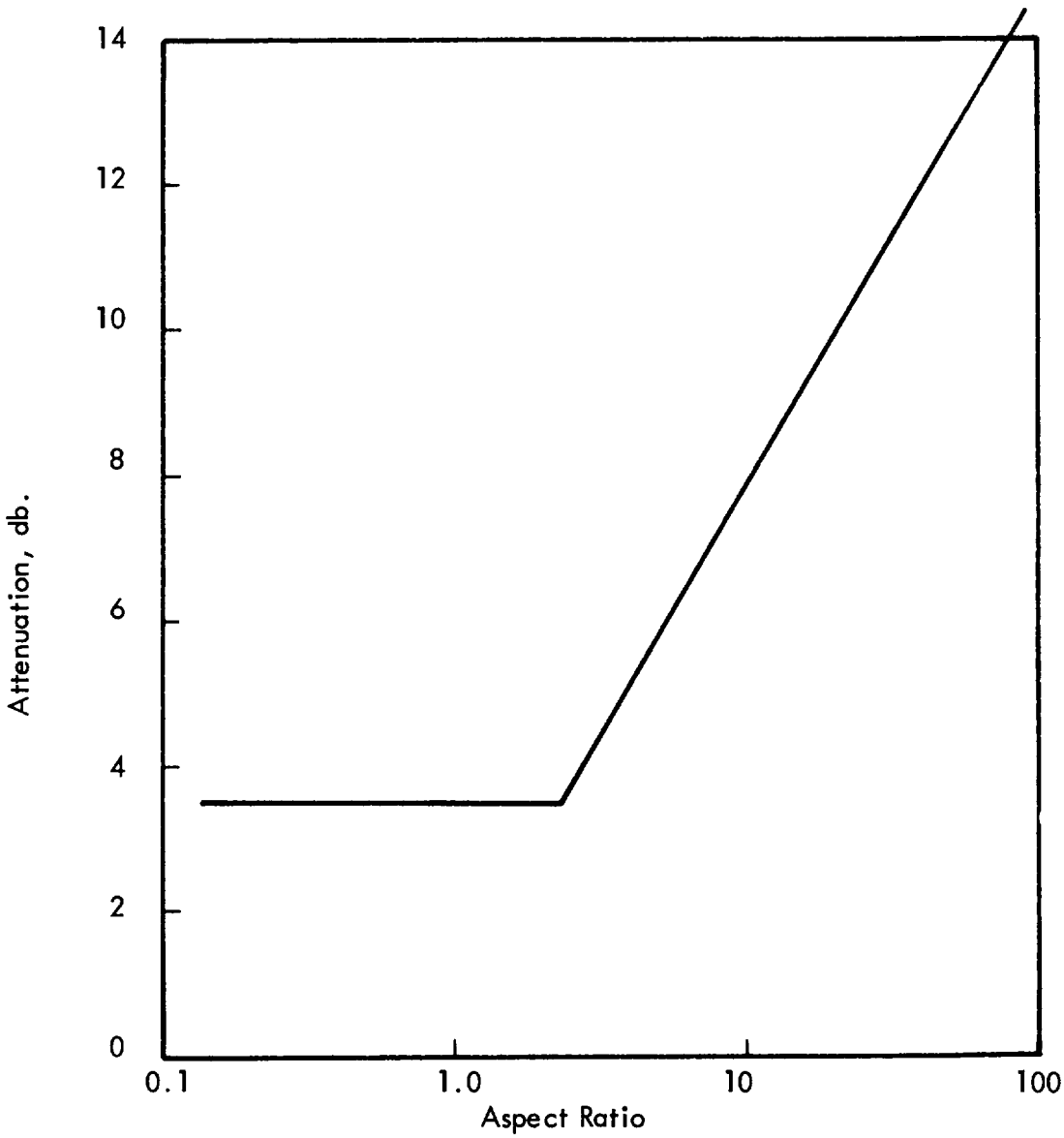


Noise Reduction off the Ends of Rectangular Nozzles at 1575 fps Relative Velocity. Tyler, Sofrin and Davies (Reference 35)

Figure 65: Attenuation of Sound Pressure Levels of Rectangular Nozzles

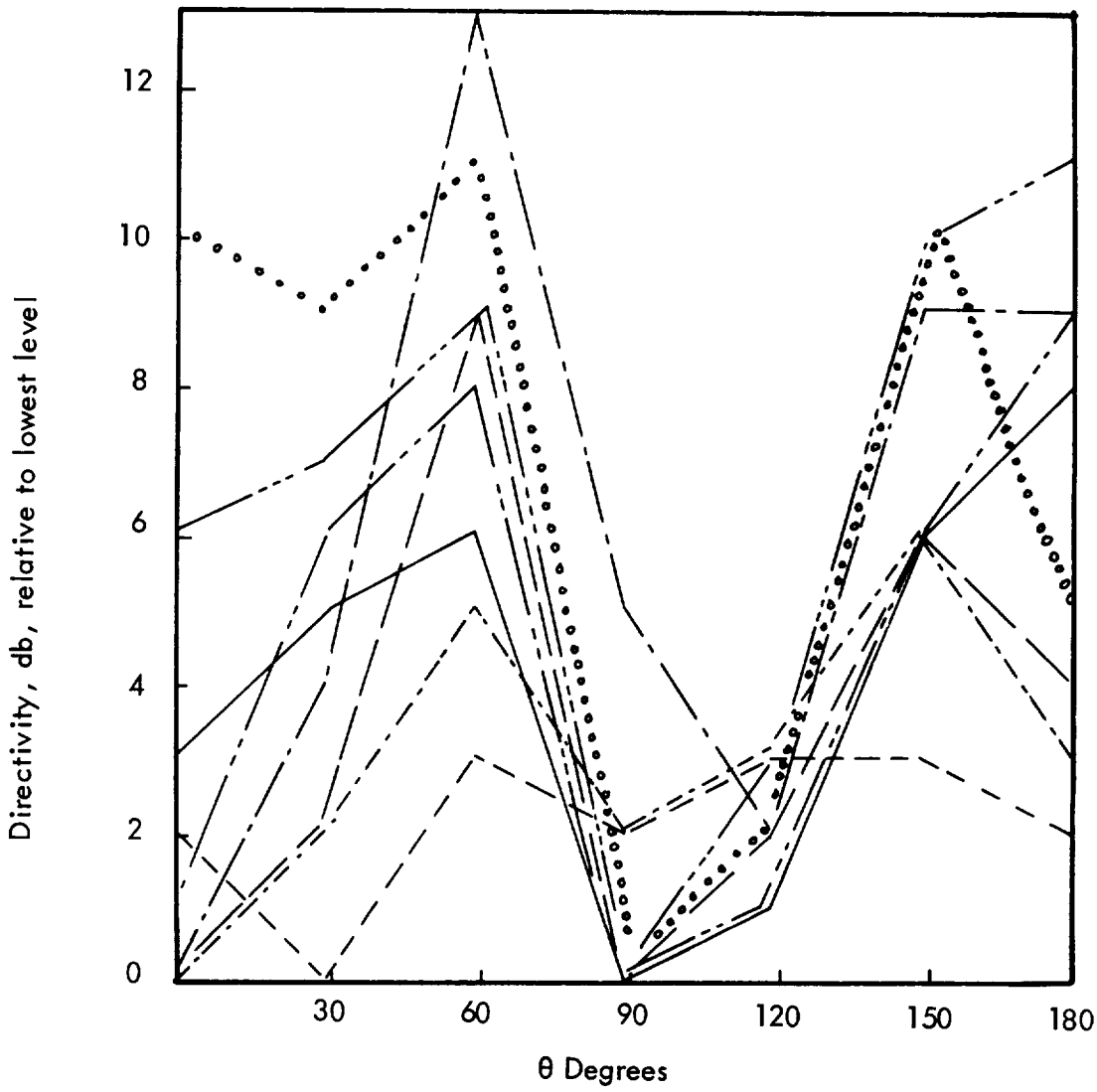


Results from Cole, et al. (Reference 11)

Figure 66: Ellipticity of Sound Field from Deflected Rocket

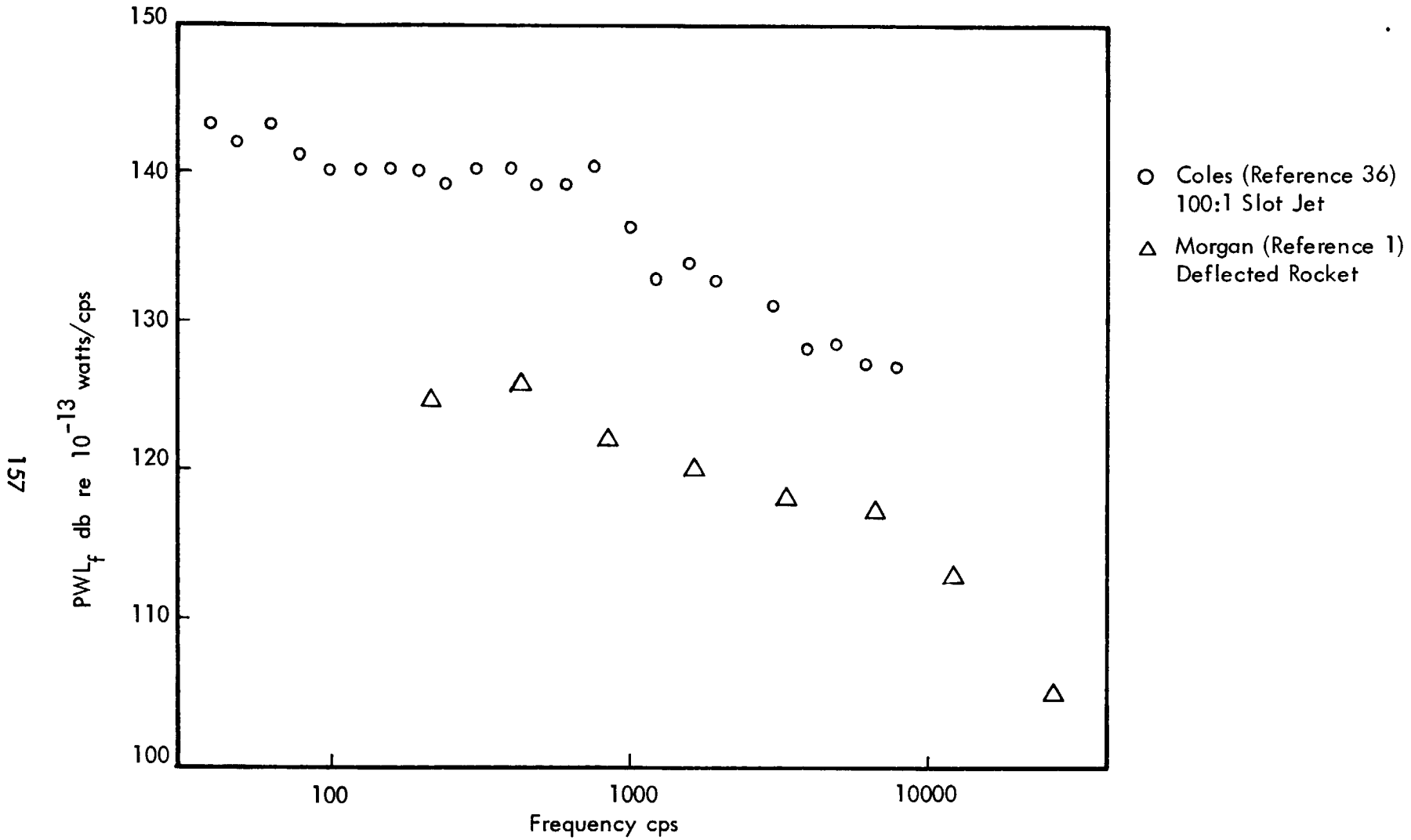


Figure 67: Spectral Density of Acoustic Power from a Slot Jet Compared with a Deflected Jet

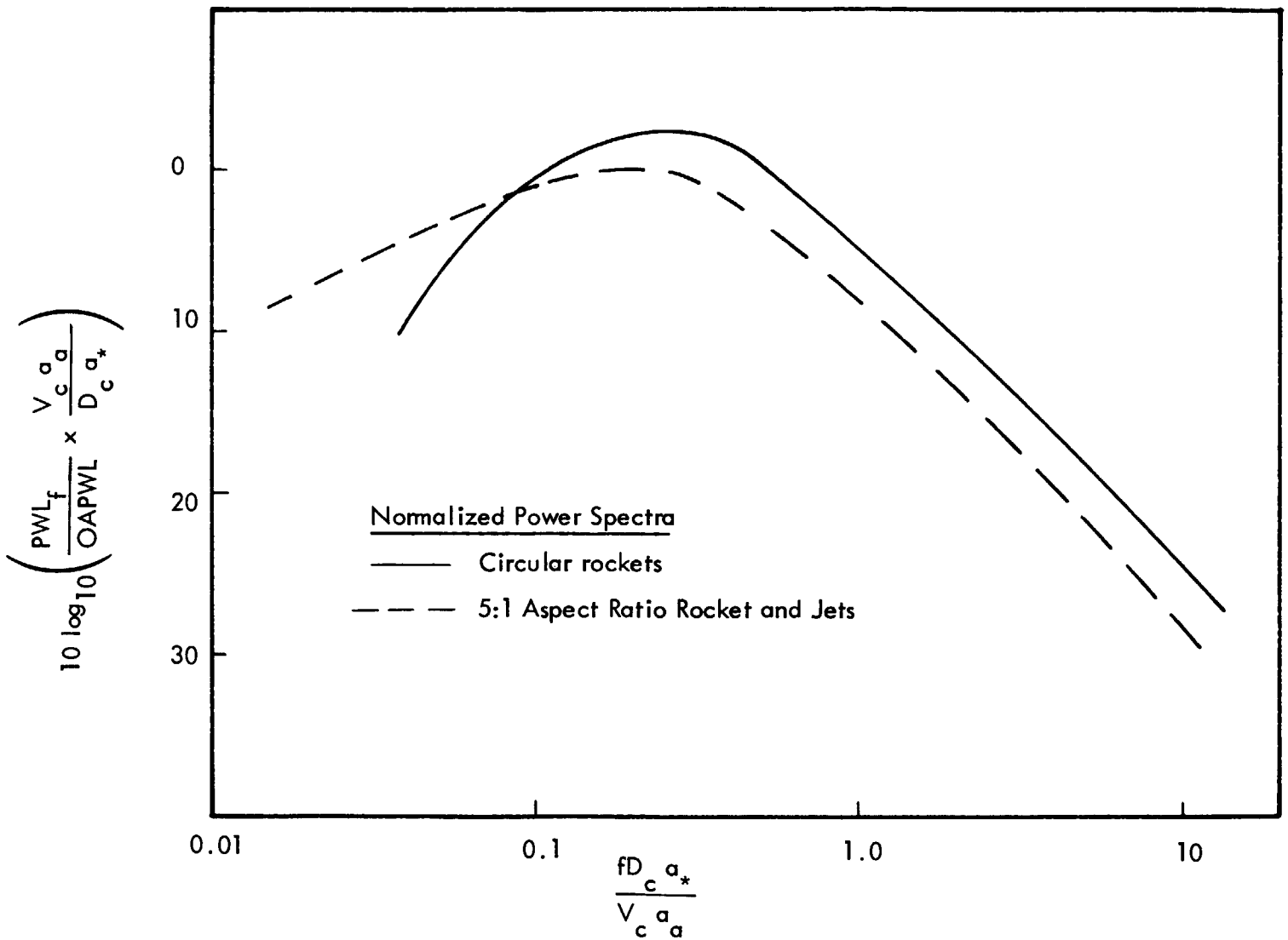


Figure 68: Normalized Power Spectra for Circular and High Aspect Ratio Flows

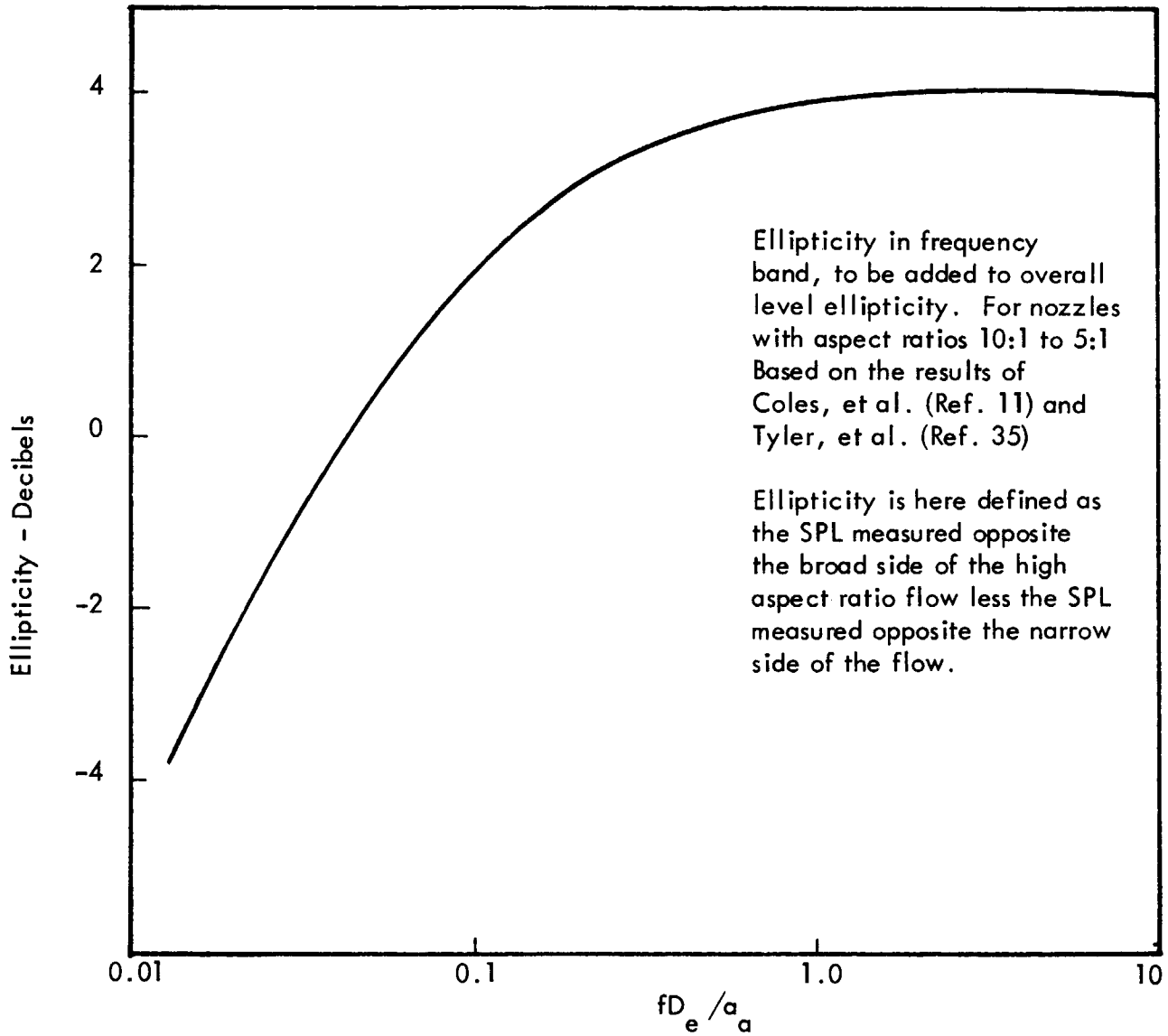


Figure 69: Ellipticity of Sound Pressure Level with Frequency for High Aspect Ratio Flows

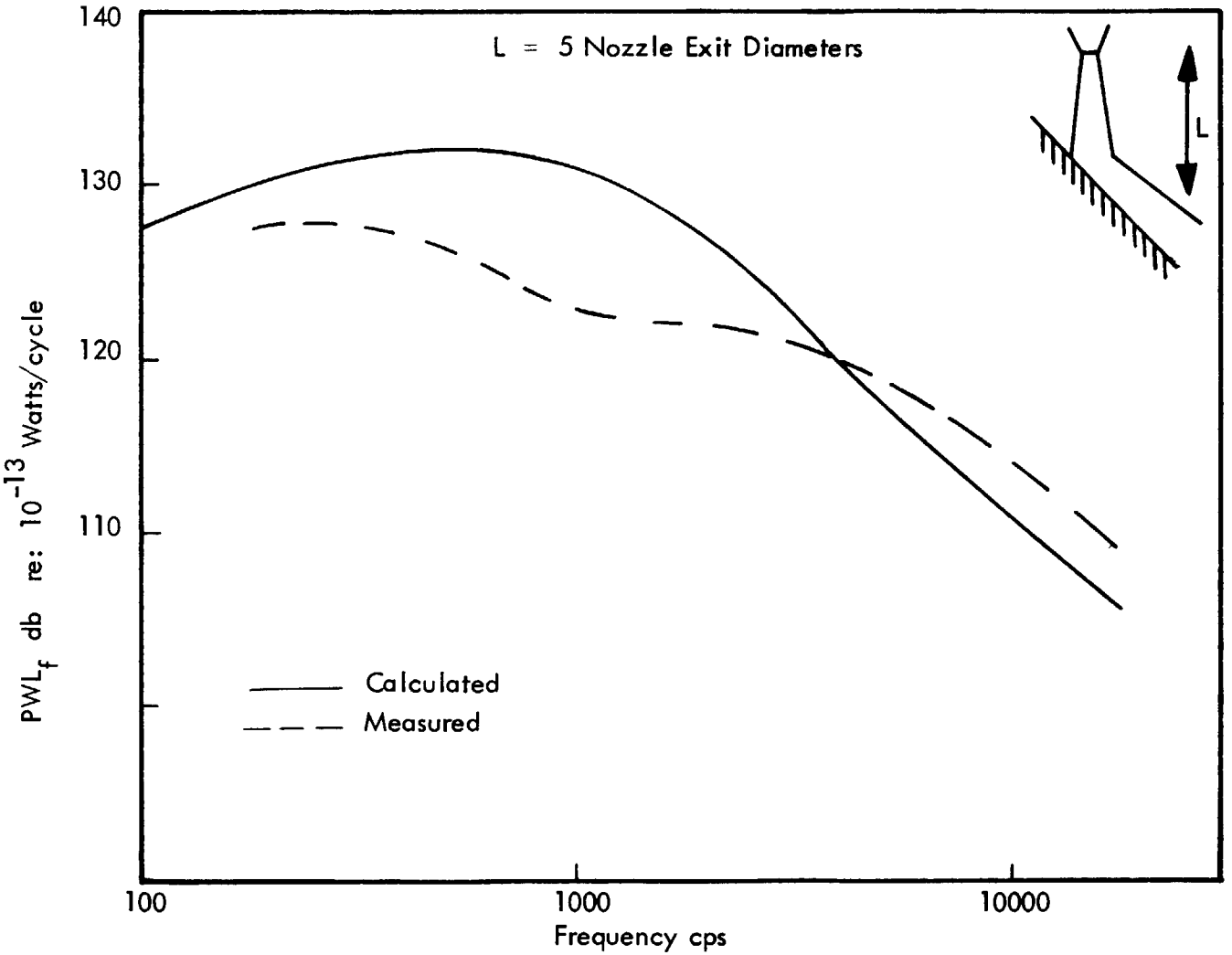


Figure 70: Total Sound Power Spectral Density for Small Rocket with Deflected Exhaust

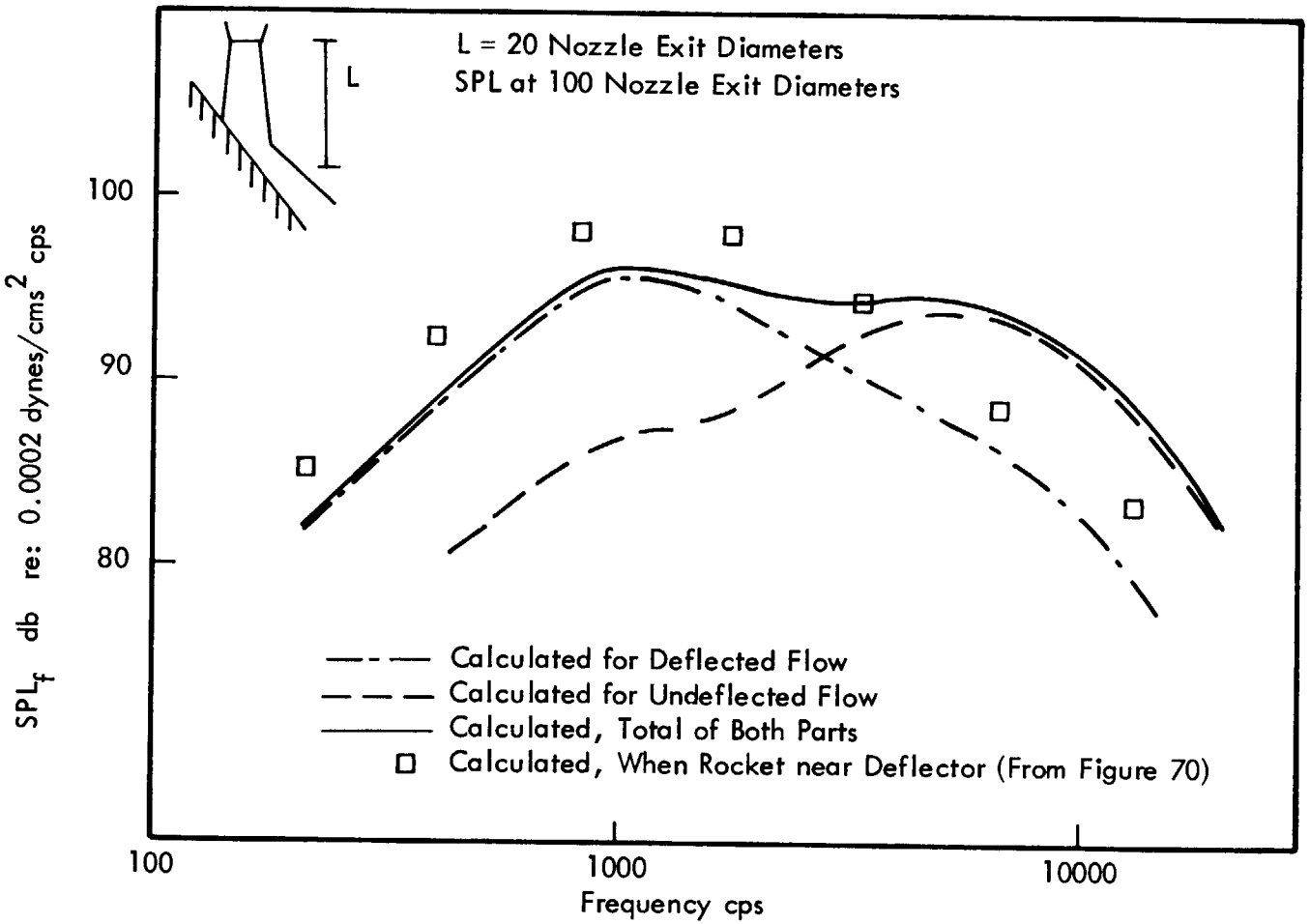


Figure 71: Spectrum of Sound Pressure Level for Small Rocket with Deflected Exhaust

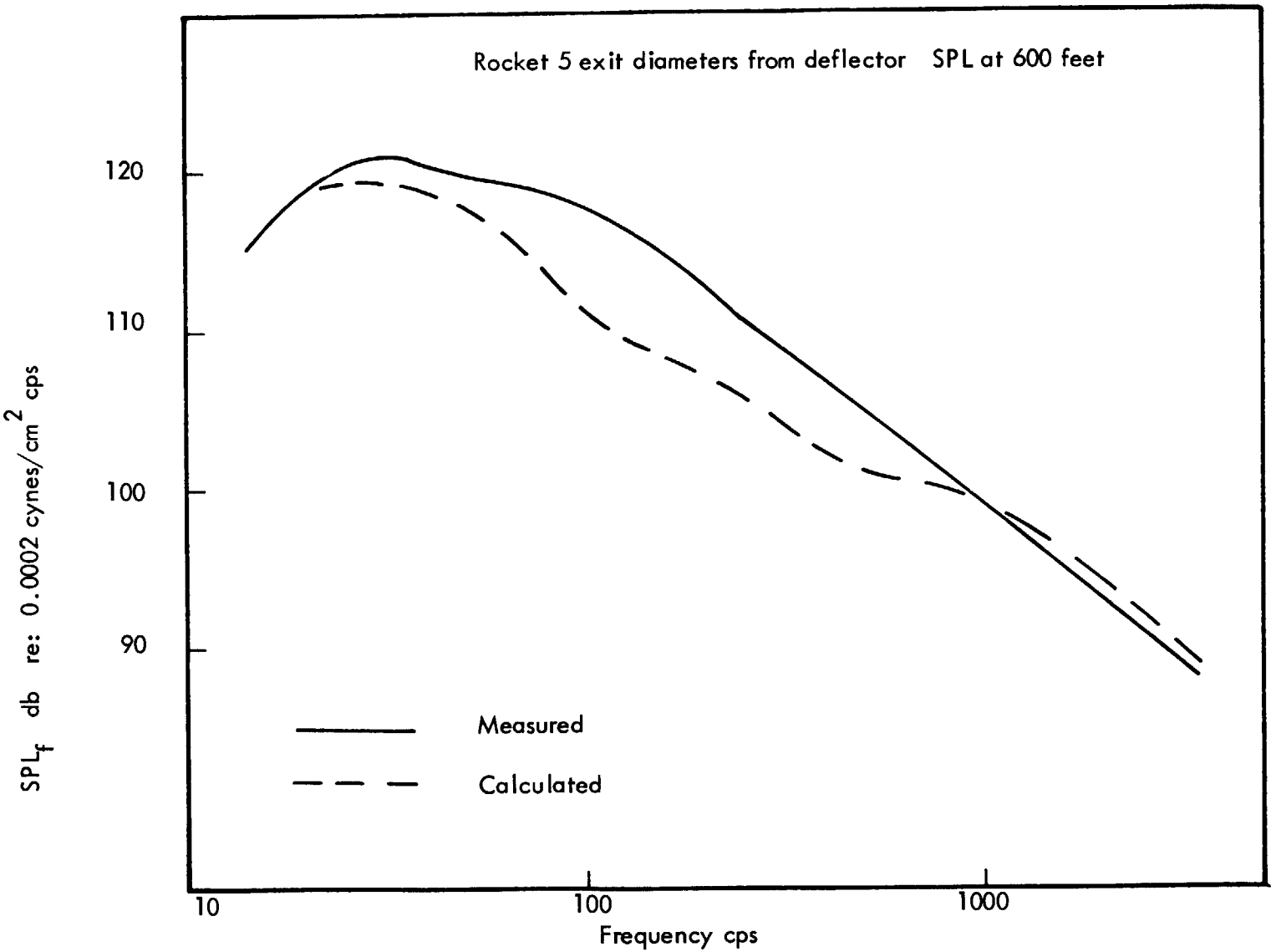


Figure 72: Spectrum of Sound Pressure Level for Large Rocket Example

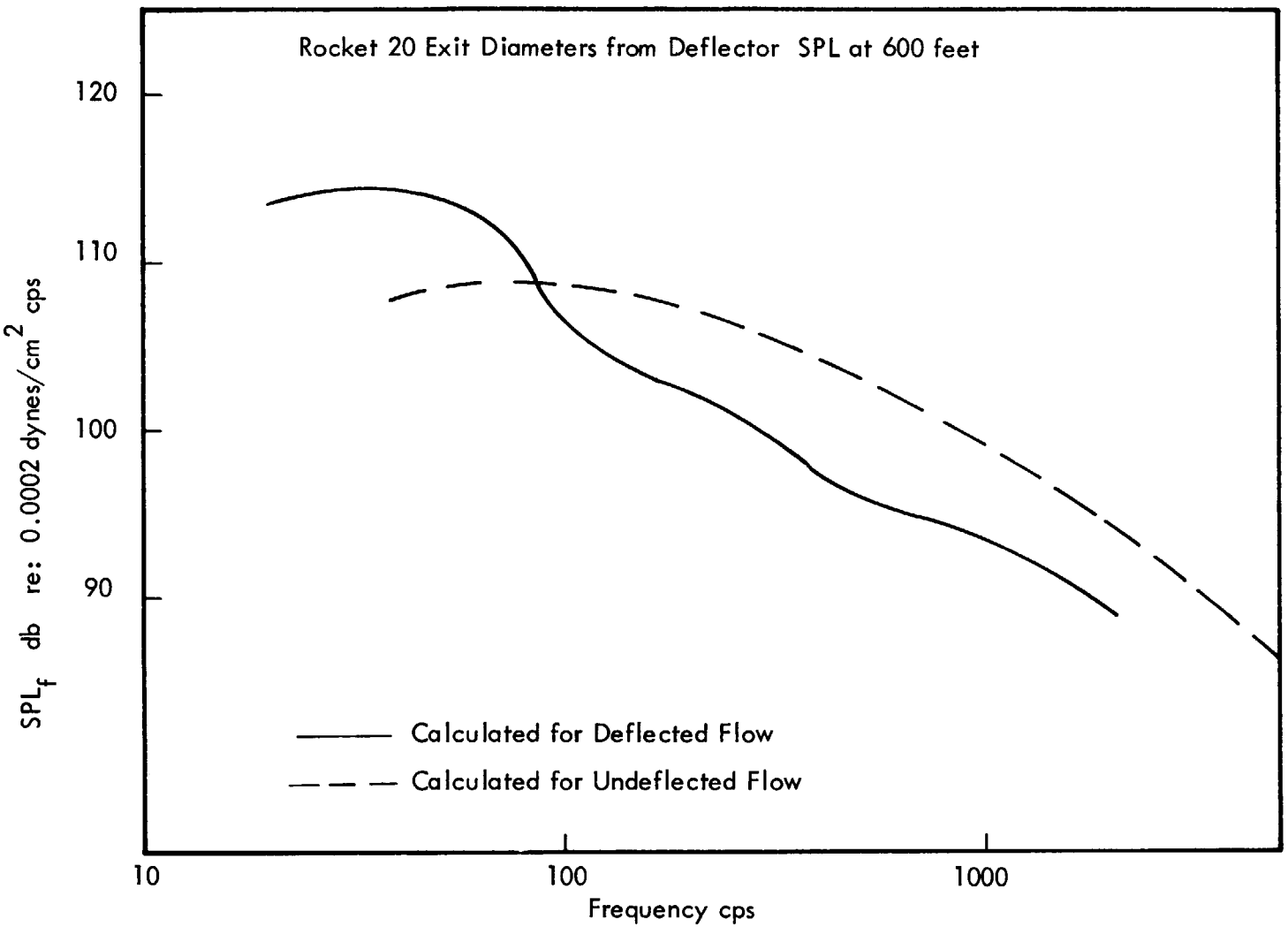


Figure 73: Spectrum of Sound Pressure Level for Large Rocket Example

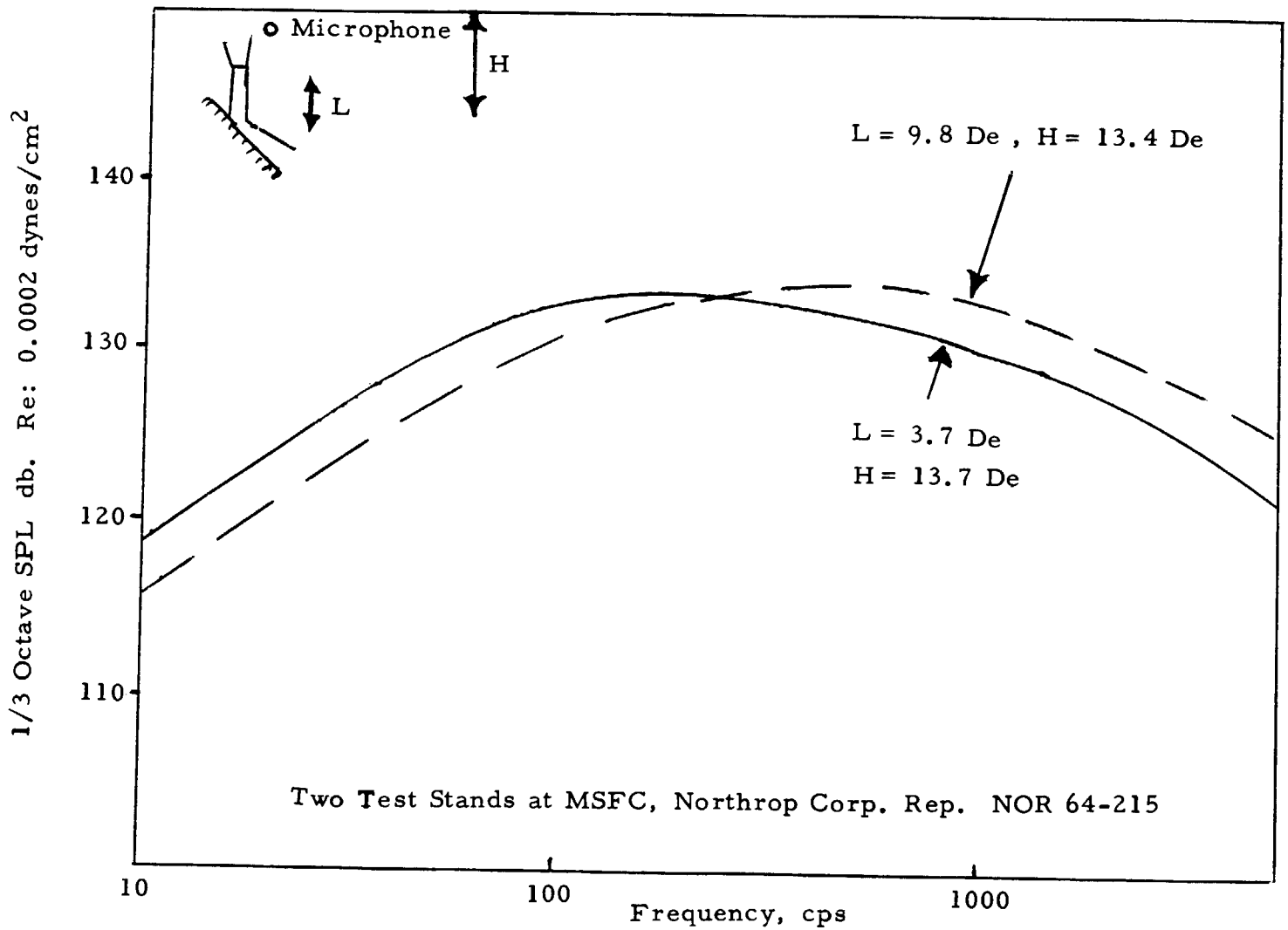


Figure 74: Spectrum of Sound Pressure Level of Noise Measured on Jupiter Rocket Case for Two Different Nozzle-Deflector Separations.

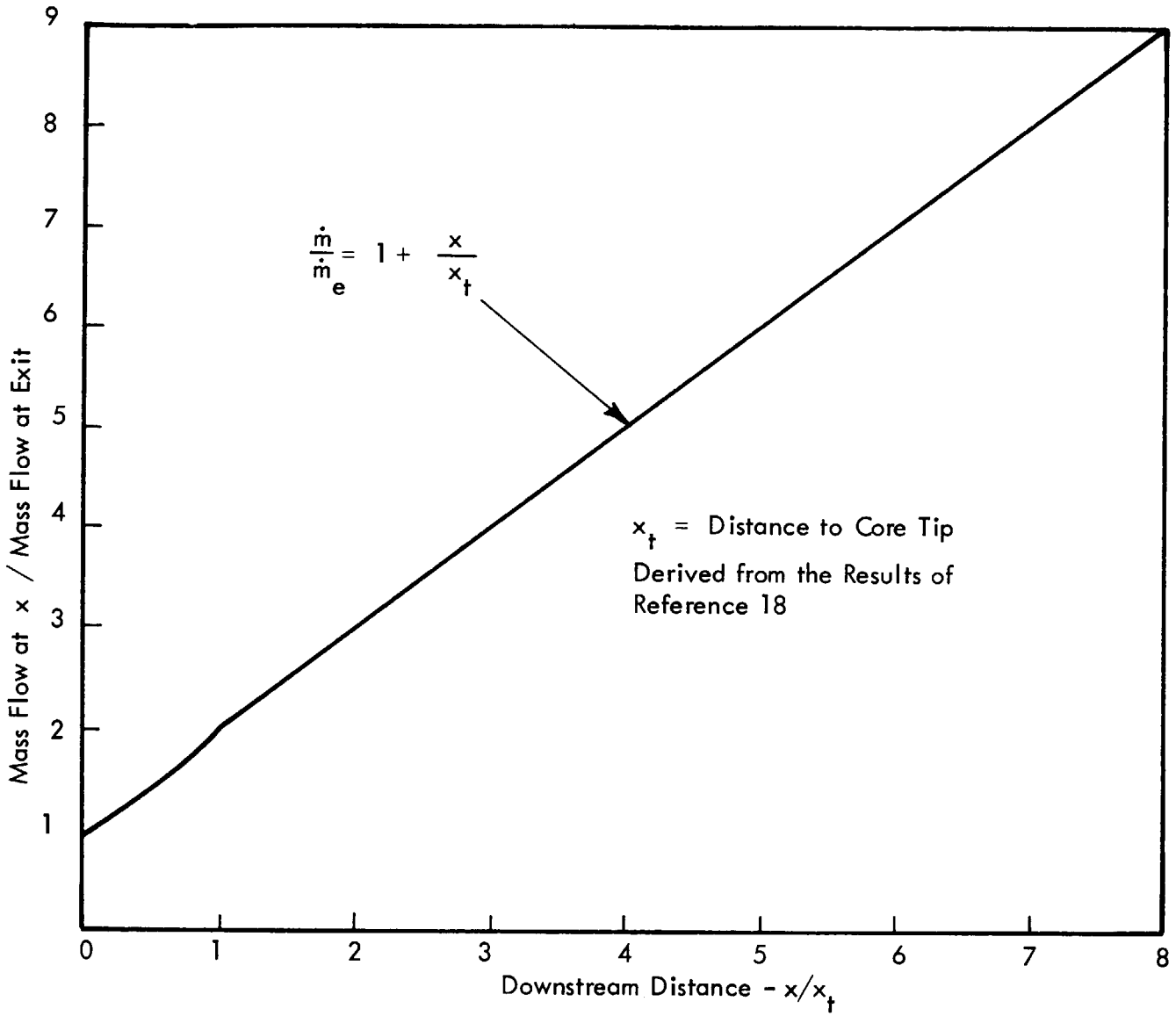


Figure A1: Mass Flow at Distance x Downstream Compared to Mass Flow at Nozzle Exit Against Downstream Distance

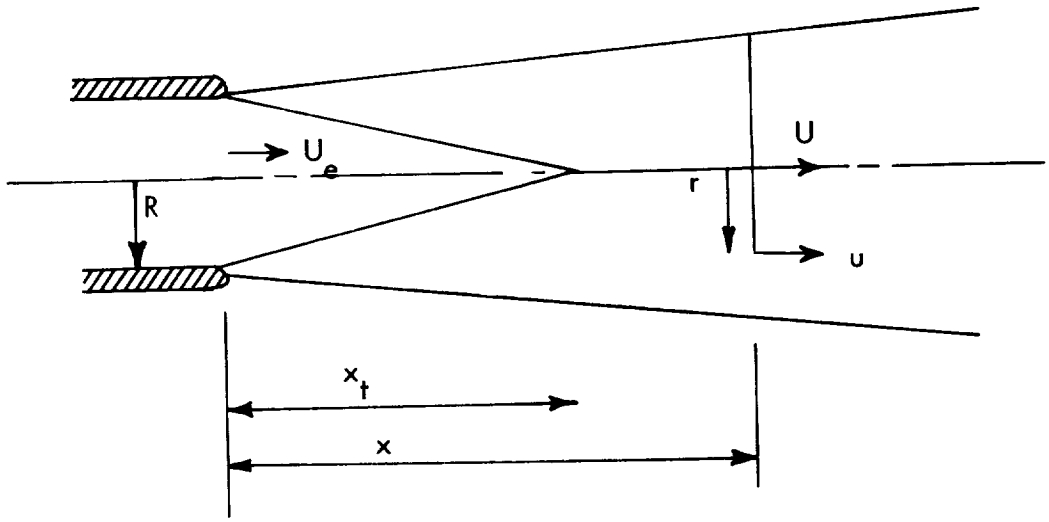


Figure D 1: Jet Parameters

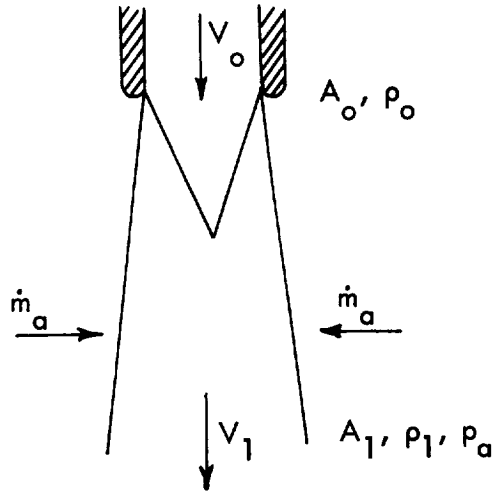


Figure D 2: Uniform Free Jet

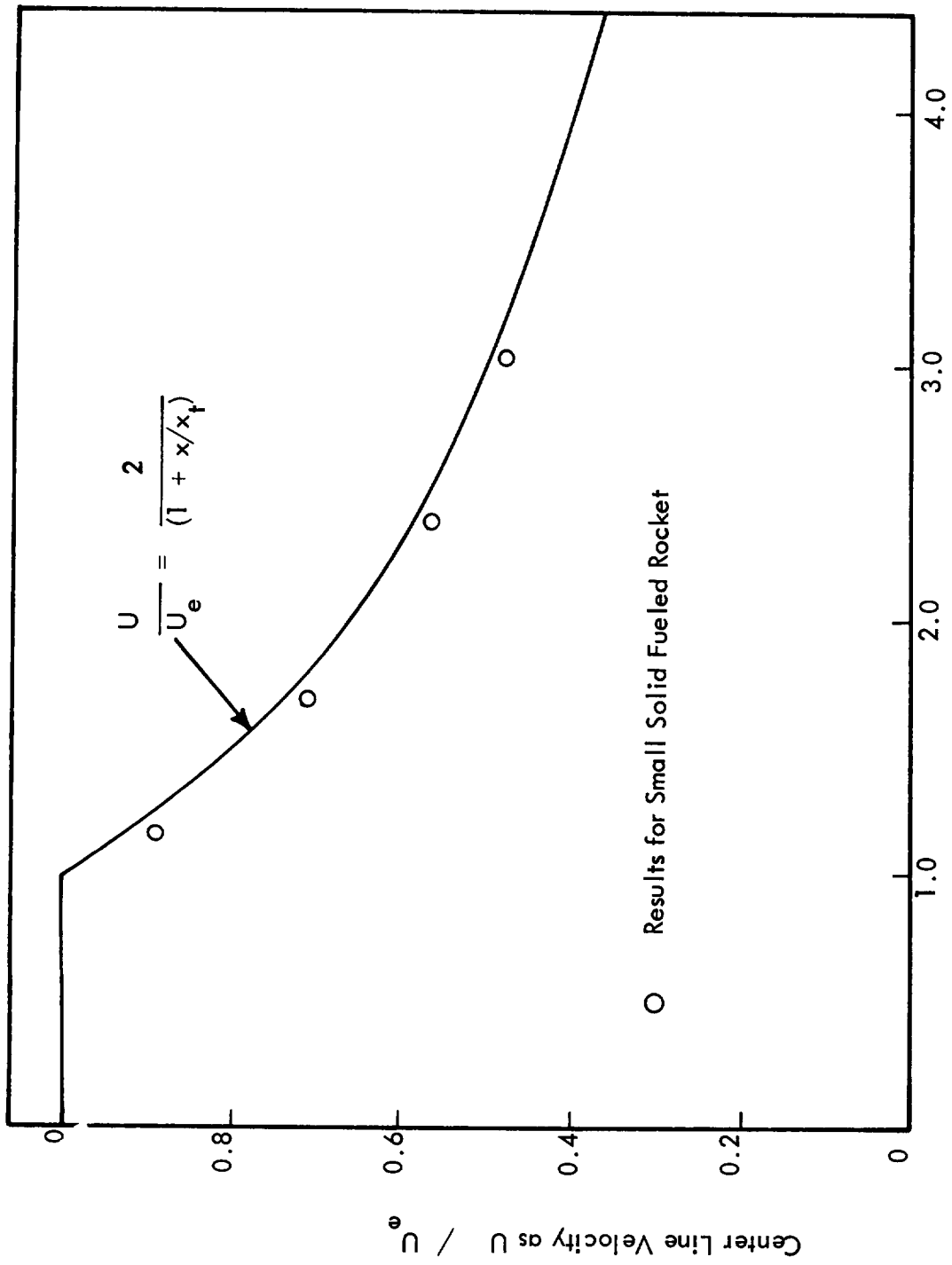


Figure D3: Comparison of Center Line Velocity Between Constant Density Jet and Calculated Results for a Small Solid Fueled Rocket